FZD-511

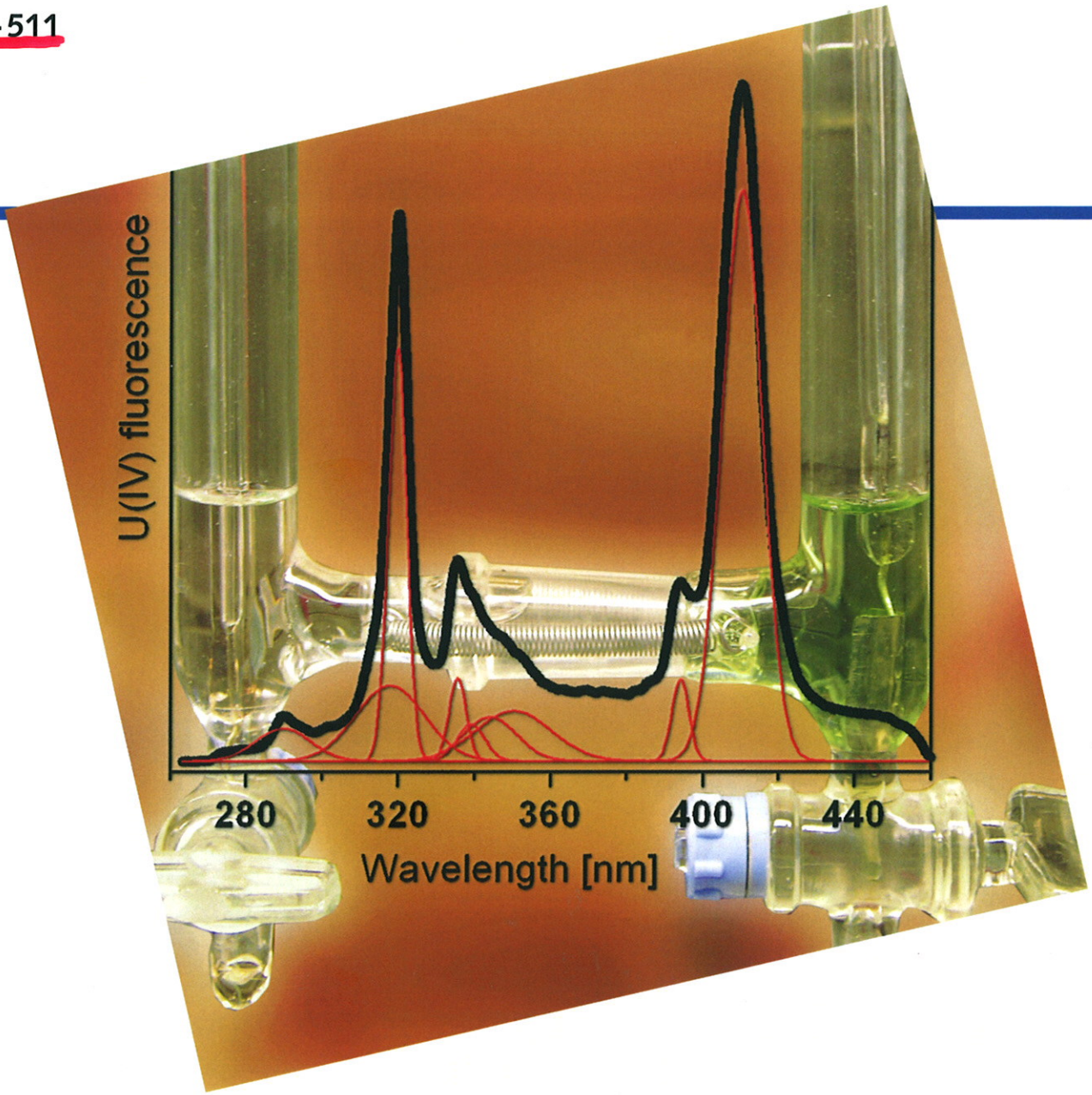

Wissenschaftlich-Technische Berichte
FZD-511 2009 · ISSN 1437-322X

ANNUAL REPORT 2008

INSTITUTE OF RADIOCHEMISTRY

Forschungszentrum Dresden Rossendorf

Wissenschaftlich-Technische Berichte
FZD-511
2009

Annual Report 2008

Institute of Radiochemistry

Editor: **Prof. Dr. G. Bernhard**

Editorial staff: **Dr. H. Foerstendorf**
Dr. A. Richter
Dr. K. Viehweger

Forschungszentrum
Dresden Rossendorf

Contact

Forschungszentrum Dresden-Rossendorf
Institut für Radiochemie

Postal Address	*Address for visitors*
P.O. Box 51 01 19	Bautzner Landstraße 400
D-01314 Dresden	D-01328 Dresden
Germany	Germany

Phone: ++49 (0) 351 260 3210
Fax: ++49 (0) 351 260 3553
http://www.fzd.de/FWR
e-mail: contact.radiochemistry@fzd.de

This report is also available at http://www.fzd.de/FWR

Cover picture

A uranium(IV) perchlorate solution is electrolytically reduced to green-emerging uranium(IV). A novel time-resolved laser fluorescence spectroscopy system for research of emitters of short-lived fluorescence was applied to study the complexation of uranium(IV) with fluoride and phosphate in aqueous solution. The stability of the complexes was characterized by determination of their corresponding complex formation constants (for details see pages 61 and 62).

Preface

The Institute of Radiochemistry (IRC) is one of the six Institutes of the Forschungszentrum Dresden-Rossendorf (FZD). Together with the Institute of Safety Research, the IRC contributes to the research program "Nuclear Safety Research" and performs basic and applied research in the fields of radiochemistry and radioecology. Motivation and background of our research are environmental processes relevant for the installation of nuclear waste repositories, for remediation of uranium mining and milling sites, and for radioactive contaminations caused by nuclear accidents and fallout. Because of their high radiotoxicity and long half-life the actinides are of special interest. The research is focused on a better understanding of the chemical behavior of actinides and other relevant long-lived radionuclides in the environment on a molecular level.

In 2007, the FZD was evaluated by the Wissenschaftsrat (German Council of Science and Humanities). This council is an advisory body to the Federal Government and the State Governments. Its function is to draw up recommendations on the development of scientific research and of the university sector as well as to contribute to the safeguarding of the international competitiveness of German science in the national and European science system (see: www.wissenschaftsrat.de). The results of the evaluation were published in spring 2008. We can proudly report that the Institute of Radiochemistry has got a very good testimonial by the Wissenschaftsrat. We will follow the given helpful hints to further improve our research work.

In the last year we have focused our research activities on two topics:

- Actinides (Metals) in Waste Repositories,
- Actinides (Metals) in Biosystems.

Following a recommendation of the Wissenschaftsrat the research work of the division of Biophysics, Institute of Radiation Physics, will be fully integrated into the topic Actinides (Metals) in Biosystems since the beginning of 2009.

In 2008, about 100 scientists, technicians, Ph.D. and diploma and bachelor students were employed at the Institute of Radiochemistry (see scheme on p. 106). More than twenty Ph.D. students are working at the institute. Promotion of young scientists is an important requirement to ensure that the competence and excellent scientific results of radiochemistry will be maintained in the future.

We accomplished many new scientific results in the past year, which are presented in this Annual Report. Among them only few can be highlighted in this preface.

We were very successful in the determination of formation pathways and structures of various actinides with biologically relevant ligands. These results contribute to a better understanding of actinide speciation during the transfer from the geo-sphere to the bio-sphere, especially with respect to the chemical processes at interfaces and in bio-fluids.
Further progress was achieved on knowledge about the microbial diversity in uranium contaminated sites and the understanding of the interaction of actinides with different bacterial strains and algae. We strengthened our research on the use of bacterial S-layers as templates for photocatalysts and chemo-optical sensors. By a combination of spectroscopic and microscopic methods with data collected by electrochemical micro-sensors we got new insights in the metabolic activity of bacteria in bio-films after adding uranium.
The long-lived fission product selenium-79 has been considered as one of the great challenges for the safe disposal of nuclear waste. Our recent investigations demonstrate that redox-processes in the near-field and the far-field of such repositories may significantly reduce the mobility of selenium-79.
Conclusions drawn from thermodynamical calculations depend on the quality of the input data. The aim of the cooperative project THEREDA is the development of a consistent and quality assured thermodynamic reference data base for all safety relevant elements. New results about data compilation for uranium and radium and the maintenance of the data consistency are presented.

Furthermore, we can report that our own radiochemical experimental facilities – the radiochemistry lab at the Rossendorf Beamline at ESRF, the radiochemical station at the Free Electron IR-Laser of the Rossendorf accelerator ELBE, and our different laser-spectroscopic and microscopic systems are continuously working on a high quantitative and qualitative level. These methods are the basis for excellent scientific results of our researchers and all the other users.

I would like to thank the visitors, German and international ones, for their interest in our research and for their participation in the institute seminars. We would also like to thank our scientific collaborators and the visiting scientists for coming to Dresden/Rossendorf in 2008 to share their knowledge and experience with us. We continue to strongly encourage the collaborations and visits by scientists in the future. Special thanks are due to the Executive Board of the Forschungszentrum Dresden-Rossendorf, the Ministry of Science and Arts of the State Saxony, the Federal Ministry of Education and Research, the Federal Ministry of Economics and Technology, the Deutsche Forschungsgemeinschaft, the European Commission, and other organizations for their support.

Prof. Dr. Gert Bernhard

Contents

SCIENTIFIC CONTRIBUTIONS

Part I: Actinides (metals) in biosystems

Part II: Actinides (metals) in waste repositories

Part III: Biophysics

PUBLICATIONS

SCIENTIFIC ACTIVITIES

Actinides (metals) in biosystems

Aqueous U(VI) complexes with tartaric acid: A combined EXAFS and UV-vis study

C. Lucks, A. Rossberg, A. C. Scheinost

The aqueous U(VI) complexes with DL-tartaric acid were investigated in the pH range from pH 1 to pH 7 by applying EXAFS und UV-vis measurements. According to the literature the complexes were identified and structures were proposed.

EXPERIMENTAL. Sample solutions were prepared by dissolving UO_3 in perchloric acid and adding the needed amount of solid DL-tartaric acid. After the pH was adjusted to pH 7, the UV-visible pH titration experiment was performed by adding negligible small volumes of highly concentrated acids. The UV-vis data was collected on a Cary 50 spectrophotometer in the spectral range from 700 to 350 nm. At seven selected pH points solutions were prepared for measuring both EXAFS and UV-vis. The uranium L_{III}-edge EXAFS measurements were performed in transmission mode at the Rossendorf Beamline BM20 (ROBL), ESRF.

RESULTS. The UV-visible pH titration data were treated using the program pHab [1]. For the computation complex stability constants from literature [2-4] were used as initial values. Figure 1 shows the measured and fitted data at one single wavelength as well as the calculated speciation. It has been approved that between pH 3 and 5 the dimeric uranyl tartrate $(UO_2)_2(H_{-1}Tar)_2^{2-}$ is the dominant species and that at higher pH values a further oligomerization to the trimer $(UO_2)_3(H_{-1}Tar)_3(OH)_2^{5-}$ occurs. Furthermore, no evidence was found for the occurrence of a tridentate monomer which was also postulated in literature [2-4]. EXAFS analyses were done using iterative target transform factor analyses. Three factors were found to be sufficient for fitting the data. The Fourier-transforms of these factors are shown in Fig. 2. According to the speciation, these factors must be the hydrated uranyl ion, the dimer and the trimer. This suggestion is supported by the fact that the relative concentrations of those factors fit very well to the speciation that was computed using the UV-vis data (Fig. 1).

Factor 2 and 3 show a strong U–U interaction at 3.93 Å and 3.81 Å respectively (Tab. 1). These distances are in fair agreement with U–U distances of dimers or trimers of the hydrolysis species in aqueous phase from DFT calculations [5]. The determined U–C distances give evidence for the formation of five or six membered rings. According to the sum formulas of both complexes, the tartrate ion connects tridentately to uranium using one hydroxyl and two carboxyl groups. These pieces of information lead to the postulation of the structures shown in Fig. 3.

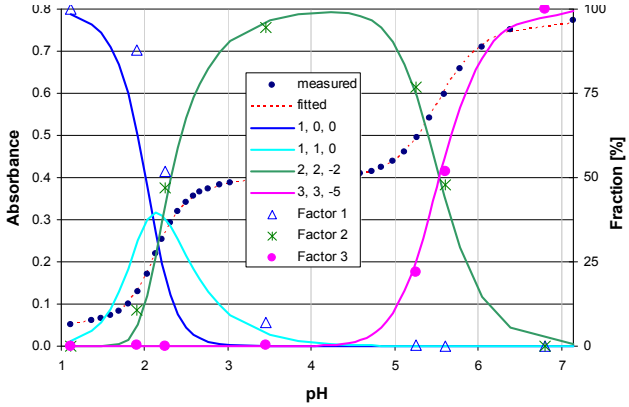

Fig. 1: Measured and fitted absorbance data at 433 nm, computed speciation and relative concentration of the factors in the U(VI)-tartrate system determined by EXAFS.

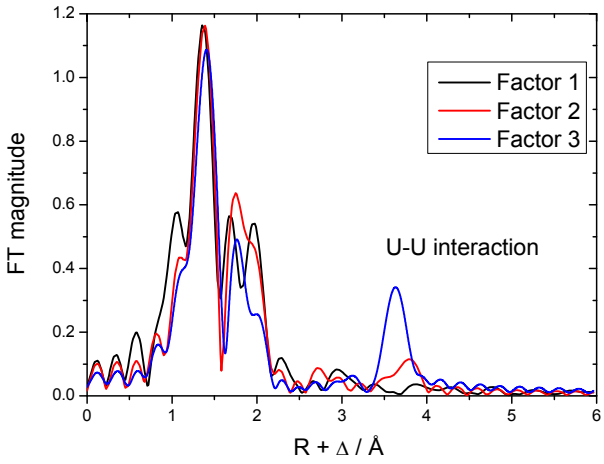

Fig. 2: Fourier-transforms of the isolated EXAFS spectra for the individual species in the U(VI)-tartrate system.

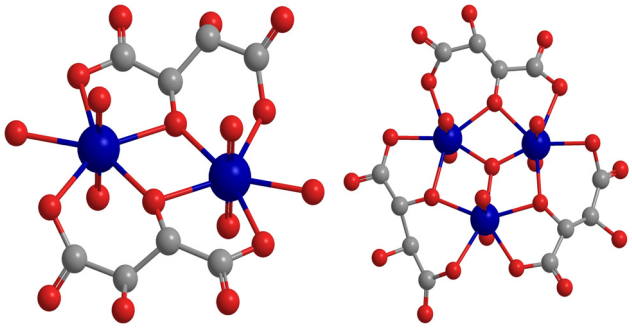

Fig. 3: Proposed structures for the uranium tartrate dimer (left) and uranium tartrate trimer (right).

Tab. 1: EXAFS structural parameters for the three factors.

	Atom	N	R	σ²
Factor 1	O_{ax}	2*	1.766(1)	0.00112(6)
	O_{eq}	5*	2.404(3)	0.0075(3)
Factor 2	O_{ax}	2*	1.787(9)	0.00129(6)
	O_{eq}	5*	2.356(2)	0.0061(2)
	C	2.1(8)	3.28(1)	0.006(3)
	U	1*	3.927(6)	0.0054(4)
	U–U distance of $(UO_2)_2(OH)_2^{2+}$: 3.87 [5]			
Factor 3	O_{ax}	2*	1.803(1)	0.00142(7)
	O_{eq}	5*	2.360(4)	0.0113(4)
	C	1.5(5)	3.29(2)	0.006*
	U	2*	3.806(2)	0.0048(2)
	U–U distance of $(UO_2)_3(O)(OH)^{3+}$: 3.83 [5]			

* fixed ()- standard deviation.

REFERENCES

[1] Gans, P. et al. (1999) *Annali di Chimica*, **89**, 45-49.
[2] Feldman, I. et al. (1960) *Annali di Chimica*, **64**, 1224-1230.
[3] Rajan, K. S. et al. (1964) *J. Inorg. Nucl. Chem.* **26**, 1927-1944.
[4] Sircar, J. K. et al. (1982) *J. Chem. Eng. Data*, **27**, 231-233.
[5] Tsushima, S. (2007) *Inorg. Chem.* **35**, 784-787.

Complexation of U(IV) by mandelic and glycolic acid studied by UV-vis spectroscopy

K. Schmeide

The complexation of uranium(IV) by mandelic and glycolic acid was studied at an ionic strength of 1.0 M by UV-vis spectroscopy. Stability constants for 1:1 and 1:2 uranium(IV) ligand complexes of the type $M_pH_qL_r$ were determined with $\log \beta_{101} = 4.53 \pm 0.09$ and $\log \beta_{102} = 8.02 \pm 0.13$ for mandelate and with $\log \beta_{101} = 4.71 \pm 0.08$ and $\log \beta_{102} = 8.25 \pm 0.15$ for glycolate.

Data for the complexation of U(IV) with inorganic and organic ligands are scarce. In this study, for the U(IV) complexation the model ligands mandelic acid and glycolic acid were chosen which stand for a variety of organic ligands in aqueous systems.

EXPERIMENTAL. Sample solutions were prepared in a glove-box (N_2 atmosphere) using CO_2-free solutions. The U(IV) concentration was kept constant at $1 \cdot 10^{-3}$ M or $5 \cdot 10^{-4}$ M, the ligand concentration was varied between 0 and 0.2 M. The concentration of hydrogen ions (1.0, 0.5, 0.1 M) was adjusted by adding aliquots of 5 M $HClO_4$ simultaneously taking into consideration the $[H^+]$ stemming from the U(IV) stock solution. The ionic strength was 1.0 M (H,Na)ClO_4. The amount of U(VI) in the samples was ≤ 1.5% of the total U as determined by fluorescence spectroscopy.
The UV-vis absorption spectra were recorded with a UV/vis/NIR spectrophotometer (CARY-5G, Varian) in the spectral range from 800 to 300 nm. The spectra were analyzed between 444 and 526 nm and between 567 and 727 nm. The stability constants were calculated with the program SPECFIT™.

RESULTS. The complexation of U(IV) has been investigated in dependance on hydrogen ion concentration. The pK_a values reported for mandelic acid and glycolic acid amount to 3.18 [1] and 3.61 [1] at I = 1.0 M, respectively. Exemplary, Fig. 1 shows the evolution of the U(IV) spectrum in the two wavelength ranges analyzed for increasing glycolic acid concentrations (0 to 0.2 M) at an acidity of $[H^+] = 0.1$ M and an ionic strength of I = 1.0 M.
The U(IV) complexation reaction can be expressed as:

$$p\ U^{4+} + q\ H^+ + r\ \text{ligand}^- \rightleftarrows U_pH_q\text{ligand}_r^{(4p+q-r)}$$

For the calculation of the stability constants, each series of experiments was analyzed within 2 wavelength ranges. Thereby, the formation of 1:1 and 1:2 complexes was detected in the mandelate and glycolate media. The stability constants were determined with $\log \beta_{101} = 4.53 \pm 0.09$ and $\log \beta_{102} = 8.02 \pm 0.13$ for mandelate and with $\log \beta_{101} = 4.71 \pm 0.08$ and $\log \beta_{102} = 8.25 \pm 0.15$ for glycolate. The U(IV) speciation, calculated for the glycolic acid system (Fig. 2), exemplifies that the U(IV) hydrolysis is impeded due to the strong complexation of U(IV) by the ligand.
To our knowledge, there are no data available on the U(IV) complexation by mandelic or glycolic acid in literature. However, as expected, the $\log \beta$ values determined for U(IV) mandelate and glycolate in this work are higher than those reported for Th(IV) mandelate and glycolate (e.g. [2-5]) but lower than those reported for U(IV) citrate [6].

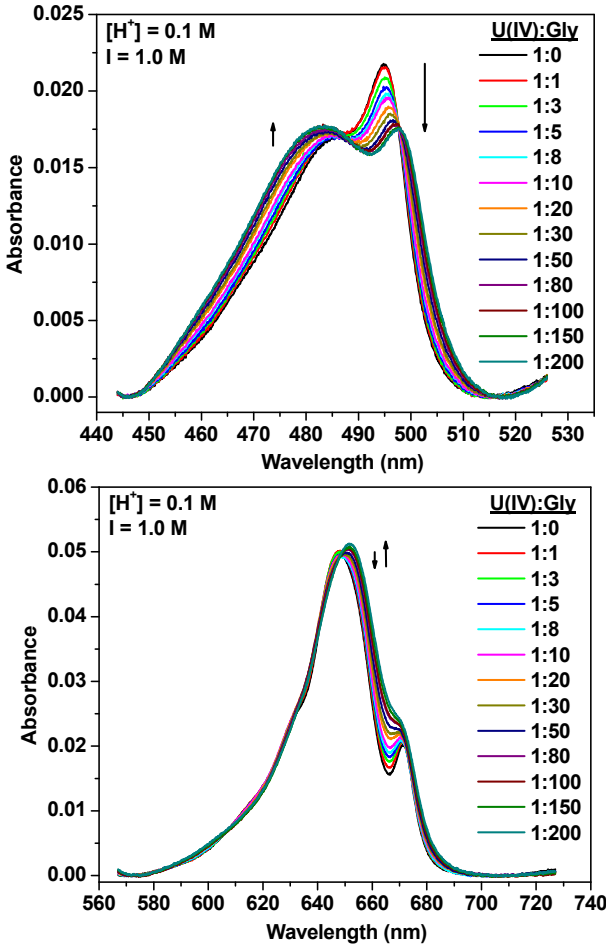

Fig. 1: Two wavelength ranges of the UV-vis spectra for $1 \cdot 10^{-3}$ M U(IV) as a function of the glycolic acid (Gly) concentration.

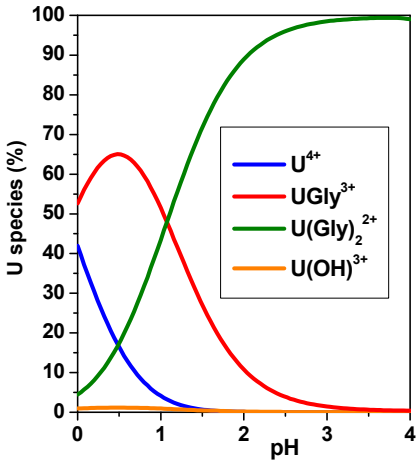

Fig. 2: U(IV) speciation in presence of glycolic acid ($[U(IV)] = 5 \cdot 10^{-4}$ M, [Gly] = 0.1 M, I = 1.0 M).

ACKNOWLEDGEMENTS. This work was funded by the BMWi under contract number 02E10156.

REFERENCES

[1] Martell, A. E. et al. (1998) *NIST critically selected stability constants of metal complexes database*, Gaithersburg, MD, U.S.A.
[2] Toraishi, T. et al. (2002) *J. Chem. Soc., Dalton Trans.*, 3805.
[3] Di Bernado, P. et al. (1978) *Thermochim. Acta* **23**, 293.
[4] Magon, L. et al. (1973) *J. Inorg. Nucl. Chem.* **35**, 4237.
[5] Charykov, A. et al. (1985) *Zh. Obshch. Khim.* **55**, 2411.
[6] Schmeide, K. et al. (2008) *Report FZD-489*, p. 16.

TRLFS study of the U(VI) / citric acid system – Measurements at cryogenic temperature

A. Günther, R. Steudtner

The complex formation of uranium(VI) with citric acid was investigated by time resolved laser-induced fluorescence measurements at cryogenic temperature and compared with previous investigations at room temperature. The formed U(VI)-citrate species UO_2cit^- and $(UO_2)_2(cit)_2^{2-}$ fluoresces at 153 K. The detected luminescence emission bands are bathochromic shifted in comparison to the bands of the free uranyl cation. The corresponding complex formation constants were calculated using spectroscopic data.

EXPERIMENTAL. The luminescence of the uranyl ion was measured after excitation with laser pulses at 266 nm (Inline laser, Continuum). Time-resolved spectra were recorded with an ICCD-camera (Princeton Instruments) in the wavelength range from 421 nm to 593 nm. The delay time after the excitation laser pulse was 20 µs. The pulse energy was 0.5 mJ. A cryostat (RDK 10-320) with an ultra pump station (PT50 KIT/DN 40 KF), compression unit RW2 and a low temperature controller LTC60 (complete system: Oerlicon Leybold, Dresden, Germany) were used for measurements at low temperature (153 K). The experiments were performed at a fixed uranyl perchlorate concentration of $5 \cdot 10^{-5}$ M. The citric acid (H_3cit) concentration was varied between 0 and $2.5 \cdot 10^{-3}$ M. All complex formation experiments were performed at an ionic strength of 0.1 M and at pH 3.5. The reference and complex solutions were prepared in dark measuring flasks and were stored at 253 K.

RESULTS. Earlier investigations demonstrated that the uranyl citrate complex species do not fluoresce or the luminescence quenching effects are too high for the detection of the complex species at room temperature. Only the decrease of the luminescence intensity of the free uranyl cation could be detected and shifts of the emission bands were not visible [1].
Figure 1 shows the normalized luminescence emission spectra of uranium(VI) as a function of the total citric acid concentration measured at 153 K. In contrast to the results of the measurements at room temperature it is shown that the uranyl luminescence signals shift significant to higher wavelengths at a concentration ratio U(VI) to citric acid of 1 :2 and higher. Therefore, it is possible to verify the complex formation by detection of the uranyl - citric acid complex species at cryogenic temperature and to determine their luminescence properties.
The time-resolved spectra show a three-exponential luminescence decay at higher citric acid concentrations. Three uranyl species are the main components in these complex solutions. The averaged luminescence lifetimes are $\tau_1 = 273 \pm 39$ µs for the free uranyl cation, $\tau_2 = 79 \pm 15$ µs and $\tau_3 = 14 \pm 5$ µs for two different complex species.
The spectra were analyzed with the factor analysis program SPECFIT™ [2]. The formed complex species are UO_2cit^- (lifetime τ_2) and $(UO_2)_2(cit)_2^{2-}$ (lifetime τ_3). The corresponding formation constants were calculated to be $\log \beta_{101} = 7.24 \pm 0.16$ and $\log \beta_{202} = 18.90 \pm 0.26$, according to the complex formation reaction:

$$x\ UO_2^{2+} + y\ H^+ + z\ cit^{3-} \xleftrightarrow{\beta xyz} [(UO_2)_x H_y cit_z]^{(2x+y-z)-}$$

The obtained formation constants are comparable with literature data [3]. Due to this fact, it was expected that the possible reduction of U(VI) to U(IV) by citric acid is negligible under the given experimental conditions. Figure 3 depicts the resulting luminescence spectra of the complex species calculated by SPECFIT™ in comparison to the spectrum of the free uranyl cation at pH 3.5. The corresponding data are summarized in Tab. 1.

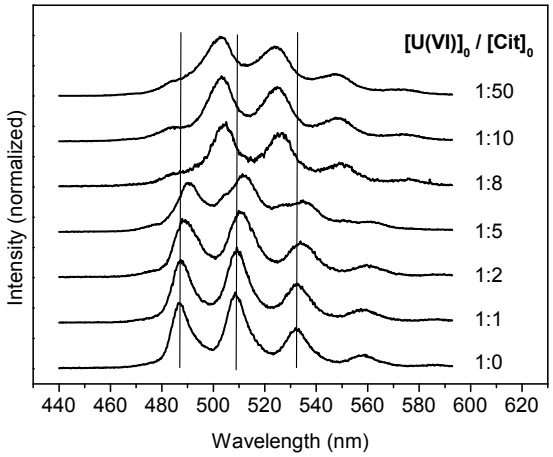

Fig. 1: Luminescence spectra of U(VI) as a function of the citric acid concentration at pH 3.5, I = 0.1 M, measured at 153 K.

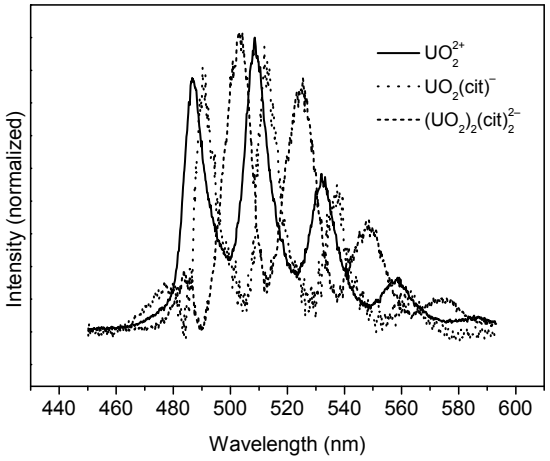

Fig. 2: Luminescence spectra of the uranyl species in the U(VI)/citric acid system at pH 3.5 and I = 0.1 M, T = 153 K.

Tab. 1: Luminescence emission bands of the different uranyl-citrate species and of the free uranyl cation at 153 K.

Species	Main emission bands (nm)				
UO_2^{2+}	473	488	509	532	558
UO_2cit^-	475	492	513	537	562
$(UO_2)_2(cit)_2^{2-}$	484	503	524	548	574

ACKNOWLEDGEMENTS. The authors thank Carlos Fajardo Uribe for the sample preparation.

REFERENCES

[1] Günther, A. et al. (2008) *Report FZD-489*, p. 17.
[2] SPECFIT 32, *Spectrum Software – Associates* (2003).
[3] Martell A. E. et al. (1998) *NIST critically selected stability constants of metal complexes database, Standard references database 46, Version 5.0,* Texas A & M University, U.S.A.

Reduction of uranium(VI) by citric acid

R. Steudtner, G. Geipel

The reduction properties of citric acid (Cit) on uranium(VI) were investigated by UV-vis spectroscopy. The influence of different pH values and of the atmosphere was studied. The formation of a U(IV)-Cit_3 complex is suggested.

Citric acid (Cit) is a naturally-occurring ubiquitous organic substance. It is an important intermediate product in the metabolism of hydrocarbons, proteins and fats in all animal and plant cells. The formation of molecule complexes with heavy metal ions an the reducing properties of Cit potentially influence the migration behavior of U(VI). The speciation of U(VI)-citrate complexes are widely available [1-3], but the reduction from U(VI) to U(IV) and the speciation of uranium(IV)-citrate species is only investigated in acid solution [4-6].

EXPERIMENTAL. The reduction experiments were conducted under aerobic and anaerobic conditions. The pH value of the solutions ranges from 1 to 10, and concentrations were set to $5 \cdot 10^{-4}$ M U(VI) and $1 \cdot 10^{-2}$ M Cit. with an ionic strength of 0.1 M $NaClO_4$. After shaking the samples for 7 days under neon lamp light the pH values were readjusted. The absorption spectroscopy measurements were performed using a CARY5G UV-vis-NIR spectrometer (Varian Co.) at room temperature. The spectra were recorded between 200 and 800 nm.

RESULTS. Figure 1 shows the relative amount of U(VI) which was reduced by citric acid at aerobic and anaerobic conditions at different pH values. At pH 1, no reduction of U(VI) was observed. Irrespective to the atmospheric conditions, the uranyl ion forms stable complexes with citric acid. The reduction of U(VI) to U(IV) was observed starting from pH 2 and pH 3 for the anaerobic and aerobic conditions, respectively. The highest reduction rates of ~ 52% for ambient and ~ 66% for inert atmosphere were determined at pH 4. Increasing the pH leads to a decreased relative amount of reduced uranium(VI). Under aerobic conditions, no reduction was observed above pH 6.5 because of the formation of stable U(VI) carbonato complexes. At nitrogen atmosphere, the reduction rate decreases to a ~ 22.3% at pH 9.
In all solutions, U(IV) was detected as dissolved species. With respect to the atmospheric conditions, the formation

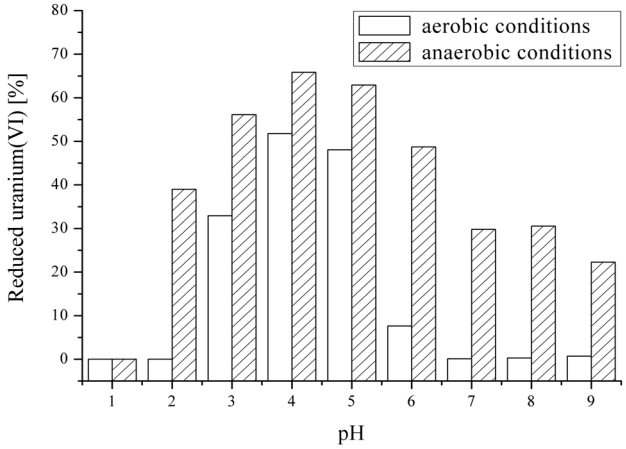

Fig. 1: Relative amount of reduced U(VI) in the pH range from 1 to 9.

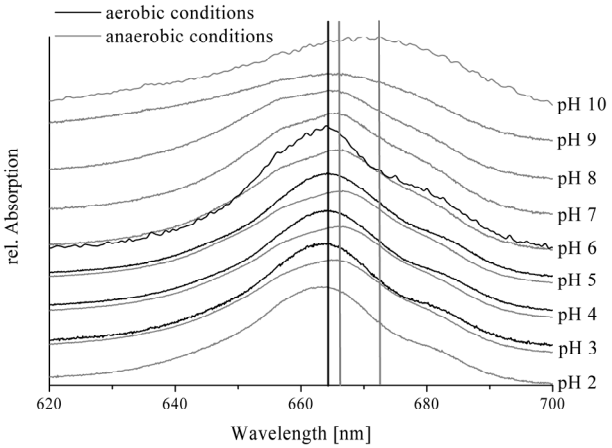

Fig. 2: Relative absorption spectra of the formed U(IV) complexes at aerobic and anaerobic conditions in the pH range from 2 to 10.

of different complexes can be derived from the absorption spectra (Fig. 2). In the aerobic system, one U(IV)-citrate species is observed showing a maximum at 664 nm in the pH range from 3 to 6. The same species is obviously present at pH 2 after the reduction in O_2-free atmosphere. At higher pH levels, further U(IV)-citrate species with absorption maxima at 666 nm (pH 3-8) and 672 nm (pH 10) are formed.
The species with the absorption at $\lambda_{max} = 664$ nm was probably observed in recent investigations and can be assigned to the 1 : 2 complex (Tab. 1). The shift of the band to 666 nm indicates the formation of a new species which presumably represents the 1 : 3 complex. However, no detailed description of this complex is available up to now. The absorption band at 672 nm was not yet observed and can not be assigned to a distinct species at this stage of knowledge.

Tab. 1: Comparison of the U^{4+} species.

U^{4+} species	C_U [mM]	U : Cit	λ_{max} [nm]	pH	Ref.
free	1	–	649	0	[4]
in citrate media	1	1 : 20	670	4; 5	
in citrate media	5	1 : 10	670	3.5	[5]
free	5	–	647	0.1	[6]
in citrate media	5	1 : 100	654 [U(IV)-Cit)] 662 [U(IV)-Cit_2]	0.1	
aerobic system	0.5	1 : 20	664	3-6	This work
anaerobic system	0.5	1 : 20	664 666 672	2 3-8 9; 10	

REFERENCES

[1] Feldman, I. et al. (1951) *J. Am. Chem. Soc.* **73**, 2312-2315.
[2] Pasilis, S. P. et al. (2003) *Inorg. Chem.* **42**, 6793-6800.
[3] Ohyoshi, E. et al. (1975) *Bull. Chem. Soc. Jpn.* **48**, 227-229.
[4] Suzuki, Y. et al. (2006) *Radiochim. Acta* **94**, 579-583.
[5] Ohyoshi, A. et al. (1974) *J. Inorg, Nucl. Chem.* **36**, 379-384.
[6] Bonin, L. et al. (2008) *Radiochim. Acta* **96**, 145-152.

Spectroscopic studies of the uranium(VI) interaction with nicotinic and anthranilic acid

B. Raditzky, K. Schmeide, S. Sachs, G. Geipel, G. Bernhard

The binding properties of uranium(VI) onto various nitrogen containing organic ligands, model substances for humic acids, were studied using time-resolved laser-induced fluorescence spectroscopy (TRLFS) at various pH values. The formation constants of the identified complexes were determined.

The aim of this work was to study the contribution of different nitrogen containing functionalities to the complexation of humic acid and uranium(VI). For that, anthranilic acid and nicotinic acid, molecules that can occur as building blocks of humic substances, were used as model ligands.

EXPERIMENTAL. Depending on the prevailing physical and chemical properties of the considered ligands two different TRLFS systems were used. To study the uranium(VI) (U(VI)) complexation by anthranilic acid (AA) which exhibits fluorescence properties, a femtosecond-laser-pulsed system (fs-TRLFS) was used. The fs-TRLFS experiments were performed at a fixed AA concentration of $1 \cdot 10^{-5}$ M by varying the U(VI) concentration from $1 \cdot 10^{-5}$ to $3 \cdot 10^{-4}$ M. For the study of the U(VI) complexation by nicotinic acid (NA), which shows no significant fluorescence emission under the studied conditions, U(VI) luminescence spectra were recorded using a pulsed Nd:YAG laser system at a total U(VI) concentration of $5 \cdot 10^{-5}$ M. The concentration of NA was varied from $5 \cdot 10^{-5}$ to $5 \cdot 10^{-4}$ M. The excitation wavelength for both TRLFS systems was 266 nm. All measurements were carried out at room temperature at pH values between pH 1.5 and 4.5. The ionic strength was adjusted to 0.1 M ($NaClO_4$). The stability constants were determined by slope analysis and using the factor analysis program SPECFIT™ [1].

RESULTS. The fluorescence emission spectrum of AA ranges from 360 to 520 nm showing a peak maximum at about 405 nm. The AA/U(VI) system is characterized by a decrease of the fluorescence intensity of AA with increasing U(VI) concentration without a shift of the main emission band. The formed complex does not show any fluorescence in the considered wavelength range. The observed decrease is a typical behavior for static fluorescence quenching processes due to the complex formation, thereby reducing the concentration of free AA. From the pKa values ($pKa_1 = 2.01$, $pKa_2 = 4.78$) reported in [2] follows that the prevailing AA species change with increasing pH value. From the experiments, three different lifetimes were obtained each relatable to the prevailing AA species. For the full protonated species at pH 1.5, a lifetime of about 1 ns was measured. Like other amino acids, AA is zwitterionic at pH values between 2 and 4 showing a lifetime of about 2.5 ns. At pH 4.5 two main species occur in solution and a biexponential fluorescence decay was observed. Two lifetimes were determined, 2.5 ns for the zwitterionic species and about 8.5 ns for the completely deprotonated AA species.

The TRLFS spectra obtained for the NA/U(VI) system show a strong decrease of the U(VI) luminescence intensity with increasing NA concentration. The luminescence decay was monoexponential in all samples. No shifts of the main emission bands were detected. The formed complex does not show any luminescence in the considered wavelength range.

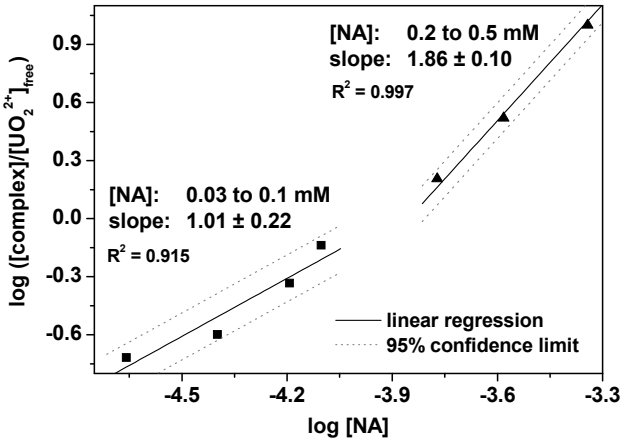

Fig. 1: Validation plot for the complexation of U(VI) with NA at pH 2.5: Separated slope analysis for different concentration areas of NA.

Using a modified logarithmic form of the mass action law the complex stoichiometries and the stability constants were determined graphically via slope analysis according to the following reactions:

$$\text{AA: } x\,UO_2^{2+} + y\,H_2NC_6H_4COO^- + z\,H^+ \rightleftarrows [(UO_2)_x(H_2NC_6H_4COO)_yH_z]^{(2x+z-y)} \quad (1)$$

$$\text{NA: } x\,UO_2^{2+} + y\,C_5H_4NCOO^- + z\,H^+ \rightleftarrows [(UO_2)_x(C_5H_4NCOO)_yH_z]^{(2x+z-y)} \quad (2)$$

For both ligands no complexation with U(VI) at pH < 2 could be determined. For AA a slope near 1 was calculated in the experiments at pH > 2, suggesting a predominant 1:1 complex. The averaged stability constant ($\log \beta_{xyz}$ for the complex species $M_xL_yH_z$, cf. Eq. 1) was determined to be $\log \beta_{111} = 7.83 \pm 0.03$. Unlike AA, the calculated slope for the experiments with NA was higher than 1, suggesting the formation of 1:2 complexes at higher ligand concentrations. Figure 1 shows the validation plot for the complexation of U(VI) with NA at pH 2.5. The stability constants for the complexes calculated via SPECFIT™ are $\log \beta_{111} = 8.57 \pm 0.04$ and $\log \beta_{122} = 17.20 \pm 0.04$.

From the pKa values of AA [2] and NA [3] follows that the nitrogen containing group is not deprotonated in the considered pH range, whereas the carboxylic group is already deprotonated. From that, it is concluded that the complexation takes place via the carboxylic group.

ACKNOWLEDGEMENTS. This study was funded by the Federal Ministry of Economics and Technology (02 E 10156).

REFERENCES

[1] Binstead, R. A. et al. (2007) SPECFIT Global Analysis System, Version 3.0.39.

[2] Martell A. E. et al. (1998) *NIST critically selected stability constants of metal complexes database, standard reference database 46, version 5.0*, Texas A & M University, U.S.A.

[3] Hallé, J. C. et al. (1996) *Can. J. Chem.* **74**, 613-620.

Fluorescence properties of Na-L-lactate studied at room temperature and low temperatures

T. Arnold, C. Wimmer, K. Großmann

Time resolved laser-induced fluorescence spectroscopy (TRLFS) measurements of a 0.1 M lactate solution were carried out at room temperature (RT) and under cryogenic conditions of 200, 100, and 10 K using an excitation wavelength of 266 nm. It was found that Na-L-lactate showed no fluorescence properties at room temperature, whereas with decreasing temperatures, increasing fluorescence intensities were recorded. The fluorescence emission maximum was found at 472 ± 2 nm. The fluorescence lifetime of lactate is also temperature dependent and follows an Arrhenius like behavior, i.e. it becomes longer with decreasing temperature. For the TRLFS measurement at 10 K, a fluorescence lifetime of 6740 ± 1.6 ns was calculated.

Natrium-L-lactat is a biochemically relevant substance and is constantly produced from pyruvate during anaerobic glycolysis in bacterial and mammalian cells [1]. The identification of such organics in biological samples may contribute to a better understanding concerning metaboling processes in cells.

EXPERIMENTAL. Sodium-L-lactate (Fluka puriss., product number 71718, ≥ 99%, total impurity ≤ 1% water) was prepared as 0.1 M standard solution. This solution was subsequently transferred in a cuvette and sealed. Then the samples were put in a freezer at −20 °C for approximately 15 hours. After that the frozen samples were measured in a refrigerator cryostat (closed cycle cryorefrigerator RDK 10-320; compressor PT50 KIT/DN 40KF and Kompressionseinheit RW2, Oerlicon Leybold, Dresden, Germany) at the desired temperature. To study the fluorescence properties of Na-L-lactate an excitation wavelength of 266 nm was used (Inlite II Laser, Continuum, Santa Clara, U.S.A.). The laser energy was 1.35 ± 0.1 mJ. It was checked with a power meter (Labmaster Ultima, Coherent, Inc., Santa Clara, U.S.A.) just before it entered the cryostat, and if necessary readjusted. The fluorescence emission was coupled into a fiber optic mounted perpendicular to the excitation beam. The fibre optic was connected to a 500 nm spectrograph (model: 1236, Acton Research, Acton, U.S.A.) and an adjacent ICCD-camera (Roper Scientific, Princeton Instruments, Stuttgart, Germany) where the fluorescence light was detected. The frozen Na-L-lactate sample was measured at temperatures of −73 °C, −173 °C, and −263 °C. Each temperature was represented by one individual sample. In addition, a 0.1 M sodium-L-lactate solution was measured at RT.

RESULTS. Na-L-lactate shows no fluorescence properties at room temperature, whereas with decreasing temperatures increasing fluorescence intensities were recorded. Figure 1 shows that the fluorescence intensity of sodium-L-lactate is strongly dependent on temperature. The fluorescence emission of sodium-L-lactate shows a broad peak with an emission maximum at 472 ± 2 nm. The fluorescence lifetime of sodium-L-lactate can be described by an Arrhenius like behavior and increases with decreasing temperature. The fluorescence lifetimes of sodium-L-lactate was calculated for the spectra with the highest fluorescence intensities at 200, 100, and 10 K. Fluorescence lifetime of 622.7, 651.0, and 6737.5 ns, respectively as shown in Tab. 1 were determined. The fluorescence decay curve of Na-L-lactate is shown in Fig. 2. The results show that Na-L-lactate in biological samples can be directly studied by laser fluorescence microscopy and laser fluorescence spectroscopy.

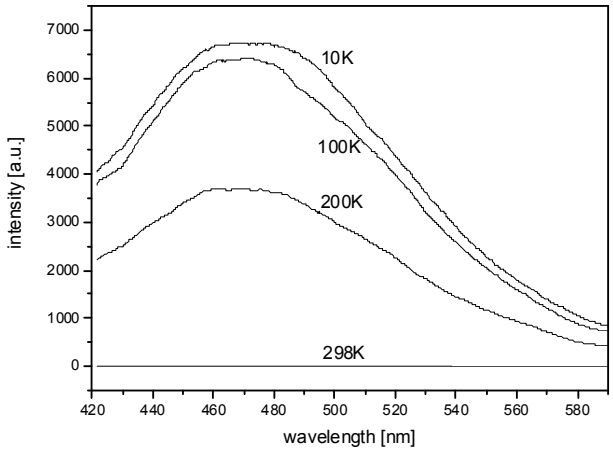

Fig. 1: Fluorescence emission spectra of sodium-L-lactate measured at 298 K, 200 K, 100 K and 10 K. The figure shows that the fluorescence intensity increases with decreasing temperature.

Tab. 1: Calculated fluorescence lifetimes of Na-L-lactate at temperatures of 200, 100, and 10 K using an excitation wavelength of 266 nm.

Temp. [K]	200	100	10
Lifetime [ns]	623 ± 0.3	651 ± 0.2	6740 ± 1.6

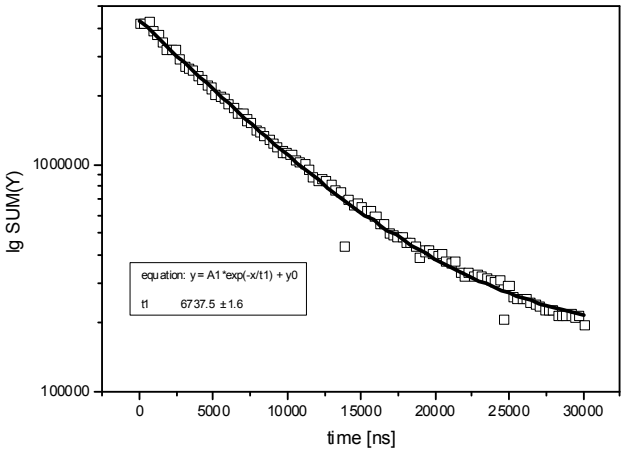

Fig. 2: Fluorescence decay curve of Na-L-lactate at 10 K.

ACKNOWLEDGMENTS. We thank the German Research Council (DFG) for financial support (project no. AR 584/1-1).

REFERENCES

[1] Berg, J. M. et al. (2003) *Biochemie,* Spektrum Akademischer Verlag, Heidelberg, Berlin.

Novel U(VI) complexes of bis(*o*-hydroxyaryl)imine ligands: Synthesis, X-ray structures and DFT calculations

H. B. Tanh Jeazet, T. Doert,[1] O. Kataeva,[2] S. Tsushima, Ke. Gloe,[1] G. Geipel, G. Bernhard, K. Gloe[1]

[1]Department of Chemistry and Food Chemistry, Dresden University of Technology, Dresden, Germany; [2]A.E. Arbuzov Institute of Organic and Physical Chemistry, Kazan, Russia

The reaction of $UO_2(NO_3)_2$ with the bis(*o*-hydroxyaryl)imine ligands L^1, L^2 and L^3 yields the mononuclear uranyl complexes $[UO_2(L^1)(NO_3)_2]$ (1) and $[UO_2(L^2)(NO_3)_2]$ (2) and the 1D coordination polymer $[UO_2(L^3)(NO_3)_2]_n$ (3).

The coordination chemistry of uranium (VI) has attracted attention due to the development of nuclear technology. The remediation of the resulting nuclear waste generated, in which uranium is a major contributor to the longterm radioactivity, is a primary concern [1]. However, the separation of actinides from lanthanides is difficult due to their similar oxidation states and ionic radii [2]. Schiff base ligands are potential candidates for selective separation as they contain multidentate mixed aza-oxo-cores and possess sufficient steric freedom, while lacking the problems associated with macrocyclic cavity size [3]. In an effort to synthesize stable uranyl–Schiff base complexes which could be used in the investigation of new means of remediation of uranium from aqueous sources or nuclear wastes, we here report the synthesis and structures of $[UO_2(L^1)(NO_3)_2]$ (**1**), $[UO_2(L^2)(NO_3)_2]$ (**2**) and $[UO_2(L^3)(NO_3)_2]_n$ (**3**) using the Schiff base ligands $\mathbf{L^1}$-$\mathbf{L^3}$ (Fig. 1).

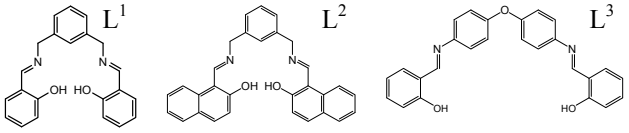

Fig. 1: Structures of Bis(*o*-hydroxyaryl)imine ligands.

EXPERIMENTAL

Ligand synthesis. The ligands $\mathbf{L^1}$, $\mathbf{L^2}$ and $\mathbf{L^3}$ were prepared *via* the previously reported methods [4,5].

Complex synthesis. Uranyl nitrate pentahydrate (23.0 mg, 0.05 mmol) in methanol (1 mL) was added to the ligand (0.05 mmol) in the mixture methanol/acetonitrile (1 :1) (1 mL). Red crystals of **1**, **2** and **3** were obtained by slow diffusion of diethylether into the resulting solution after one week. The crystals were collected, washed with ether, and dried under vacuum. Found for **1**: C, 37.38%, H, 3.00%, N, 7.50%. Cal. for $[UO_2(L^1)(NO_3)_2]$; C, 35.78%, H, 2.73%, N, 7.59%. *m/z* (ESI): 613, $[UO_2(L^1)]^+$; 676, $[UO_2(L^1)(NO_3)]^+$; 771, $[UO_2(L^1)(NO_3)_2 + MeOH]^+$. Found for **2**: C, 41.52%, H, 2.98%, N, 6.97%. Cal. for $[UO_2(L^2)(NO_3)_2]$; 42.97%, H, 2.88%, N, 6.68%. *m/z* (ESI): 713, $[UO_2(L^2)]^+$; 838, $[UO_2(L^2)(NO_3)_2]^-$.

RESULTS AND DISCUSSION. The solid-state structures of compounds **1-3** were solved from single crystal X-ray diffraction data and confirmed by DFT calculation. The asymmetric unit of the compounds contains one U(VI) ion, one ligand molecule and two NO_3^- anions. The structures of these complexes are shown in Fig. 2. The geometry around the uranyl atoms is closest to hexagonal-bipyrimidal with axial O=U=O moiety and six oxygen atoms in equatorial position.

In **1** and **2**, the U(VI) ion is coordinated by the OH functions of the ligands and two nitrate ions while in **3**, each U(VI) is coordinated by two OH functions of two ligands

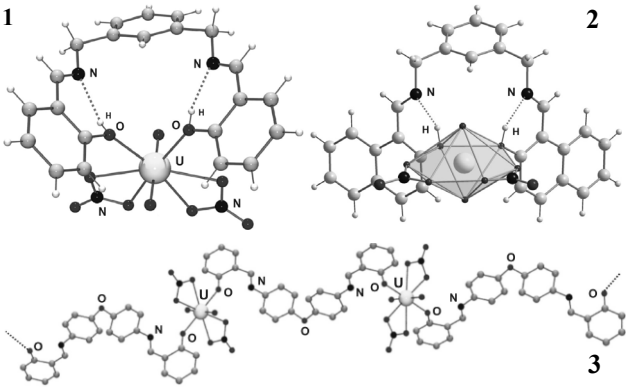

Fig. 2: Molecular structure of uranyl complexes.

molecules and further two nitrate ions leading to a 1D coordination polymer. To our knowledge, these are the first examples of U(VI) complexes formed with neutral phenolic Schiff base ligands. The U–O distances for the UO_2^{2+} entities in **1, 2** and **3** are almost identical (1.78(2) Å). The U–OH distances in **1** (2.311 and 2.324 Å), **2** (2.345 and 2.358 Å), and **3** (2.333 and 2.341 Å) are comparable to distances observed in $[(UO_2)(Salophen)]_2$ (2.387-2.463 Å) [6] and bridged dinuclear uranyl compounds involving alkoxide (2.340-2.390 and 2.360-2.389 Å) [7]. The U-$O_{nitrate}$ bond lengths are in the range 2.519-2.596 Å, 2.504-2.547 Å, 2.537-2.582 Å, in **1**, **2** and **3** respectively. The hydrogen atoms of the hydroxyl groups interact strongly with the imine nitrogen atoms. The distances are 1.98-1.94 Å, 1.81-1.85 Å, 1.82-1.88 Å in **1**, **2** and **3** respectively. DFT calculations with the neutral ligands in MeOH show that the complexes with U(VI) in the ligand periphery (Fig. 3a) are more stable as in the case of an arrangement in the pseudo-ring formed (Fig. 3b) confirming our experimental results.

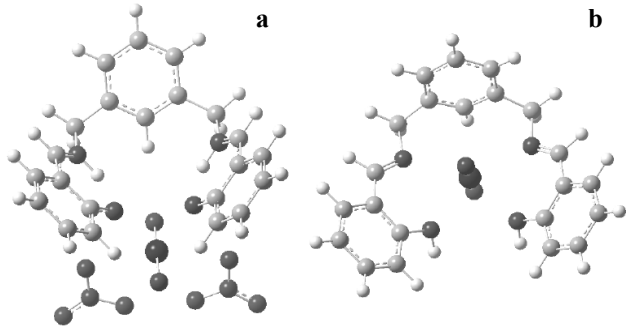

Fig. 3: The structures of the uranyl complexes optimized in CH_3OH at the B3LYP level.

REFERENCES

[1] Bruno, J. et al. (2007) *Elements* **2**, 343-349.
[2] Nash, K. L. (1993) *Solvent. Extr. Ion Exch.* **11**, 729-768.
[3] Bharara, M. S. et al. (2007) *Inorg. Chem*. **46**, 8309-8315.
[4] Maverick, A. W. et al. (2005) *Dalton Trans.* 200-206.
[5] Yoshida, N. et al. (1999) *J. Chem. Soc. Perkin Trans.* 975-983.
[6] Takao, K. et al. (2007) *Inorg. Chem*. **46**, 1550-1562.
[7] Sopo, H. et al. (2006) *Polyhedron*. **25**, 1223-1232.

Solvent extraction of U(VI) by bis(*o*-hydroxyaryl)imine and amine ligands

H. B. Tanh Jeazet, Ke. Gloe,[1] G. Geipel, G. Bernhard, K. Gloe[1]
[1]Department of Chemistry and Food Chemistry, Dresden University of Technology, Dresden, Germany

Liquid-liquid extraction studies of Eu(III) and U(VI) have been carried out using bis(*o*-hydroxyaryl)imine ligands and their new amine derivatives.

Interest in the coordination chemistry of uranium has recently increased for several reasons. That are the reduction of nuclear waste along with the extraction of uranium from seawater, groundwater, soil, human tissues and waste remediation from actinide decorporation [1]. Uranium and other actinides are major contributors to the long-term radioactivity of nuclear wastes. The separation of actinides from the lanthanides is most difficult due to their similar oxidation state and ionic radii [2]. Various ligand systems have been used for the selective extraction of uranium(VI) including organic phosphorus oxides [3], crown ethers, azacrowns, calixarenes [4,5], and Schiff base ligands [6]. The potential use of Schiff base ligands for the selective coordination of uranyl ions may be due to the multidentate mixed aza- and oxo-core and the backbone flexibility that they possess [1,6]. It is the aim of this studies to prove the extraction ability of the ligands **L**[1]-**L**[4] (Fig. 1) towards Eu(III) and U(VI).

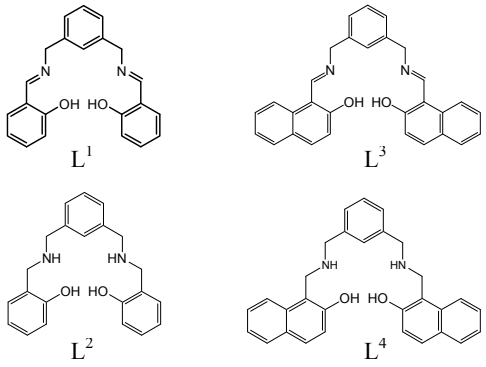

Fig. 1: Structures of bis(*o*-hydroxyaryl)imine and amine ligands.

EXPERIMENTAL

Ligand synthesis. **L**[1] and **L**[3] were prepared *via* the previously reported method [7]. The reduction of these ligands by KBH_4 gave **L**[2] and **L**[4] respectively.

Liquid–liquid extraction. The liquid–liquid extraction experiments were performed at 23 ± 1 °C in microcentrifuge tubes (2 mL) by means of mechanical shaking. The phase ratio $V_w : V_{org}$ was 1 : 1 (0.5 mL each). The shaking time was chosen as 60 min. because the extraction equilibrium was reached in all cases during this period (Fig. 3). After extraction, all samples were centrifuged and the phases separated. The determination of the Eu(III) ions concentration in both phases was carried out radiometrically by γ-radiation of ^{152}Eu with NaI(Tl)-scintillation counter (Cobra II/Canberra-Packard) while that of U(VI) ions in aqueous phase was made by the mean of ICP-MS method.

RESULTS AND DISCUSSION. The extraction behaviour of the different ligands towards Eu(III) and U(VI) was studied using the extraction system $Eu(NO_3)_3$ or $UO_2(NO_3)_2$–buffer–H_2O/ligand–$CHCl_3$. This separation system remarkably exhibited high selectivity for U(VI) over Eu(III) driven by amine ligands. Figure 2 shows an overview of the extraction strength for all the ligands

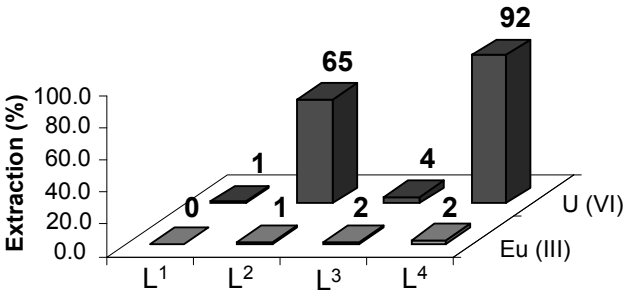

Fig. 2: Extraction of Eu(III) and U(VI). [L] = 0.01 M in $CHCl_3$; [U(VI)] = [Eu(III)] = 10^{-4} M, [$NaNO_3$] = $5 \cdot 10^{-3}$ M, pH = 5,2 (HEPES/HNO_3 buffer), T = 23 ± 1°C.

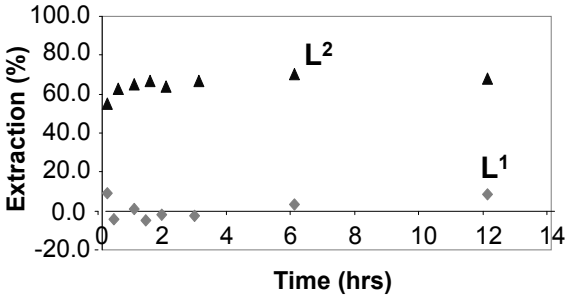

Fig. 3: Time dependence of U(VI) extraction with L^1 and L^2. [L] = 0.01 M in $CHCl_3$; [U(VI)] = 10^{-4} M, [$NaNO_3$] = $5 \cdot 10^{-3}$ M, pH = 5,2 (HEPES/HNO_3 buffer), T = 23 ± 1 °C, t = 10 min.-12 h.

studied. In each case, the distribution ratio of U(VI) was higher than that of Eu(III). This tendency reflects the fact that these ligands favour U(VI) over Eu(III). The extraction results show that the amine ligands extract U(VI) better than the Schiff base ligands (Figs. 2,3). The lower extractability by the Schiff bases is caused obviously by structural differences of the complexes.

For more information about the extraction equilibrium, the influence of pH on the extraction of U(VI) by L^2 was investigated (Fig. 4). With increasing pH, the extractabilities of this ligand increase. This trend is in agreement hwith the changing protonation state of the ligands.

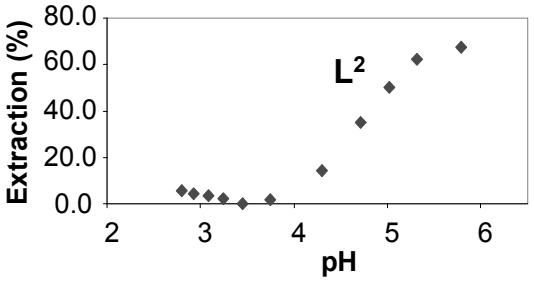

Fig. 4: Extraction of U(VI) with L^2 as a function of pH. [L^2] = 0.01 M in $CHCl_3$; [U(VI)] = 10^{-4} M, [$NaNO_3$] = $5 \cdot 10^{-3}$ M, pH = 2-6 (HEPES/HNO_3 buffer), T = 23 ± 1 °C.

REFERENCES

[1] Bharara, M. S. et al. (2007) *Inorg. Chem*. **46**, 8309-8315.
[2] Nash, K. L. (1993) *Solvent. Extr. Ion Exch.* **11**, 729-768.
[3] Wilson, P. D. E. (1996) *Nuclear Fuel Cycle: From Ore to Waste*; Oxford Science Publications, Oxford.
[4] Eller, P. G. et al. (1976) *Inorg. Chem*. **15**, 2439-2442.
[5] Thuery, P. et al. (1995) *New J. Chem.* **19**, 619-625.
[6] Sessler, J. L. et al. (2006) *Coord. Chem. Rev*. **250**, 816-843.
[7] Maverick, A. W. et al. (2005) *Dalton Trans.* 200-206.

Synthesis and characterization of sulfur-containing humic acid model substances

S. Sachs, S. Heller, T. Reich,[1] J. Drebert[1]

[1]Institute of Nuclear Chemistry, Johannes Gutenberg-Universität Mainz, Mainz, Germany

Sulfur-containing humic acid model substances were synthesized and characterized with regard to their elemental composition, structure and functionality. Using X-ray photoelectron spectroscopy (XPS) reduced sulfur functionalities (thiols, dialkylsulfides and/or disulfides) were identified as the main sulfur species in humic acid M1-S-1.

Depending on their origin, humic substances contain different amounts of sulfur ranging from 0.1 to 3.6% and 0.5 to 1.43% in soil and aquatic humic substances, respectively [1]. Reduced (e.g., sulfides, disulfides, thiols, thiophenes), intermediately oxidized (e.g, sulfoxides, sulfonates) and highly oxidized (e.g., sulfates) sulfur functionalities occur in humic substances [2]. However, their importance for the metal ion complexation by humic substances is still unclear.
Sulfur-containing humic acid model substances have been synthesized and characterized for the study of the influence of sulfur functionalities on the metal ion complexation by humic substances.

EXPERIMENTAL. The synthesis of sulfur-containing humic acids type M1-S was performed in aqueous solution based on the synthesis of humic acid type M1 [3]. Syntheses starting from xylose (2.83 M), phenylalanine (0.76 M) and varying amounts of glycine and cysteine were performed. The initial concentration of cysteine was increased from 0 to 0.83 M to obtain humic acids with different sulfur contents. In parallel, the glycine concentration was reduced for the same amount from 0.83 to 0 M, ensuring constant amino acid concentrations in the synthesis mixtures. The resulting synthetic products were characterized for their elemental composition, structure and functionality by elemental analysis, FT-IR spectroscopy and potentiometric titration, respectively. First XPS measurements of humic acid M1-S-1 were performed in comparison to L-cysteine to identify sulfur species in the synthetic product.

RESULTS. Table 1 shows sulfur content and proton exchange capacity (PEC) of the synthesized humic acids. Both, sulfur content and PEC increase with increasing initial cysteine concentration in the reaction mixtures. However, independent of the sulfur content, all synthetic products show comparable FT-IR spectra (not shown) indicating similar overall structures. No FT-IR absorption bands pointing to sulfur-containing functional groups were observed in the FT-IR spectra. This is attributed to the low sulfur content of the humic acids and the overlapping of IR absorption bands of sulfur functionalities with those of other structural elements of the humic acids.

Tab. 1: Sulfur content and proton exchange capacity (PEC) of humic acid model substances synthesized with varying cysteine concentrations.

HA	$[Cysteine]_0$ (M)	S (%)	PEC (meq/g)
M1	0	0	1.56 ± 0.13
M1-S-1	0.26	1.94 ± 0.01	1.63 ± 0.16
M1-S-2	0.57	3.94 ± 0.04	1.90 ± 0.17
M1-S-3	0.83	7.72 ± 0.05	2.71 ± 0.13

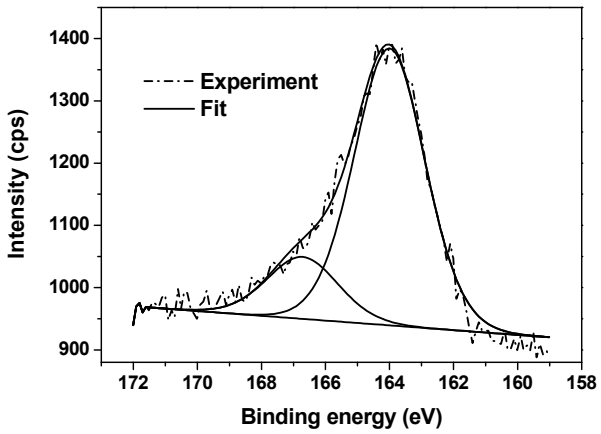

Fig. 1: S 2p XPS spectrum of humic acid M1-S-1.

Figure 1 shows the S 2p XPS spectrum of humic acid M1-S-1. In this spectrum two components were detected indicating the occurrence of at least two different sulfur species in humic acid M1-S-1. Table 2 summarizes the S 2p binding energies of L-cysteine and humic acid M1-S-1.

Tab. 2: S 2p binding energies of cysteine and humic acid M1-S-1 in eV.

	S 2p binding energy (eV)	
L-cysteine	163.8	–
M1-S-1	164.0	166.7

Electrostatic charging of the sample surface was corrected by setting the C1s binding energy of M1-S-1 to 285.0 eV.

Based on literature data [4] and on the binding energy of cysteine, an assignment of the binding energies of humic acid M1-S-1 to different sulfur species was performed.
The XPS signal at 164.0 eV can be retained to reduced sulfur species such as thiols, dialkylsulfides and/or disulfides. About 82% of sulfur in humic acid M1-S-1 occurs in this reduced form. The binding energy at 166.7 eV is attributed to sulfoxides, representing about 18% of the sulfur species. From that it is concluded that the main part of sulfur groups in humic acid M1-S-1 occurs in reduced form which is due to the use of L-cysteine as precursor.
Further XPS measurements are performed to characterize the sulfur species in the humic acid model substances with higher sulfur content. The results will be compared to those of natural humic acids. Furthermore, the newly developed sulfur-containing humic acid model substances are used in complexation studies with uranium(VI) to determine the influence of the identified sulfur species on the uranium(VI) complexation by humic acids. The results will be used to assess the impact of sulfur-containing humic acid functionalities on the uranium(VI) complexation by humic acids in comparison to oxygen and nitrogen functionalities.

ACKNOWLEDGEMENTS. The Federal Ministry of Economics and Technology funded this work (02 E 10156).

REFERENCES

[1] Xia, K. et al. (1998) *Soil Sci Soc. Am. J.* **62**, 1240-1246.
[2] Solomon, D. et al. (2003) *Soil Sci Soc. Am. J.* **67**, 1721-1731.
[3] Pompe, S. et al. (1996) *Radiochim. Acta* **74**, 135-140.
[4] Lindberg, B. J. et al. (1970) *Phys. Scripta* **1**, 286-298.

ATR FT-IR investigation of U(VI) complexation with EDC modified phosvitin

B. Li, J. Raff, H. Foerstendorf

In order to reduce the impact of the carboxylic groups of the phosvitin on the U(VI) binding, 1-ethyl-3-(3-dimethylaminopropyl) carbodiimide hydrochloride (EDC) was used to block the carboxylic groups on phosvitin. From the ATR FT-IR spectra of the EDC modified phosvitin solution, it has to be assumed that the modification occurs on both carboxylic groups and phosphate groups. After its complexation with 10^{-3} M U(VI) in solution at pH 4, the spectra suggests a preferential binding to the phosphate groups than to carboxylic groups.

In our previous work, the affinity of U(VI) to phosphorylated amino acid side chains was shown by infrared spectra of U(VI)-phosvitin complexes with a initial U(VI) concentration of 10^{-4} M [1]. These results are expected to be confirmed by blocking the carboxylic groups and subsequent complexation with U(VI) at millimolar concentration. Thus, 1-ethyl-3-(3-dimethylaminopropyl) carbodiimide hydrochloride (EDC) was recruited in the study. The nucleophilic properties of EDC can be used for the selective activation of carboxylic groups of proteins [2], as crosslinker between DNA and protein or between protein and protein [3].

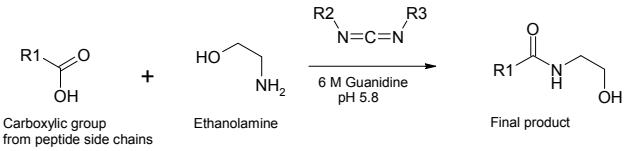

Fig. 1: Scheme of the chemical reaction for the activation of carboxylic groups using EDC as a nucleophile agent.

EXPERIMENTAL.

EDC modification. 50 mg phosvitin (Sigma-Aldrich) was dissolved in 5 mL 50 mM propionic acid buffer pH 5.8 containing 6 M guanidine. Carboxylic groups on the protein were activated for 30 min by incubating with 1200 fold molar excess of EDC to phosvitin, are then blocked with 200 fold molar excess of ethanolamine for 24 hours at room temperature. The reaction was stopped by dialyzing the solution against water for 2 hours in a dialysis tube with a molecular cut-off of 14 kDa. The protein concentration of the end product was determined with Lowry method. In order to quantify the ethanolamine binding to the protein, tryptophan was added to the solution instead of ethanolamine. Its concentration remained in the solution is determined spectrophotometrically at 278 nm.

U(VI) incubation of phosvitin. 2.5 mg of modified phosvitin was shaken in 25 mL 0.1 M NaCl and 1 mM UO_2Cl_2 at pH 4, for two days at room temperature. The binding complex was harvested by centrifugation. The U(VI) concentration in the supernatant was measured with ICP-MS. Washing steps with 1 mL 0.1 M NaCl pH 4 were carried out to remove unbound U(VI) on the pellet.

ATR FT-IR measurements. The infrared spectra have been measured on a Bruker Vertex 80/v FTIR instrument equipped with a flow cell ATR accessory.

RESULTS. The spectrophotometric determination of the tryptophan implies that the amount of the ethanolamine binding to the protein is equal to blocking ~19% of the total carboxylic groups on the protein (data not shown). In correlation, the uranyl binding capacity decreases of ca. 20% from 510 µg to 410 µg per mg protein.

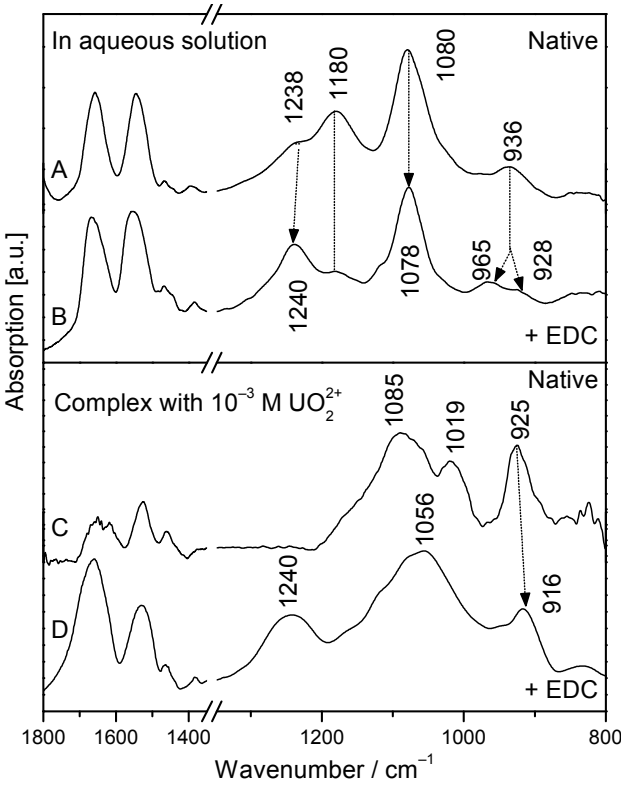

Fig. 2: FT-IR spectra of phosvitin. IR spectra of aqueous solutions of native phosvitin (A) and after EDC modification (B). IR spectra of resuspensions of the U(VI) complexes. Native phosvitin (C), EDC-modified phosvitin (D).

The EDC-modification is mainly reflected in the frequency range below 1300 cm^{-1} (Fig. 2, top). The increased intensity of the band at 1240 cm^{-1} is assigned to formation of secondary amines upon EDC-modification (Fig. 1). The slight changes in the spectral range where generally phosphate groups absorb (1200-900 cm^{-1}) suggest also the formation of amino phosphate groups.

The spectral differences of the U(VI) complexes are mainly observed in the same spectral regions. However, the band of the antisymmetric stretching vibration mode of UO_2^{2+} is shifted from 925 to 916 cm^{-1} upon EDC-modification. The lower frequency suggest a preferred coordination of the UO_2^{2+} ion to phosphate groups in the modified system, as it was observed for the U(VI)-phosvitin complex at lower U(VI) concentrations [1].

In conclusion, the complexation of 1 mM U(VI) with modified phosvitin is obviously dominated by U-phosphate interactions confirming the high affinity of UO_2^{2+} ions to phosphorylated amino acid side chains.

REFERENCES

[1] Li, B. et al. (2007) *Report FZD -489*, p. 36.
[2] Hoare, D. G. et al. (1967) *J. Biol. Chem.* **242**, 2447.
[3] Hermanson, G. T. (1996) *Bioconjugate Techniques*, Academic Press, San Diego.

Neptunium(V) complexation with pyoverdins secreted by a groundwater strain of *Pseudomonas fluorescens*

H. Moll, A. Johnsson,[1] K. Pedersen,[1] G. Bernhard
[1]Department of Cell and Molecular Biology, University of Gothenburg, Gothenburg, Sweden.

The interaction between Np(V) and pyoverdins was studied using NIR spectroscopy. Two NpO_2^+–*P. fluorescens* (CCUG 32456) pyoverdin species, NpO_2HL^{2-}, and NpO_2L^{3-}, with large formation constants of $\log \beta_{111} = 20.14 \pm 0.56$ and $\log \beta_{101} = 12.84 \pm 0.55$ could be identified.

Pyoverdins (LH_4) secreted by ubiquitous fluorescent *Pseudomonas* species, have a great potential to complex and thus to mobilize actinides in the environment [1,2]. The unknown interaction between Np(V) and the pyoverdins released by *P. fluorescens* (CCUG 32456) isolated from the granitic rock aquifers at the Äspö Hard Rock Laboratory (Äspö HRL), Sweden, is the subject of this study.

EXPERIMENTAL. The test solutions were prepared in a glove-box (N_2 atmosphere) using CO_2-free solutions. The NpO_2^+ concentration was fixed to $1.8 \cdot 10^{-4}$ M. The Np(V)-to-ligand ratio was varied between 1 :0.09 and 1 :1 while the pH was changed between 3 and 9. A Cary-5G UV/Visible/Near IR spectrophotometer (Varian, Inc.) was used. The spectra were obtained between 920 and 1070 nm with a resolution of 0.1 nm. The neptunium concentration in all acidic test solutions without adding a ligand was determined by spectrophotometric analysis at 980 nm using a molar extinction coefficient of 395 L mol^{-1} cm^{-1} [3].

RESULTS. An overview of the absorption spectra of $1.8 \cdot 10^{-4}$ M Np(V) in 0.1 M $NaClO_4$ measured in the *P. fluorescens* (CCUG 32456) pyoverdin system is presented in Fig. 1.
As previously observed [4], indications for two isosbestic points approximately at 985 and 996 nm can be found in Fig. 1. This suggests the occurrence of at least two neptunyl pyoverdin species. It is interesting to note that in the Np(V)–pyoverdin system, the neptunyl complexation started even at metal-to-ligand ratios below 1 :1 (data not shown). The program SPECFIT™ was used to extract the metal-ligand stability constants, single component spectra (see Fig. 2) and the molar absorptivities of the metal-ligand species. As a result, the variations observed in the absorption data (see Fig. 1) could be described by the following equilibria:

$$NpO_2^+ + H^+ + L^{4-} \rightleftharpoons NpO_2HL^{2-} \quad (1)$$

$$NpO_2^+ + L^{4-} \rightleftharpoons NpO_2L^{3-} \quad (2)$$

Formation constants for reactions (1) and (2) were calculated to be $\log \beta_{111} = 20.14 \pm 0.56$, and $\log \beta_{101} = 12.84 \pm 0.55$, respectively.

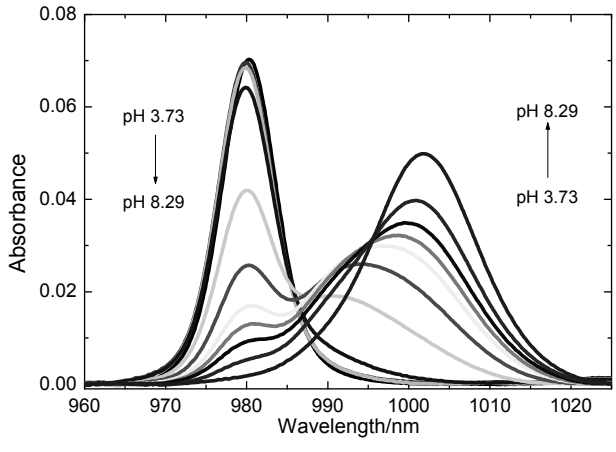

Fig. 1: Spectrophotometric titration of $1.8 \cdot 10^{-4}$ M Np(V) in 0.1 M $NaClO_4$ measured at a fixed pyoverdin concentration of [LH_4] $2.0 \cdot 10^{-4}$ M as a function of pH.

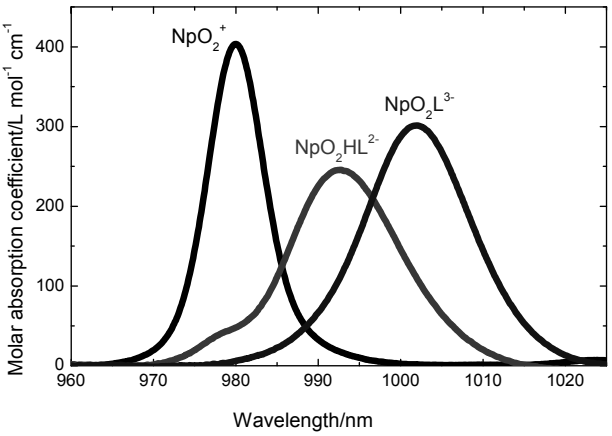

Fig. 2: NIR absorption spectra of the single components in the NpO_2^+–*P. fluorescens* (CCUG 32456) pyoverdin system, as derived by peak deconvolution using SPECFIT™.

By comparing these results with those obtained with the pyoverdin model ligands [4] it follows that Np(V) forms the strongest complexes with the natural pyoverdins. Both (a) the absorption maxima and (b) the stability constants showed increased values in the order BHA, SHA, NAP to LH_4. This suggests a stronger affinity of NpO_2^+ to the catechol functionality of the pyoverdin molecule. By comparing our Np(V) complexation studies with pyoverdins and related model compounds with results in the literature one can conclude a strong affinity of NpO_2^+ to complexing agents containing hydroxamate and catechol functionalities.

ACKNOWLEDGEMENTS. This work was funded by BMWi under contract number 02E9985.

REFERENCES

[1] Moll, H. et al. (2008) *Geomicrobiol. J.* **25**, 157-166.
[2] Moll, H. et al. (2008) *BioMetals* **21**, 219-228.
[3] Keller, C. (1971) *The Chemistry of the Transuranium Elements.* Verlag Chemie, Weinheim, p. 294.
[4] Moll, H. et al. (2009) this report, p. 22.

Complex formation of neptunium(V) with pyoverdin model compounds studied by NIR spectroscopy

H. Moll, G. Bernhard

We investigated the unknown interaction of NpO_2^+ with simple hydroxamate (SHA, BHA) and catechol (NAP) ligands by NIR spectroscopy over a wide pH range. Strong 1 : 1 and 1 : 2 NpO_2^+ bioligand species of the type $M_xL_yH_z$ could be identified from the spectrophotometric titrations.

Fluorescent *Pseudomonas* species are ubiquitous soil and groundwater bacteria that synthesize bacterial pyoverdin-type siderophores. The pyoverdin molecule provides different functional groups for metal ion coordination (e.g., catechol groups of the chromophore and hydroxamate groups). For an estimate which functional group contributes more in NpO_2^+ binding simple hydroxamate (salicylhydroxamic acid: SHA and benzohydroxamic acid: BHA) and a catecholate (2,3-dihydroxynaphthalene: NAP) ligand were investigated. To the best of our knowledge, the characteristics of the complexation of these ligands with pentavalent actinides (e.g., neptunium) are unknown.

EXPERIMENTAL. The test solutions were prepared in a glove-box (N_2 atmosphere) using CO_2-free solutions. The NpO_2^+ concentration was fixed to $1.8 \cdot 10^{-4}$ M. The Np(V)-to-ligand ratios were varied between 1 : 2 and 1 : 30 while the pH was changed between 3 and 10.
A Cary-5G UV/Visible/Near IR spectrophotometer (Varian, Inc.) was used. The spectra were obtained between 920 and 1070 nm with a resolution of 0.1 nm. The neptunium concentration in all acidic test solutions without adding a ligand was determined by spectrophotometric analysis at 980 nm using a molar extinction coefficient of 395 L mol^{-1} cm^{-1} [1].

RESULTS. The results of the spectrophotometric titrations of the NpO_2^+ test solutions are shown in Fig. 1. In all experiments indications for two isosbestic points approximately at 985 and 996 nm can be found in Fig. 1 suggesting the occurrence of at least two neptunyl bioligand species in each system.

Tab. 1: Stability constants of Np(V) bioligand complexes in 0.1 M $NaClO_4$.

	BHA	SHA	NAP
$\log \beta_{111}$		13.68 ± 0.05	
$\log \beta_{110}$	4.57 ± 0.01	6.09 ± 0.10	8.23 ± 0.17
$\log \beta_{120}$	7.59 ± 0.05	9.32 ± 0.20	13.60 ± 0.05

The program SPECFIT™ was used to extract the metal-ligand stability constants, single component spectra and the molar absorptivities of the metal-ligand species. The calculation procedure is based on the formal complex formation equation:

$$x\ NpO_2^+ + y\ L^- + z\ H^+ \rightleftharpoons [(NpO_2)_x(L)_yH_z]^{x(x-y+z)+}$$

Np(V) forms strong complexes with the selected model ligands providing hydroxamate and catechol functionalities for Np(V) binding as shown in Tab. 1. Within the SHA system two different 1 : 1 species were identified. At a metal-to-ligand ratio of 1 : 30 also the formation of a 1 : 2 : 0 species could be confirmed. BHA forms two Np(V) species with metal-to-ligand ratios of 1 : 1 and 1 : 2. The difference between SHA and BHA is the phenolic OH group next to the hydroxamate group in SHA. Interestingly, this structural difference is also pronounced in the spectrophotometric titration results. A direct comparison of the 1 : 1 and 1 : 2 species might indicate an involvement of the phenolic OH group in the binding of Np(V) to SHA.

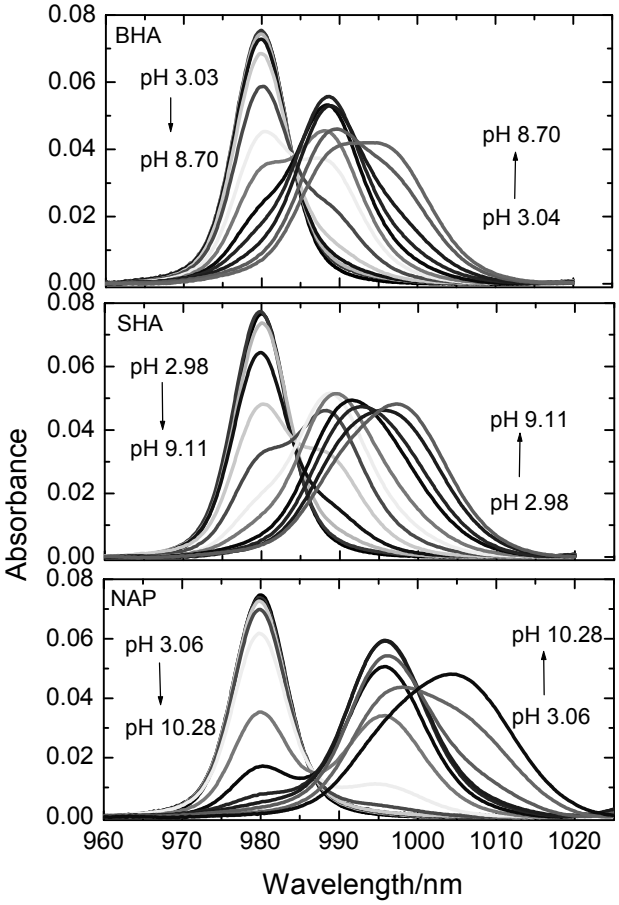

Fig. 1: Spectrophotometric titrations of $1.8 \cdot 10^{-4}$ M NpO_2^+–bioligand solutions in 0.1 M $NaClO_4$. BHA: $3.69 \cdot 10^{-3}$ M; SHA $5.4 \cdot 10^{-3}$ M; NAP $1.7 \cdot 10^{-3}$ M.

NAP forms the strongest 1 : 1 and 1 : 2 complexes with Np(V). The largest red shift of the absorption band, 996.2 nm, for a 1 : 1 model complex in this study and the magnitude of the stability constant indicate the formation of a four-membered chelate ring.

ACKNOWLEDGEMENTS. This work was funded by BMWi under contract number 02E9985.

REFERENCES

[1] Keller, C. (1971) *The Chemistry of the Transuranium Elements.* Verlag Chemie, Weinheim, p. 294.

Curium(III) complexation with desferrioxamine B (DFO) investigated using fluorescence spectroscopy

H. Moll, G. Bernhard

Curium(III) forms with desferrioxamine B (DFO) three complexes, CmH_2DFO^{2+}, $CmHDFO^{+}$, and CmDFO in aqueous solution which were characterized using TRLFS. Complex stability constants were calculated, main luminescence bands and the luminescence lifetimes were determined.

Hydroxamate-type siderophores like desferrioxamine B (DFO) are the most common siderophores ubiquitously found in the environment. These chelating substances have the potential to enhance the solubility and mobility of actinides by forming soluble complexes. DFO is a microbial produced trihydroxamate ligand which is commercially available and occurs naturally in soils. Recently, Essen et al. [1] demonstrated the production of desferrioxamine siderophores by *Pseudomonas stutzeri* (CCUG 36651) which had been isolated at the Äspö Hard Rock Laboratory. The unknown interaction between curium(III) and aqueous DFO species is the subject of this study.

EXPERIMENTAL. The TRLFS experiments were performed under N_2 atmosphere at 25 °C. The [Cm(III)] was fixed to $3 \cdot 10^{-7}$ M. TRLFS spectra were recorded using a pulsed flash lamp pumped Nd:YAG-OPO laser system. Details on the experimental set-up and the sample preparation are summarized in [2].

RESULTS. An overview of the emission spectra of $3 \cdot 10^{-7}$ M Cm(III) in 0.1 M $NaClO_4$ measured in the DFO system is presented in Fig. 1.
The spectral variations depicted in Fig. 1 are clear indications for a strong interaction of aqueous DFO species with Cm^{3+}. The emission maximum of Cm^{3+} at 593.8 nm decreased with: (a) increasing DFO amounts at fixed pH and (b) increasing pH at fixed [DFO]. No influence of the Cm^{3+} aquo ion could be detected in the measured sum TRLFS spectra at pH ≥ 6.2. At the same time, the amount of a first Cm(III)–DFO species increased having an emission maximum at approximately 600 nm. The formation of the second Cm(III)–DFO species is shown by the strong changes in the emission spectra between pH 5.8 and 6.2. Then, the spectra are independent from pH until pH 8.7. The again red shifted emission maximum at pH 9.8 indicates the increased influence of the third Cm(III)–DFO complex.
The spectral changes detected (see Fig. 1) were used in the SPECFIT™ factor analysis program to describe the complex formation reactions occurring in the Cm^{3+}–DFO system.

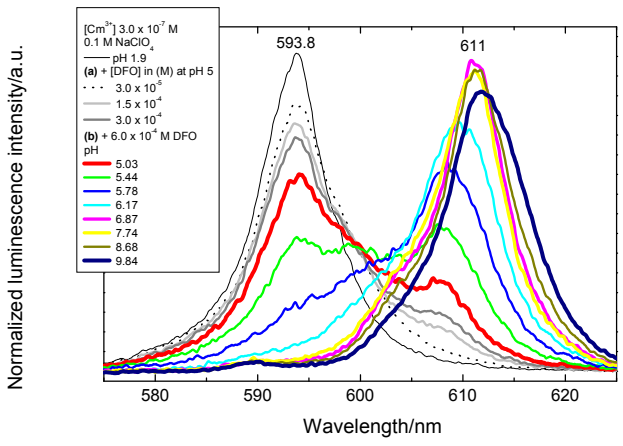

Fig. 1: Luminescence spectra of $3 \cdot 10^{-7}$ M curium(III) measured as a function of [DFO] at pH 5.0 (not all data shown) and at fixed [DFO] of $6 \cdot 10^{-4}$ M as a function of pH (not all data shown).

$$Cm^{3+} + DFO^{3-} + 2H^{+} \rightleftharpoons CmH_2DFO^{2+} \quad (1)$$

$$Cm^{3+} + DFO^{3-} + H^{+} \rightleftharpoons CmHDFO^{+} \quad (2)$$

$$Cm^{3+} + DFO^{3-} \rightleftharpoons CmDFO \quad (3)$$

Formation constants for reactions (1) to (3) were calculated to be $\log \beta_{121} = 31.62 \pm 0.23$, $\log \beta_{111} = 25.73 \pm 0.17$, and $\log \beta_{101} = 16.80 \pm 0.40$, respectively [2]. These results indicate the formation of strong 1 : 1 DFO complexes with curium(III). No published data exist for curium(III) providing a basis for comparison. The corresponding single component spectra of the individual species are summarized in Fig. 2.

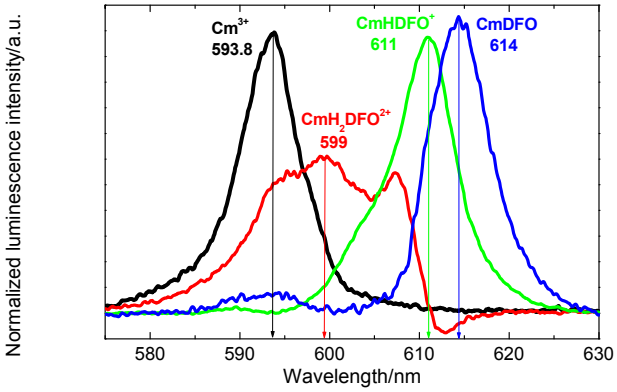

Fig. 2: Luminescence spectra of the single components in the Cm(III)–DFO system, as derived by peak deconvolution using SPECFIT™.

An indirect excitation mechanism for the Cm^{3+} luminescence was observed in the presence of DFO. The spectroscopic speciation determined at 360 (indirect excitation) and 395 nm (direct excitation) is in agreement. Speciation calculations showed that the Cm(III)–DFO species dominate over a wide curium concentration and pH range. This indicates the great potential of trihydroxamate siderophores to mobilize curium(III) in the biologically relevant pH range.

ACKNOWLEDGEMENTS. This work was funded by BMWi under contract number 02E9985.

REFERENCES

[1] Essen, S. A. et al. (2007) *Appl. Environ. Microbiol.* **73**, 5857-5864.
[2] Moll, H. et al. (2008) *Bull. Chem. Soc. Jpn.* **81**, 857-862.

Complexation of curium(III) and europium(III) with urea studied by TRLFS

A. Heller, A. Barkleit, G. Bernhard

The complex formation of Cm(III) and Eu(III) with urea in aqueous solution has been studied over a wide pH range. For Cm(III) a red shift of the luminescence peak is observed upon complexation, while for Eu(III) a significant change in splitting of the emission wavelengths occurs. Two complexes of the type ML^{3+} and $MLOH^{2+}$ are formed by both metals [1].

In case of incorporation, radionuclides pose a serious health risk to humans. Unfortunately, little is known about the metabolism of trivalent actinides. To address this lack of knowledge, the speciation of Cm(III) and its lanthanide analogue Eu(III) is investigated in human urine. For this purpose, their complexation with single constituents has to be known. Since urea is the most abundant component of mammal urine, its interactions with Cm(III) and Eu(III) has been investigated first.

EXPERIMENTAL. TRLFS measurements were performed under nitrogen atmosphere at room temperature and a constant ionic strength of 0.1 M ($NaClO_4$). The metal concentrations were fixed at $3 \cdot 10^{-5}$ M Eu(III) and $3 \cdot 10^{-7}$ M Cm(III). The urea concentration ranged from 0.01 to 5 M and the pH varied between 1 and 8. Analyses of the luminescence spectra were done by Origin™ and Specfit™ and speciation calculations were carried out with HySS2006.

RESULTS. In aqueous solution, the Cm(III) luminescence spectrum exhibits one characteristic emission peak at 593.5 ± 0.3 nm and a lifetime of 67.5 ± 1.3 µs. These data are in good agreement with the literature [2]. Upon complexation with urea this emission peak decreases and a new one at 598.7 ± 0.2 nm evolves (Fig. 1) [1].
Emission spectra of Cm(III) + 1.5 M urea show no differences up to pH 5 but at higher pH the emission wavelength is further red shifted to 601.2 nm. Since this shift and the resulting spectrum is not identical with one of the Cm(III) hydroxides [3], the formation of a mixed urea hydroxo complex was concluded.
In contrast to the actinide, the luminescence spectrum of Eu(III) in aqueous solution exhibits two characteristic emission peaks around 590 and 615 nm each of them split into two peaks at 588.6 ± 0.1 and 591.8 ± 0.2 nm and 612.1 ± 0.1 and 616.2 ± 0.2 nm, respectively, and a lifetime of 108.9 ± 1.5 µs. All data are in good agreement with literature [4,5]. Upon complexation with urea the emission wavelengths remain unaltered but the splitting of peaks is changed and the luminescence at 612 nm is significantly enhanced. For a detailed discussion of the peak splitting see [1]. Luminescence spectra of Eu(III) in aqueous solution at pH 4, I = 0.1 M and 24 °C under nitrogen atmosphere as a function of urea concentration are given in [6].

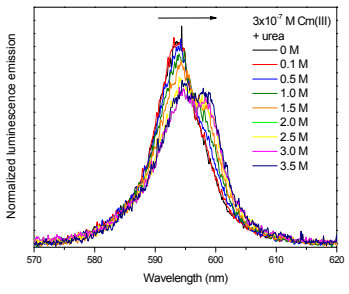

Fig. 1: Luminescence spectra of Cm(III) in aqueous solution at pH 4, I = 0.1 M and 24 °C under nitrogen atmosphere as a function of urea concentration; spectra are scaled to the same peak area.

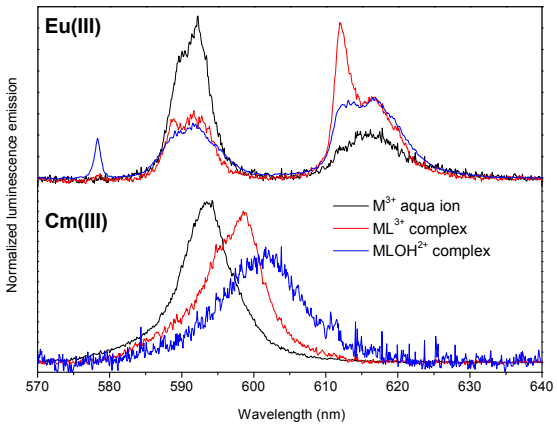

Fig. 2: Luminescence spectra of the single components as derived from peak deconvolution using Specfit™.

Analysis of the TRLFS spectra resulted in increasing lifetimes with increasing urea concentration for both heavy metals. Discussion and interpretation of this fact is given elsewhere [1]. For Cm(III) the lifetime is prolonged to 75-85 µs and for Eu(III) to 120-150 µs.
Stability constants were determined under consideration of all spectra recorded at various pH, ligand concentrations and formation of the metal hydroxides. For Cm(III), the stability constants were calculated to be $\log \beta_{110} = -0.28 \pm 0.12$ and $\log \beta_{11-1} = -7.01 \pm 0.15$. For Eu(III), slightly larger values were found ($\log \beta_{110} = -0.12 \pm 0.05$, $\log \beta_{11-1} = -6.86 \pm 0.15$) [1].
Speciation calculations were carried out to predict the distribution of both metals over a wide pH-range and are shown in Fig. 3 [1].

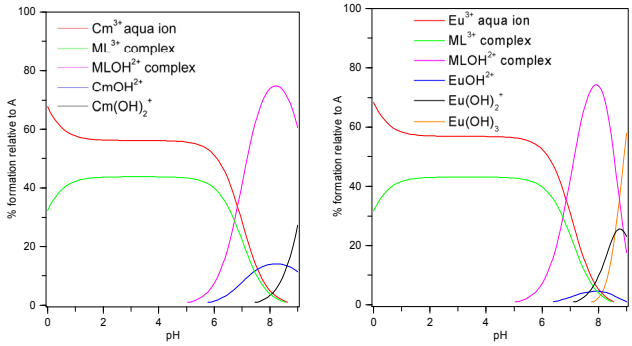

Fig. 3: Species distribution of $3 \cdot 10^{-7}$ M curium(III) at a fixed urea concentration of 1.5 M (left) and $3 \cdot 10^{-5}$ M europium(III) at a fixed urea concentration of 1 M (right) as a function of pH as derived from Hyss2006.

ACKNOWLEDGEMENTS. This work was funded by the Deutsche Forschungsgemeinschaft under contract number BE 2234/10-1.

REFERENCES

[1] Heller, A. et al. (2009) *Inorg. Chim. Acta*, in press.
[2] Moll, H. et al. (2008) *Biometals* **21**, 219-228.
[3] Fanghänel, T. et al. (1998) *J. Alloy. Compd.* **271**, 728-737.
[4] Moulin, C. et al. (1999) *Anal. Chim. Acta* **396**, 253-261.
[5] Plancque, G. et al. (2003) *Anal. Chim. Acta* **478**, 11.
[6] Heller, A. et al. (2007) *Report FZD -489*, p. 28.

Luminescence spectra of Eu(III) and Cm(III) in urine samples – A first step towards the speciation of trivalent lanthanides and actinides in human urine

A. Heller, A. Barkleit, G. Bernhard

Luminescence spectra of Eu(III) and Cm(III) in 10 original human urine samples were recorded and the composition of all samples was analyzed. Surprisingly, the electrolyte matrix does not seem to have a great influence on the dominant metal species. In contrast, the pH seems to be the crucial parameter. At lower pH, organic species, namely complexes with citric acid, are formed while at pH above 6 inorganic complexes are dominant [1].

In case of incorporation, radionuclides pose a serious health risk to humans. Unfortunately, little is known about the metabolism of trivalent actinides. To address this lack of knowledge, the speciation of Cm(III) and its lanthanide analogue Eu(III) in human urine is investigated. Besides the determination of the complexation behavior of both metals with single constituents [2], also luminescence spectra of 10 original human urine samples spiked in vitro with Eu(III) or Cm(III) were recorded and analyzed in regard to the dominant metal species and whether the pH or the electrolyte matrix plays the more important role.

EXPERIMENTAL. Analysis of the urine samples were done by mass spectrometry with inductive coupled plasma (ICP-MS) and ion chromatography (IC). TRLFS measurements were performed under nitrogen atmosphere and at room temperature. The metal concentrations were fixed at $3 \cdot 10^{-5}$ M Eu(III) and $3 \cdot 10^{-7}$ M Cm(III). Analysis of the luminescence spectra were done by Origin™.

RESULTS. ICP-MS and IC analysis showed that sodium, potassium and chloride are the main electrolytes in human urine (Tab. 1). Additionally, the samples exhibit a wide variation in regard to the concentration of a single ion which can vary up to one order of magnitude. A pH dependency is also observed (Tab. 1).
Luminescence spectra of urine samples spiked in vitro with Eu(III) are shown in Fig. 1 and can be divided into two groups. The first one exhibits 6 and the second one 7 luminescence maxima. Both groups can be clearly distinguished by the more or less pronounced luminescence at 578 nm, the shape of the sum spectrum of the three emission peaks in the 600-630 nm range, and the different lifetimes of 140-160 µs and 400-900 µs for group 1 and 2, respectively.

Tab. 1: Inorganic composition (mg/L) and pH values of the samples investigated.

Ion	P1	P2	P3	P4	P5	P6	P7	P8	P9	P10
Na^+	2170	4320	2670	210	1770	2260	2880	4713	7017	1367
K^+	2220	4220	3070	324	2300	609	1053	1420	2000	1220
Ca^{2+}	170	172	32	69	107	23	36	113	78	84
Mg^{2+}	159	95	32	20	69	17	40	55	87	24
Cl^-	3050	5870	3920	186	2390	1955	2380	4700	6285	1140
CO_3^{2-}	52.3	11.5	355	25.4	72.4	19.5	100	273.5	24.4	1595
NO_2^-	39.7	107	10	7.3	26	2	10.6	2	2	2
NO_3^-	57	64.5	19.3	7.5	29.4	8.3	17.3	14	53.3	20.5
PO_4^{3-}	4070	5380	1230	587	1950	449	1055	1305	2735	620.5
SO_4^{2-}	2110	2200	920	437	1150	313.5	673.5	1095	1540	509
pH	5.60	5.75	7.09	5.51	6.00	5.7	6.09	5.89	5.78	6.36

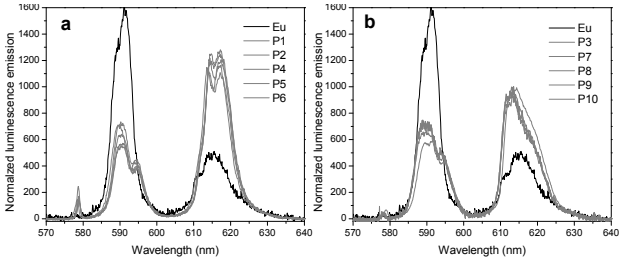

Fig. 1: Luminescence spectra of $3 \cdot 10^{-5}$ M Eu(III) in human urine samples; spectra are normalized to the same peak area and divided into a) group 1 and b) group 2 according to their shape and luminescence properties.

Luminescence spectra of urine samples spiked in vitro with Cm(III) were recorded for samples P1-P5 and are depicted in Fig. 2. Comparable to those of Eu(III) the luminescence spectra in samples P1, P4 and P5 are nearly identical (group 1) while the one in sample P3 differs significantly (group 2).

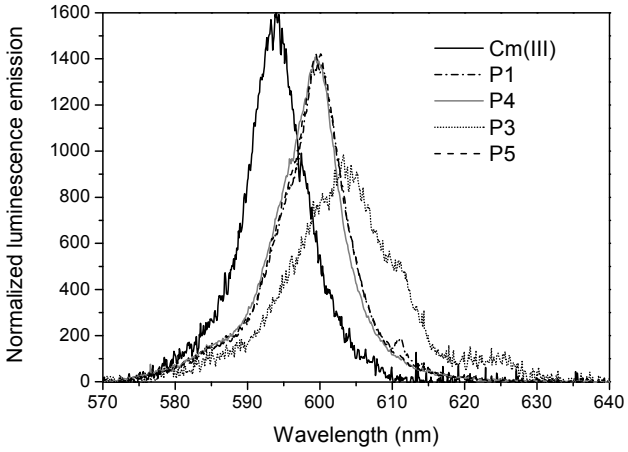

Fig. 2: Luminescence spectra of $3 \cdot 10^{-7}$ M Cm(III) in human urine samples; spectra are normalized to the same peak area.

A comparison of the inorganic composition and luminescence spectra of all samples provides no correlation between the electrolyte matrix and the emission spectrum. In contrast, comparing the pH of the samples shows that all samples exhibiting luminescence spectra of group 1 show values near or below 6, while those belonging to group 2 show higher pH values. Therefore, the pH seems to be the crucial factor in determination of the dominant metal species formed.
Since the luminescence spectra in all urine samples differ from those of both metals with urea in aqueous solution [2], other ligands were investigated and the spectra compared to those in the samples. For group 1, the emission spectra and spectroscopic data are in good agreement with a metal citrate species (unpublished data), while for group 2 inorganic species, presumably phosphate or sulfate, seem to be most likely.

ACKNOWLEDGEMENTS. This work was funded by the Deutsche Forschungsgemeinschaft (BE 2234/10-1).

REFERENCES

[1] Heller, A. et al. (2008) *NRC7 – Proceedings,* Budapest.
[2] Heller, A. et al. (2009) *Inorg. Chim. Acta*, in press.

Investigation of biological samples beyond the diffraction limit

T. Günther, J. Raff, K. Pollmann

The examination of the biological microcosm with light microscopy is limited by the diffraction limit of light. However, since the development of the AFM by Binning, Quate and Gerber in 1986, this can be bypassed. The MFP3D-Bio from Asylum Research is one of the most versatile AFMs on the market for biological research. It combines an inverted fluorescence microscope and a multimode AFM especially for biological applications.

We are able to analyze soft samples at the nano scale in air and even in liquids. The current project is treating the field of photo catalytic degradation of organic compounds in waste water. Therefore, we are developing catalytic active coatings. These coatings are based on metal binding bacterial surface layers (S-layer) that are forming two dimensional paracrystalline arrays. The AFM is used for characterization of surfaces such as live imaging of protein array recrystallization with pattern below 15 nm. But also detailed imaging of bacteria, spores and eucaryotic cells is possible. Phase imaging provides information about surface properties in AC mode. Further applications are force measurements to gain material specific data that could be easily combined with information about electrical conductivity.

EXPERIMENTAL. The S-layer proteins were derived from waste pile isolate *Lysinibacillus sphaericus* JG A12 by a standard S-layer preparation [1] (monomers from supernatant). The recrystallization of S-layer was processed on cleaned silicon within the closed fluid cell of the MFP3D-Bio. The cleaning of the wafers was done by incubation in piranha solution (30% hydrogen peroxide and sulphuric acid 1 :1) followed by intense rinsing with ultrapure water and subsequent UV radiation. The recrystallization buffer contained 0.5 mM TrisHCl (pH 9.0) and 10 mM $CaCl_2$. Adding S-layer to a final concentration of 0.3 mg/mL starts the recrystallization process. Immobilization of bacteria was done by drying a washed sample of an *E. coli* culture on a cover glass slide. Samples imaged in air were vacuum dried overnight. Imaging was done with silicone cantilever (1 N/m, 75 kHz) in air and silicon nitride cantilever (0.1 N/m, 7.5 kHz) in liquid.

RESULTS. The observed layers of recrystallized proteins offered a height of about 8 nm (Fig. 1A), which is consistent with monolayer data from other *Bacillus* strains [2]. The lattice exhibits a p4-symmetry with a unit cell of 12 to 13 nm and angle of 90° (Fig. 1B). During the S-layer preparation, the protein envelope is removed due to a lysozyme treatment. After this step, a sample was taken, vacuum dried and imaged in air. The height and phase images are shown in Fig. 2. In the height image (Fig. 2A) the detached protein sheets are clearly visible beneath the bacteria. The phase image is generated due to the phase shift during AC measurement. It provides information about surface properties. Some of the protein sheets appear darker then others. Light and dark sheets originate from different sites of the S-layers that possess different hydrophilicity. The AFM does not only bypass the borders of diffraction limit but with the height information it is possible to create three dimensional maps of the sample as shown in Fig. 3.

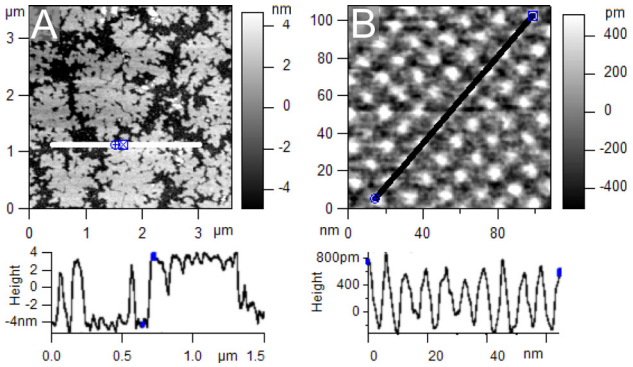

Fig. 1: AFM height image of assembling protein monolayer in buffer on silicon surface, the graph shows the height profile beyond the white line (A); AFM height image of S-layer lattice and the corresponding height profile along the black line (B).

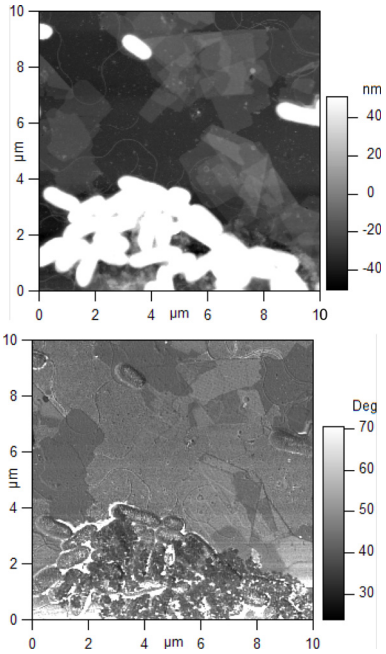

Fig. 2: Sample of lysozyme treated *Lysinibacillus sphaericus* JG A12, AC mode in air. Height image, full greyscale corresponds to 100 nm, bacteria appear in white for their height is exceeding the scale. Detached S-layer sheets are located beside the bacteria (A). Phase-image of the sample reveals some differences in surface constitution. The two different sides of the protein sheets appear in different color (B).

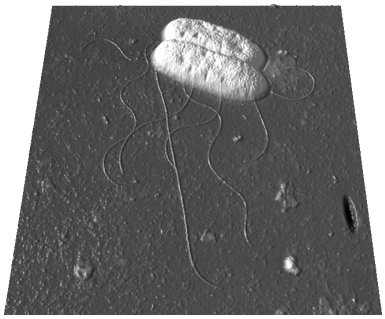

Fig. 3: 3D image of *E. coli*, vacuum dried on a glass slide, AC mode in air. Flagella, which can not be seen in light microscopy, are clearly visible in the AFM image. Overall height of the dried bacteria is about 200 nm.

ACKNOWLEDGEMENTS. This work is supported by the German Federal Ministry of Education and Research (BMBF), grant NanoFoto - BMBF/DLR 01SF0717.

REFERENCES

[1] Raff, J. (2002) Thesis, University of Leipzig, Leipzig.
[2] Györvary, E. S. et al. (2003) *J. Microsc.-Oxf.* **212**, 300-306.

Enhanced photocatalytic activity of S-layer supported ZnO-nanoparticles

K. Pollmann, A. Marquard, J. Raff

ZnO-nanoparticles were produced using S-layer as organic template. The nanocomposites were used to degrade diclofenac. Produced S-layer supported nanoparticles show enhanced photocatalytic activity in comparison to free ZnO-particles.

ZnO-nanoparticles are well known for their high photocatalytic activity [1]. Exposure of aqueous media to UV-light results in formation of highly reactive hydroxyl radicals which can subsequently decompose organic pollutants in waters. However, the application of such materials for cleaning-up waste waters requires a long-lasting immobilization of the particles. Here we present the synthesis of photocatalytic nanocomposites based on ZnO-nanoparticles immobilized on self-assembling S-layer proteins.
In our approach, the produced nanoparticles are used for photocatalytic degradation of the pharmaceutical diclofenac. The widespread occurrence of pharmaceutical residues in the environment has been reported in numerous investigations [2], thus establishing these compounds as a new class of pollutants. Therefore, the need of novel technologies for removal of these compounds has become evident.

EXPERIMENTAL. S-layer proteins of *Lysinibacillus sphaericus* were isolated as described previously [3]. ZnO-particles were synthesized by incubation of 10 mg S-layer in 20 mL 20 mM $ZnCl_2$ solution and subsequent addition of 25% NH_3 [4]. The glassy precipitate, consisting of $Zn(OH)_2$-complexes, was dialyzed overnight against H_2O, resulting in a white precipitate.
For XRD-analyses of S-layer bound particles, suspensions were centrifuged and the precipitates were dried at 30 °C in a vacuum oven.
For catalytic experiments, 1 mL of ZnO/S-layer suspension was added to 10 mL of a solution of 100 µM diclofenac in a quartz glass beaker. Suspensions were irradiated with UV-light (365 nm) and samples of 200 µL were taken at defined time points. HPLC-analyses were performed for monitoring the degradation of diclofenac. For every sample, 2 µL of the supernatants were injected and analyzed with a HPLC-system Agilent 1200 equipped with a DAD-detector 1200 (Agilent Technologies) and a column RP Zorbax Eclipse XDB-C 18, 150 x 4.6 mm x 5 µm. The aqueous system (flow rate 1 mL/min.) contained 85% methanol und 15% 20 mM KH_2PO_4 (pH 2.5) buffer. Diclofenac was identified and quantified by comparison with a standard.

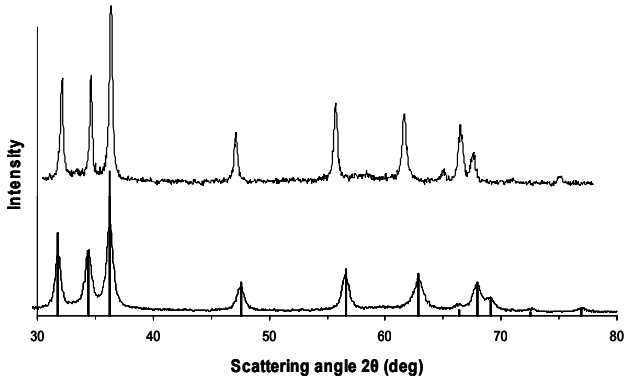

Fig. 1: X-ray diffraction pattern of S-layer templated ZnO-nanoparticles (upper graph) and ZnO-particles prepared without protein (lower graph); the measured diffraction lines (bars) are indexed; the different peak intensities of both samples correspond directly to the amount of material that was measured.

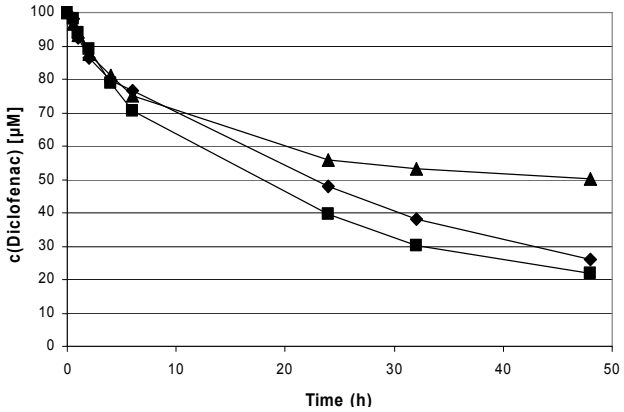

Fig. 2: Photocatalytic degradation of diclofenac. 100 µM diclofenac were incubated with 1 mg ZnO, without S-layer (▲), produced with 30 mg S-layer (♦), produced with 10 mg S-layer (■).

RESULTS. XRD-analyses of samples (Fig. 1) demonstrate the formation of ZnO-particles of a size of about 14 nm on S-layer (upper graph). In comparison, ZnO-particles produced in parallel without protein have a size of about 23 nm (lower graph).
Irradiation of ZnO-particles in aqueous medium with UV light of a wavelength of 365 nm results in the formation of highly reactive hydroxyl radicals. These radicals react with organic molecules, causing their decomposition. Figure 2 shows the decomposition of the pharmaceutical diclofenac using S-layer templated ZnO-particles. After 48 h irradiation, about 80% of applied diclofenac was degraded. In comparison, ZnO-particles produced without protein show a significant lower activity, showing a degradation rate of only 50% after 48 h.

CONCLUSIONS. Experiments have demonstrated the suitability of S-layer proteins as protein template for the synthesis of ZnO-nanoparticles. S-layer supported nanoparticles show enhanced photocatalytic activity in comparison to ZnO-particles produced without protein. Future goal is the development of photocatalytic surfaces that are based on the use of S-layer proteins for the coating of different substrates and as templates for the synthesis of ZnO-particles as the catalytic compound.

ACKNOWLEDGEMENTS. The work was supported by the German Federal Ministry of Education and Research (BMBF), grant NanoFoto - BMBF/DLR 01SF0717. We thank A. Scholz (FZD) for XRD-analysis.

REFERENCES

[1] Evgenidou, E. et al. (2007) *Catal. Today* **124,** 156-162.
[2] Wiegel, S. et al. (2004) *Chemosphere* **57**, 107-126.
[3] Raff, J. (2002) Thesis, University of Leipzig, Leipzig.
[4] Shao, S et al. (2008) *Mater. Lett.* **62**, 1200-1203.

Influence of different S-layer supports on the photocatalytic degradation of diclofenac by ZnO nanoparticles

J. Raff, F. Behrendt, A. Marquard, K. Pollmann

S-layer proteins allow the simple production of photocatalytic active ZnO nanoparticles of defined size. The aim of this study was to determine the influence of protein supports on structural properties and catalytic activities of produced nanoparticles. As demonstrated by the experiments, different S-layer supports have no influence on the structural properties of the produced nanoparticles but on their catalytic activity.

One important parameter influencing the activity of catalytic active nanoparticles is their size and their surface area. Therefore, the big challenge in producing catalytic active nanoparticles is to control the size and to achieve a narrow size distribution of the particles. A very elegant method to control these parameters is the use of bacterial S-layer proteins as structural support for the nanoparticle formation. Furthermore, the protein support avoids aggregation and release of the produced nanoparticles. The method is also applicable for the production of photocatalytic active nanoparticles composed of ZnO or TiO_2 particles. Photocatalysts based on such nanoparticles are very prospective for the elimination of pharmaceuticals in water [1]. However, for their technical application, the efficiency of such nanoparticles has to be increased. Therefore, the biggest challenges are the development of visible-light-responsive photocatalysts and the general enhancement of the radical formation efficiency. The latter is the focus in this study. As different protein lattice structures may have an influence on the structural properties of formed nanoparticles and also on their catalytic activity, different S-layer supports were tested for their influence on the photocatalytic diclofenac degradation. Diclofenac is one example for a persistent, in the environment detectable pharmaceutical with negative long-term effects [2,3].

EXPERIMENTAL. Different S-layer proteins were isolated from the uranium mining waste pile bacteria *Lysinibacillus sphaericus* JG-12, *Lysinibacillus* sp. JG-B7 and the *Bacillus* strains JG-B53, JG-B58 and JG-B62 by using standard procedures. ZnO-particles were synthesized and analyzed according to [1]. The immobilization of ZnO-nanoparticles on S-layer proteins were analyzed by means of SDS gel electrophoresis and ICP-MS measurements, described in reference [4]. For the diclofenac degradation tests, 1 mL of ZnO/S-layer suspension was mixed in a quartz glass beaker with 1 mL 1 mM diclofenac solution and 8 mL ultra pure water. The samples were irradiated with UV-light (365 nm), aliquots of 200 µL were taken after 0.5, 1, 2, 4, 6, 24, 30 and 48 hours and analyzed by means of HPLC-analyses as specified in [1].

RESULTS. Both methods, SDS gel electrophoresis and ICP-MS measurements, demonstrate the binding of the ZnO-nanoparticles to the S-layer proteins. The amount of ZnO bound by the S-layer proteins vary from 32 to 40 ± 2%. The XRD-analyses of the produced nanoparticles demonstrate the formation of pure ZnO phases on the S-layer protein with same particle size in respect to the error range. In contrast to that, the S-layer supported ZnO-nanoparticles show significant differences in the ability to degrade diclofenac photocatalytically dependent

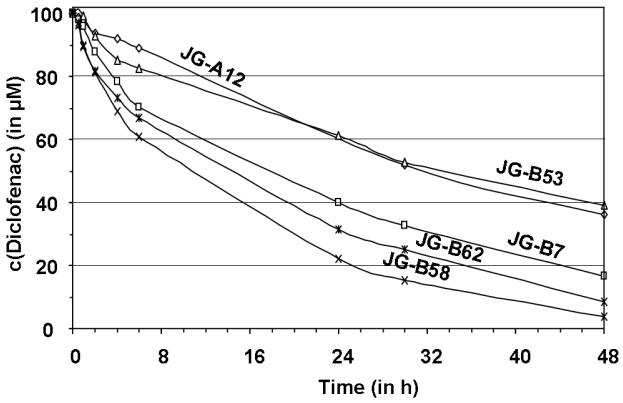

Fig. 1: Degradation of diclofenac by ZnO-particles bound to different S-layer supports from the indicated *Bacillus* and *Lysinibacillus* strains, normalized to 3 mg Zn.

of the S-layer protein variant (Fig. 1). Best degradation rates were obtained with ZnO-nanoparticles bound to S-layer protein from the uranium mining waste pile isolate *Bacillus* sp. JG-B58.
This S-layer protein possesses a p4 symmetry and a lattice constant of 16.5 nm. Up to now, the latter is compared to all other S-layer proteins the largest lattice constant. Furthermore, B58-S-layer possesses the highest uranium binding capacity and the highest phosphorus content among all investigated S-layer proteins [5]. But neither the structural differences nor the known biochemical properties are sufficient to explain the differences in activity . Possibly, differences in the particle binding and/or an influence of the S-layer proteins on the radical formation efficiency may explain these results. In any case, further investigations are necessary to understand the ZnO-protein interaction.

CONCLUSIONS. S-layer proteins are well suited for the production of photocatalytic active ZnO-nanoparticles. Although current degradation rates are unsatisfactory, they are in the typical range of a non-optimized photocatalytic diclofenac degradation. Moreover, the S-layer based production of nanoparticles offers several possibilities to enhance their photocatalytic activity. Therefore work is planed regarding an expanded screening for the identification of an ideal S-layer as nanoparticle support, the production of a biocomposite composed of ZnO-particles/S-layer/carrier and the doping of nanoparticles.

ACKNOWLEDGEMENTS. The work was funded by German Federal Ministry of Education and Research (grant NanoFoto BMBF/DLR 01SF0717). We thank U. Schäfer for the ICP-MS measurements, A. Scholz (FZD) for XRD-analysis and S. Matys (IfWW, TU Dresden) for structural characterization of the S-layer proteins.

REFERENCES

[1] Pollmann, K et al (2009) this report, p. 27.
[2] Wiegel, S. et al. (2004) *Chemosphere* **57**, 107-126.
[3] Triebskorn, R. et al. (2007) *Anal. Bioanal. Chem.* **387**, 1405-1416.
[4] Behrendt, F. (2008) Diploma thesis, University of Applied Sciences, Dresden.
[5] Raff, J, et al (2006) *Report FZR- 443*, p. 29.

Bacterial S-layer as matrix for the construction of chemo-optical sensors

U. Weinert, K. Großmann, G. Geipel, J. Raff

S-layer proteins of isolates from the uranium mining waste pile "Haberland" in Saxony bind more selective higher amounts of uranium and other heavy metals than comparable proteins [1]. They can self assemble in solution and on different surfaces to highly regular monomolecular lattices. The proteins themselves contain up to 20 mol-% amino and carboxyl groups. By linking two specific fluorescence dyes to these groups fluorescence resonance energy transfer (FRET) can be generated. The latter can be used for the development of chemo-optical sensors.

FRET is a nonradiative energy transfer from one fluorescence dye (donor) to another fluorescence dye (acceptor). The result is a decrease of the emission of the donor and an increase of the emission of the acceptor. The efficiency of FRET is dependent on a high overlap between emission spectra of the donor and extinction spectra of the acceptor and the distance between both dyes. Also heavy metals cause a disturbance of FRET what is detectable.

EXPERIMENTAL. The isolate *Lysinibacillus sphaericus* JG-A12 was grown over night at room temperature in Nutrient Broth medium (6 g/L, Mast Group Ltd., Merseyside, UK). S-layer proteins were extracted according to the protocol in reference [2]. The S-layer proteins were modified with the fluorescence dyes Alexa488 and Alexa555 (Molecular Probes, Invitrogen, Eugene, U.S.A.) with a ratio of 1 : 2. 1-ethyl-3-(3-dimethylaminopropyl) carbodiimid (EDC) was used as coupling reagent. EDC initiates the formation of a peptide bond between protein and fluorescence dye. Free fluorescence dye was removed by ultra filtration (vivaspin 100 kDa MWCO) and the modified proteins were washed several times (at least 5 times). The detection of a possible FRET was measured with two different methods described below.

RESULTS. It was possible to modify the proteins with both fluorescence dyes at the same time. The amount of S-layer bound dye was almost the same for both dyes (0,7 $mol_{Alexa488}/mol_{S-L}$ and 0,9 $mol_{Alexa555}/mol_{S-L}$). The modification had no influence on the formation of polymeric S-layer structures like sheets and tubes. (Fig. 1a-c). UV-vis spectra of modified protein confirmed both findings (Fig. 2).

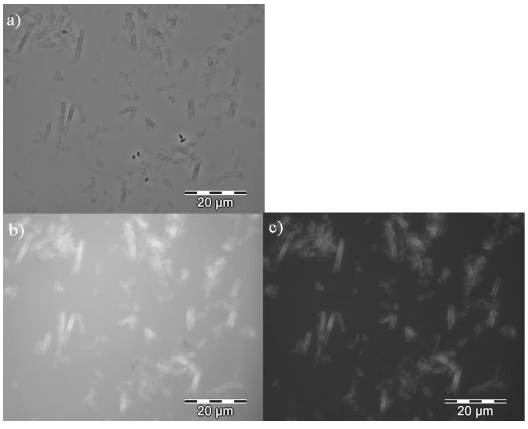

Fig. 1: Phase contrast (a) and fluorescence pictures of JG-A12 S-layer proteins modified with Alexa488 (b) Alexa555 (c).

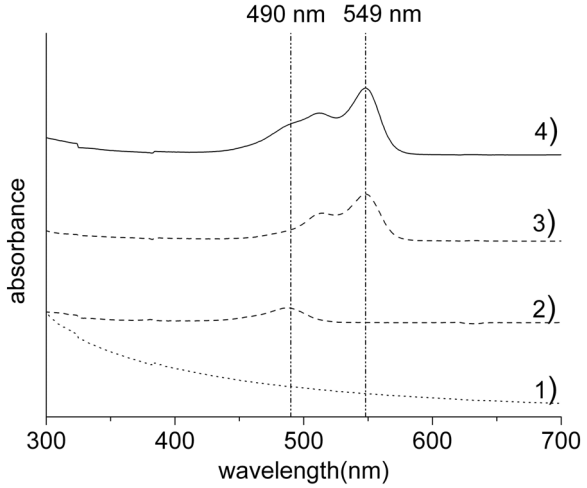

Fig. 2: UV-vis spectra of native S-layer protein (1) and S-layer protein modified with (2) Alexa488, (3) Alexa555 and (4) Alexa4888 and Alexa555 absorbance maxima of Alexa488 is 490 nm and of Alexa555 549 nm.

As first method for FRET detection confocal laser scanning microscopy was used. Measurements were performed with the method of acceptor bleaching. This method did not give any evaluable result because of the high photostability of the fluorescence dyes. For reliable results, a 90% bleaching of the acceptor is necessary [3].
As second method for detecting FRET time resolved laser induced fluorescence spectroscopy (TRLFS) was used for the determination of the fluorescence lifetimes of the two dyes Alexa488 and Alexa555 bound to the S-layer proteins. The measurements were carried out with S-layer proteins modified with only one fluorescence dye and with S-layer proteins modified with both fluorescence dyes. In case of FRET, the fluorescence lifetime of the donor decreases and the fluorescence lifetime of the acceptor increases compared to those of the fluorescence dyes bound separately to the protein. The investigations showed a change in lifetime but contrarily to what is expected on Alexa488/Alexa555 modified S-layer proteins. The fluorescence lifetime of Alexa488 increases and that of Alexa555 slightly decreases.

Tab. 1: Fluorescence lifetimes of the dyes Alexa488 and Alexa555 linked to the S-layer of JG-A12, 1) Alexa488 and Alexa555 are linked separately to the S-layer protein 2) both fluorescence dyes are linked together to the S-layer protein.

Lifetime of*	Alexa488	Alexa555
1)	4.5 ± 0.7	22.5 ± 2.1
2)	17.4 ± 3.0	16.2 ± 3.2

*calculated with programm Origin™, model expdecay2.

As obvious from the experiments, S-layer proteins can be successfully modified with two fluorescence dyes and also an energetic interaction between both dyes is detectable. But for technical application, further optimization of the dye coupling is necessary to obtain a clear and detectable FRET.

REFERENCES

[1] Pollmann, K. et al. (2006) *Biotechn. Appl*. **24**, 58-68.
[2] Raff, J. (2002) Thesis, University of Leipzig, Leipzig.
[3] Berney, C. et al. (2003) *Biophys. J.* **84**, 3992-4010.

Coating of different materials with S-layer proteins for technical applications

F. Lehmann, T. Günther, J. Raff

S-layer proteins can be used for the development of different multifunctional coatings. For technical applications materials need to be easy to produce as well as mechanical and chemical stable. Therefore, we are testing different SiO_2- and Al_2O_3-materials for their suitability to work as carrier for multifunctional S-layer coatings. As demonstrated by the experiments, the amount of bound S-layer proteins highly depends on the surface area and on the surface fine structure of the material.

Surface-layer (S-layer) proteins are the outermost cell component of many bacteria and archea. They form paracrystalline protein lattices with different structures and are able to self assemble in vivo and in vitro as monomolecular layer on surfaces [1]. Furthermore they possess two different sides, a negatively charged, hydrophilic side and a neutral charged more hydrophobic side. These properties can be used for the simple coating of different materials, and for a durable immobilization of the protein layer. The latter is crucial for the development of materials for technical applications, such as photocatalysts [2], chemo-optical sensors [3] and metal specific filter material [4]. In this work, we use S-layer monomer solutions either obtained from the isolation procedure itself or produced from S-layer suspensions for a controlled recrystallization and a deposition of a protein layer on different carriers. This is a very simple method and upscaling is easily possible.

EXPERIMENTAL. The isolate *Lysinibacillus sphaericus* JG-A12 was grown over night at room temperature in Nutrient Broth medium (6 g/L, Mast Group Ltd., Merseyside, UK). S-layer protein was isolated according to the protocol in reference [5]. Supernatants obtained after the digestion of the peptidoglycan of the bacterial cell wall and after the recrystallization by dialysis were collected and the protein content was determined using the Lowry protein assay [6]. For further experiments, the protein content was adjusted to 0.2 to 2 mg protein per mL. In addition, S-layer solutions were prepared by adding 100 mM EDTA to purified S-layer suspensions until the suspension became clear. Solubilized S-layer proteins containing EDTA were again adjusted to protein concentrations of 0.2 to 2 mg protein per mL, dialysed against ultra pure water and used for coating experiments. For the controlled recrystallization, a buffer containing 5 mM TRIS and 10 mM $CaCl_2$, pH 9 was used. All samples were incubated for 48 hours at a temperature of 8 °C. Bound S-layer protein was calculated from the residual S-layer content of the supernatant. For visualization, S-layer protein solutions were supplemented with Alexa 488-labeled S-layer protein monomers and were also used for the particle coating. Alexa488 labeled proteins were produced as described in [3].

Tab. 1: S-layer coating of different materials.

Material	mg S-layer per g material
Fomed clay pellets (< 0.63 mm)	62
Foamed clay pellets (0.63-2 mm)	39
Foamed clay pellets (2-4 mm)	34
Glas foam (< 0.63 mm)	56
Glas foam (0.63-2 mm)	34
Glas foam (2-4 mm)	26
Industrial ceramic (< 0.63 mm)	56
Industrial ceramic (0.63-2 mm)	32
Industrial ceramic (2-4 mm)	16
Industrial ceramic (spherically Ø 3 mm)	10
Silicagel G 62	68
Puralox (Al_2O_3)	55
MCM 41 (meso-porous SiO_2)	116
SBA 15 (nano-porous SiO_2)	53

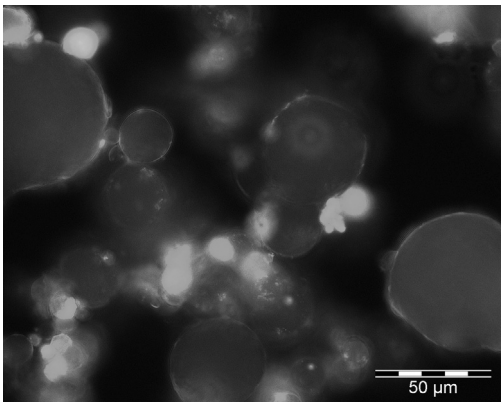

Fig. 1: Coating of mesoporous Al_2O_3 with fluorescent labeled S-layer protein.

RESULTS. As demonstrated by AFM investigations, the applied method is suitable for the production of monomolecular S-layer lattices on SiO_2-surfaces [7]. By using longer incubation time and different supports, AFM studies indicate also the formation of multi-layer coatings (data not shown). The coating of Al_2O_3 carriers was also demonstrated by using Alexa488-labeled S-layer proteins (Fig. 1). Interestingly, the amount of bound S-layer protein depends not only on the surface area (different particle size of used materials; Tab. 1) but also on the surface fine structure of the carriers, e.g. MCM 41 in comparison to SBA 15 (Tab. 1). Next experiments will focus on the chemical and mechanical stability of the coatings and on methods for the covalent linking of the proteins to the supporting carrier.

ACKNOWLEDGMENTS. Industrial ceramics were provided by Fa. Letscher. MCM41, SBA15 and Puralox were provided by N. Steinfeldt (Leibniz Institute for Catalysis, Rostock, Germany).

REFERENCES

[1] Sleytr, U. B. et al. (2001) *Prog. Surf. Sci.* **68**, 231-278.
[2] Pollmann, K. et al. (2009) this report, p. 27.
[3] Weinert, U. et al. (2009) this report, p. 29.
[4] Raff, J et al. (2003) *Chem. Mat.* **15**, 240-244.
[5] Raff, J. (2002) Thesis, University of Leipzig, Leipzig.
[6] Lowry, O. H. et al. (1951) *J. Biol. Chem.* **193**, 265-275.
[7] Günther, T. et al. (2009) this report, p. 26.

Heterologous expression of the silent S-layer protein gene *sllB* of *Lysinibacillus sphaericus* JG-A12 in *E. coli*

F. Lederer, K. Pollmann

The plasmid located silent S-layer protein gene *sllB* of the uranium mining waste pile isolate *Lysinibacillus sphaericus* JG-A12 was cloned as polymerase chain reaction product in the expression vector pET-30 Ek/LIC and heterologously expressed in *Escherichia coli* Bl21(DE3).

Surface layer proteins are characteristic structures of archaea and lots of bacteria. They protect the cells against pathogens, difficult environmental conditions and in some cases they form the cell shape. These bacterial envelope proteins have the ability to fix heavy metals on their surface. To produce S-layer proteins in a cost efficient way, selected S-layer protein genes were cloned and heterologously expressed in the bacterial expression strain *E. coli* Bl21(DE3). To investigate the structure of the silent S-layer protein SllB, *sllB* was cloned into *E. coli* Bl21(DE3). The addition of His tags to the N-terminus enabled the purification of the recombinant protein by Ni-chelating chromatography.

EXPERIMENTAL. The silent S-layer protein gene *sllB* of *Lysinibacillus sphaericus* JG-A12 was cloned as PCR product in the vector pET-30 Ek/LIC and heterologously expressed in *E. coli* Bl21(DE3). The gene expression was induced by addition of IPTG.
For maximal protein expression the growth temperature of the cells needs to be optimized. Samples of cell cultures incubated at different temperatures were taken each hour for 26 hours. The optical density was determined using a photospectrometer (Pharmacia Biotech) and total cell extracts of each sample were analyzed by means of SDS-PAGE gel and stained with Coomassie Brilliant Blue.
The recombinant protein, carrying six histidine residues at the N-terminus, was purified by Ni-chelating chromatography using the His Bind Kit (Novagen) under denaturing condition. The used method was modified after [3]. The heterologous expression of the recombinant S-layer protein was measured with Bradford reagent (BioRad) and SYPRO Ruby protein stain.

RESULTS. As presented in Fig. 1 the expression strain carrying *sllB* incubated at room temperature (RT) shows lowest growth rate but highest cell density ($OD_{600} > 4$). In comparison, bacterial strains growing at higher temperatures show higher growth rates but lower cell densities.

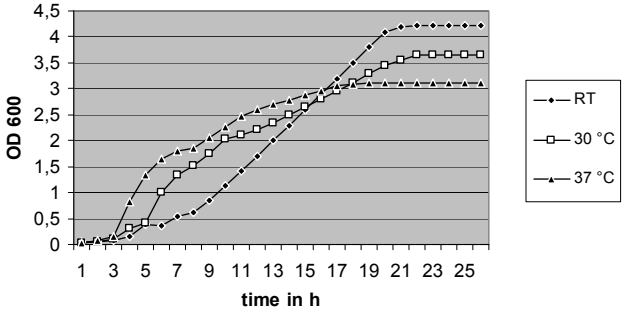

Fig. 1: Growth curve of expression strain *E. coli* Bl21(DE3) carrying the recombinant silent S-layer protein gene *sllB* at different temperatures. Growth was monitored at different growth temperatures by measuring the optical density at 600 nm.

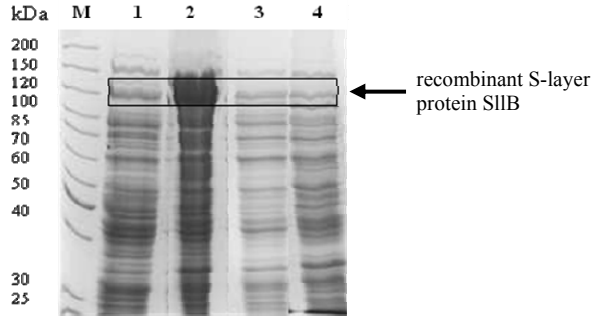

Fig. 2: Expression of the recombinant silent S-layer protein SllB. Cell extracts were analyzed by using a 7,5% SDS gel, stained with Coomassie Brilliant Blue. Protein ladder (**M**), expression strain grown for 48 h (**1**-**4**), at RT without IPTG addition (**1**), at RT with IPTG addition (**2**), at 30 °C with IPTG addition (**3**) and at 37 °C with IPTG addition (**4**).

As shown in Fig. 2 *E. coli* carrying SllB was producing the recombinant protein most efficiently when growing at RT compared to those grown at higher temperatures.
As presented in Tab. 1 the total expression of recombinant S-layer protein of *E. coli* grown at RT is more than 3 times higher than for *E. coli* grown at higher temperatures.

Tab. 1: Comparison of amount of total protein and recombinant S-layer per 100 mL culture volume of expression strain grown at different temperatures for 48 hours.

	RT	**30 °C**	**37 °C**
Culture volume [mL]	100	100	100
Total protein content [mg]	917,3	376,8	512,6
S-layer content per culture volume]mg]	25,0	7,1	6,9

CONCLUSIONS. The cloning and heterologous expression of the silent S-layer protein gene *sllB* of *Lysinibacillus sphaericus* JG-A12 were successful. The expression of the recombinant S-layer protein strongly depends on cultivation temperature, time and IPTG addition.

REFERENCES

[1] Sleytr, U. B. et al. (1997) *Trends Biotechnol.* **15**: 20-26.
[2] Pollmann, K. et al. (2005) *Microbiology* **151**, 2961-2973.
[3] Pollmann, K. et al. (2007) *Appl. Microbiol. Biotechnol.* **75**, 1079-1085.

Microbial diversity in highly contaminated uranium mining wastes. Part A: Archaeal diversity

G. Radeva,[1] V. Buchvarova,[1] K. Flemming, T. Reitz, S. Selenska-Pobell
[1]Institute of Molecular Biology, Bulgarian Academy of Sciences, Sofia, Bulgaria

Archaeal diversity was compared between U wastes samples contaminated differently with U. The low contaminated samples were occupied by group 1.1a of *Crenarchaeota*, while the highly contaminated samples were dominated by the group 1.1b. This indicates that the members of the group 1.1b are more resistant to U then those of the group 1.1a. This suggestion is consistent with our results demonstrating a strong shifting from *Crenarchaeota* 1.1a to 1.1b after addition of uranyl nitrate to the low contaminated samples.

Recent meta-genomic studies revealed that *Archaea* are widely spread in nature and that they should play important role in a wide variety of environmental processes [1,2]. Because only a very small fraction of these organisms was cultivated up to date, our knowledge about their metabolic pathways and ecological properties is rather limited. Distribution of *Archaea* in U mining wastes and their interactions with radionuclides are not well studied in contrast to those of bacteria [3]. Up to date, only the ability of one hyperthermophilic archaeon to reduce U(VI) [4] and by one halophilic archaeon to biosorp U(VI) [5] are described. These two organisms are, however, not relevant to uranium mining wastes.

EXPERIMENTAL. The following natural soil samples were involved in the comparative analyses of archaeal diversity: BuhC (containing 200 mg U/kg) and BuhD (78.4 mg U/kg) collected from a uranium mill tailings called Buhovo; Sliv (374 mg U/kg) collected from uranium mine Sliven Bulgaria; JG35 (26 mg U/kg) collected from a uranium mining waste pile of Johanngeorgenstadt, Germany. In addition, four sub-samples of JG35 treated with uranyl nitrate to reach concentrations of 100 mg U/kg (JG35U1, JG35U4) and 300 mg U/kg (JG35U2A and JG35U3) were involved in the analyses. The archaeal diversity was estimated via the 16S rRNA gene retrieval as described earlier [3,6,7].

RESULTS. As evident from the results presented in Fig. 1, all archaeal 16S rRNA gene sequences identified in the studied samples were affiliated with the mesophilic *Crenarchaeota*. The sequences identified in the naturally highly contaminated samples BuhC, BuhD and Sliv represented populations belonging to the 1.1b group of this phylum and formed three clusters (A, B and C). The highest number of clones in the cluster A was retrieved from the most contaminated sample Sliv (sequences Sliv-Ar22 and Sliv-Ar32), followed by the BuhC and BuhD clones represented by sequences BuhC-Ar48 and BuhD-Ar100 and Ar111. The sequence Sliv-Ar32 shares a high identity at the level of species with the recently described ammonia-oxidizing organism "Candidatus Nitrososphera gargensis" which was identified in a cultured enrichment consortium containing also representatives of *Beta-* and *Gammaproteobacteria* [8]. The cluster B was smaller and included mainly populations found in the low contaminated sample JG35 represented by the sequences JG35-TR-Ar19 and JG35-TR-Ar78. In the cluster B only one clone (BuhC-Ar44), originating from the highly contaminated natural sample BuhC and 2 clones retrieved from the U(VI) supplemented sample JG35U2A (sequence JG35U2A-TR-Ar57) were affiliated.

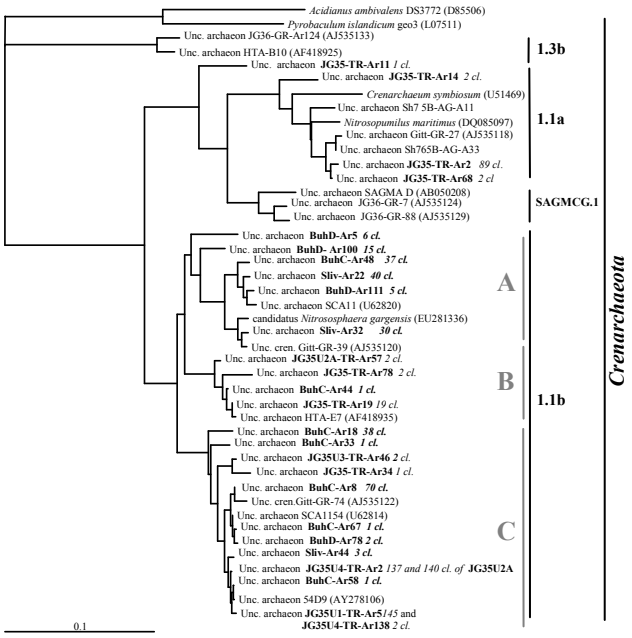

Fig. 1: Phylogenetic tree of the retrieved archaeal 16S rRNA gene sequences. The tree was rooted with the 16S rRNA genes of *Pyrobaculum islandicum* geo3 and *Acidianus ambivalens* DS3772.

Cluster C was the biggest and it incorporated over 70% of the clones retrieved in the sample BuhC (sequences BuhC-Ar18, BuhC-Ar33, BuhC-Ar8, BuhC-Ar67, BuhC-Ar58) and some clones from BuhD and Sliv samples. This cluster includes almost all the clones found in the four uranium treated samples JG35U1, JG35U4, JG35U2A, and JG35U3 which are represented by sequences JG35U4-TR-Ar2 and JG35U1-TR-Ar5 in Fig. 1. None of the sequences retrieved in the highly naturally or laboratory contaminated samples was affiliated with the group 1.1a. Into this group, exclusively sequences retrieved in the low contaminated sample JG35 were clustered, namely JG35-TR-Ar2, JG35-TR-Ar68, JG35-TR-Ar14, and JG35-TR-Ar11. Our results indicate that the populations belonging to the 1.1b group of *Crenarchaeota* are very adaptive and that they can tolerate higher amounts of uranium than those belonging to the group 1.1a. Earlier, crenarchaeal populations, also exceeding the group 1.1a, were found in another highly U polluted sample (JG36) collected from higher depths then the samples studied here [9] (see clusters 1.3b and SAGMCG.1 in Fig. 1).

REFERENCES

[1] Chaban, B. et al. (2006) *Can. J. Microbiol.* **52**,73-116.
[2] Schlepper, C. et al. (2005) *Nat. Rev. Microbiol*. **3**, 479-488.
[3] Geissler, A. (2007) Thesis, TU Bergakademie Freiberg, Freiberg.
[4] Kashefi et al. (2008) *Geobiology* **6**, 147-154.
[5] Francis, A. J. et al. (2004) *Radiochim. Acta* **92**, 481-488.
[6] Geissler, A. et al. (2005) *Geobiology* **3**, 275-285.
[7] Reitz, T. et al. (2007) *Report FZD-459*, p. 42.
[8] Hatzenpichler, R. et al. (2008) *Proc. Natl. Acad. Sci. U.S.A.* **105**, 2134-2139.
[9] Radeva, G. et al. (2002) *Report FZR-373,* p. 29.

Microbial diversity in highly contaminated uranium mining wastes. Part B: Bacterial diversity

G. Radeva,[1] K. Flemming, V. Buchvarova,[1] S. Selenska-Pobell
[1]Institute of Molecular Biology, Bulgarian Academy of Sciences, Sofia, Bulgaria

Composition of bacterial communities in soil samples collected from two different uranium contaminated habitats in Bulgaria was site-specific and very complex. Observed differences in the biodiversity are possibly depending on the geographic environment and on the different grade of uranium pollution.

A number of studies have shown that environments polluted with radionuclides and heavy metals are occupied by unusual bacteria well adapted to the extreme conditions [1-5]. Understanding how bacteria alter the toxicity of heavy metals and influence their behavior in the environment is important for the development of the bioremediation strategies. Uranium mining waste piles, mill tailings and disposal sites exist in several regions in Bulgaria. No biological monitoring for assessing the environmental effects of the uranium mining in Bulgaria was ever applied.

EXPERIMENTAL. The three soil samples studied in this work were BuhC, BuhD, and Sliv described in [6]. Bacterial diversity was estimated via the 16S rRNA gene retrieval according to [1-3].

RESULTS. The natural bacterial communities in the samples of the studied highly contaminated uranium wastes in Bulgaria were composed of highly diverse organisms distributed within the following eight phyla (*Proteobacteria, Acidobacteria, Bacteroidetes, Verrucomicrobia, Gemmatimonadetes, Actinobacteria, Chloroflexi,* and *Planctomycetes*).

Most part of the bacteria found in the samples BuhC, BuhD and Sliv were affiliated with various members of *Proteobacteria* which are shown in Fig. 1. As evident from the figure, bacterial community of the most U contaminated sample (Sliv) was predominated by representatives of *γ-Proteobacteria* (sequences Sliv-7 and Sliv-13), *α-Proteobacteria* (sequences Sliv-23, Sliv-29, Sliv-66), and *β-Proteobacteria* (Sliv-21, Sliv-75, Sliv-144, Sliv-76). The most predominant group of *γ-Proteobacteria*, represented by the sequence Sliv-7 was affiliated with 94% of similarity with *Aquicella lusiana.* This is in contrast with our previous studies where mostly members of *Pseudomonas* spp. were found in the highly polluted with U samples [1]. Representatives of *γ-Proteobacteria* but in lower numbers were retrieved also in the samples from Buhovo (sequences BuhC-2 and BuhD-10). Abundance of *Alphaproteobacteria* was higher in the sample BuhD then in BuhC. In the latter sample *β-Proteobacteria* were found to predominate (sequences BuhC-11 and BuhC-95). The representatives of *δ-Proteobacteria* were found only in the sample BuhD (sequence BuhD-66).

The second predominant group of bacteria were the representatives of *Acidobacteria*. They represented 42% of the retrieved 16S rRNA sequences in the relatively low polluted sample BuhD [6], 28% in the sample BuhC, and only 5% in the Sliv sample. Interestingly, *Acidobacteria* were the most predominant group found in several German uranium wastes polluted with uranium at a similar level as BuhD [4, 5].

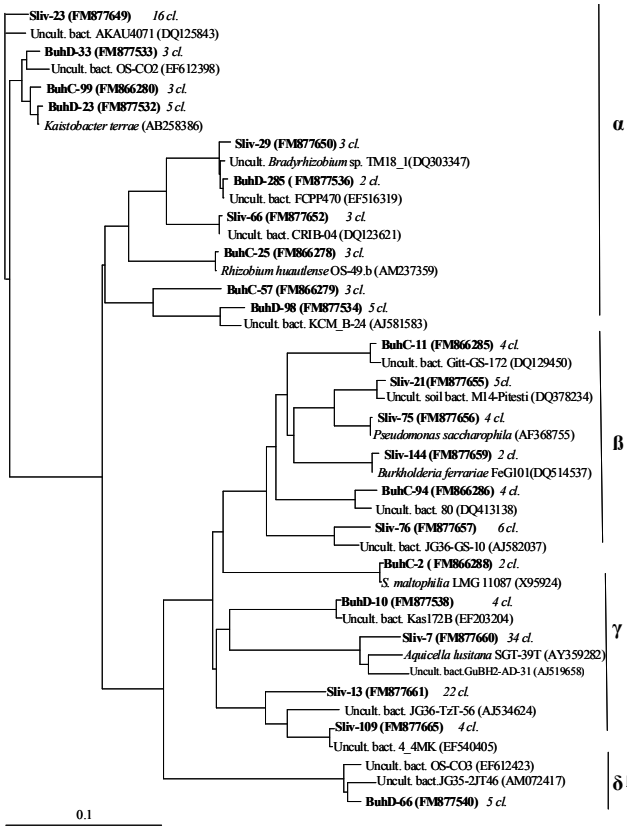

Fig. 1: Phylogenetic tree of the retrieved 16S rRNA gene sequences from the studied habitats affiliated with *Proteobacteria*. The scale bar represents 10% nucleotide difference.

Another predominant group in the studied samples was affiliated with *Bacteroidetes* and enclosed 31% of the clones found in Buh C, 11% of the Sliv clones, and only 3% of those found in BuhD. *Verrucomicrobia* populations comprised 15% in the sample BuhD and only 1% in Buh C, but they were not found in the sample Sliv. *Gemmatimonadetes* were present in a low density in all samples (BuhC: 6%, BuhD: 2%, Sliv: 3%). The representatives of *Actinobacteria* were found only in the Sliv sample. Single representatives of *Chlorofexi* were identified in the U mill tailings samples BuhC and BuhD. A few sequences, affiliated with 97 to 94% of 16S rRNA gene similarity with *Planctomycetales* were retrieved in the samples Sliv and BuhD. The found differences in the diversity and the composition of the bacterial communities in the studied samples can be explained by their different geographic and geologic origin and also by the different grade of metal contamination in them.

REFERENCES

[1] Geissler, A. et al. (2005) *Geobiology* **3**, 275-285.
[2] Nedelkova, M. et al. (2005) *Underground injection science and technology*, p. 531-536, Elsevier, Amsterdam.
[3] Radeva, G. et al. (2005) *Can. J. Microbiol.* **51**, 910-923.
[4] Selenska-Pobell, S. (2002) *Interactions of Microorganisms with Radionuclides*, p. 225-254, Elsevier Science Ltd., Oxford.
[5] Selenska-Pobell, S. (2002). *Uranium in the Aquatic Environment,* p. 455-464, Springer, Berlin.
[6] Radeva, G. et al. (2009) this report, p. 32.

Halophilic archaeal populations in Arava Desert (Israel) as examined by using direct molecular and cultivation methods

V. Buchvarova,[1] U. Jankowski, K. Flemming, S. Selenska-Pobell
[1]Institute of Molecular Biology, Bulgarian Academy of Sciences, Sofia, Bulgaria

Hyper saline environments are considered as perspective repositories of radioactive wastes. They are, however, occupied by extreme halophilic microorganisms, which can influence mobility of radionuclides. In this study, archaeal diversity in two hyper saline samples collected from the Arava Desert was analysed. All identified archaeal populations, including one cultured isolate, were affiliated to the family *Halobacteriaceae.*

EXPERIMENTAL. The Arava Valley is laying between the Dead Sea and the Gulf of Eilat and contains many hyper saline regions. Two samples (7EY and 10EY) were collected from the salt crust of one such region called Ein Yahav. The samples 7EY collected from the surface and 10EY (from a depth of 0-3 cm) were stored at −20 °C. The elemental composition of the samples was measured by ICP-MS. The most abundant elements in both samples were Si (139 mg Si/kg in 7EY, 115 mg Si/kg in 10EY) and Na (111 mg Na/kg in 7EY, 103 mg Na/kg in 10EY). Two archaeal 16S rRNA clone libraries were constructed for the two samples. For this two archaea-specific primers (A21f and A958r) were used. The cloned 16S rDNA gene fragments were amplified and analyzed by using two different restriction enzymes, *Msp*I and *Hae*III. Based on the RFLP patterns, the clones from both 16S rDNA clone libraries were divided into 15 groups. One clone from each group was selected for sequencing and phylogenetic analyses.

RESULTS. Our results revealed that both samples were occupied by populations of the family *Halobacteriaceae*. As shown in Fig. 1., the 16S rRNA gene sequences recovered from the two studied samples were grouped in nine clusters. Clusters I, II, III and V were formed by sequences that had no close affiliation with any cultivated member of *Archaea*. The closest relative to the sequences 10EY-Ar102 and 7EY-Ar14 from the cluster I was the uncultured haloarchaeon WN-HAS 17 found in sediments of a hyper saline lake of Wadi an Natrun in Egypt [1]. Cluster II included the largest number of clones which were affiliated with another uncultured haloarchaeon DIE1 and which was found in a heap of a potassium mine in Germany [2]. Clusters IV and VI contained the cultured archaeal representatives *Halosimplex carlsbadense* 2-9-1 and *Haloplanus natans*, respectively. The latter was found in Dead Sea/Red Sea water mixtures in an experimental outdoor pond [3]. One sequence (10EY-Ar57) together with *Natronobacterum sp*. 2-24-1formed cluster VII. Two sequences retrieved from the sample 10EY were allied with *Halobacterium halobium* into cluster VIII. Our first isolate was also situated into this cluster, called *Halobacterium sp. UJ-EY-1*, cultivated in an enrichment culture from the studied samples [5]. Interestingly, it was demonstrated that a strain from the species *Halobacterium halobium* accumulates uranium extracellulary on the cell surface [4].
Into the last cluster IX, 21 clones were affiliated with *Halosimplex carlsbadense* 2-9-1. The explanation for this very surprising grouping is the finding of Vreeland et al. [6] who found that this halophilic archaeon, in contrast to

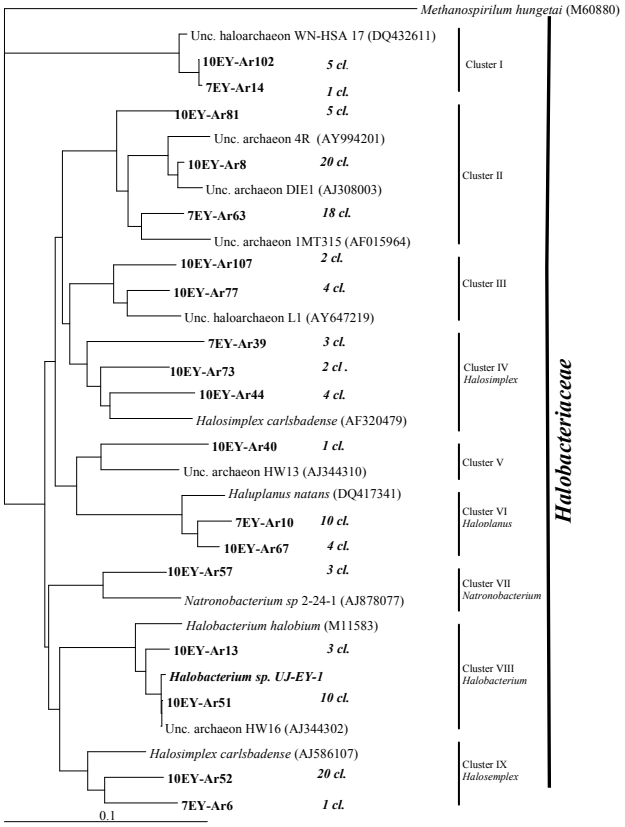

Fig 1: Phylogenetic tree of archaela 16S rRNA gene sequencer retrieved from the studied samples. The scale represents a 10% nucleotide sequences difference.

the majority of all the studied microorganisms, has three dissimilar 16S rRNA genes. Two of them showed only 97% similarity to each other and the third gene possesses only 92-93% similarity to the other two. This unusual microorganism was isolated from unsterile salt crystals from a 25-million-year old Salado in a formation in southeaster New Mexico [6].
Efforts to culture more representatives of the above described haloarchaeal groups found in the studied hyper saline environments are in progress in our laboratory. Studies on the interactions with radionuclides of such isolates are of importance for the risk assessments of the possible perspective to deposit radioactive wastes in hyper saline geological formations.

ACKNOWLEDGEMENTS. This work was supported by grant SMWK4-7531.50-04-844-08/2 by Saxonian Ministry of Science and Arts, Dresden, Germany. We thank Dr. I. Soares and O. Gillow (University of the Negev, Israel) for their help in collecting the samples 7EY and 10EY.

REFERENCES

[1] Mesbah, M. N. et al. (2007) *Microb. Ecol.* **54**, 598-617.
[2] Ochsenreiter, T. et al. (2002) *Extremophiles* **6**, 267-274.
[3] Bardavid, R. E et al (2007) *Int. J. Syst. Evol. Microbiol.* **57**, 780-783.
[4] Francis, A. J. et al. (2004) *Radiochim. Acta* **92**, 481-488.
[5] Jankowski, U. et al. (2009) this report, p. 35.
[6] Vreeland, R. H. et al. (2002) *Extremophiles* **6**, 445-452.

Characterization of a *Halobacterium* sp. isolate cultivated from samples collected from Arava Desert

U. Jankowski, K. Flemming, S. Selenska-Pobell

The Arava Desert is a hostile oligotrophic, extremely dry and hyper saline environment in Israel. Such environments are usually inhabited by microorganisms called extremophiles. In this study, an extreme halophilic Archaeon was cultivated from sand samples of the Arava Desert. The interactions of this archaeal isolate with radionuclides will be studied in the next future. Such studies are important because saline environments are perspective sites for deposition of radioactive wastes.

EXPERIMENTALS. The Arava Desert is a part of the Great African Rift Valley located between the Gulf of Eliat and the Death Sea. The sand contains high salt concentrations because of the geographical location of the desert. Two sand samples were used for the preparation of enrichment cultures of halophilic microorganisms – 8EY collected from the surface of the salt crust and 11EY from a depth of 0-3 cm. These samples represented portions of the samples 7EY and 10EY [1] but instead at −20 °C they were stored at room temperature in order to avoid lysis of the indigenous microorganisms by the freezing.
The resuscitation of the microbes in the samples was performed in the following way: Portions of 3.5 g from each sample were homogenized with a sterile pestle. 1 g fractions of the crushed material were transferred into two sets of three parallel screw-capped centrifuge tubes filled with 100 mM MOPS buffer, containing 2, 3 or 4 M NaCl, and 100 mM $MgSO_4 \cdot 7H_2O$, 50 mM KCl, 2 mM $CaCl_2 \cdot 2H_2O$, and 0.1 vol.-% trace elements solution ($(Fe(NH_4)_2(SO_4)_2 \cdot 6H_2O$, $CuSO_4 \cdot 5H_2O$, $MnSO_4 \cdot H_2O$ and $ZnSO_4 \cdot 7H_2O$). All samples were mixed gently for 5 min. Afterwards, they were placed at 12 °C over night. 300 µL of the resuscitations mixtures were spread on agar plates, containing modified R2A medium supplemented with 2, 3 or 4 M NaCl and adapted for halophilic microorganisms [2]. The plates were incubated at 37 °C and checked for growing every week. Individual microbial colonies were separated by plating on freshly prepared agar plates and finally analysed by using light microscope (Olympus BX61) and molecular methods.
Total DNA from the cultured isolates was recovered according to [3] and 16S rRNA gene analysis was performed as described earlier [1].

RESULTS. The first microbial colonies of the 8EY and 11EY samples appeared after 3 weeks on the plates containing 4 M NaCl. One week later, colonies were grown on the plates with 3 M NaCl. In Fig. 1 a picture of one of the cultivated enrichment cultures on an agar plate is shown. The colonies were colored from white/beige to deep red which can be seen as white/light gray and black stains. The form of the colonies was mainly circular, and nearly all colonies were surrounded by a slimy shape.
For a better characterization, of the microbes they were cultivated in the corresponding liquid medium (without agar). The light microscopic analyses demonstrated that one of the cultured organisms called *Halobacterium sp.* UJ-EY-1 was rode shaped with a length of about 2 µm and a width of about 0.5 µm (Fig. 2).

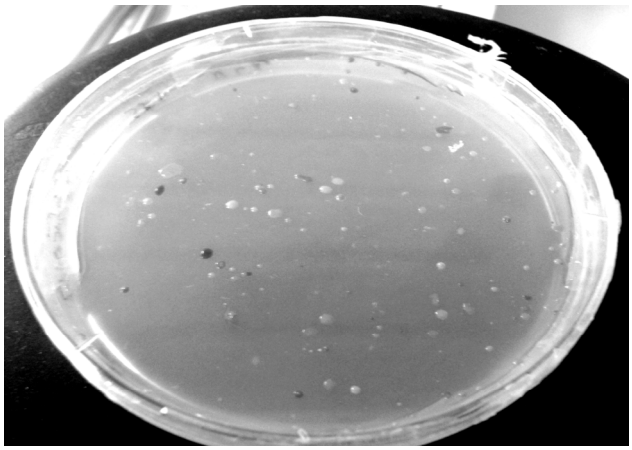

Fig. 1: Agar plate with 4 M NaCl after 9 weeks of cultivation.

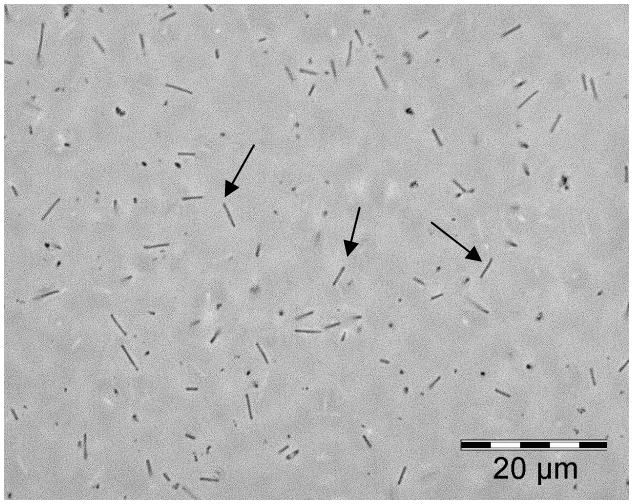

Fig. 2: Microscopic picture of a liquid culture (4 M NaCl) containing the isolate ***Halobacterium sp. UJ-EY-1*** (arrows)**.**

The analysis of the 16S rRNA gene of this organism and of 30 additional orange colonies demonstrated that they all belong to a novel species of the genus *Halobacterium* with 96% of 16S rRNA identity to *Halobacterium halobium* and *Halobacterium salinarum* [4].
Interestingly, one of the predominant 16S rRNA sequences found by using direct molecular analyses of the same samples [1] shared 99% of identity with the gene of the isolate *Halobacterium* sp. UJ-EY-1. This finding indicates that the populations of this archaeal species play an important role in the studied habitat. It was demonstrated that *Halobacterium halobium* accumulates considerable amounts of uranium [5]. The capability of the newly described strain, representing a novel species, to interact with U will be studied in the next future.

REFERENCES

[1] Buchvarova, V. et al. (2009) this report, p. 34.
[2] Robinson, J. L. et al. (2005) *J. Bacteriol.* **187**, 923-929.
[3] Nedelkova, M. et al. (2007) *FEMS Microb. Ecol.* **59**, 694-705.
[4] Gruber, C. et al. (2004) *Extremophiles* **8**, 431-439.
[5] Francis, A. J. et al. (2004) *Radiochim. Acta* **92**, 481-488.

Interactions of *Sulfolobus acidocaldarius* with U(VI) as estimated by EXAFS and TRLF spectroscopic analyses

T. Reitz, M. Merroun, S. Selenska-Pobell

The structural parameters of the U(VI) complexes formed by the cells of the crenarchaeon *S. acidocaldarius* at acidic conditions were investigated by using extended X-ray absorption fine structure (EXAFS) spectroscopy and time-resolved laser-induced fluorescence spectroscopy (TRLFS). The results demonstrate that the cells of this archaeal strain bind U(VI) mainly through organic phosphate groups.

Microorganisms are known to play an important role in the migration behavior of uranium in the environment [1]. In contrast to the well studied interactions of bacteria with uranium, little is known about the processes implicated in the complexation of this radionuclide by representatives of the second microbial domain of life, the "*Archaea*".

EXPERIMENTAL. *S. acidocaldarius* was cultivated at pH 2.5 and 70 °C in a mineral salt medium [2] supplemented with 0.1% tryptone and 0.005% yeast extract. Cells grown to the late exponential phase were harvested by centrifugation and washed twice with 0.1 M $NaClO_4$. Three parallel cell suspensions were prepared with pH 1.5, 3.0 and 4.5. They were shaken at room temperature in 10 mL uranium solution (0.5 mM $UO_2(NO_3)_2 \cdot 6H_2O$, pH 1.5, 3.0, 4.5). The sample preparation and the set-up of the X-ray absorption spectroscopic measurements were performed as described earlier [3]. For TRLFS analyses, U(VI) spectra were recorded between wavelengths of 444 and 594 nm with an excitation at 410 nm.

RESULTS. Quantitative fit results of the EXAFS data indicated that at all acidic conditions studied (pH 1.5, 3.0, 4.5) the adsorbed U(VI) has the common linear trans-dioxo structure: two axial oxygen atoms at about 1.76-1.79 Å, and an equatorial shell of 4 to 6 oxygen atoms at 2.29-2.30 Å. The U–Oeq_1 bond distance is within the range of previously reported values for phosphate bound to uranyl [4,5]. The FT spectra of the U-treated microbial samples contain a FT peak at about R + Δ ~ 2.3 Å, interpreted as a contribution from oxygen neighbors (Oeq_2). The fourth FT peak, which appears at R + Δ ~ 3 Å (radial distance R = 3.58-3.62 Å) is a result of the back-scattering from phosphorus atoms. This distance is typical for a monodentate coordination of U(VI) by phosphate [4,5]. The phosphate groups implicated in the coordination of U could have organic origin since the EXAFS spectrum shows high similarity to those resulting from the uranium complexes with organic phosphate groups, e.g. fructose phosphates as shown in Fig. 1. At pH 4.5, a high Debye-Waller factor of the U–Oeq_1 shell was calculated. This suggests the existence of more than one oxygen atom bond in the equatorial plane. The shell may be split into a shorter U–Oeq_1 distance, from the back-scattering contribution of phosphate oxygen(s) in a monodentate binding mode, and a longer bond distance from oxygen(s) of hydroxyl or carboxyl groups.

To confirm these results TRLFS studies were performed. Figure 2 shows the fluorescence spectra of the U(VI) complexes build by the cells of *S. acidocaldarius* at pH 3.0 and 4.5, respectively.

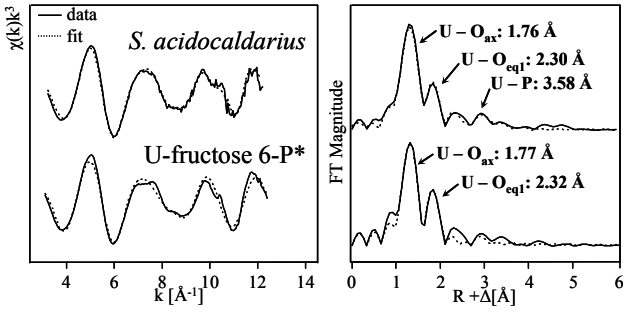

Fig. 1: Uranium L_{III}-edge k^3-weighted EXAFS spectra (left) and corresponding Fourier transforms (right) of the U(VI) complexes formed by *S. acidocaldarius* at pH 4.5 and those of the reference compound U-fructose 6-P[6].

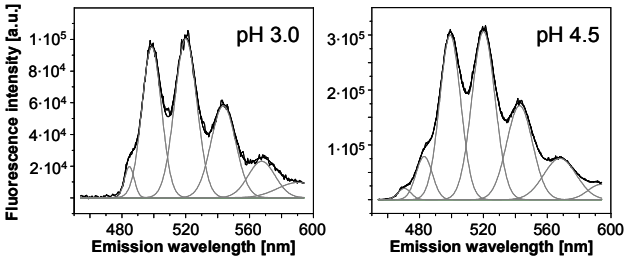

Fig. 2: TRLF spectra of the U(VI) complexes formed by the cells of *S. acidocaldarius* at pH 3.0 (left) and pH 4.5 (right). Displayed spectra were recorded after a delay time of 100 ns.

Tab. 1: Fluorescence emission maxima of the measured TRLFS spectra.

pH	Fluorescence emission maxima [nm]*					
1.5		483.6	**498.3**	**520.3**	**543.6**	569.2
3.0		484.7	**498.7**	**520.0**	**543.6**	567.6
4.5	470.4	482.9	**499.2**	**520.0**	**542.7**	568.0

*: Main fluorescence emission bands were pointed out by bold letters.

The presented fluorescence spectra, as well as the spectrum of the sample incubated at pH 1.5 (not shown), exhibit characteristic fluorescence emission maxima of U(VI) coordinated to phosphate groups (Tab. 1) as it was determined from the complexation of U(VI) by phospholipids [7] as well as by sugar phosphates [6]. Time-resolved analyses (not shown) demonstrated the presence of at least two U(VI) fluorescence lifetimes in all samples. This indicates at least two complexation sites or modes that cannot be distinguished by their fluorescence emission maxima. In accordance to the EXAFS data, the spectrum of the sample incubated at pH 4.5 differed significantly. An extra fluorescence peak was observed at a wavelength of 470.4 nm which indicates the formation of an additional U(VI) complex.

ACKNOWLEDGEMENTS. We acknowledge the assistance of Dr. G. Geipel (TRLFS) and the ROBL group at the ESRF, Grenoble, France (EXAFS).

REFERENCES

[1] Pedersen, K. et al. (2005) *J. Nucl. Radiochem. Sci.* **6**, 11-15.
[2] Brock, T. D. et al. (1972) *Arch. Microbiol.* **84**, 54-68.
[3] Reitz, T. et al. (2008) *Uranium, Mining and Hydrogeology*, p. 703-710, Springer-Verlag, Berlin.
[4] Hennig, C. et al. (2001) *Radiochim. Acta* **89**, 625-631.
[5] Merroun, M. et al. (2003) *Radiochim. Acta* **91**, 583-591.
[6] Koban, A. et al. (2004) *Radiochim. Acta* **92**, 903-908.
[7] Barkleit, A. et al (2008) *Dalton Trans.* **21**, 2879-2886.

Complexation of uranium(VI) with peptidoglycan

A. Barkleit, H. Moll, G. Bernhard

We investigated the interaction of the uranyl cation (UO_2^{2+}) with peptidoglycan (PG) from *Bacillus subtilis* in aqueous solution by using potentiometry and time-resolved laser-induced fluorescence spectroscopy (TRLFS). With both methods, we determined three UO_2^{2+} PG complexes: Two complexes with carboxyl coordination, and a third one with additionally amino or hydroxyl coordination.

Bacteria are very important for the bioremediation of the environment because they are able to adsorb radionuclides and other heavy metals. Peptidoglycan is the main part of the cell wall of Gram-positive bacteria. It consists of polysaccharides chains, which are cross-linked with tetrapeptide strings [1]. The main binding sites for heavy metal ions are carboxyl, hydroxyl, and amino groups.

EXPERIMENTAL. Peptidoglycan (PG) from *B. subtilis* was purchased from Fluka. All experiments were carried out under inert gas atmosphere (nitrogen). For potentiometric titrations, 0.1 g/L PG and 10^{-4} mol/L UO_2^{2+} were used. The solutions were acidified with $HClO_4$ to obtain a starting pH of about 4 and titrated with NaOH. TRLFS spectra were measured at fixed UO_2^{2+} concentration of 10^{-5} mol/L and varying PG concentration of 0.01 to 0.2 g/L at pH 2.5 and 4.0, and at fixed PG concentration of 0.1 g/L with varying pH between 2.0 and 9.0. The experimental equipment and the analysis of the data was the same as described in [2].

RESULTS. The potentiometric titrations of the pure biomacromolecule PG resulted in three different functionalities. We could distinguish two different carboxylate groups of the peptide strain. For amino and hydroxyl groups only a cumulative constant could be calculated. The deprotonation constants, site densities and the assignment to the appropriate functionalities are summarized in Table 1.

The potentiometric titrations of the uranyl PG complex mixture results in three different complexes, the 1 : 1 and 1 : 2 uranyl carboxyl complexes R–COO–UO_2^+ and $(R–COO)_2–UO_2$, and one with additional amino or hydroxyl coordination ($R–COO–UO_2^{(+)}–A_i–R$; $A_i = NH_2$ or O^-). The stability constants are listed in Table 2.

The TRLFS measurements of the uranyl PG system in dependency of pH are depicted in Fig. 1. Between pH 2.0 and 3.0 a slight decrease of the luminescence intensity, connected with a strong red shift of the peak maxima of about 8 nm can be observed. Above pH 3.0 up to pH 5.6 the luminescence intensity increases again (Fig. 1A). From pH 5.6, the luminescence intensity decreases once more (Fig. 1B). For comparison, the luminescence spectra of uranyl at pH 2.0 (UO_2^{2+}(aq)) (Fig. 1A) and pH 6.2 (Fig. 1B) are included. The changes in the luminescence spectra implicate that three complexes are formed: one, which occurs at low pH with a lower luminescence intensity than the free uranyl ion, a second one with a higher luminescence intensity, which dominates until pH 5.6, and a third one, which appears from pH 5.6 and shows no luminescence properties. The two measurement series at fixed pH 2.5 and 4.0 and with varying PG concentration confirmed these observations. The time-resolved measurements gave the same information: one uranyl PG complex with a luminescence lifetime of 7.3 ± 1.4 µs begins to form at pH 3 ($R–COO–UO_2^+$), but will be overlapped soon by a second uranyl PG complex with stronger luminescence intensity and a luminescence lifetime of 0.7 ± 0.1 µs ($(R–COO)_2–UO_2$). A third complex, which appears at pH about 6, shows no luminescence properties ($R–COO–UO_2^{(+)}$-A_i–R; $A_i = NH_2$ or O^-).

The peak maxima of the two complexes with luminescence properties were calculated to be 466, 482, 518, 539, 566, and 595 nm (both).

The stability constants were calculated with the computer program SPECFIT™. They are summarized in Table 2.

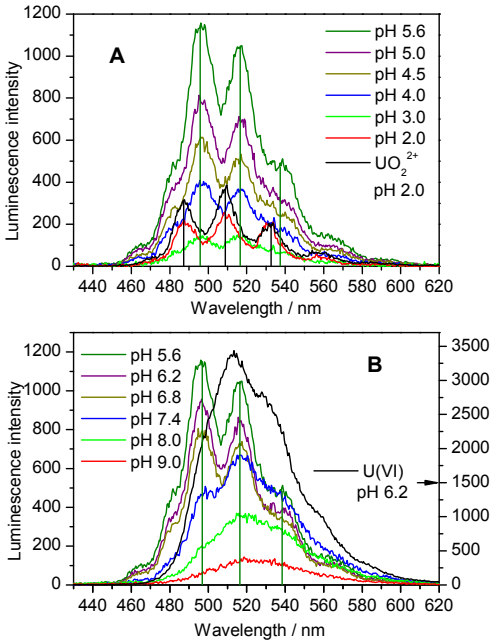

Fig. 1: Luminescence spectra of 10^{-5} M U(VI) with 0.1 g/L PG in dependency of pH. A: pH = 2.0 to 5.6; B: pH = 5.6 to 9.0.

Tab. 1: Calculated pK_a values and site densities from potentiometric titration for PG from *B. subtilis* (25 ± 1 °C, 0.1 M $NaClO_4$).

pK_a	Site density /mmol (g PG)$^{-1}$	Functionality
4.21 ± 0.07	0.62 ± 0.19	Carboxyl
6.01 ± 0.11	0.82 ± 0.09	Carboxyl
9.72 ± 0.20	3.05 ± 0.60	Amine / hydroxyl

Tab. 2: Calculated complex species and stability constants of the uranyl PG system (25 ± 1 °C, 0.1 M $NaClO_4$).

Species	log β	Method
$R–COO–UO_2^+$	5.17 ± 0.06	Potentiometry
	5.31 ± 0.32	TRLFS
$(R–COO)_2–UO_2$	10.13 ± 0.20	Potentiometry
	10.26 ± 0.17	TRLFS
$R–COO–UO_2^{(+)}–A_i–R$	13.75 ± 0.24	Potentiometry
($A_i = NH_2$ or O^-)	13.37 ± 0.38	TRLFS

ACKNOWLEDGEMENTS. This work was funded by the BMWi under contract number 02E9985.

REFERENCES

[1] Johnson, K. J. et al. (2006) *Geochim. Cosmochim. Acta* **70**, 5075-5088.
[2] Barkleit, A. et al. (2008) *Dalton Trans.* 2879-2886.

Transport and accumulation of fluorescent nanoparticles in biofilms

S. Brockmann,[1] T. Arnold, E. Krawczyk-Bärsch
[1]Dresden University of Technology, Dresden, Germany

The transport of nanoparticles through a multispecies biofilm was studied by confocal laser scanning microscopy (CLSM) using fluorescent nanoparticles with a diameter of 1 µm. The particles were mostly found as agglomerates in pores and open water-channels.

The interaction of nanoparticles with microorganisms associated in biofilm communities is an important issue for assessing the surface and subsurface transport behavior of heavy metal containing colloidal particles in the environment. Such metal-laden nanoparticles could possibly be immobilized in biofilms and hence, may help to avoid the dispersion of such metals in the environment.

EXPERIMENTAL. The fluorescent nanoparticles (Invitrogen, Eugene, U.S.A.) used in this study were carboxylate-modified microspheres referred to as "FluoSpheres Blue". These spherical particles show a diameter of 1.0 µm. The biofilm used in our studies was a multispecies biofilm, grown in an annular rotating biofilm reactor, similar to the reactor type described by Lawrence et al. [1]. The biofilm cultivation is described in details by Krawczyk-Bärsch et al. [2]. The glass slide with the biofilm was removed from the reactor and positioned in a flow-through cell. During the experiment, 40 mL of the culture media with the added microspheres was pumped through the flow cell in a closed circuit. The microspheres were added to a final concentration of $5 \cdot 10^{10}$ particles/L. The pump was stopped after 96 h of circulation. The biofilm was then taken out of the flow cell and stained with Syto59, a red fluorescent nucleic acid stain to visualize bacterial cells in the biofilm. Fluorescence microscopic investigations were performed with a CLSM (Leica TCS SP2) using an excitation wavelength of 364 nm for the FluoSpheres Blue particles and 633 nm for the Syto59 fluorescent dye, respectively. Details on the CLSM system and the lasers are summarized in [3]. Subsequently, the generated images or images-stacks were analyzed using Imaris 6.0 (Bitplane, Zürich, Switzerland).

Tab. 1: Excitation and emission wavelengths of the microspheres and the fluorescent dye.

	Excitation Optimum/used [nm]	**Emission** [nm]
Blue particles	365 / 364	415
Syto59	622 / 633	645

RESULTS. To see if the particles were agglomerated, the FluoSpheres Blue were visualized by the CLSM system prior to the addition to the biofilm. A fluorescence image of the particles is shown in Fig. 1. It shows that most particles exist as individual particles and that there were hardly any agglomerates. The biofilm through which the culture media, including the fluorescent nanoparticles, was pumped through for 96 h was investigated by CLSM. The distribution of the fluorescent particles in a three-dimensional representation is shown in Fig. 2. It shows the stained bacterial cells in red color as iso-surface and the FluoSpheres Blue particles in green color.

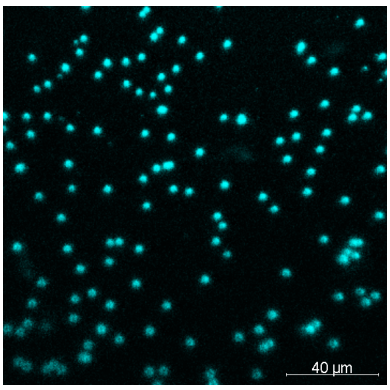

Fig. 1: FluoSpheres Blue, sphere diameter 1 µm.

The FluoSpheres Blue particles are mostly situated as single particles in the open water channels around the biofilm or as agglomerated particles on the biofilm surface (biofilm-water interface). Only a very small number of particles were observed within the EPS-matrix, indicating that the particle dimension of 1 µm in diameter was too big to freely penetrate the microbial agglomerates surrounded by EPS matrix. However, the used particles were useful to visualize pores and water-channels in the biofilm.

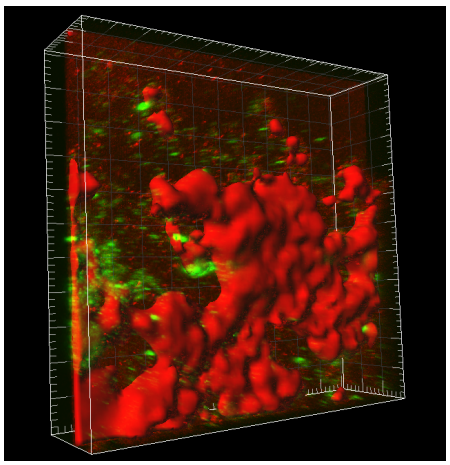

Fig. 2: Three-dimensional image of the biofilm (red iso-surface) with the Blue particles (fluorescence pictured in green).

For a better understanding of the transport behavior of nanoparticles in biofilm systems, further studies using smaller particles are required. Such smaller particles may penetrate the dense EPS matrix surrounding the microbial cells.

ACKNOWLEDGEMENTS. The authors thank S. Aleithe for her assistance with the experiments and the German Research Council (DFG AR 584/1-1) and the Projektträger Jülich (03NUK002F) for financial support.

REFERENCES

[1] Lawrence, J. R. et al. (2000) *J. Microbiol. Methods* **42**, 215-224.
[2] Krawczyk-Bärsch, E. et al. (2008) *Geochim. Cosmochim. Acta* **72,** 5251-5265.
[3] Großmann, K. (2008) Thesis, Dresden University of Technology, Dresden.

Stress response to U(VI) of biofilms from a microbial suspension from a uranium tailing

E. Krawczyk-Bärsch, T. Arnold, S. Hofmann[1]

[1]Institute of Microbiology, Dresden University of Technology, Dresden, Germany

Oxygen concentration and redox potential profiles were measured in a biofilm from a microbial suspension before and after the exposure to uranium by electrochemical microsensors. Before the addition of uranium to the biofilm the high metabolic activity of the aerobe microorganisms and the reduction processes of anaerobic microorganisms have led to a high oxygen consumption rate and to a decrease of the redox potential. After the exposure to uranium in ecologically relevant concentration the microorganisms used mechanisms for the maintenance of the physiological function of the cells. The metabolic activity of the microorganisms was reduced and the redox potential showed very high values from the top to the bottom of the biofilm.

EXPERIMENTAL. In cooperation with the Dresden University of Technology, soil samples were taken from four different levels from a uranium tailing with an averaged uranium concentration of 100 mg/kg. The mixture has been suspended by adding a physiological saline solution. Afterwards, the suspension was transferred in an annular biofilm reactor and exposed to a special nutrient solution for soil extracts under sterile conditions and at room temperature (20 °C). The nutrient solution was pumped through the biofilm reactor with a flow-rate of 15.2 mL/min. After some months, a biofilm with a thickness of approximately 500 µm has been cultured on the slides. The biofilm-coated slides were removed from the reactor and transferred in a flow cell where concentration profiles of oxygen and redox potential versus biofilm depths were measured by electrochemical microsensors. The measurements were limited to a short period of some hours to avoid changes of the microbial diversity of the biofilm when measuring under non-sterile conditions. The used sensors had a tip diameter of 10 µm and were slowly moved downward in 20 µm steps in the x-axis by a motor-driven micromanipulator.

To obtain kinetic information on the microbial response to uranium the nutrient solution, which was pumped through the flow cell, was fed with $UO_2(ClO_4)_2$ to adjust a total uranium concentration in ecologically relevant concentration ($1 \cdot 10^{-5}$ M). The first microprofile in this biofilm was recorded 4 hours after the addition of uranium. Over a period of 5 days, the changings of the oxygen concentration and redox potential were studied in certain time intervals.

RESULTS. Before expososure to uranium, both the oxygen concentration and the redox potential are decreasing in a similar way with increasing biofilm depth (Figs. 1,2). At a depth of approximately 400 µm, no oxygen was detectable anymore and the redox potential reached its lowest value (Figs. 1,2). It can be assumed that in the upper zone of 400 µm the high metabolic activity of the aerobe microorganisms and the reduction processes of anaerobic microorganisms have led to a high oxygen consumption rate and to a decrease of the redox potential. After the addition of uranium in ecologically relevant concentration, the metabolic activity of the microorganisms was reduced dependent on time. Already 50 hours after the exposure to uranium, relatively high oxygen concentrations have been detected in the upper as well as in the lower zone of the biofilm (Fig. 1). The redox potential showed a similar behavior with very high values from the top to the bottom of the biofilm (Fig. 2). We assume that the bacteria, which were isolated from the radionuclide loaded habitat Seelingstädt and cultured in the laboratory under sterile condition, hold a multitude of mechanisms of detoxification and strategies to survive. During the exposure to uranium, these mechanisms maintain the physiological function of the cells.

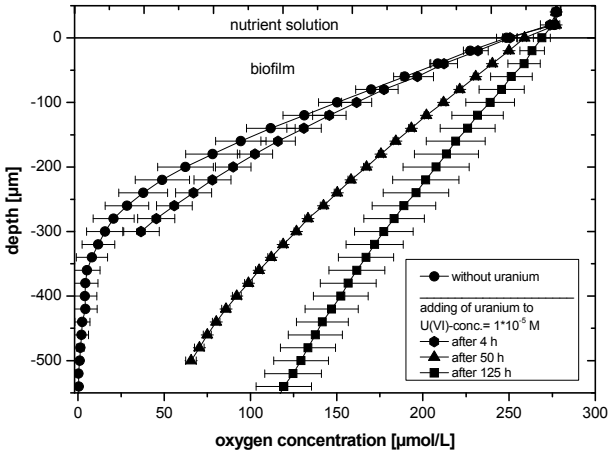

Fig. 1: Oxygen concentration profiles in a biofilm from a microbial suspension before and after the addition of uranium.

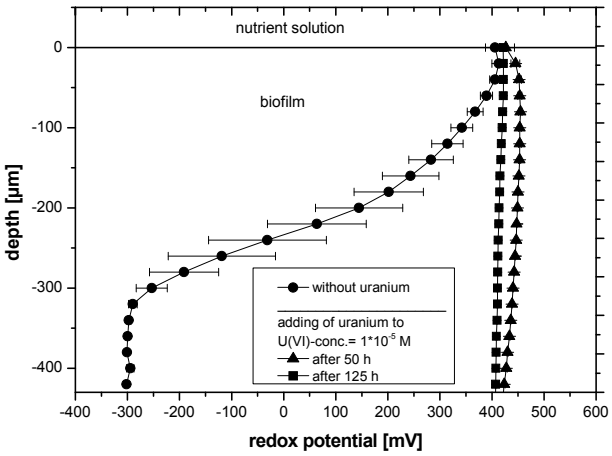

Fig. 2: Redox potential profiles in a biofilm from a microbial suspension before and after the addition of uranium.

ACKNOWLEDGEMENTS. Funding by the German Research Council (DFG) under the Contract No. AR 584/1-1 and by the EU within the FUNMIG project is gratefully acknowledged.

Investigation of the U(VI) interaction with metabolic active green algae *Chlorella vulgaris*

M. Vogel, A. Günther, J. Raff

The green alga *Chlorella vulgaris* has the ability to bind high amounts of U(VI) depending on pH and speciation in the growth medium. The uranium removal by metabolic active algae is almost complete at pH 4.4 in mineral medium whereas at pH 7.1 in tap water only 30% of the uranium was removed. Laser-induced fluorescence spectroscopy was used for the characterization of the uranyl species in solution and in/on algal biomass.

The aim of this study was to characterize the molecular structure of the U(VI) complexes formed on/in metabolic active *C. vulgaris* cells using time-resolved laser-induced fluorescence spectroscopy (TRLFS) and the quantitative analysis of the sorption process under the given experimental conditions.

EXPERIMENTAL. Living algal cells were resuspended in tap water or mineral medium [1]. The sorption experiments started with a biomass concentration of 0.76 g algae dry weight/L and an initial uranium concentration of $1 \cdot 10^{-4}$ M. A Nd-YAG laser (Minilite, Continuum) with laser pulses at 266 nm and a beam energy of about 250 µJ was used for laser-induced fluorescence measurements on contaminated algal biomass and used media [1]. The uranium concentration in solutions was quantified by ICP-MS analyses (ELAN 9000, Perkin Elmer). Dilution series of the algal culture were streaked on agar plates with solid algal full medium to determine the number of colony forming units in the day of sampling during the sorption experiments [1].

RESULTS. In the mineral medium at pH 4.4 the free uranyl ion (57.2%) dominates the U(VI) speciation. Additionally, UO_2SO_4 (26.8%) and hydroxides (12.1%) are formed in a remarkable amount. In tap water at pH 7.1 uranyl carbonates are the main species with $Ca_2UO_2(CO_3)_3$(aq) (85.1%), $(UO_2)_2CO_3(OH)_3^-$ (9.9%) and $UO_2(CO_3)_2^{2-}$ (2.8%).
Algal cells could remove 87.7% of the uranium from the mineral medium within 96 h. From the tap water, only low uranium amounts were removed by metabolic active algal cells within the same time (30.4% of the initial uranium amount). Differences in the sorption behavior of the metabolic active *C. vulgaris* cells can be explained by the formation of different uranyl species in tap water and mineral medium due to differences in the chemical composition and pH values of the two media [1]. The uranyl species formed in tap water were poorly accumulated by algal cells. In fact, in mineral medium nearly no cells survived (0.03%) because of the high amount of accumulated uranium whereas 26% of the cells survived in tap water (data not shown). This indicates that several uranium species in tap water are not bio-available for the algae. In the case of algal cells incubated in mineral medium, uranium directly affects the viability of the cells.
The uranium species occurring in tap water, mineral medium and bound on the algae were investigated by TRLFS verifying the calculated U(VI) species by determined spectral lines (Fig. 1). The luminescence spectra of the different uranyl species were compared to those cited in literature. Uranyl species were successfully detected on/in the algal biomass grown in mineral medium (M_{Bio}) and in tap water (TW_{Bio}). Uranium remained in the oxidation state VI after the immobilization on algal cells. The spectral lines of the uranyl-algae-complexes M_{Bio} and TW_{Bio} are shifted compared to the maxima of the initial solutions (Fig. 1) indicating the formation of different species accumulated by the algal cells. Between the algal luminescence spectra of the systems M_{Bio} and TW_{Bio} spectral differences occurred. Since the differences are very small, the identification of two different uranyl-algae-complexes has to be verified in future investigations. Under the given sorption conditions, the TRLFS spectral lines of the metabolic active algal biomass demonstrate an interaction of uranium with different complexes on algal cells as it was detected for metabolic inactive algal cells at pH 6 [2] or for higher plants [3]. The results for the uranyl-algae-complexes are comparable to those emission maxima obtained for model uranyl complexes with organic phosphate groups and/or carboxylic ligands [1].

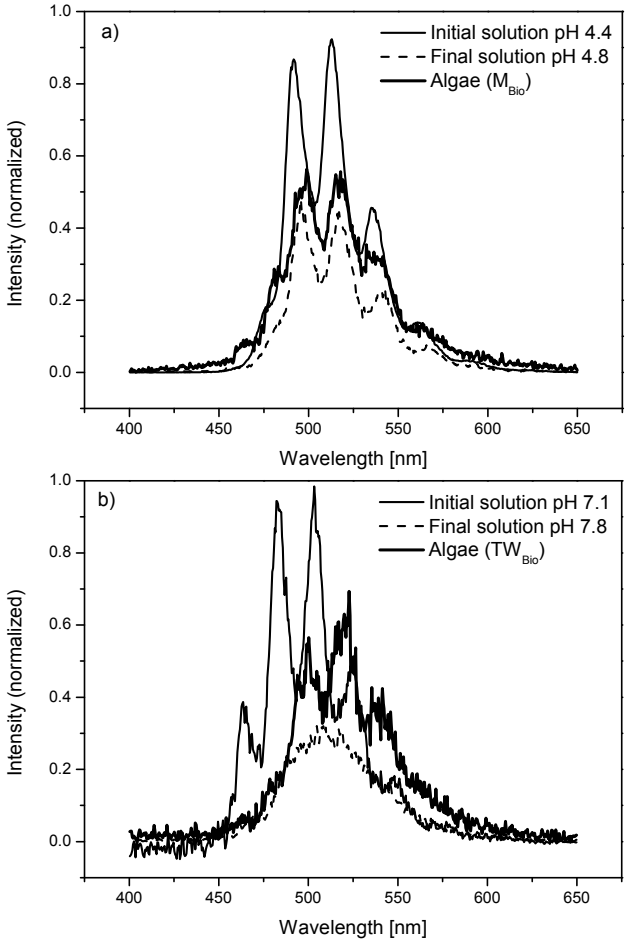

Fig. 1: Luminescence spectra of U(VI)-algal complexes formed in mineral medium (a) and tap water (b), the initial solution with $1 \cdot 10^{-4}$ M U(VI) and the final solution after 96 h contact time.

REFERENCES

[1] Vogel, M. et al. (2008) *Uranium, Mining and Hydrogeology*, p. 693-702, Springer Verlag, Berlin.
[2] Günther, A. et al. (2008) *BioMetals* **21**, 333-341.
[3] Günther, A. et al. (2003) *Radiochim. Acta* **91**, 319-328.

Flavonoids as an example for an extracellular defence mechanism against uranium

K. Viehweger, G. Geipel

Cell suspensions of canola (*Brassica napus*) released flavonoids in their culture medium after contact with the heavy metal uranium (U). Due to a strong complex formation between the flavonoid and the metal this phytoalexin could be a main part of an extracellular defence reaction against U.

EXPERIMENTAL. Acidic hydrolysis was achieved by heating with 2 M HCl under reflux conditions after sequential extraction of cell culture medium with different solvents. Subsequent thin-layer-chromatography (TLC) was performed according to Stahl [1]. Commercially available quercetin was used for absorption spectroscopy.

RESULTS. After U exposure to canola cell suspensions, a time dependent release of fluorescent compounds in the culture medium occurred (Fig. 1). Acidic hydrolysis of the culture medium and subsequent analysis by TLC (detection with Natural Product Reagent A) revealed a strong correspondence with the flavonol quercetin.

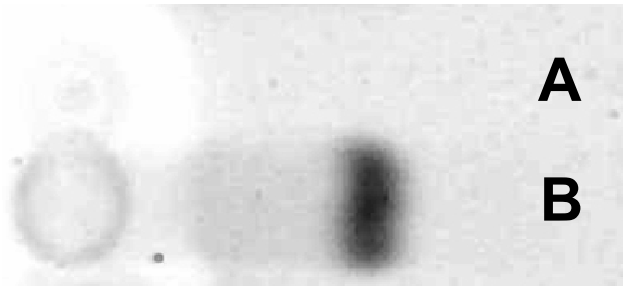

Fig. 1: TLC of culture medium after acidic hydrolysis. (A) before U contact, (B) 15 min. after U contact of cells. Detection with Natural Product Reagent A, fluorescence λ_{ex} 366 nm, inverted image.

Since the excretion of quercetin occurs only in the presence of U (Fig. 1), a complex between the phytoalexin and the metal could probably be formed. Figure 2 shows the decrease of the quercetin absorbance after addition of U. It is crucial for this drop to use the culture medium of cells contacted with U. Hence, we suppose that a further component likely a protein is involved.

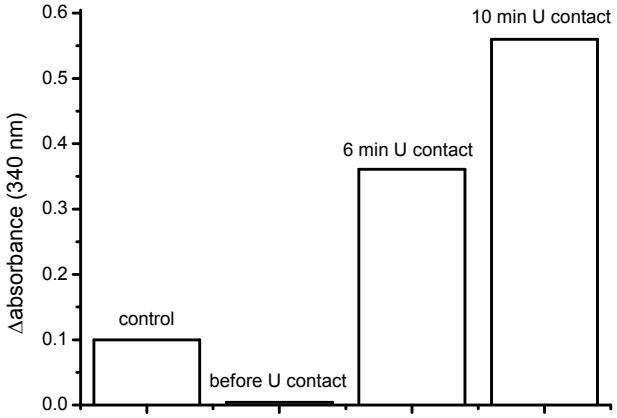

Fig. 2: Shifts of absorbance of quercetin (2 µg/mL) after addition of U (1 mM), control sample contained buffer, other samples contained cell culture medium taken at indicated time points.

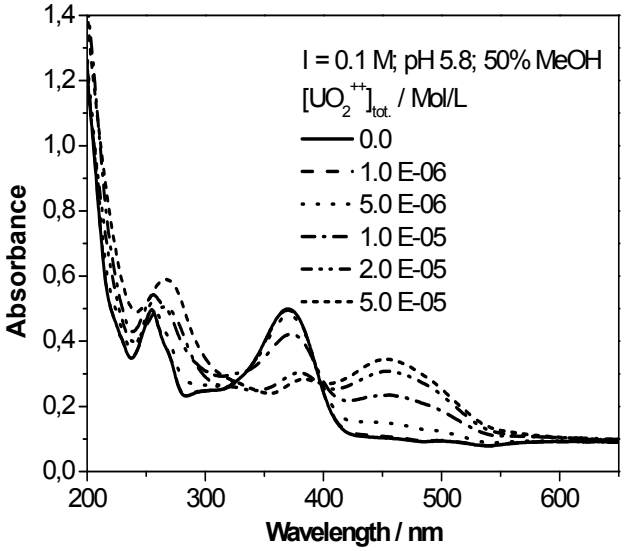

Fig. 3: Absorption spectra of a constant quercetin concentration combined with increasing U concentrations.

Absorption spectroscopy was used for the in-vitro characterisation of the U-quercetin complex. As it could be seen in Fig. 3, there are isosbestic points indicating a clear interaction. Based on this experiments, a stability constant was calculated using factor analysis „Specfit/32™“ (Eq. 1).

$$UO_2^{2+} + C_{15}H_5O_7^{5-} + 3\ H^+ \rightarrow UO_2C_{15}H_8O_7 \qquad (1)$$
$$\log K = 41.4 \pm 0.4$$

Speciation diagrams revealed a dramatic change in the uranium speciation in the mid pH range indicating a predominance of a quercetin-U complex.
Concerning this exorbitant high stability constant and the conversion of quercetin in presence of U, we suppose that extracellular excretion of the flavonoid is a part of an extracellular defence mechanism against U.

ACKNOWLEDGEMENTS. We thank S. Gürtler and G. Grambole for skilled technical assistance.

REFERENCES

[1] Stahl, E. (1967) *Dünnschicht-Chromatographie*, Springer, Berlin.

Actinides (metals) in waste repositories

Uranium(VI) sorption on montmorillonite and bentonite: Prediction and experiments

C. Nebelung, V. Brendler

The sorption of U(VI) on bentonite and montmorillonite was investigated in batch experiments to understand the near-field behavior in geological nuclear waste repositories. The sorption was predicted using thermodynamic data of aqueous and solid species, protolysis data and surface complex constants from literature, and the characterization data of the solids. The predicted and experimental sorption data show a good agreement. With such predictions the sorption experiments can be optimized, verified and reduced.

PREDICTIONS. A scientifically founded description of sorption processes at the mineral-liquid surface is possible with the surface complexation models (SCM), the ion adsorption on surface sites as complexation reaction. We use the diffuse double layer model (DDL) to predict the sorption of uranium on montmorillonite and bentonite. For the modeling, the code MINTEQA2 was used (Version 4.03, US EPA May 2006). Thermodynamic data of aqueous and solid species were taken from the NEA-TDB [3]. The mineral characterization and the respective protolysis data and surface complex constants were calculated for a site density of 2.31 sites/nm^2.
Uranium sorption on montmorillonite and bentonite was calculated with protolysis constants from [4] and surface complex constants from [5] using DDL:

»Al-OH	$pK_1 = 7.98$,	$pK_2 = -9.37$
»Si-OH		$pK_2 = -6.94$
»Si-OH + UO_2^{2+} = »Si-O-UO_2^+ + H^+		logK = 2.34
»Si-OH + 3UO_2^{2+} + 5H_2O = »Si-O-$(UO_2)_3(OH)_5$ + 6H^+		logK = −15.55
»Al-OH + UO_2^{2+} = »Al-O-UO_2^+ +H^+,		logK = 2.35
»Al-OH + 3UO_2^{2+} +5H_2O = »Al-O-$(UO_2)_3(OH)_5$ + 6H^+		logK = −15.29

EXPERIMENTAL. Sorption parameters were determined in batch tests. The sorption on bentonite (MX80) was studied at different pore water compositions referring to the dry bulk densities of the clay (1.3, 1.6, 1.9 g/cm^3), at pH 8 for the U(VI) concentration dependance (10^{-4} to 10^{-9} M). U(VI) sorption experiments were carried out additionally as comparative tests on the pure mineral montmorillonite (Wyoming montmorillonite SWy-2) in 0.1 M $NaClO_4$ (concentration dependance at pH 5.5, pH dependance between pH 3 and 11). Detailed experimental conditions were given in [1,2].

RESULTS. The modeling of the sorption on montmorillonite versus U(VI) concentration (Fig. 1) shows a good agreement of measured and predicted values up to 10^{-5} M. At 10^{-4} M no precipitation is observed, but at 10^{-3} M a small precipitation is possible. A good agreement between measured and predicted values even for the precipitation is achieved in case of sorption on bentonite at all three pore water types (Fig. 2), also correctly reflecting the effect of the changed pore water composition. The prediction of U(VI) sorption on montmorillonite at the pH dependance (Fig. 3) shows also a good prediction. At higher pH the CO_2 equilibrium was not reached (triangles). So we have modeled with the ambient CO_2 (black) up to pH 9.5, from pH 10 with the measured values (grey). After addition of $NaHCO_3$, no precipitation was found (squares).

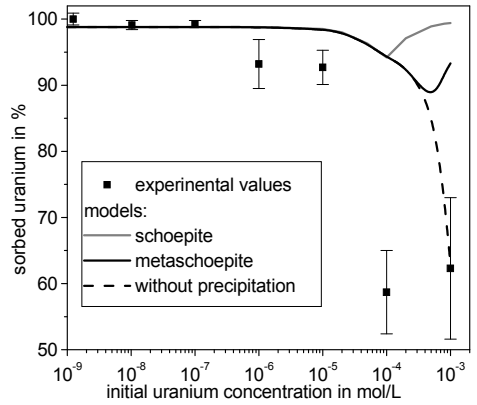

Fig. 1: U(VI) sorption on montmorillonite, concentration dependance.

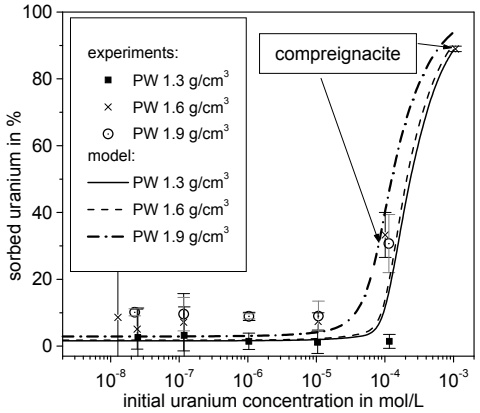

Fig. 2: U(VI) sorption on bentonite, concentration dependance.

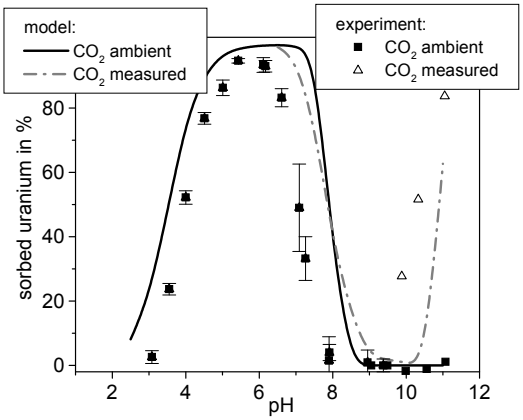

Fig. 3: U(VI) sorption on montmorillonite, pH dependance.

ACKNOWLEDGEMENTS. Funding by the European Commission (NF-PRO C2-ST-C-01) is gratefully acknowledged.

REFERENCES

[1] Nebelung, C. (2006) *Report FZR-443*, p. 40.
[2] Nebelung, C. et al. (2006) *Report FZR-443*, p. 39.
[3] Guillaumont, R. et al. (2003) *Update on the Chemical Thermodynamics of U, Np, Pu, Am, Tc*, Elsevier, Amsterdam.
[4] Pabalan, R. T. et al. (1997) *Aquat. Geochem.* **2**, 203-226.
[5] Pabalan, R. T. et al. (1998) *Adsorption of metals by geomedia*, p. 99-130, Academic Press, San Diego.

K_d values in performance assessment: Effects of scaling based on specific surface areas

V. Brendler, T. E. Payne,[1] C. Nebelung, M. J. Comarmond[1]

[1]Australian Nuclear Science and Technology Organisation, PMB 1, Menai, NSW Australia 2234.

Adsorption processes play an important role in retarding contaminant plumes. Their integration into risk assessments will benefit from normalization with regard to specific surface areas of the sorbent.

Sorption phenomena are often described by conditional distribution coefficients (K_d), which are simplified empirical parameters subsuming many basic processes. It is easy to incorporate them into reactive transport codes but their capability for inter- and especially extrapolation is limited. It seems reasonable that, as sorption is a surface process, K_d should be proportional to the specific surface area (SSA). Furthermore, statistical correlations have been found between K_d and SSA [1]. Thus it has been proposed [2] to normalize K_d values according to Eq. (1):

$$K_a = K_d / SSA \quad (1)$$

DATABASE AND MODELING. Most literature studies involve sorption experiments with a single solid (a small set of solids) across a range of conditions (pH, ionic strength, etc.). Hence, even extensive literature databases may only include a small number of materials with varying SSA. So we focus on uranium for which a larger amount of experimental data is available. The data are summarized in Fig. 1a, showing raw K_d data for the sorption of U(VI) on a number of minerals: hydrous ferric oxide (HFO) [3]; two types of weathered rock [3], montmorillonite [4] and two kaolinite samples [3, 5], measured under similar conditions of ionic strength, U concentration (~1 µM) and across a broad pH range (3-7, in equilibration with air). The U sorption increases from a relatively low amount (< 10%) to nearly total adsorption. This is a similar behavior to a number of other radionuclides and heavy metals in this pH range. In Fig. 1b the same raw data have been converted to K_a values using the relationship in Eq. (1).

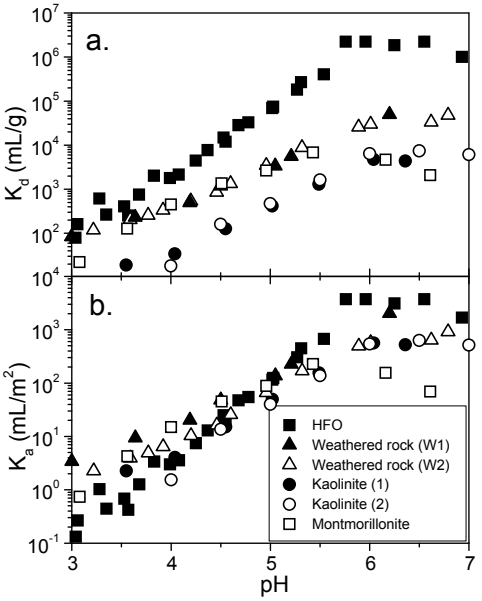

Fig. 1: U(VI) sorption on different minerals on the low pH 'sorption edge' expressed as (**a**) Distribution coefficients (K_d) and (**b**) Surface area normalized distribution coefficients (K_a).

RESULTS AND DISCUSSION. Comparison of Fig. 1a and 1b shows that the recalculation of K_d values as K_a values considerably reduced the scatter in values obtained for U sorption. The K_a curves are much closer together than the K_d curves – the effect of SSA is largely removed by the normalization.

Figure 2 shows the K_a data for the solid materials in comparison to fitted curves obtained by Pabalan et al. [2], but this time across the entire pH range. It is immediately apparent that there is considerably more scatter at the high pH values, although the general trend of [2] is followed. This may be due to experimental parameters which affect the pCO_2 and hence the speciation of U. The K_a data are approximated by the curves for simple oxide minerals (solid line) and complex minerals (zeolites and layer silicates - dotted) presented in [2]. There, the authors suggested an arbitrary correction to superimpose both their fitted curves. But, as the steepness of the low pH-edge for HFO is greater than for the clay systems, these curves will not adequately represent HFO across a wide pH range, regardless of how they are normalized.

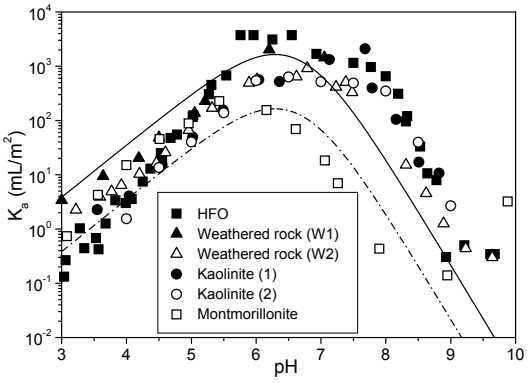

Fig. 2: Comparison of computed K_a values with curves fitted for simple oxides (solid) and layer silicates (dotted) from Pabalan et al. [1998].

CONCLUSION. Sorption is related to specific surface area, and correlations between K_d and SSA are often apparent for sets of experiments under comparable conditions. The concept of normalizing K_d values using the measured SSA of the solid was tested using uranium sorption data obtained in both simple model mineral systems and also more complex materials such as soils or rock assemblages. It was demonstrated that the K_a concept harmonizes various divergent sorption data for uranium reasonably well.

REFERENCES

[1] Payne, T. E. et al. (2009) *J. Environ. Radioact.,* submitted.
[2] Pabalan, R. T. et al. (1998) *Adsorption of metals by geomedia*, Academic Press, p. 99-130, San Diego.
[3] Payne, T. E. (1999) Thesis, University of New South Wales, Sydney.
[4] Křepelová, A. (2007) Thesis, Dresden University of Technology, Dresden.
[5] Nebelung, C. et al. (2007) *Report NF-PRO 2.5.15*., Contract No. FI6W-CT-2003-02389, EC-EURATOM.

Uranium(VI) and humic acid sorption onto kaolinite and opalinus clay

C. Joseph, K. Schmeide, S. Sachs, G. Bernhard

The ternary system U(VI) - humic acid - clay was investigated. The main U(VI) species in the used background electrolyte synthetic opalinus clay pore water is the complex $Ca_2UO_2(CO_3)_3(aq)$. The comparison of opalinus clay with kaolinite shows that kaolinite offers more binding sites for U(VI) as well as for humic acid than opalinus clay.

Beside salt rock and granite rock, also clay is a possible host rock for nuclear waste disposal. Therefore, the investigation of the actinide interaction with natural clay and the determination of the influence of clay organic matter on this system is of high interest. Organic matter, such as humic acid (HA), is known for its ability to bind metal ions. For these experiments, the well studied reference clay kaolinite and, as natural clay, opalinus clay were used.

EXPERIMENTAL. The sorption experiments were performed at room temperature under ambient atmosphere ($pCO_2 = 10^{-3.5}$ atm). Synthetic ^{14}C-labeled HA type M42 [1], kaolinite KGa-1b [2] (BET = 11.7 m^2/g [3]) from the Clay Minerals Society Source Clay Repository and opalinus clay BHE-241 (BET = 42 m^2/g) from the underground rock laboratory in Mont Terri, Switzerland were applied. The background electrolyte was synthetic opalinus clay pore water (pH 7.6, I = 0.42 M, Tab. 1) and the solid-liquid ratio was 4 g/l. The pH was adjusted by addition of dilute HCl or NaOH. The suspensions were equilibrated for 72 h (kaolinite) and 1 h (opalinus clay). The final concentrations of HA in the suspensions were 10 or 50 mg/l and of U(VI) $1 \cdot 10^{-6}$ M. The contact time with U(VI) and/or HA was 2.5 d. The samples were analyzed by ICP-MS and LSC for the final U(VI) and HA concentration, respectively. Prior to the measurements of the U(VI) concentrations in the samples in presence of HA, HA was removed by digestion in a microwave oven.

Tab. 1: Synthetic opalinus clay pore water, pH 7.6, I = 0.42 M [4].

Salt	g/L
NaCl	12.38
KCl	0.120
$MgCl_2 \cdot 6H_2O$	3.457
$CaCl_2 \cdot 2H_2O$	3.793
$SrCl_2 \cdot 6H_2O$	0.136
Na_2SO_4	2.000
$NaHCO_3$	0.040

RESULTS. In a previous study, $NaClO_4$ was applied as background electrolyte of the system U(VI) – HA – kaolinite [3]. Significantly lower amounts of U(VI) adsorb onto kaolinite if opalinus clay pore water is used instead of $NaClO_4$. This difference in the sorption behavior of U(VI) can be explained by its speciation. The speciation of U(VI) in opalinus clay pore water at pH 7.6 shows that about 99% of U(VI) exist as the aquatic complex $Ca_2UO_2(CO_3)_3$ (Fig. 1). This complex is electroneutral and adsorbs supposedly worse than the carbonato/hydroxo species, which exist at pH 7.6 in the $NaClO_4$ system (not shown).
Batch experiments with the two different clays show, that kaolinite adsorbs significantly more U(VI) than opalinus clay. Thus, the U(VI) mobility is higher in the opalinus clay system than in the kaolinite system. Furthermore, opalinus clay is a seemingly somewhat stronger adsorbent for HA than kaolinite. However, taking the higher specific surface of opalinus clay into account (Tab. 2), it can be concluded, that kaolinite is also the better adsorbent for HA. The sorbed HA offers additional binding sites for U(VI) on the clay, thus the amount of sorbed U(VI) increases with increasing HA concentration. The sorption behavior of opalinus clay is unexpected, because amongst others opalinus clay consists of kaolinite and different iron minerals, which are very good U(VI) adsorbents [5]. This phenomenon has to be investigated further.

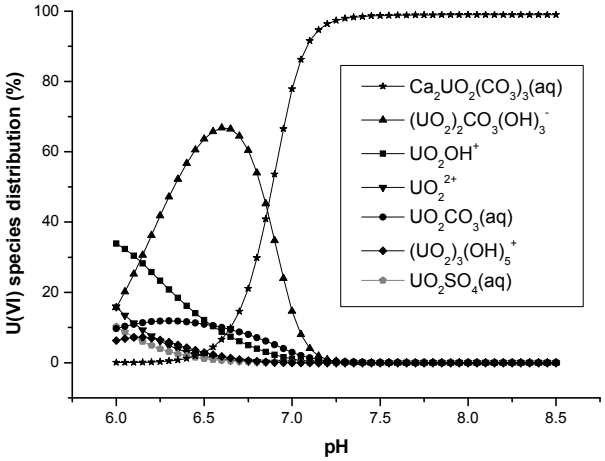

Fig. 1: Speciation of U(VI) ($1 \cdot 10^{-6}$ M) in synthetic opalinus clay pore water ($pCO_2 = 10^{-3.5}$ atm) (only species > 5% are shown).

Tab. 2: U(VI) and humic acid (HA) sorption onto kaolinite and opalinus clay in synthetic opalinus clay pore water (data in µg/m^2 clay).

	Kaolinite		Opalinus clay	
	Sorbed U(VI)	Sorbed HA	Sorbed U(VI)	Sorbed HA
[U] = $1 \cdot 10^{-6}$ M	2.83 ± 0.21	–	0.34 ± 0.01	–
[U] = $1 \cdot 10^{-6}$ M + [HA] = 10 mg/l	2.37 ± 0.22	166.67 ± 4.27	0.30 ± 0.04	40.48 ± 2.38
[U] = $1 \cdot 10^{-6}$ M + [HA] = 50 mg/l	2.49 ± 0.22	451.28 ± 8.55	0.38 ± 0.03	149.52 ± 7.62
[HA] = 10 mg/l	–	161.54 ± 7.69	–	39.05 ± 2.38
[HA] = 50 mg/l	–	376.92 ± 47.86	–	155.48 ± 1.67

ACKNOWLEDGEMENTS. The Federal Ministry of Economics and Technology funded this work (02E10156).

REFERENCES

[1] Sachs, S. et al. (2004) *Report FZR-399*, p. 49.
[2] Pruett, R. J. et al. (1993) *Clays Clay Miner.* **41**, 514-519.
[3] Křepelová, A. et al. (2006) *Radiochim. Acta* **94**, 825-833.
[4] Pearson, F. J. (1998) *PSI Internal report TM-44-98-07*, Paul Scherrer Institut, Villigen, Switzerland.
[5] Schmeide, K. et al. (2000) *Radiochim. Acta* **88**, 723-728.

Characterization of U(VI) sorption complexes onto different TiO_2 samples using *in situ* ATR FT-IR spectroscopy

T. Meusel, K. Müller, H. Foerstendorf

The sorption process of U(VI) onto seven different TiO_2 samples was studied using ATR FT-IR spectroscopy. The influence of both the TiO_2 modification and the specific surface area on the sorption complex was studied.

The assessment of the mobility and bioavailability of heavy metals in the environment requires a comprehensive understanding of the molecular interactions at the solid-water-interfaces. TiO_2 is often used as a model for the investigation of sorption phenomena. [1-3] ATR FT-IR spectroscopy is a convenient technique to characterize sorption complexes *in situ*.

EXPERIMENTAL. The used TiO_2 samples are summarized in Tab. 1. The U(VI) concentration was set to 20 µM at an ionic strength of 0.1 M adjusted by NaCl at pH 5 and normal atmosphere. The ATR FT-IR accessory was described previously. [4]
A thin TiO_2 layer was prepared on the ATR crystal by a five times repeated deposition of 1 µL of a 2.5 g/L TiO_2 suspension. The TiO_2 density on the ATR crystal was approximately 0.1 mg/cm^2. For the *in situ* sorption experiments a flow cell was used to pass the solutions through the TiO_2 film. To equilibrate the oxide film before U(VI) sorption in a 1st conditioning step, a blank solution, i.e., water under the same conditions (pH, ionic strength, temperature) flushed the film for 60 min. The sorption process lasted 90 min, then, a 2nd conditioning step with the same solution as in the 1st step was performed for additional 30 min.

Tab. 1: Characteristics of the TiO_2 samples.

Sample	Origin	Composition	BET in m^2/g
S1	Alfa Aesar	80-90% anatase 10-20% rutile	374
S2	Degussa	86% anatase 14% rutile	56.4
S3	CERAC Inc.	90% rutile 10% anatase	5.20
S4	Tronox	100% rutile	5.88
S5	S3 calcinated	100% rutile	2.19
S6	MTI Corp.	100% anatase	234
S7	Aldrich	91% anatase 9% rutile	9.18

RESULTS. The composition of the TiO_2 samples shows different anatase/rutile ratios. The specific surface area (BET) of the samples ranges from 5 to 380 m^2/g. In general, a high BET area is related to a high fraction of anatase (Tab 1).
Figure 1 shows exemplarily the obtained ATR FT-IR spectra of the three stages during the *in situ* sorption experiments of the sample S6. Since no bands were observed in the difference spectrum of the 1st conditioning stage, the stability of the prepared TiO_2 film on the ATR crystal is confirmed under the given conditions.
Upon U(VI) sorption several bands increase in intensity with time. The band at ~ 900 cm^{-1} is assigned to the antisymmetric stretching vibrational mode (ν_3) of the uranyl ion. Compared to the fully hydrated species UO_2^{2+} in acidic solutions the strong shift of ~ 60 cm^{-1} upon surface

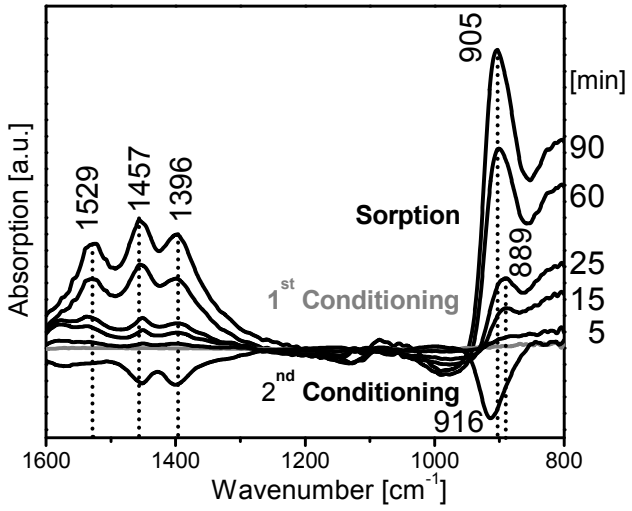

Fig. 1: ATR FT-IR spectra of 20 µM U(VI) sorbed onto TiO_2 (S6, pH 5.0, 0.1 M NaCl). Indicated values are in cm^{-1}.

bonding on TiO_2 suggests the formation of inner-spheric complexes. [2,5] At a lower U(VI) loading, the band is observed at 889 cm^{-1}, but shifts to 905 cm^{-1} when U(VI) concentration on the TiO_2 increases. This might be related to the formation of different surface species. The bands at 1200-1000 cm^{-1} possibly represent rearrangement processes at the TiO_2 surface upon U(VI) complexation. Similar spectral observations are made with other cationic sorbates such as Np(V), Mg(II) and Cs(I) (cf. [6]).
In the 2nd conditioning step outer-spheric, i.e. slightly surface bounded species are presumably flushed out of the pores reflected by a negative band at 916 cm^{-1}.
Up to now, the spectral region above 1300 cm^{-1} can not be accurately interpreted but similar spectral changes have already been observed in the spectra of aqueous actinyl(VI) hydrolysis species. [5] The band at 1396 cm^{-1} seems to be specific for the TiO_2-U(VI) system.
A comparison of the IR spectra of U(VI) sorption experiments onto different TiO_2 samples shows similar results. No great changes of the significant spectral characteristics are observed, indicating similar U(VI) sorption complexes on anatase and rutile However, the signal-to-noise ratio strongly correlates with the specific surface area and, thus, with the amount of sorbed U(VI).
In conclusion, this ATR FT-IR study has shown that U(VI) forms the same molecular complexes on anatase and rutile surfaces. The present work can be used as a reference system of actinide sorption on oxides for further investigations on the scale of international cooperation.

ACKNOWLEDGEMENTS. The authors are grateful to Dr. G. Lefèvre, ENCSP, Paris, F, Dr. J. Comarmond, ANSTO, Menai, AU, C. Eckardt and U. Schaefer.

REFERENCES

[1] Jakobsson, A. M. et al. (1998) *Radiochim. Acta* **82**, 257-262.
[2] Lefèvre, G. et al. (2008) *J.Colloid Interface Sci.* **327**, 15-20.
[3] Vandenborre, J. et al. (2007) *Inorg. Chem.* **46**, 1291-1296.
[4] Müller, K. et al. (2007) *Report FZD-489*, p. 25.
[5] Müller, K. et al. (2008) *Inorg. Chem.* **47**, 10127-10134.
[6] Müller, K. et al. (2009) this report, p. 50.

In situ formation of ternary uranyl(VI) carbonato complexes on ferrihydrite as probed by ATR FT-IR spectroscopy

K. Heim, H. Foerstendorf

The sorption complexes of uranium(VI) on ferrihydrite (Fh) were investigated under inert gas and ambient atmosphere by *in situ* ATR FT-IR spectroscopy. The atmospheric carbon dioxide shows a high affinity to the UO_2^{2+} ions already sorbed to the mineral phase. This implies the formation of ternary surface complexes at the Fh-water interface.

In our previous report of the sorption complexes of U(VI) on Fh, we demonstrated the applicability of ATR FT-IR spectroscopy for the detection of the formation of such complexes [1]. However, the derivation of molecular structures of the sorption complexes can only be given by spectroscopic results from selective modified systems. In this work, we studied the influence of dissolved atmospheric CO_2 on the sorption processes.

EXPERIMENTAL. The experiments were performed as already described [1]. All experiments were carried out using solutions of 50 µM U(VI) chloride at pH 5.5. Preparation of sample and solutions for experiments under inert gas conditions were carried out in glove boxes and were kept under constant conditions during the IR measurements. Infrared spectra were recorded with a Bruker Vertex 80/v instrument using a diamond ATR accessory equipped with a flow cell. Spectral resolution was 4 cm^{-1} and difference spectra were calculated in such a way that positive bands represent the chronologically later spectrum of the sorption process.

RESULTS. The spectra of the U(VI) sorption experiments in inert gas and in ambient atmosphere are shown in Fig. 1A and B, respectively. In both spectra, bands at 903 cm^{-1} with a shoulder around 935 cm^{-1} are observed which can be assigned to the ν_3 stretching mode of the uranyl ion bound to the Fh phase and to surface OH-modes of the iron hydroxide phase, respectively, latter reflecting structural alterations of the Fh-film during the

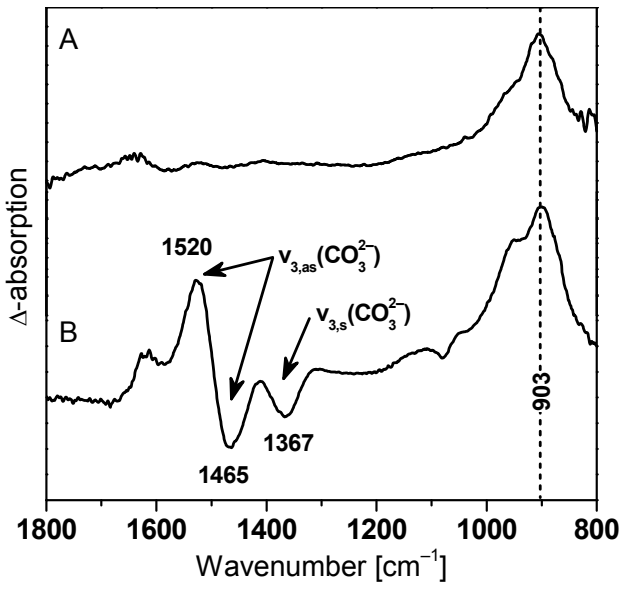

Fig. 1: *In situ* ATR FT-IR spectra of the sorption of 50 µM U(VI) onto Fh under inert gas (A), and in ambient atmosphere (B).

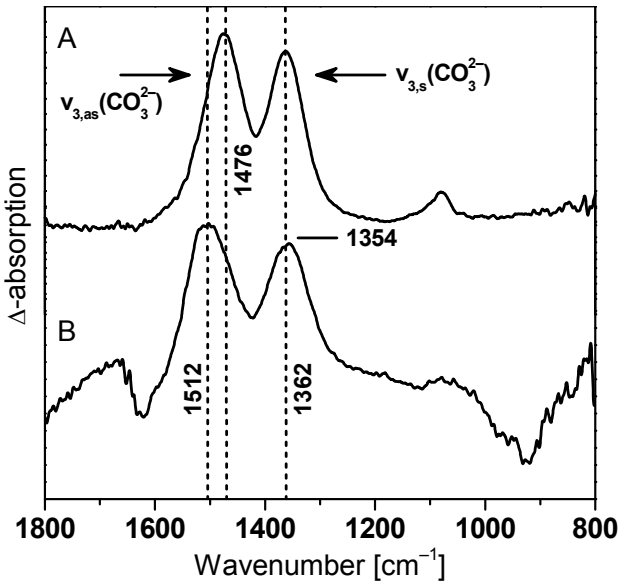

Fig. 2: *In situ* ATR FT-IR difference spectra of the sorption of dissolved CO_2 onto Fh under inert gas conditions. Spectrum of sorption onto pristine Fh (A), and after prolonged sorption of UO_2^{2+} as shown in Fig. 1A (B).

sorption processes. The spectrum recorded in presence of atmospheric CO_2 shows additional bands between 1520 and 1350 cm^{-1} (Fig. 1B). These bands have to be attributed to structural changes of carbonate ligands sorbed onto Fh.

In order to gain more information about the uranyl carbonate surface complexes on Fh, sorption experiments using carbonate as the sorbate were carried out (Fig. 2). First, the spectrum of the sorption of carbonate on a pristine Fh phase under inert gas conditions shows two bands at 1476 and 1362 cm^{-1} representing the $\nu_{3,as}$ and $\nu_{3,s}$ of the anion, respectively. In a second experiment, the aqueous solution equilibrated with air was added after the exhaustive sorption of UO_2^{2+} under inert gas atmosphere. Again, two bands appear in the spectrum which can be assigned to the ν_{as} (1512 cm^{-1}) and ν_s modes (1354 cm^{-1}) of the carbonate anion. The splitting of these bands has considerably increased. From the degree of splitting of the ν_3 bands, the type of binding of the carbonate anions to the iron mineral phase can be deduced [2]. Since the carbonate is known to be monodendately bound on pristine Fh [3], the increased spectral distance of these bands in Fig. 2B is interpreted as a more bidendate binding. This can only be explained by the formation of ternary complexes where the carbonate ions bind directly to the UO_2^{2+} ions which are sorbed to the iron hydroxide phase.

In summary, *in situ* ATR FT-IR spectroscopy provides deep insight into the molecular course of sorption processes of uranyl(VI) ions on the mineral-water interface. From this work, the presence of bidendate inner-sphere ternary [OCO_2···UO_2···Fh] complexes can be derived.

REFERENCES

[1] Foerstendorf, H. et al. (2006) *Report FZR-443*, p. 52.
[2] Lefèvre, G. (2004) *Adv. Colloid Interface Sci.* **107**, 109-123.
[3] Su, C. et al. (1997) *Clays Clay Min.* **45**, 814-825.

In-situ study of the sorption of Np(V) on surfaces of TiO_2 and SiO_2 by ATR FT-IR spectroscopy

K. Müller, H. Foerstendorf

The sorption of Np(V) on surfaces of titanium and silicium oxides has been investigated *in-situ* by application of ATR FT-IR spectroscopy. From the obtained spectral data the formation of similar Np(V) inner-sphere surface complexes is concluded.

Oxides of the transition metals play an important role in regulating the mobility of contaminants, due to their widespread presence and high sorption capacity [1]. For the investigation of sorption phenomena, TiO_2 often serves as a model due to its high thermal stability, low solubility over a wide pH range, and its well-known structure and surface properties [2,3]. In-situ time-resolved ATR FT-IR analysis provides an insight in the formation of Np(V) surface complexes.

EXPERIMENTAL. The micromolar concentrated Np(V) solutions were prepared from a deuterated 0.02 M neptunyl chloride stock solution (D_2O content: $\geq$ 99.99%, Sigma Aldrich). Ionic strength was 0.1 M maintained by addition of NaCl. The solutions were prepared and analyzed under nitrogen atmosphere in a glove box. The sorbents titanium and silicium dioxide are commercial powders obtained from Alfa Aesar and Merck, respectively. The TiO_2 sample is a mixture of anatase (about 80%) and rutile. The specific surface areas of TiO_2 and SiO_2 are 374 and 505 m^2/g, respectively. The set-up of the in-situ ATR FT-IR analysis is described elsewhere [4].

RESULTS. The IR absorption maxima of ν_3 of the neptunyl(V) cation occur at frequencies around 800 cm^{-1}. To avoid strong interferences with water absorption bands, the isotopic shift of deuterium oxide is used. Thus, in aqueous solution the detection limit was reduced by three orders of magnitude to a level of 50 µM (Fig. 1a). The band at 818 cm^{-1} is assigned to the antisymmetric stretching mode (ν_3) of the fully hydrated NpO_2^+ species, which dominates the speciation at pH 2-10 at this concentration level [5,6].
Upon sorption of NpO_2^+, the frequency of the ν_3 mode is red-shifted. For both TiO_2 and SiO_2 strong absorption is observed at 788 cm^{-1} (Fig. 1b,c,f). The respective shift of 30 cm^{-1} compared to the solution species might be due to surface complexation with one or more species. However, with respect to the same frequency of the absorption band of the sorption complex found for titania and silica a similar Np(V) surface complex can be derived (Fig. 1c,f).
Upon increasing the sorption pH from 4.0 to 7.6, no significant shifts of the IR band maxima could be observed, indicating the presence of the same sorption complexes, i.e. inner-sphere coordination, present at both conditions (Fig. 1b,c). The increased intensity reflects a different level of Np(V) uptake at different pH values. This is in agreement with previous macroscopic studies [2].
Additionally, the spectra of Np(V) sorption onto TiO_2 exhibit further absorption bands in the frequency range 1200-950 cm^{-1} (Fig. 1b,c). Their assignment to interactions of the background electrolyte or of heavy water with the TiO_2 can be ruled out, since the spectra obtained during the conditioning stage of the TiO_2 with 0.1 M NaCl in D_2O solution give no evidence for any complexation. To

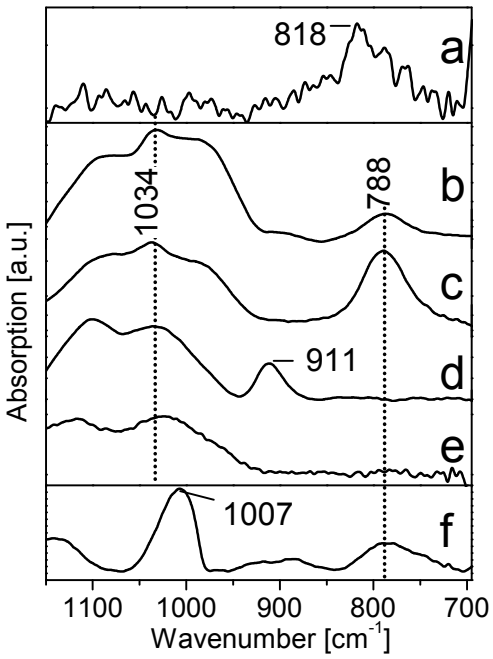

Fig. 1: ATR FT-IR spectra of 50 µM Np(V) (a) in aqueous solution at pH 6, (b) sorbed on TiO_2 at pH 4.0, (c) sorbed on TiO_2 at pH 7.6, (d) 1 µM U(VI) sorbed on TiO_2 at pH 4.0 (e) 50 µM Cs sorbed on TiO_2 at pH 7.6 and (f) 50 µM Np(V) sorbed on silica gel at pH 7.6. All measurements were performed in D_2O, at 0.1 M NaCl under nitrogen atmosphere. Indicated values are in cm^{-1}.

verify the specificity of these bands, in-situ ATR FT-IR sorption experiments using Cs and U(VI) as representative sorbates for monovalent and divalent actinyl cations, respectively. All obtained spectra show very similar results in this spectral region (Fig. 1d,e). It is obvious that the interaction of cations on the TiO_2 surface provokes specific bands in the IR spectra with high bandwidths and slightly shifting maxima. They might be specific for TiO_2 and depend on the size and charge of the reacting cation. The band at 1007 cm^{-1} observed for Np(V) sorption to SiO_2 is probably attributed to Si-O vibrations (Fig. 1f).
In conclusion, Np(V) surface complexes on TiO_2 and SiO_2 have been investigated for the first time by *in-situ* ATR FT-IR spectroscopy. Structural similar inner-sphere complexes are derived from the resulting spectra.

ACKNOWLEDGEMENTS. This work was supported by the DFG, Grant FO 619/1-1. The authors are grateful to Dr. A. Ikeda-Ohno, Dr. G. Lefèvre and C. Eckardt.

REFERENCES

[1] Tochiyama, O. et al. (1996) *Radiochim. Acta* **73**, 191-198.
[2] Jakobsson, A. M. et al. (1998) *Radiochim. Acta* **82**, 257-262.
[3] Lefèvre, G. et al. (2008) *J. Colloid Interface Sci.* **327**, 15-20.
[4] Meusel, T. et al. (2009) this report, p. 48
[5] Guillaumont, R. et al. (2003) *Update on the chemical thermodynamics of U, Np, Pu, Am and Tc*., Elsevier, Amsterdam.
[6] Jones, L. H. et al. (1953) *J. Chem. Phys.* **21**, 542-544.

Selenite reduction by Fe^{II}-bearing minerals: Towards a better understanding of Se retention processes in the near-field and far-field of nuclear waste repositories

A. C. Scheinost, L. Charlet,[1] S. Nikitenko,[2] T. Missana[3]

[1]Laboratoire de Géophysique Interne et Tectonophysique, UJF, Grenoble, France; [2]Laboratoire de Sonochimie, CEA Marcoule, Bagnols-sur-Cèze, France; [3]Departamento de Medioambiente, CIEMAT, Madrid, Spain

The fission product ^{79}Se is commonly considered as one of the key risks of nuclear waste disposal sites due to its long half-live of 1.1 Ma and due to the suspected predominance as anionic aqueous species ($Se(IV)O_3^{2-}$ and $Se(VI)O_4^{2-}$) with high environmental mobility. Ferrous Fe, either sorbed to clay minerals or as structural component of minerals, is ubiquitous in the near-field and far-field of nuclear waste repositories, and reduces selenite to Se(0) and Se(−II) species with very low solubility [1-3]. The extent and kinetics of reduction as well as the end products of the reaction, however, show a high variability. Some of the control mechanisms will be discussed in the following.

INTERFACIAL VS. AQUEOUS REDUCTION. Selenite is not significantly reduced by aqueous Fe^{2+} [1]. In clay systems, aqueous Fe^{2+} reduces selenite only in a pH range, where both Fe^{2+} and selenite are adsorbed, i.e. below pH 7 (provided that some Fe^{2+} is sorbed by pH-independent cation exchange) [3]. Furthermore, selenite reduction is not triggered by solution Eh alone, since complete reduction was observed even at Eh > 200 mV in the presence of magnetite [3]. Both observations give clear evidence that the electron transfer is catalyzed by the mineral/water interface.

PROCESSES AT THE MAGNETITE/WATER INTERFACE. Selenite was completely reduced within 24 h by magnetite [2,3], while in two other experiments with similar duration, selenite reduction was not detectable [4,5]. One of the reasons for the absence of reduction is the much higher surface loading of 60 μmol/m^2 in the latter experiment (compared to 0.3 μmol/m^2 in the former experiments), restricting electron transfer from the magnetite surface to attached selenite. Furthermore, acidic pH and anoxic conditions favor the topotactic transformation of magnetite to (Fe^{II}-less) maghemite [6], which is not able to reduce selenite. The aqueous Fe^{2+} released during the magnetite-maghemite transformation is also not able to reduce selenite, in line with our earlier observation [1]. Instead, Fe and selenite co-precipitate to form a Fe selenite at acidic pH [5].

CONTROLS OF REDOX KINETICS. Depending on the type of mineral, reduction kinetics and end product greatly varied. While selenite reduction by Fe-sorbed clay and siderite ($FeCO_3$) was slow, leading to an incomplete reduction within days or weeks, selenite reduction was completed within 24 h in the presence of mackinawite (FeS), green rust (GR) and magnetite (Fe_3O_4). The fast reactions of FeS, GR and Fe_3O_4 are in line with the small band gap of these minerals (about 1 eV), which facilitates electron transfer from the structure to the solid-water interface [7]. The slow reduction by siderite reflects the large band gap of this mineral. Similarly, reduction by sorbed Fe^{2+} seems to depend on the formation of activated surface complexes and/or the formation of H_2-species [8], but the kinetics remain slow [1,3].

NATURE OF REDUCED END PRODUCTS. Interestingly, the Se redox products depend on the reduction kinetics. Slow reductions (>> 24 h) favor formation of elemental Se, while fast reductions (complete reduction within 24 h) favor formation of FeSe species [1-3]. These results are in striking contrast to thermodynamic calculations using the most recent data [9], which predict formation of elemental Se for the investigated FeS, GR and Fe_3O_4 systems, while formation of ferroselite ($FeSe_2$) is predicted for the $FeCO_3$ and clay systems [3]. This obvious contradiction can be easily resolved by assuming that the reduction of selenite to the reduced aqueous species HSe^- is rate-limiting, while the precipitation of the solids is proceeding more rapidly. Although the end products are in obvious thermodynamic disequilibrium, subsequent mineral transformations towards equilibrium may need very long periods, since they can proceed only via a dissolution/re-precipitation reaction, which is greatly hindered by the extremely low solubilities of these solid phases.

CONSEQUENCES FOR THE SAFETY OF NUCLEAR WASTE REPOSITORIES. Our experiments suggest that selenite reduction should be a common process at the surface of (corroding) steel claddings and clay liners in the near-field of nuclear waste repositories, as well as in deep-underground rocks and sediments and aquifers, where Fe(II) minerals are commonly present. After complete reduction and precipitation, Se concentrations dropped below the ICP-MS detection limit, $6.3 \cdot 10^{-8}$ M, suggesting an efficient scavenging of Se from groundwater. Even when reduction was not completed within the relatively short time scale of our experiments, we anticipate a complete reduction for longer time periods representative for underground migration processes (years to millennia). Although the observed Se phases have most likely a nanoparticulate nature, we did not observe a tendency to form potentially mobile Se colloids [3]. However, this has to be investigated in more detail. Furthermore, in some cases, where we would have expected selenite reduction, the reduction did not happen. The reasons seem to be only partly understood, and further investigations are needed. Finally, there is only little work published demonstrating that not only selenite, but also selenate is reduced by Fe(II) systems [10].

REFERENCES

[1] Charlet, L. et al. (2007) *Geochim. Cosmochim. Acta* **71**, 5731-5749.
[2] Scheinost, A. C. et al. (2008) *Environ. Sci. Technol.* **42**, 1984–1989.
[3] Scheinost, A. C. et al. (2008) *J. Contam. Hydrol.* **102**, 228-245.
[4] de Arroyabe Loyo, R. L. et al. (2008) *Environ. Sci. Technol.* **42**, 2451-2456.
[5] Missana, T. et al. (2009) *Geochim. Cosmochim. Acta*, submitted.
[6] White, A. F. et al. (1994) *Geochim. Cosmochim. Acta* **58**, 1859-1875.
[7] Tronc, E. et al. (1984) *J. Chem. Soc.-Faraday Transactions I* **80**, 2619-2629.
[8] Géhin, A. et al. (2007) *Geochim. Cosmochim. Acta* **71**, 863–876.
[9] Olin, A. et al. (2005) *Chemical thermodynamics of selenium*, Elsevier, Amsterdam.
[10] Myneni, S. C. B. et al. (1997) *Science* **278**, 1106-1109.

X-ray photoelectron spectroscopy investigation of Se^{IV} and Sb^{V} reduction by mackinawite (FeS)

D. Banerjee, R. Kirsch, A. C. Scheinost

Both Se and Sb exist in nature in a wide range of oxidation states and can be potential hazardous contaminants depending on their speciation and reactivity. In this study, we employed cryogenic-XPS in order to understand the redox processes involving Se^{IV} and Sb^{V} at the surface of mackinawite. Results from Fe 2p and S 2p XPS spectra of the reacted samples from both Se^{IV}-mackinawite and Sb^{V}-mackinawite systems revealed the presence of Fe^{III} and S^{0} species at the surface. These observations suggest that both Fe^{II} and S^{-II} atoms at the surface of mackinawite were oxidized and were therefore responsible for the reduction of Se^{IV} and Sb^{V}.

EXPERIMENTAL. The mackinawite (FeS) suspension (0.3 M Fe) was prepared by mixing 100 mL of a 0.6 M Fe(II) solution ($Fe(NH_4)_2(SO_4)_2 \cdot 4H_2O$) with 100 mL of a 0.6 M S^{-II} solution Na_2S (60-62%, Riedel de Häen). This recipe gives a disordered tetragonal mackinawite structure, with a specific surface area of 380 m^2g^{-1} (HRTEM). Mackinawite samples were prepared and stored as suspensions under strictly anoxic conditions (< 1 ppmv O_2) in the Jacomex glovebox. Sorption experiments with Se and Sb were also conducted in the same glovebox under anoxic conditions.

X-ray Photoelectron Spectroscopy (XPS) spectra of frozen wet pastes of mackinawite samples were collected with a cryogenic KRATOS Axis Ultra electron spectrometer under monochromatic Al Kα radiation (1486.6 eV), equipped with hybrid lens system containing a magnetic lens and a charge neutralizer. Analysis pass energy of 160 eV with a step size of 1 eV was used for survey scans while pass energy of 20 eV with a step size of 0.1 eV was used for narrow scans for individual elements. The binding energy (BE) scale was referenced to the C 1s peak of aliphatic carbon contamination, which is ubiquitous in XPS analyses, at 285.0 eV. In order to prevent exposure of samples to atmosphere, the wet pastes were applied on the XPS sample holders in a glove bag under Ar atmosphere and were transferred to the precooled (−160 °C) XPS introduction chamber likewise. The samples were analyzed in the liquid nitrogen cooled (−155 °C) analytical chamber of the instrument. All the elemental spectra were fitted using KRATOS vision processing software.

RESULTS. Fe 2p XPS spectrum of pure mackinawite surface revealed presence of both Fe^{II}–S and Fe^{III}–S species and the proportion of the latter increased when reacted to Se^{IV} suggesting oxidation of surface Fe^{II}. In addition, presence of elemental S at the surface of the reacted sample suggested oxidation of sulfur as well (Fig. 1). These results suggest that Se reduction is coupled to both S^{-II}/S^0 and Fe^{II}/Fe^{III} redox half reactions [1].

Fe 2p XPS spectra of the mackinawite sample reacted with Sb^{V} revealed an increased abundance of Fe^{III}–S species and presence of Fe^{III}–O species on the surface at the expense of Fe^{II}–S species, suggesting a Fe oxidation coupled to Sb reduction. According to the O 1s spectra, there is a small contribution of surface hydroxyl groups after the reaction which is most likely due to the formation of Fe^{III} hydroxides. Presence of S^0 was also observed on the surface after reaction with Sb^{V} (Fig. 2). Therefore Sb^{V} is reduced by electron transfer from both Fe^{II} and S^{-II} [2]. In both Se^{IV}-Mackinawite and Sb^{V}-Mackinawite systems it seems ⅔ of total electrons, responsible for reducing Se^{IV} and Sb^{V}, respectively, are contributed by Fe atoms and ⅓ by S atoms.

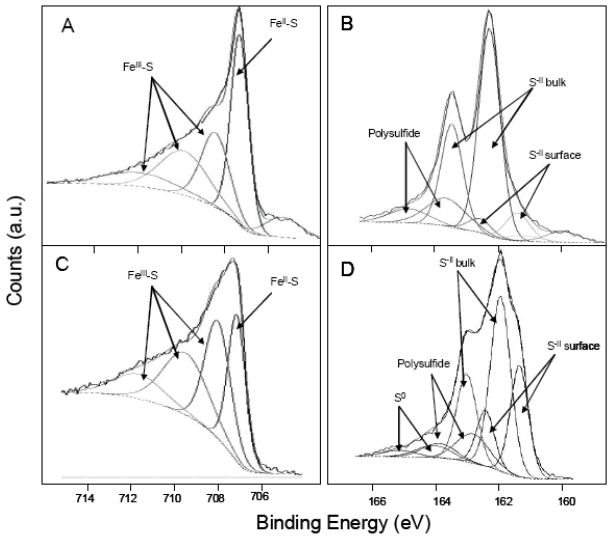

Fig. 1: Fitted Fe $2p_{3/2}$ and S 2p cryo-XPS spectra of pure mackinawite (A,B) and when reacted with Se^{IV} in aqueous solution (C,D). Interpretations of the fits are provided in the text.

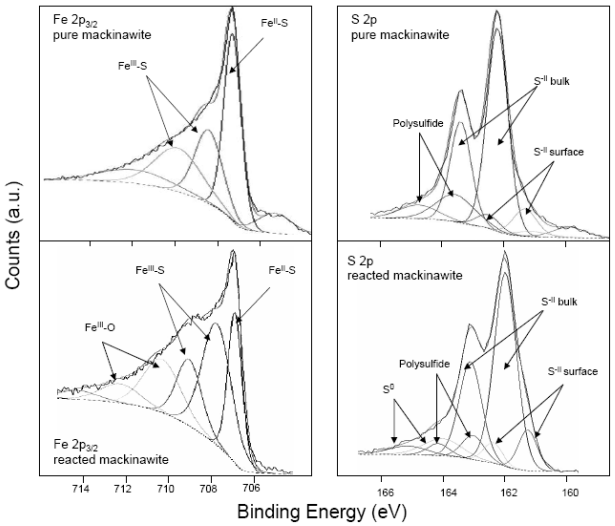

Fig. 2: Fitted Fe $2p_{3/2}$ and S 2p cryo-XPS spectra of pure mackinawite and when reacted with Se^{IV} in aqueous solution. Interpretations of the fits are provided in the text.

REFERENCES

[1] Scheinost, A. C. et al. (2008) *J. Contam. Hydrol.* **102**, 228-245.
[2] Kirsch, R. et al. (2008) *Mineral. Mag.* **72**, 185-189.

Reaction of antimony with nano-particulate magnetite, mackinawite and siderite – An EXAFS investigation

R. Kirsch,[1,2] A. C. Scheinost, L. Charlet[1]

[1]Earth and Planetary Science Department, University of Grenoble-I, Grenoble, France; [2]Institute of Radiochemistry, Forschungszentrum Dresden-Rossendorf, Dresden, Germany

Iron(II) minerals occur naturally in anoxic soils and form as intermediate corrosion products of reactive barriers and waste containers. The structural Fe(II) is able to reduce a range of metal(loid)s, including Se, As, Cr, Pu and Np [1-5], thereby influencing the mobility of these contaminants. In addition, surface sorption/precipitation reactions play a considerable role in determining the environmental impact of toxic contaminants. We show here that aqueous Sb^{III} and Sb^{V} species form inner-sphere sorption complexes on the surface of magnetite ($Fe^{II}Fe^{III}_2O_4$), mackinawite ($Fe^{II}S$) and siderite ($Fe^{II}CO_3$), and that Sb^{V} is reduced to Sb^{III} by magnetite and mackinawite.

EXPERIMENTAL. Magnetite [6], mackinawite [7] and siderite [8] were synthesized in a glove box under anoxic conditions and were subsequently reacted in 25 mM $CaCl_2$ with Sb(III) (Sb_2O_3 in 2 M HCl) or Sb(V) ($KSbOH_6$) ([Sb] = 0.1 mM; 40 or 3 g/L Fe_3O_4; 25 or 1.9 g/L FeS, 10 g/L $FeCO_3$) at pH values from 4 to 9 and for reaction periods from 1 h to 67 d. In a closed-cycle Helium cryostat at 15 K XANES and EXAFS spectra at the Sb-K-edge were collected in fluorescence mode on wet pastes obtained by centrifugation; an Sb foil was used for energy calibration.

RESULTS. Reaction of siderite with Sb(V) for up to 7 days at near-neutral pH resulted in no reduction of Sb(V) (XANES, not shown). Sb(V) is adsorbed via inner-sphere surface complexation with Sb–Fe distances of 3.18 Å and 3.55 Å, characteristic of edge and corner-sharing arrangements between $Sb(O,OH)_6$ and $Fe(O,OH)_6$ octahedra.

Reaction of mackinawite with Sb(V) caused a fast (~1 h) and complete reduction to Sb(III) and formation of a surface complex with a $Sb(S)_3$-structure, characterized by a (Sb–S) distance of 2.48 Å.

Reaction of magnetite with Sb(V) also produced Sb(III), the extent of reduction being dependent on reaction pH and time. Under our experimental conditions, Sb reduction was complete for pH > 6.5 and reaction times > 7 days (further depending on the solid/liquid ratio). The reduction process is orders of magnitude slower than adsorption of Sb(V) to the surface, which is complete within 30 min. The resulting surface complex of Sb(III) is characterized by corner sharing of an $Sb(III)O_3$-pyramide with up to 6 $Fe(O,OH)_6$-octahedra, a position else occupied by $Fe(III)O_4$ tetrahedra in the magnetite-structure (Figs. 1,2). The identified structure of the Sb(III) surface complex is similar to the one found for As(III) on {111} faces of magnetite [9].

CONCLUSION. The structure of the surface complexes of Sb(III) and Sb(V) on the surface of magnetite, mackinawite and siderite could be determined by shell fitting [10]. However, a number of questions remain to be answered concerning the reduction mechanisms of Sb by magnetite and mackinawite. While Sb(V) is reduced by FeS over a wide pH range, the respective roles of Fe^{II} and

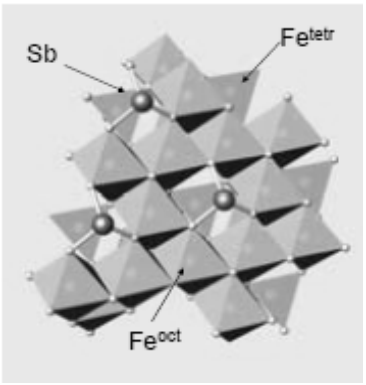

Fig. 1: Model of Sb(III)-complex on {111}-faces of magnetite.

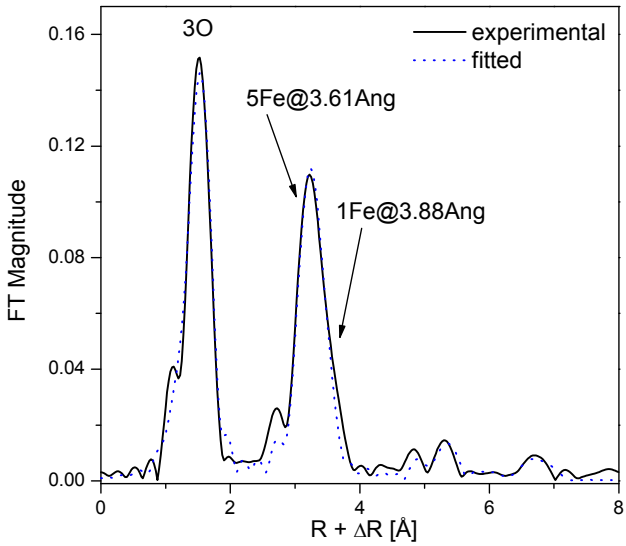

Fig. 2: Sb K-edge EXAFS Fourier-transform of the Sb(III)-complex on {111}-faces of magnetite, and fit results.

S^{2-} in this process remain to be clarified. It also remains open whether the lower reductive capacity of magnetite at low pH is solely due to the progress of its topotactic transformation to maghemite [11] that occurs in anoxic solutions according to

$$Fe^{II}Fe_2^{III}O_4 + 2H^+ \rightarrow \gamma\text{-}Fe_2^{III}O_3 + Fe^{2+} + H_2O \qquad (1)$$

or whether other mechanisms come into play.

REFERENCES

[1] Scheinost, A. C. et al. (2008) *Environ. Sci. Technol.* **42**, 1984-1989.
[2] Gallegos, T. J. et al. (2007) *Environ. Sci. Technol.* **41**, 7781-7786.
[3] Mullet, M. et al. (2004) *Colloids Surf. A* **244**, 77-85.
[4] Powell, B. A. et al. (2004) *Environ. Sci. Technol.* **38**, 6016-6024.
[5] Nakataka, K. et al. (2004) *Radiochim. Acta* **92**, 145-149.
[6] Jolivet, J. P. et al. (1992) *Clay Clay Miner.* **40**, 531-539.
[7] Rickard, D. (1969) *Stockholm Cont. Geol.* **20**, 67-95.
[8] Charlet, L. et al. (1990) *Geochim. Cosmochim. Act.* **54**, 2329-2336.
[9] Wang, Y. et al., (2008) *Geochim. Cosmochim. Act.* **72**, 2573-2586.
[10] Kirsch, R. et al. (2008) *Mineral. Mag.* **72**, 185-189.
[11] White, A. et al. (1994) *Geochim. Cosmochim. Act.* **58**, 1859-1875.

Aqueous suspensions of carbon nanotubes: Surface oxidation and colloidal stability

A. Schierz,[1] H. Zänker

[1]Department of Chemistry and Biochemistry, University of South Carolina, Columbia, U.S.A.

The formation of stable colloidal suspensions of carbon nanotubes due to functionalization by surface oxidation is demonstrated.

In [1] we showed that carbon nanotubes (CNTs) functionalized by surface oxidation are able to adsorb considerable amounts of uranium. Here, we test if CNTs can form colloidal solutions in near-neutral waters. If so, they might be mobile in the aquatic environment and might prove to be a danger to man and animals due to their toxicity and to their ability to transport contaminants (such as uranium) in the water, possibly up to the inside of living cells (cf. [2]).

EXPERIMENTAL. Multiwall CNTs (Ilo-litech, Germany) were functionalized with concentrated HNO_3/H_2SO_4 as described in [3]. They were investigated by FT-IR to identify the produced functional groups. Their behavior in colloidal suspension was studied by measuring the zeta potential using laser Doppler velocimetry and by sedimentation tests after agitation with ultrasound and measuring the scattered light intensity (SLI) of the solution at a scattering angle of 90° (count rate of our BI 90 photon correlation spectroscope). For a detailed description of the experiments see [3].

RESULTS. The FT-IR spectra of the CNTs are given in Fig. 1. All three spectra exhibit a band at 1587 cm^{-1} which results from stretching vibrations of isolated C=C double bonds (for the pristine CNTs it is superposed by a water band). The IR spectra of the functionalized CNTs show that two peaks appear and become stronger during oxidation. These bands around 1212 and 1738 cm^{-1} can be assigned to the C–O and the C=O stretching vibrations of the carboxylic group. With increasing reaction time the bands broaden, indicating that the content of carboxylic groups at the outer surface of the CNTs increases.
Figure 2 shows the pH dependance of the zeta potential, ζ, for modified and pristine CNTs. With a pH rise from 2 to 11 a decline in zeta potential from −10 mV to −35 mV is observed for the modified CNTs (modification time 16 h). We explain this decrease by the deprotonation of functional groups. According to Fig. 1, these groups should primarily be carboxylic groups. The pH response of the pristine CNTs in Fig. 2 is much less.

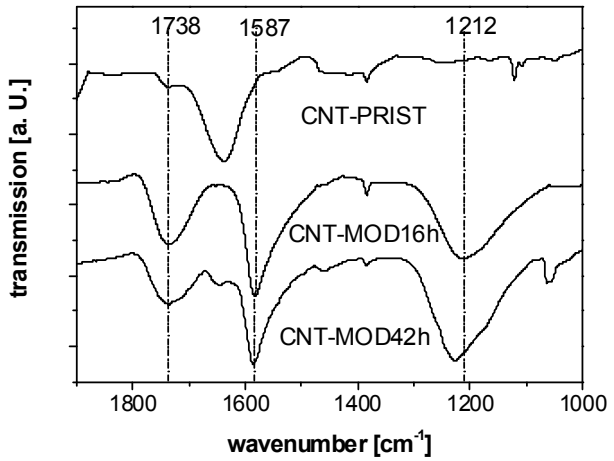

Fig. 1: FT-IR spectra (KBr pellet) of the pristine CNTs (CNT-PRIST) and the modified CNTs (CNT-MOD16h and CNT-MOD24h).

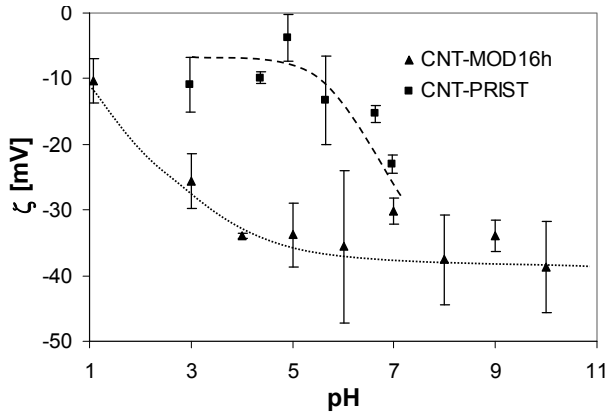

Fig. 2: Zeta potential of pristine and modified CNTs in dependence on pH (I = 10 mM NaCl, error bars: 2 σ, 3 replicates).

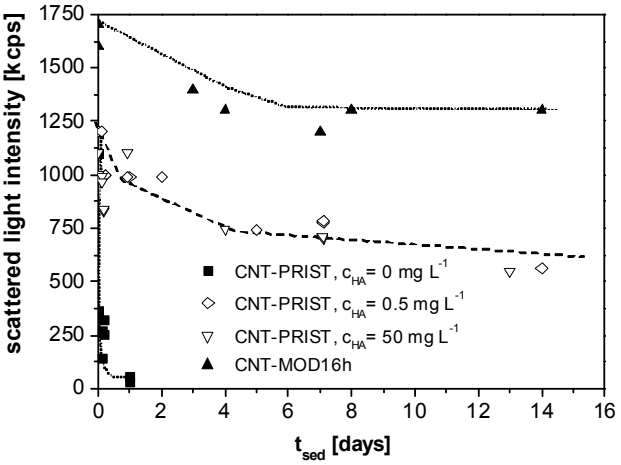

Fig. 3: Sedimentation behaviour of pristine CNTs in the presence of humic acids and sedimentation behaviour of modified CNTs (pH 7, $c_{CNT} \leq 100$ mg L^{-1}).

Figure 3 shows the time dependance of the SLI of the CNT suspensions after sonication. It can be seen that the SLI decreased from 1100 to 32 kcps within 24 h for the pristine CNTs. By contrast, the SLI of the suspended modified CNTs remained nearly constant over a period of more than 14 days (decrease ~ 25%), i.e. this colloidal suspension proved to be stable. CNTs can also be stabilized in aqueous solutions by surfactants. These can be synthetic surfactants as well as natural organic matter (NOM). As shown in Fig. 3, a significant decrease of the sedimentation rate of pristine CNTs, even at a humic acid (HA) concentration as low as 0.5 mg L^{-1}, is observed.
From these findings we conclude that transport of heavy metals (e.g. uranium) bound to CNTs through natural aquatic systems and even into biological systems ("Trojan Horse effect") is at least conceivable. Considering the interactions between CNTs and certain environmental contaminants, the properties of CNTs in aquatic systems should be further investigated in order to enable prognoses of their effects if released to the environment.

REFERENCES

[1] Schierz, A. et al. (2007) *FZD Report-459*, p. 56.
[2] Porter, A. E. et al. (2007) *Nat. Nanotechnol.* **2**, 713-717.
[3] Schierz, A. et al. (2009) *Environ. Pollut.*, in press.

Uranium(IV) colloids in near-neutral solutions: Influences on particle size

I. Dreißig, S. Weiß, H. Zänker, G. Bernhard

Light scattering (LS) and ultracentrifugation (UC) results revealed that the size of the U(IV) colloids in near-neutral solution is controlled by the silicate concentration and the pH of the solution.

Uranium(IV) is only sparingly soluble in near-neutral solutions. Therefore, it is usually assumed to be immobile in the aquatic environment which makes it very different from uranium(VI). As a consequence, uranium is expected to be immobilized under reducing conditions. However, it is well known that also insoluble compounds can be mobile in natural waters which happens when they form colloids. We tested in [1] if U(IV) is able to form colloids under near-neutral conditions. We found that the tetravalent uranium can be transferred into a colloidal form under such conditions if it is reduced in an alkaline carbonate solution and neutralized in the presence of significant amounts of silicate. Here we investigated how certain chemical conditions influence the size of these colloids. Particle size is an important property of a colloidal system. It influences the behavior of the colloids in small pores and filters, the Brownian diffusion, the aggregation kinetics and so forth.

EXPERIMENTAL. The U(IV) colloids were generated as in Experiment C of [1], i.e. by the galvanostatic reduction of a 20 mM $UO_2(ClO_4)_2$ solution in 1 M $NaHCO_3$, dilution by a factor of 20 with a silicate solution of the adequate silicate concentration and neutralization with perchloric acid. Measurement of the scattered light intensity (SLI) and photon correlation spectroscopy (PCS) were carried out with a BI-90 PCS device from Brookhaven Instruments. UC was performed with an Optima XL 100K ultracentrifuge (Beckman Coulter) at a centrifugal acceleration of 170000 x g.

RESULTS. Typically, the colloids produced did not reach their final particle size immediately but showed a certain growth phase of about one week. This could be seen from both PCS and simple SLI measurements. Fig. 1 shows the increase of the particle diameter as determined by PCS (method of cumulants according to [2]) and the rise in SLI (count rate) for a sample of U(IV) colloids. The count rate of the pure Membrapure water (blank) is about 2 kcps. Two influences control the SLI: particle size and particle concentration. Considering that the concentration of colloidal matter is largely constant during the growth period, particle growth is bound to reduce particle concentration (number concentration) which reduces SLI. However, this reduction in SLI is outweighed by the increase in SLI due to particle diameter increase since the SLI depends significantly stronger on particle size than on particle number. Therefore, the SLI is a semiquantitative measure of particle growth in our experiment. Figure 2 shows the SLI at various initial silicate concentrations (concentration of the free dissolved silicate decline during the experiment due to colloid formation) and pH values (steady SLIs after 7 days). The highest SLIs were measured in the solutions of the lowest silicate content (sample 1), solutions of higher silicate content produced lower SLIs.

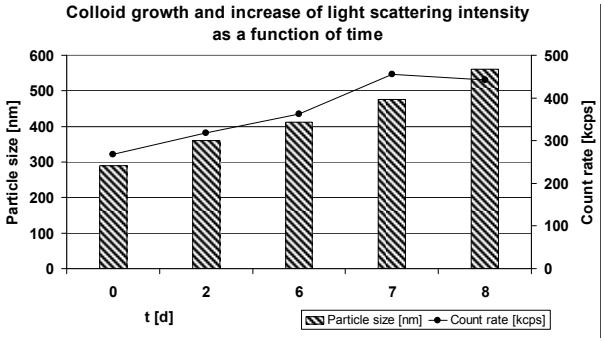

Fig. 1: Time dependency of PCS particle size and SLI of a sample of U(IV) colloids (U: 0.85 mM; initial silicate: 1.66 mM; pH 9.62).

All samples exhibited an increase in SLI with decreasing pH. Obviously, very small colloidal particles are generated at high pH and/or high silicate concentration and larger ones at low pH and/or low silicate concentration. At pH < 7 sedimentation occurred in sample 1, whereas at higher silicate concentration (samples 2 and 3) the colloids were still stable at the pH range below 7.

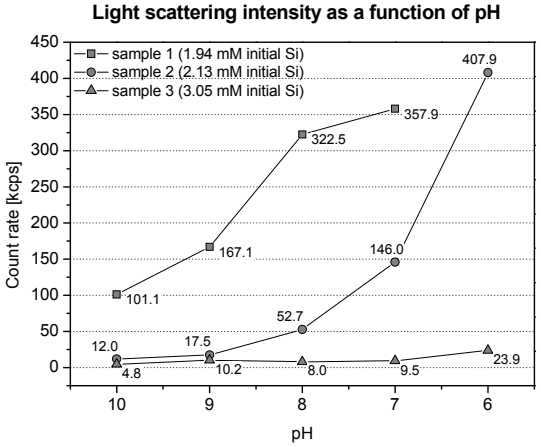

Fig. 2: Equilibrium SLI in dependence on silicate content and pH.

This silicate and pH dependency is confirmed by our UC results (Tab. 1). The smaller the colloids, the longer the time they need for separation at the given centrifugal acceleration. After 1 h of UC the supernatants of samples A and D still contained significantly higher U concentrations than samples B and C. After 5 h UC time almost all the uranium was removed, indicating that truly dissolved uranium did not play a significant part in the system, i.e. almost all U was colloidal.

Tab. 1: Ultracentrifugation results.

Sample	A	B	C	D
pH	7.7	7.8	8.4	9.4
initial Si conc. [mM]	5.4	3.3	2.8	5.4
initial U conc. [mM]	0.97	0.81	1.01	0.97
U conc. after 1 h UC [mM]	0.62	0.18	0.10	0.62
U conc. after 5 h UC [mM]	0.10	0.02	0.11	0.09

REFERENCES

[1] Dreißig, I. et al. (2008) *Report FZD-489,* p. 57.
[2] Koppel, D. E. (1972) *J. Chem. Phys.* **57**, 4814-4820.

Comparison of uranium(VI) sorption on milk proteins from water and synthetic milk ultrafiltrate (SMUF)

K. Schreppel, S. Weiß, H. Zänker, K. Gloe,[1] T. Henle,[1] G. Bernhard
[1]Department of Chemistry and Food Chemistry, Dresden University of Technology, Dresden, Germany

The adsorption of UO_2^{2+} on sodium caseinate and whey proteins was studied using two different media: water and SMUF solution. The sorption capacity for UO_2^{2+} proved to be higher for whey protein than for sodium caseinate whereas the sorption affinity was higher for caseinate than for the whey protein. For caseinate the solution employed (water or SMUF) did not influence these sorption characteristics. For whey protein they did.

The adsorption of U(VI) by milk proteins is interesting from two points of view. The first is related to the toxicity of uranium in the food chain and the second is connected to the possible use of such proteins for uranium separation. In order to prove the influence of the environment on the adsorption of U(VI) by milk proteins, sodium caseinate and whey proteins were studied in both water and SMUF solution. The latter is used in dairy technology to simulate milk and is characterized by a high free phosphate content. Therefore, this leads to the question whether the dissolved inorganic phosphate has an influence on the adsorption behavior of UO_2^{2+} on milk proteins.

EXPERIMENTAL. The general proceeding is in accordance with [1]. A solution of SMUF was prepared according to [2] with the pH adjusted to 4.6. The U(VI) solutions were prepared from $UO_2(NO_3)_2 \cdot 6\ H_2O$ with concentrations between $1 \cdot 10^{-7}$ M and $1 \cdot 10^{-5}$ M at a pH value of 4.6. Sodium caseinate or lyophilized whey proteins were suspended in water or in SMUF solution and added to the U(VI) solutions leading to concentrations of 14.2 mg/L sodium caseinate or 3.2 mg/L whey proteins. The differentiation between uranium adsorbed to the milk proteins and free uranium was performed by phase separation using 10 kD ultrafilters and ICP-MS analysis for U in the ultrafiltrate (cf. [1]).

RESULTS AND DISCUSSION. The experimental results of the adsorption studies are summarized in Fig. 1. The data were fit to the Langmuir isotherm and both the adsorption capacity, q_{max}, and the Langmuir adsorption constant, K_L, were derived (cf. [1]). Due to the scatter in data, the fit is not very good. However, estimates of q_{max}, and K_L could be provided. They show that whey proteins possess a much higher adsorption capacity for U(VI) (ca. 280 mg/g in H_2O and 190 mg/g in SMUF) than sodium caseinate (approx. 70 mg/g in H_2O and 80 mg/g in SMUF) under comparable conditions. It is conceivable that the carboxylate groups effect the adsorption capacity while the adsorption affinity (as represented by K_L) is controlled by the phosphoserine residues present (or absent) in the protein. This can be seen in the case of sodium caseinate whose Langmuir constant K_L is higher (ca. 110 L/mg in H_2O and 120 L/mg in SMUF) than those of the whey proteins (approx. 20 L/mg in H_2O and 1 L/mg in SMUF). However, in the case of whey proteins the Langmuir parameters q_{max} and K_L are influenced by the different media whereas for sodium caseinate these parameters are nearly identical for the two solutions. As

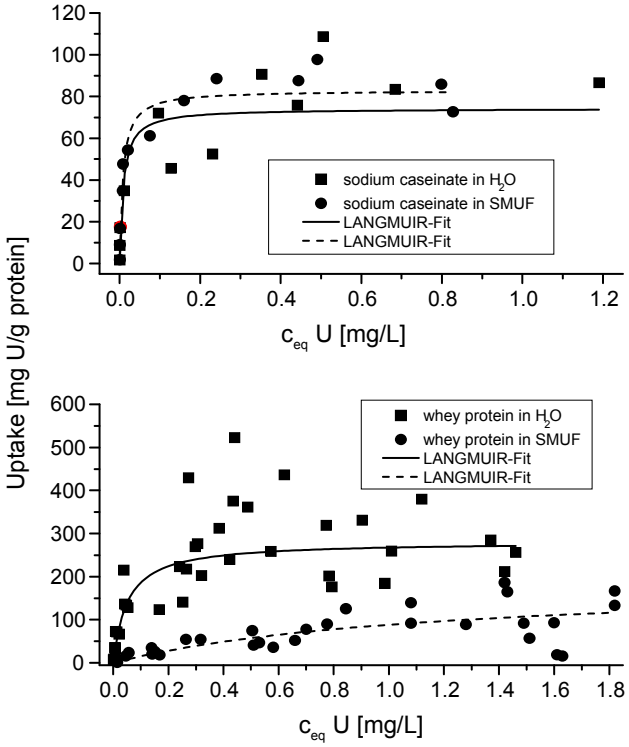

Fig. 1: Experimental data and the fitted Langmuir isotherms of the adsorption of U(VI) on sodium caseinate (top) and whey proteins (bottom) in water (squares) and in SMUF solution (circles).

Tab. 1: Composition of bovine casein and amount of P-Ser/molecule [4].

	% of whole casein	M_W [kDa]	No. P–Ser residues
α_{S1}-casein	38	23.6	8
α_{S2}-casein	10	23.2	11
β-casein	36	24	5
κ-casein	13	19	1

SMUF solution contains free phosphate which forms stable complexes with UO_2^{2+} [3], it should decrease U adsorption to the proteins. This can be seen in the case of whey proteins. For sodium caseinate the situation is different since caseinate itself has phosphate groups. The four main components of bovine casein are characterized by defined numbers of phosphoserine residues (P-Ser) per molecule (Tab. 1) which all can contribute to the binding of UO_2^{2+}. In conclusion, the different U(VI) adsorption behavior observed is obviously caused by several influences, among them interactions of U(VI) with the free and bound phosphate. The results with sodium caseinate point to a stronger binding of UO_2^{2+} by protein bound phosphate groups in comparison with the free phosphate ions of SMUF, i.e. dissolved phosphate hinders the adsorption of UO_2^{2+} on proteins without protein bound phosphate groups but not on phosphate-containing proteins.

REFERENCES

[1] Schreppel, K. et al. (2008) *FZD Report-489*, p. 38.
[2] Jenness, R. et al. (1962) *Neth. Milk Dairy J.* **85**, 153-164.
[3] Ansoborlo, E. et al. (2006) *Biochimie* **88**, 1605–1618.
[4] Schlimme, E. et al. (1999) *Milch und ihre Inhaltsstoffe*, Verlag Th. Mann, Gelsenkirchen.

Thermodynamic reference database THEREDA: 1. Data compilation for uranium and radium

A. Richter, V. Brendler, S. Gester, H. Moog,[1] V. Neck,[2] C. Marquardt,[2] M. Altmaier[2]

[1]Gesellschaft für Anlagen- und Reaktorsicherheit mbH, Braunschweig, Germany; [2]Institute for Nuclear Waste Disposal, Forschungszentrum Karlsruhe, Karlsruhe, Germany

The cooperative project THEREDA aims at the development of a consistent and quality assured thermodynamic reference database for all safety relevant elements, temperature and pressure ranges [1]. Among other things, FZD is responsible for the work package "Database of uranium and radium". This concerns the data review, validation and selection of the thermodynamic data.

REQUIREMENTS AND REALIZATION. The importance of reliable thermodynamic data for the long-term safety analyses of geological repositories has been acknowledged internationally since decades. For selected actinides (U, Np, Pu, Am) and fission products (Tc, Zr, Ni, Se) a thermodynamic database from the Nuclear Energy Agency (NEA) is available and updated [2,3]. However, as a result of high demands for quality this database is rather restrictive and therefore incomplete for extensive modeling calculations. For example, there are 197 solids in the NEA uranium database, but only five uranium minerals out of about 250 natural occurring ones made their way into the recommended data set. This has been pointed out (but unfortunately not corrected for) also by the Nagra/PSI data base [4]. The use of further established databases (NBS tables, CODATA, IUPAC) is limited, especially when dealing with solutions of high ionic strength. Moreover, they lack data on many relevant radionuclides and other toxic metals. So, these (and other, site specific) databases cannot adapt directly to the specific requirements in Germany.

We seek to compile data of high quality, internal consistency and traceability (see [5]). Persistent data gaps are closed via data of higher uncertainty or estimated values. The provision of such marked uncertain or estimated data is important: As it has been shown in several case studies, a comprehensive thermodynamic equilibrium calculation with (documented) estimated data is better than an incomplete parameter file. Therefore, each data included in the database is categorized with respect to type of experiment, bibliographic source (+ reviewing) and quality.

TECHNICAL APPROACH. THEREDA will represent a source of information on thermodynamic data that will be publicly accessible and free of charge. We realize this with PostgreSQL™, an relational system for the administration of databanks, running on an Apache web server. The database will be provided via our website (URL: http://www.thereda.de). In the current start-up phase of the project, a large number of data are recorded using Excel™ spreadsheets. This task will be taken over bit by bit by a system of PHP-scripts, designed to aid in data import, to trigger internal calculations and to export subsets into parameter files. PHP is a widely used general-purpose scripting language that is especially suited for web development and can be embedded into HTML. It generally runs on a web server, taking PHP code as its input and creating web pages as output.

DATABASE FOR URANIUM. The NEA-TDB [3] is the major source for uranium data. Additional sources provide information concerning uranium(IV), coordination chemistry (mixed complexes, complexes at pH > 8 and ϑ > 25 °C), saline systems (SIT and Pitzer parameters) and secondary mineral phases. The following uranium constituents are recorded: hydrolysis products, sulphates, carbonates, arsenates, silicates, phosphates, nitrates, halogenides, solid uranites. Examples for secondary mineral phases are the uranyl silicates Haweeite, (Na-)Weeksite, (Na-)Boltwoodite and the uranyl phosphate Saleeite. Data for gaseous species and high temperature solids are not relevant for German requirements, therefore, they have not been imported in the database. The main parameters are data relating to chemical elements (most stable modification in standard state, formation enthalpy, function of heat capacity), stoichiometry factors and reaction equations, reaction data including phase transitions, parameters of ion interaction models (SIT, Pitzer) and, if available, confidence interval. Additional remarks provide further information (literature reference, validity limits, underlying analogon or method of estimation). Up to now, the following information are recorded in the database:

- 113 species including 38 solid phases (thereof 22 are not covered by the NEA & Nagra/PSI database) and
- about 700 entries of respective reaction and formation data with uncertainty (if available), reference and quality label.

DATABASE FOR RADIUM. In case of radium, which is not part of any of the established databases, the task of FZD is the compilation of relevant species and validation of the published data. Thermodynamic data for radium are published sparely [6,7]. They are based on estimations and correlations regarding to data of barium and its compounds because of the similar ionic radius and the equal ionic charge of both elements. Notwithstanding the low quality label, we recorded 44 thermodynamic data for 6 relevant aqueous species and 5 solid phases (hydrolysis products, carbonates, sulphates, chlorides). Unfortunately, no uncertainties of these data are documented in the original literature.

ACKNOWLEDGEMENTS. Financial support by the BMWI (contract No. 02E10136), the BMBF (contract No. 02C1436), and the BfS is gratefully acknowledged.

REFERENCES

[1] Richter, A. et al. (2007) *Report FZD-459*, p. 71.
[2] Mompean, F. J. et al. (2003) *Radiochim. Acta* **91**, 617-621.
[3] Guillaumont, R. et al. (2003) *Update on the Chemical Thermodynamics of U, Np, Pu, Am and Tc*, Elsevier, Amsterdam.
[4] Hummel, W. et al. (2002) NAGRA/PSI Chemical Thermodynamic Data Base 01/01, NAGRA Technical Report NTB 02-16, Universal Publishers, Parkland, Florida.
[5] Gester, S. et al. (2009) this report, p. 58.
[6] Langmuir, D. et al. (1985) *Geochim. Cosmochim. Acta* **49**, 1593-1601.
[7] Phillips, S. L. et al. (1988) *Report NUREG/CR-4864*, Lawrence Berkeley Laboratory, Berkeley, California.

Thermodynamic reference database THEREDA: 2. Check and maintenance of the consistency of thermodynamic data

S. Gester, V. Brendler, A. Richter, H. Moog,[1] V. Neck[2]

[1]Gesellschaft für Anlagen- und Reaktorsicherheit mbH, Braunschweig, Germany; [2]Institute for Nuclear Waste Disposal, Forschungszentrum Karlsruhe, Germany

It is necessary to make reliable estimations about the amount of mobilized toxic substances that can reach the biosphere to evaluate the safety of a final repository for nuclear waste. These estimations will be made by geochemical speciation codes calculating chemical equilibria by use of thermodynamic data. If the available thermodynamic data are heterogeneous (of various origin and quality) the obtained estimations are not comparable to each other. One task of the joint project THEREDA [1] is to check the consistency of the covered thermodynamic datasets and to maintain the consistency during updates of the common database. This will ensure the comparability and reliability of estimations attained by thermodynamic data from THEREDA.

OUTLINE. Today, a lot of thermodynamic data derived from experimental research are known [2,3]. However, these data are incomplete (resp. unknown) for many systems especially for temperatures higher than 25 °C. So, to obtain reliable predictions, one often has to complete the available thermodynamic data with data from own measurements or different literature sources, but origin and quality of these data are often not specified. Therefore calculations with heterogeneous datasets of different quality are leading to incomparable results.
Another problem occurs if it is disregarded that a particular thermodynamic datum is valid only in combination with other data. Consistent datasets become inconsistent if single data thereof are modified or new data are entered. This causes miscalculations of chemical equilibria.
Therefore it is necessary to have a comprehensive quality assured database that considers the relationships between single thermodynamic data.

METHODOLOGY. In the present state of the database THEREDA, we distinguish between different levels of consistency:

1. Data consistency. Thermodynamic data within the database must be convertible following the thermodynamic relations (Eq. 1):

$$\Delta_r G^0 = \Delta_r H^0 - T \cdot \Delta_r S^0 = -R \cdot T \cdot \ln K \qquad (1)$$

This implicates:

- a technical framework which enforces internal consistency by automatically triggered internal calculations and
- a clear distinction between "entered" data, which are not subject to internal calculations, and "internally calculated" data.

For each datum to be calculated internally a clear specification should exist by which thermodynamic relation this will be done. This information implies also which other data the specific datum depends on.
This kind of consistency is established within the input tools and also integrative part of the database itself.

2. Algorithm consistency. Two different cases fall into this category of consistency.
First, conditional equilibrium constants should be extrapolated applying the same model for activity coefficients. Equilibrium constants exist which were derived from constants at different ionic strengths, extrapolated applying SIT parameters, while others were derived applying the Pitzer model. Those equilibrium constants must not be combined in a single calculation of thermodynamic equilibrium.
Second, also SIT or Pitzer parameters for the calculation of activity coefficients may be derived using slightly different formulas, superficially being assigned to SIT or Pitzer theory. Therefore all equations used for parameter optimization (including constants such as the Debye-Hückel limiting slope at various temperatures) must be agreed upon and held stringently throughout the work. In addition, such conventions are to be documented for those who apply the database.

3. Correlation consistency. While it is obvious for some data that they are interrelated (e.g. those contained in the Gibbs-Helmholtz relation), for others it is not. One might have been determined some Pitzer parameters by assuming a certain solubility constant for a specific solid phase. Leaving the Pitzer parameters at their original values but changing the solubility constant for the solid phase involved in their determination, will lead to erroneous results in future calculations with the modified database. Binary and ternary Pitzer parameters within a certain system also belong to this category of consistency. Such data therefore have to be combined in a set and appropriate warning messages will be issued when an editor tries to modify parts of the set individually.

4. Species consistency. For some complex species (namely highly charged ones), Pitzer parameters are not accessible. Such species may be exported to parameter files, if and only if it is not intended to make calculations with Pitzer parameters. In the thermodynamic database THEREDA they get a special identification mark.

ACKNOWLEDGEMENTS. Financial support by the BMWI (contract No. 02E10136), the BMBF (contract No. 02C1436), and the BfS is gratefully acknowledged.

REFERENCES

[1] Richter, A. et al. (2006) *Report FZD-459*, p. 71.
[2] Wagman, D. D. et al. (1982) *J. Phys. Chem. Ref. Data* **11,** Suppl. 2, 1-392.
[3] Cox, J. D. et al. (1989) *CODATA key values for thermodynamics*, Hemisphere Publishing Corp., New York.

Species distribution and coordination of U(VI) chloride in acetonitrile

C. Hennig, K. Servaes,[1] P. Nockemann,[1] R. Van Deun[1]
[1]Department of Chemistry, Katolieke Universiteit Leuven, Belgium

The complex formation of UO_2^{2+} with chloride ions was investigated by factor analysis of UV-vis absorption spectra and U L_3–edge EXAFS spectra. Five different species were indicated.

Chloride coordination alters the stability of actinide complexes in solution. The solubility of actinides in highly concentrated chloride solutions is about one order of magnitude higher than in solutions with noncoordinating electrolytes. Nevertheless, the chloride anion is in aqueous solution a weak ligand for UO_2^{2+} which is reflected by the fact that only two stability constants are reported in the actual NEA thermodynamic database [1]. In contrast to aqueous solutions, the chloride anion forms strong complexes with U(VI) in organic solvents. The aim of this study is to correlate the species distribution and the coordination of uranyl chloro complexes by combining UV-vis and EXAFS spectroscopy [2]. The UV-vis spectra of UO_2^{2+} arise from electronic transitions $(\sigma_u^+)^2 \rightarrow \sigma_u^+\delta_u$ and $(\sigma_u^+)^2 \rightarrow \sigma_u^+\phi_u$ [3]. Because both orbitals have 5f character, the observed f-f transition is Laporte forbidden and the UV-vis absorption spectra show typical vibronic features. EXAFS spectra contain information on the distances R_i and coordination numbers N_i of the first coordination shells. Several backscattering atoms can be separated from each other due to differences in R_i.

EXPERIMENTAL. $UO_2(ClO_4)_2 \cdot 6H_2O$ was mixed with tetrabutylammonium chloride in acetonitrile to obtain 50 mM UO_2^{2+} and a systematic variation of the $[UO_2^{2+}]:[Cl^-]$ ratio ranging from 1 :0 to > 1 :4.

RESULTS. The UV-vis absorption spectra have been statistically analyzed by factor analysis [2]. The resulting species distribution is shown in Fig. 1.
The limiting species are the pure solvated ion, $[UO_2(solv)_n]^{2+}$, and $[UO_2Cl_4]^{2-}$. The tetrachloro complex exhibits a significant vibrational fine structure indicating the centrosymmetric D_{4h} symmetry. Due to the correlation with the $[Cl^-]/[UO_2^{2+}]$ ratio, the intermediate species can be assigned to $[UO_2Cl]^+$, $[UO_2Cl_2]^0$, and $[UO_2Cl_3]^-$.

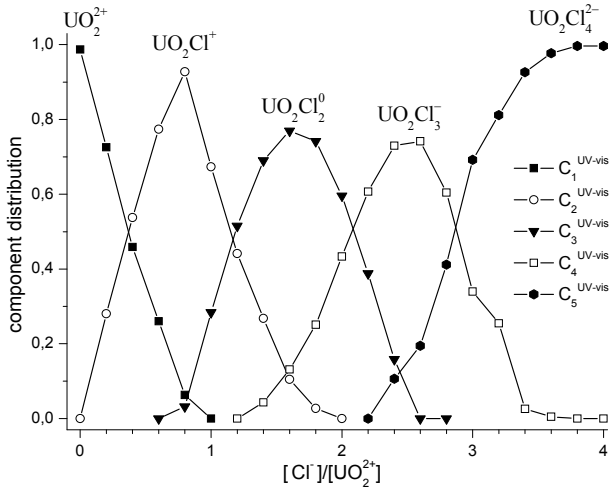

Fig. 1: Component distribution revealed from the UV-vis absorption spectra. The components represent the individual solution species.

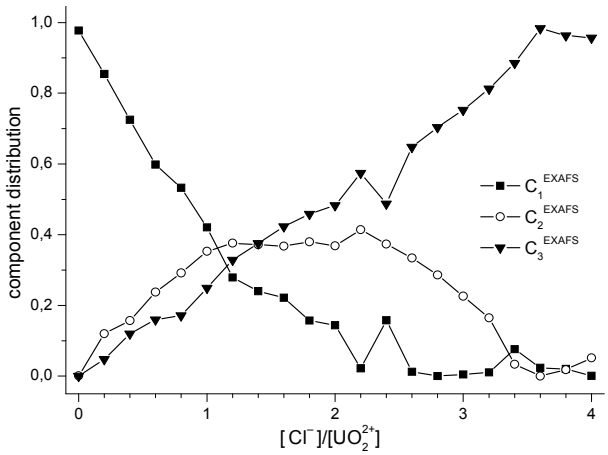

Fig. 2: Component distribution revealed from the EXAFS spectra. The components represent the following dinds in the equatorial shell: C_1^{EXAFS}:U–O, C_2^{EXAFS}: U–N, and C_3^{EXAFS}: U–Cl.

U L_3-edge EXAFS spectra have been obtained from the same sample series [2]. Figure 2 shows the distribution function which is related with the U–O bond from coordinating water, the U–N bond from MeCN and the U–Cl scattering contribution. These three bonds correspond to the components C_1^{EXAFS}, C_2^{EXAFS} and C_3^{EXAFS}. There is a small effect from a [*2p4f*] double-electron excitation [4], which is constant in the whole sample series and occurs therefore not as spectral component.
The determined distances in the first coordination sphere are: U–Oax = 1.77 Å, U–OH_2O = 2.43 Å, U–NMeCN = 2.53 Å and U–Cl = 2.68 Å. The next task is to combine the data from UV-vis and EXAFS spectroscopy to reveal the remaining solvent molecules. The following five monomeric species have been observed: $[UO_2(H_2O)_5]^{2+}$, $[UO_2Cl(H_2O)_2(MeCN)_2]^+$, $[UO_2Cl_2(H_2O)(MeCN)_2]$, $[UO_2Cl_3(MeCN)_2]^-$ and $[UO_2Cl_4]^{2-}$ (Fig. 3).

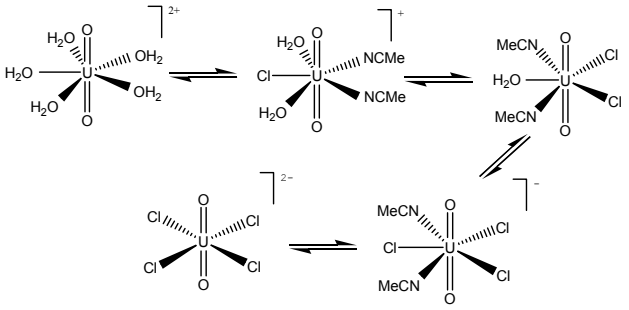

Fig. 3: Coordination of the U(VI) chloride series.

This study shows that a combination of UV-vis and EXAFS is able to reveal both, the species distribution as well as the coordination of the individual species.

REFERENCES

[1] Guillaumont, R. et al. (2003) *Update on the Chemical Thermodynamics of U, Np, Pu, Am and Tc*, Elsevier, Amsterdam.
[2] Hennig, C. et al. (2008) *Inorg Chem.* **47**, 2987-2993.
[3] Denning, R. (2007) *J. Phys. Chem. A* **111**, 4125-4143.
[4] Hennig, C. (2007) *Phys. Rev. B* **75**, 035120.

Luminescence of the uranyl carbonate complex $UO_2(CO_3)_3^{4-}$ in the temperature range of −20°C to 0°C

C. Götz, G. Geipel

TRLFS spectra of frozen solutions with uranyl ions and carbonate ions were collected in the temperature range of −20 °C to 0 °C for the fist time. The intensity shows a strong decrease with increasing temperature. The spectral form is identical in the range from pH 7 to pH 10 and in the uranium concentration range from 10^{-6} M to $5 \cdot 10^{-5}$ M. The spectra are very similar to the spectra of natural and synthetic carbonate containing uranium minerals.

The uranyl carbonate complexes play an import role in the mobility of uranium in the environment and they are very well investigated by solubility investigations, potentiometric titrations and spectroscopic studies. Because the uranyl carbonate complexes show no luminescence at room or elevated temperatures [1], there is a lack of TRLFS studies. In this work, it is shown for the first time, that TRLFS investigations are possible with frozen solutions in the temperature range of −20 °C to 0 °C.

EXPERIMENTAL. Different solutions containing various uranium concentrations and 0.1 M sodium hydrogen carbonate were prepared in the range from pH 5 to pH 11. The solutions were filled in plastic cuvettes (CVD-UV1S from Ocean Optics), frozen and stored in a refrigerator. The cuvettes were set to a precooled cuvette holder (Quantum Northwest Flash 300) with temperature control (Quantum Northwest TC 125). The samples were excited with a Continuum Inlite Laser at the excitation wavelength of 266 nm and the emission light was focused on a fiber which is connected to a spectrograph. The spectra were collected with an intensified CCD-Camera (more details in [2,3]).

RESULTS. The spectra show six observable, slight overlapping bands at 468, 487, 507, 529, 551 and 576 nm. The spectral form is identical to them from natural minerals [4-6] and their synthetic analogues, the emission bands are similar. These minerals are salts of the $UO_2(CO_3)_3^{4-}$ ion, which should be predominant in the prepared solutions. In Tab. 1 a comparison between the emission bands of the frozen solution and of some salts is shown. For the same uranium concentration, the spectra are identical in the range of pH 7 to pH 11. Small changes are observable for pH 6, which implies the presence of other uranyl species at these conditions. A lower content of total inorganic carbon in the solution of 0.029 M can explain the difference. The spectrum at pH 5 shows stronger differences, so the $UO_2(CO_3)_3^{4-}$ ion should not be the predominant uranyl species in this case. Figure 1 shows the decrease of the luminescence intensity by increasing the temperature to −3 °C. When the temperature is further increased, the structure of the spectrum will be lost and a single very broad band appears. If the sample reaches the liquid state, no luminescence is observable. The luminescence lifetimes at pH 7 in Tab. 2 between −18 °C and −3 °C show small changes until the melting process begins.

ACKNOWLEDGEMENTS. The authors thank U. Schaefer for ICP measurements and C. Eckardt for the determinations of the Total Inorganic Carbon content.

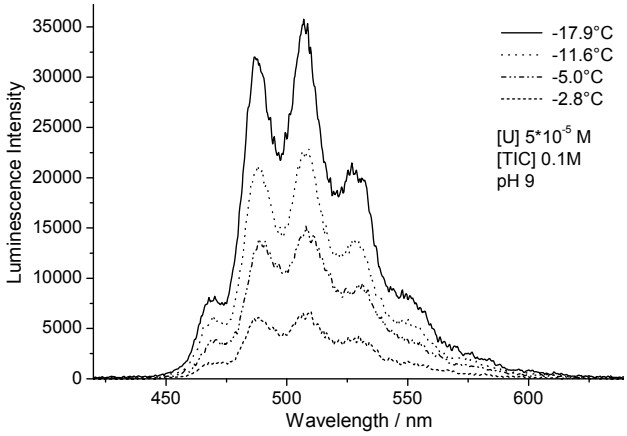

Fig. 1: Luminescence spectra of $UO_2(CO_3)_3^{4-}$ at different temperatures.

Tab. 1: Emission band positions of the luminescent species.

Species	Emission band positions [nm]				
$UO_2(CO_3)_3^{4-}$ present work [a]	468.0 ± 1.0	487.4 ± 0.5	506.5 ± 0.4	528.5 ± 0.7	550.6 ± 0.6
andersonite [4,6]	466.4	485.2	504.8	526.2	549.6
$Na_2Ca[UO_2(CO_3)_3] \cdot 6\ H_2O$ [4]	470.6	486.1	505.4	526.7	549.6
liebigite [6]	466.9	483.1	502.7	524.1	545.9
$Ca_2[UO_2(CO_3)_3] \cdot 10\ H_2O$ [6]	465.4	482.9	502.7	524.5	545.4
$Mg_2[UO_2(CO_3)_3] \cdot 18\ H_2O$ [6]	471.3	487.7	506.9	527.6	551.4
$Ba_2[UO_2(CO_3)_3] \cdot 18\ H_2O$ [6]	469.9	487.7	507.3	528.9	552.2
$CaMg[UO_2(CO_3)_3] \cdot 12\ H_2O$ [6]	472.3	488.9	509.2	531.0	554.7

[a]: frozen solution at ~ −18 °C:

Tab. 2: Luminescence lifetimes for the solution at pH 7.[a]

Temperature [°C]	Luminescence lifetime [µs]
−17.9	282.4 ± 4.6
−11.6	282.2 ± 4.7
−5.0	264.8 ± 3.6
−2.8	256.9 ± 4.5
+3.0[b]	no luminescence observable

[a]: solution with $5 \cdot 10^{-5}$ M uranium.
[b]: after the melting process was completed.

REFERENCES

[1] Bernhard, G. et al. (1996) *Radiochim. Acta* **74**, 87-91.
[2] Götz, C. et al. (2007) *Report FZD -489*, p. 24.
[3] Steudtner, R. et al. (2006) *Report FZD -459*, p. 16
[4] Amayri, S. et al. (2004) *Environ. Sci. Technol.* **38**, 6032-6036.
[5] Bernhard, G. et al. (2001) *Radiochim. Acta* **89**, 511-518.
[6] Amayri, S. et al. (2005) *J. Solid State Chem.* **178**, 567-577.

A novel time-resolved laser fluorescence spectroscopy system for research on the complexation of uranium(IV)

S. Lehmann, G. Geipel, G. Grambole, G. Bernhard

Research on short-lived fluorescence emitting metal ions like uranium(IV) has been very limited to date due to a lack of the technical prerequisites. We overcame these problems and set up a laser system applicable for investigation on the speciation of U(IV). We determined the detection limit of U(IV) in perchloric acid to be $1 \cdot 10^{-6}$ M and its fluorescence decay time with $\tau = 2.73$ ns ± 0.40 ns. Furthermore, we focused on the complexation behaviour of U(IV) using fluoride as a first and well-investigated representative. We found a U(IV) : F ratio of 1 : 1 of the compound formed during reaction. The corresponding complex formation constant was determined to be $\log \beta^{o}(UF^{3+}) = 9.43 \pm 1.94$.

EXPERIMENTAL. The novel laser system consists of a Nd:YAG laser combined with a MOPO-SL (Spectra-Physics Laser) as excitation source, a spectrograph (Acton Research SpectraPro 300i) and an intensified CCD camera (PicoStar HR, LaVision). For our experiments, we set an excitation wavelength of 245 nm. The corresponding pulse width averages 2 ns delivering a pulse energy of 3-4 mJ at a repetition rate of 20 Hz. The room temperature was kept constant at 21 ± 1 °C to ensure stable working conditions during laser operation. Preparation of all samples as well as the TRLFS measurements were carried out in a glove box under inert atmosphere (N_2) at a constant temperature of 21.5 ± 1°C. Fluorescence spectra were recorded in the range between 265 nm and 465 nm.
A U(IV) stock solution was electrolytically reduced from U(VI) in perchloric acid. First, dilution series with U(IV) concentrations between $1 \cdot 10^{-2}$ M and $1 \cdot 10^{-8}$ M were prepared. Additionally, sample series with a constant U(IV) concentration were prepared and fluoride from a sodium fluoride stock solution was added in tenfold stoichiometrical deficiency up to tenfold stoichiometrical excess with respect to the U(IV) concentration. All samples were measured using TRLFS.

RESULTS. Spectra recorded from the dilution series were deconvoluted and evaluated. With a correlation coefficient of $R^2 = 0.982$, nine peaks were identified: at 290, 318, 320, 336, 339, 344, 350, 394 and 410 nm, with the peaks at 320 and 410 nm being the two most prominent ones (Fig. 1). These peak wavelengths are in accordance with literature data [1,2]. Evaluation of the fluorescence decay resulted in the finding of a monoexponential decay. This fact combined with the peak wavelengths determined prove the occurrence of exclusively U^{4+}. The corresponding fluorescence lifetime of U(IV) in perchloric acid was evaluated to 2.73 ns ± 0.40 ns.
In the same manner, the U(IV) fluoride samples were measured (Fig. 2). A great deficiency in the fluoride concentration has no effect on the fluorescence spectrum of U(IV). Enhancing the fluoride concentration up to approximately one third the U(IV) concentration results in a decreasing fluorescence intensity. A further increase of the fluoride concentration changes the shape of the spectrum. The original U(IV) spectrum can no longer be observed. Instead, a new peak at 320 nm appears as well as a broad band without a defined structure between 350 nm and 450 nm. At a stoichiometrical U(IV) : F concentration ratio, the novel spectrum has fully developed. Enhancement of the fluoride concentration up to an excess results exclusively in an increase of the fluorescence intensity until a maximum at a fluoride concentration twofold the U(IV) concentration.

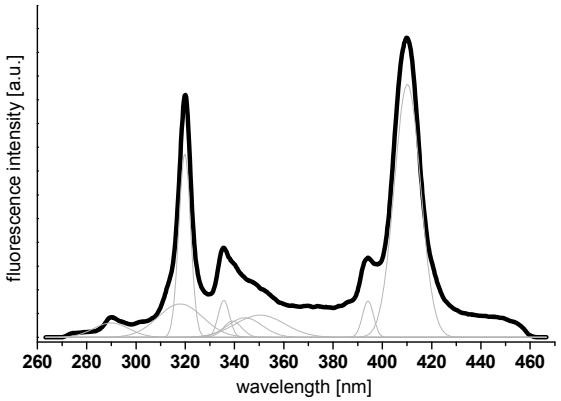

Fig. 1: Deconvolution of a U(IV) fluorescence spectrum(IV) in perchloric acid.

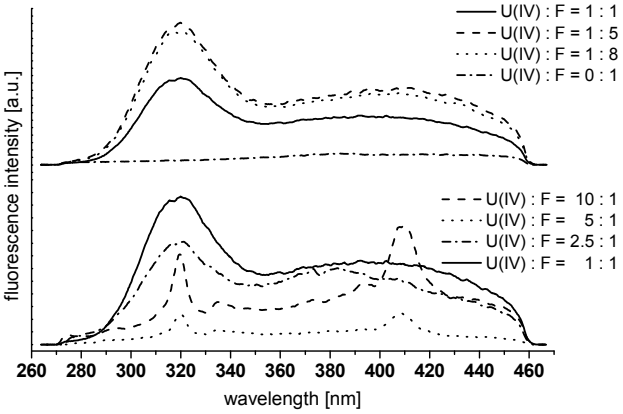

Fig. 2: Fluorescence spectra of the uranium(IV) fluoride complex formation.

All the spectra recorded were evaluated and a 1 : 1 (U(IV) : F) complex was found. The corresponding complex formation constant was determined to be $\log \beta^{o}(UF^{3+}) = 9.43 \pm 1.94$. This value is in high agreement with the one given in [3]. Conclusively, our novel TRLFS system provides a powerful tool for speciation research on elements emitting short-lived fluorescence like U(IV) in submicromolar concentration ranges, which is essential for environmental trace analysis.

ACKNOWLEDGEMENTS. The authors would like to thank the German Research Council (DFG) for financial support (contract no. GE 1011/4-1).

REFERENCES

[1] Kirishima, A. et al. (2003) *Chem. Commun.* **7**, 910-911.
[2] Geipel, G. (2003) *Report FZR -400,* p. 1.
[3] Guillaumont, R. et al. (2003) *Update on the Chemical Thermodynamics of U, Np, Pu, Am and Tc*, Elsevier, Amsterdam.

Investigation on the complexation of uranium(IV) with phosphate using TRLFS

S. Lehmann, G. Geipel, G. Grambole, G. Bernhard

Only few data on uranium(IV) phosphates in solution can be found in literature. Challenging part in research concerning this topic is the low solubility of U(IV) phosphates. A novel TRLFS system enables us to study these compounds in a solved state. By applying this laser fluorescence spectroscopy system, we identified the formation of a complex of the composition $UH_2PO_4^{3+}$. The determination of the corresponding complex was carried out using two different data analysis software packages: (1) Origin 6.1™ and (2) SpecFit/32™. The complex formation constant determined are (1) log β ($UH_2PO_4^{3+}$) = 24.15 ± 0.57 and (2) log β ($UH_2PO_4^{3+}$) = 23.08 ± 0.20.

EXPERIMENTAL. All preparative work as well as the TRLFS measurements were done in a glove box under inert atmosphere (N_2). Uranium(IV) was prepared by electrolytic reduction of a U(VI) perchlorate solution. Several sample series with a constant uranium concentration were prepared. Phosphate was added in terms of a phosphoric acid stock solution. The phosphate concentration varied between tenfold stoichiometric deficiency and tenfold stoichiometric excess with respect to the U(IV) concentration. Experiments were done at an ionic strength of I = 0.1 M. For the determination of the amount of hydrogen released from phosphoric acid during reaction, several sample series with constant U(IV) : PO_4^{3-} ratios (with the phosphate concentration varied between deficiency and excess) were prepared and the hydrogen concentration was varied between 0.01 M and 2 M by the addition of perchloric acid.

RESULTS. To identify the number of phosphate ligands bound to U(IV) during reaction, the fluorescence spectra recorded for the samples with varying phosphate concentration were evaluated. Figure 1 provides an overview of the development of the fluorescence.
Uranium(IV) without phosphate provides a spectrum with the highest fluorescence intensity of all spectra recorded. Addition of phosphoric acid results in a decrease of the fluorescence measured. The original U(IV) fluorescence spectrum is observable up to a phosphate concentration that is stoichiometrical to U(IV). As soon as the phosphate concentration exceeds the U(IV) concentration, fluorescence is no longer measurable. Furthermore, there is no shift of peaks in the spectra or a change in the shape of the spectrum in general (vanishing of single peaks, building up of new peaks or bands) observable. Evaluation of these spectra resulted in the finding of a 1 : 1 complexation of U(IV) : phosphate.

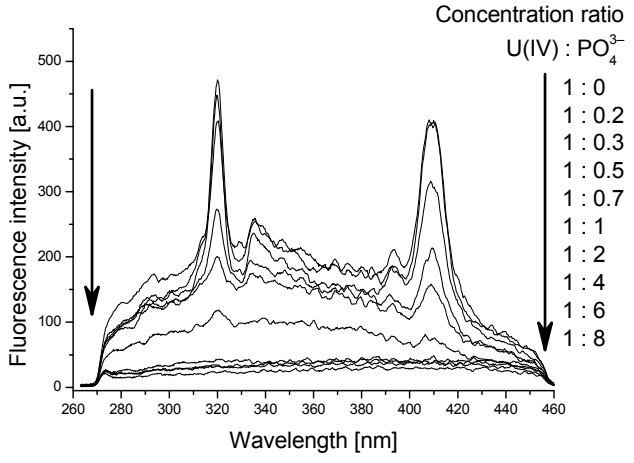

Fig. 1: Fluorescence spectra of the complexation of uranium(IV) with phosphate.

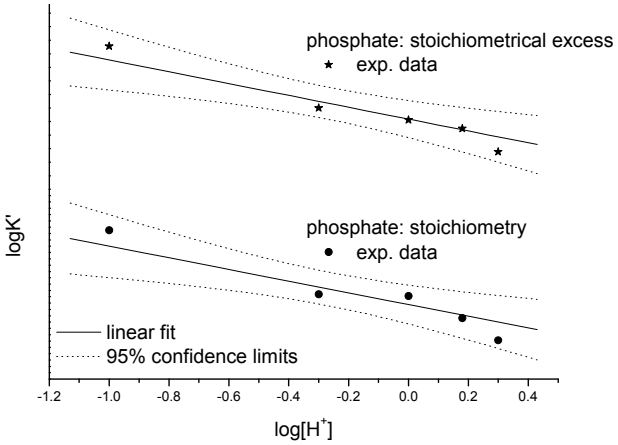

Fig. 2: Release of hydrogen from phosphoric acid during complexation.

For identification purposes of the ligand as $H_2PO_4^-$, HPO_4^{2-} or PO_4^{3-}, the fluorescence spectra of the sample series with varying hydrogen concentration were evaluated. The evaluation procedure is described in [1]. Figure 2 provides exemplarily two graphs.
The slope of the stoichiometric phosphate concentration graph was determined to be (−0.92 ± 0.23), the second slope is (−1.09 ± 0.26). These values show that one hydrogen is released from the ligand during complexation. Therefore, the overall reactions that have taken place are described as follows:

$$H_3PO_4 \rightleftarrows H_2PO_4^- + H^+$$
$$U^{4+} + H_2PO_4^- \rightleftarrows UH_2PO_4^{3+}$$

Table 1 summarizes the complex formation constants log β determined for $UH_2PO_4^{3+}$ via Origin 6.1™ and SpecFit/32™.

Tab. 1: Overview of the complex formation constants of $UH_2PO_4^{3+}$.

Origin 6.1™	SpecFit/32™	Ref. [1]
24.15 ± 0.57	23.08 ± 0.20	25.23 ± 0.13*

* extrapolated to infinite dilution.

To the best of our knowledge, there is only one literature value of log β provided for $UH_2PO_4^{3+}$. All three data imply that uranium(IV) forms a highly stable complex with phosphate in low pH-ranges (~ 1).

ACKNOWLEDGEMENTS. The authors highly acknowledge the financial support by the German Research Council (DFG) (contract no. GE 1011/4-1).

REFERENCES

[1] Merkel, B. J. et al. (2002) *Uranium in the aquatic environment*, p. 369-376, Springer, Berlin.

In-situ UV-vis-NIR absorption spectroelectrochemistry of uranyl(V/VI) carbonates

K. Takao, S. Takao, A. C. Scheinost, C. Hennig

In-situ UV-vis-NIR absorption spectroelectrochemical experiment was demonstrated using a redox couple of uranyl(V/VI) carbonates.

Actinide elements are present in various oxidation states. Therefore, electrochemistry is able to reveal thermodynamic parameters. However, electrochemical experiments normally provide only limited data, e.g., potential-current or time-current functions. Furthermore, their interpretations are not always simple. To solve this situation, many attempts to combine electrochemistry and spectroscopy, the so-called "*spectroelectrochemistry*", have been made [1-3]. One of the most popular techniques is the combination with UV-vis-NIR absorption spectroscopy using an optical transparent thin layer electrode cell (OTTLE cell). This technique provides helpful insights into an electrochemical reaction of interest. In this report, we applied a combination of UV-vis spectroscopy and electrochemistry to study a redox reaction of uranyl(V/VI) carbonates (Eq. 1) [4-8].

$$U^{VI}O_2(CO_3)_3^{4-} + e^- \rightleftarrows U^{V}O_2(CO_3)_3^{5-} \qquad (1)$$

EXPERIMENTAL. An initial solution of $U^{VI}O_2(CO_3)_3^{4-}$ (21.8 mM) was prepared from $Na_4U^{VI}O_2(CO_3)_3$ and 1.21 M Na_2CO_3 aq. The OTTLE cell from BASi was equipped with 3 electrodes (a Pt mesh working electrode as OTTLE, a Pt wire counter electrode, an Ag/AgCl reference electrode) and a PTFE tube inert gas inlet. The Pt mesh was placed in a thin layer (ca. 1 mm) between quartz windows of the cell. The effective optical path length was spectrophotometrically determined at 0.55 mm. The applied potential (E) on OTTLE was varied in a range from –0.600 to –0.850 V vs. Ag/AgCl stepwise by AUTOLAB PGSTAT302. Prior to starting this experiment, argon gas was passed through the sample to expel dissolved oxygen. The absorption spectrum at each E was recorded by a Varian Cary 5G spectrophotometer.

RESULTS AND DISCUSSION. The obtained spectra at various potentials are shown in Fig. 1. These spectra are reported in difference absorbance (ΔAbs) from $U^{VI}O_2(CO_3)_3^{4-}$ due to difficulties in reproducing the exact beam position of the optical path in the OTTLE cell.
In Fig. 1a, isosbestic points were clearly observed at 367 and 388 nm, indicating that only Eq. 1 is valid in this system. The absorbance variation in Fig. 1 corresponds to the fractions of $U^{VI}O_2(CO_3)_3^{4-}$ and $U^{V}O_2(CO_3)_3^{5-}$ at each E, and should follow the modified Nernstian equation.

$$E = E^\circ + \frac{RT}{nF}\ln\frac{|A - A_R|}{|A_O - A|} \qquad (2)$$

where $E°$, n, F, R, and T are standard potential, electron stoichiometry, Faraday constant, gas constant, and absolute temperature, respectively. The absorbance at each E is denoted by A, and those of oxidant and reductant are indicated by subscripts $_O$ and $_R$, respectively. From the Nernstian plot shown in Fig. 2, n and $E°$ at 298 K were evaluated as 1.05 ± 0.02 and -0.740 ± 0.001 V vs. Ag/AgCl, respectively. The former quantity is the evidence for Eq. 1, and the latter is similar to those reported previously (–0.7459 V [4], –0.751 V [7] in 1.0 M Na_2CO_3 aq.). The production of $U^{V}O_2(CO_3)_3^{5-}$ was also confirmed by its characteristic absorption in Fig. 1b [5-8].

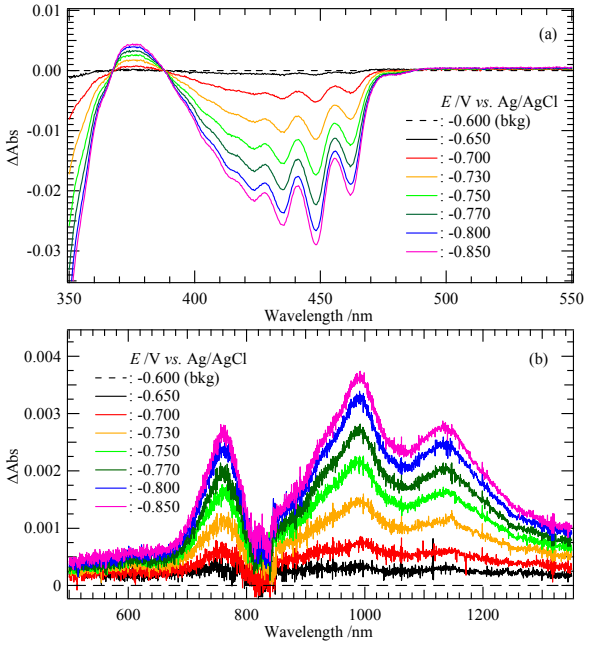

Fig. 1: Difference absorption spectra of $U^{V}O_2(CO_3)_3^{5-}/U^{VI}O_2(CO_3)_3^{4-}$ redox couple at various E (total [U(V/VI)] = 21.8 mM, $[Na_2CO_3]$ = 1.21 M). (a) 350-550 nm, (b) 500-1350 nm.

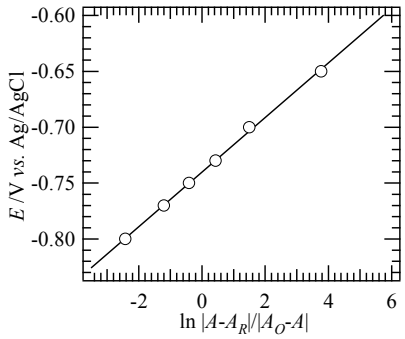

Fig. 2: Nernstian plot for absorbancies at 448 nm in Fig. 1. Smooth line is the best fit of Eq. 2.

CONCLUSION. In this report, it was demonstrated that n and $E°$ can be determined in the *in-situ* spectroelectrochemical experiment. One can obtain the absorption spectra of both oxidant and reductant even if one of them is unstable (e.g. U(V) species), unless any successive reactions take place after the reaction of interest. The small sample volume (ca. 2 mL) is an advantage especially for the actinide experiments. Because the OTTLE cell is made of transparent quartz, it may be used for other spectroelectrochemical techniques like fluorescence and Raman spectroscopy.

REFERENCES

[1] DeAngelis, T. P. et al. (1976) *J. Chem. Edu.* **53**, 594-597.
[2] Heineman, W. R. (1983) *J. Chem. Edu.* **60**, 305-308.
[3] Endo, A. et al. (1995) *Anal. Sci.* **11**, 457-459.
[4] Grenthe, I. et al. (1992) *Chemical Thermodynamics of Uranium*, OECD/NEA North-Holland, Amsterdam, 2003 updated.
[5] Cohen, D. D. (1970) *J. Inorg. Nucl. Chem.* **32**, 3525-3530.
[6] Mizuoka (Takao), K. et al. (2005) *Inorg. Chem.* **44**, 4472-4474.
[7] Mizuoka (Takao), K. et al. (2005) *Inorg. Chem.* **44**, 6211-6218.
[8] Ikeda, A. et al. (2007) *Inorg. Chem.* **46**, 4212-4219.

UV-vis spectroscopy of Am(III)-salicylate complexation at low metal concentrations

M. Müller,[1] M. Acker,[2] S. Taut,[2] G. Bernhard

[1]Institute of Analytical Chemistry, Dresden University of Technology, Dresden, Germany; [2]Section of Radiation Protection, Dresden University of Technology, Dresden, Germany

The complexation of the trivalent americium ion with salicylic acid was investigated using a Long Path Flow Cell (LPFC) for UV-vis spectroscopy, enabling measurements at low metal concentrations. At pH 4 and an ionic strength of 0.1 M ($NaClO_4$) a 1 :2 complex with log β_{122} = 32.28 ± 0.07 was determined.

The knowledge of the complexation and sorption behavior of radionuclides in the environment is important for the assessment of long term safety of nuclear waste disposal sites, providing information about the mobility of these elements when released in the host rock. Therefore, thermodynamic data concerning the reactions between radionuclides and the organic and inorganic constituents in argillaceous rock have to be collected.
We studied the complexation reaction of the trivalent Am ion with salicylic acid (Sal; 2-hydroxybenzoic acid) in aqueous solution via UV-vis spectrometry. We used a Long Path Flow Cell (LPFC) as cuvette, which provides a path length of 200 cm. Due to this very long optical path it is possible to measure the absorbance of the Am(III) ion at much lower concentrations than it would be possible with a conventional cuvette.

EXPERIMENTAL. The complexation experiments were carried out at an inert gas atmosphere (N_2) at room temperature and at a total Am concentration of $5 \cdot 10^{-7}$ M. The absorption between 480 and 530 nm was measured as a function of Sal concentration, which was varied between $6.1 \cdot 10^{-5}$ M and $3.3 \cdot 10^{-3}$ M. The ionic strength of the sample was adjusted to 0.1 M ($NaClO_4$) and the pH was kept constant at 4.0 with $HClO_4$ and NaOH. The spectra were recorded with a fiber optics spectrometer (MCS 601, Carl Zeiss, Jena, Germany) and evaluated using the factor analysis program SPECFIT™ (version 3.0).

RESULTS. At pH 4.0, the main ligand species in solution is the single protonated form $SalH^-$ [1], which is known to form 1 :1 and 1 :2 complexes with trivalent lanthanides, e.g. Eu(III) [2]. To prove whether a complexation with Am(III) occurs we measured the absorption spectra of Am(III) in dependency to the ligand concentration. The recorded spectra are shown in Fig. 1. With increasing ligand concentration, both a decrease in absorption and a slight red shift of the absorption maxima were observed indicating the formation of one or two complex species. We analyzed the spectra with SPECFIT™ trying different hypotheses with respect to the occurrence of the 1 :1, the 1 :2 or both complexes. Just the assumption that only the 1 :2 complex is present results in a good fit of the data. The stability constant for the 1 :2 complex was determined to be log β_{122} = 32.28 ± 0.07. The corresponding speciation in Fig. 2 and the red line in Fig. 1, which represent the absorption spectra of the pure 1 :2 complex species, was given out by SPECFIT™. The obtained log β_{122} of the Am(III)-salicylate system is higher than that of the Eu(III)-salicylate system which has been investigated by several working groups and different techniques. Two europium complexes with average values of log β_{111} = 15.46 and log β_{122} = 30.74 were described [2,3]. Since Eu and Am have similar chemical properties in many aspects these differences in speciation have to be discussed critically and investigated by further measurements.

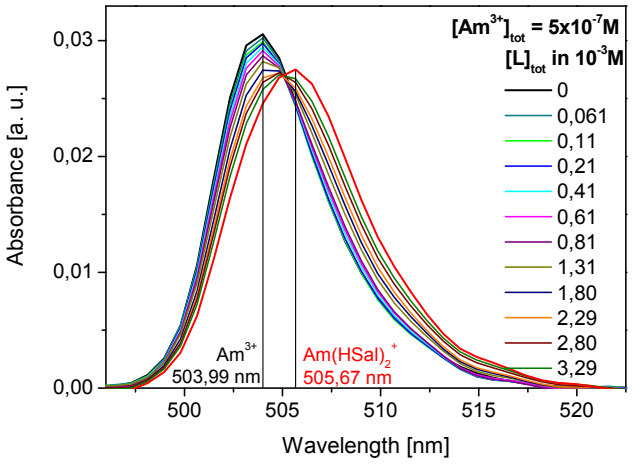

Fig.1: The absorption spectra of Am(III) at different salicylic acid concentrations in 0.1 M $NaClO_4$ solution at pH 4.0. The red line marks the spectra of the pure complex species as predicted from SPECFIT™.

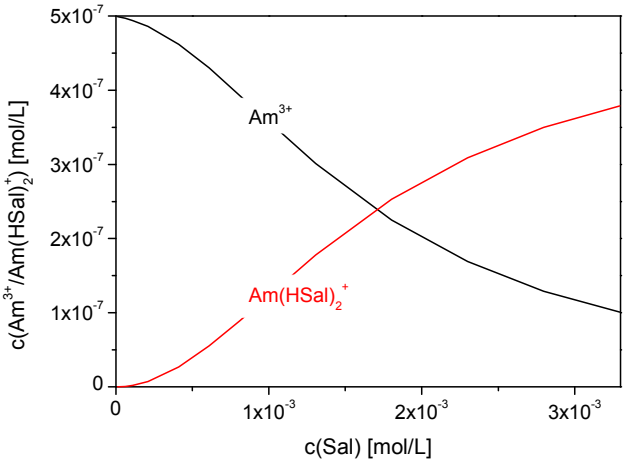

Fig. 2: The proposed concentration distribution of the two Am(III) species in solution at an ionic strength of 0.1 M ($NaClO_4$) and at pH 4.0, calculated with the log β_{122} from SPECFIT™.

ACKNOWLEDGEMENT. This work is funded by BMWi under contact number 02E10417.

REFERENCES

[1] Lajunen, L. H. et al. (1997) *Pure Appl. Chem.* **69**, 329-381.
[2] Hasegawa, Y. et al. (1989) *Bull. Chem. Soc. Jpn.* **62**, 1486-1491.
[3] Aoyagi, N. et al. (2004) *Radiochim. Acta* **92**, 589-593.

Inversion of the EXAFS equation by a recursive iteration method. Part I – Theory

H. Funke, A. Rossberg

The Landweber iteration approach is used to construct the radial pair distribution function (PDF) from an EXAFS spectrum. The radial PDF as solution of the fundamental EXAFS integral equation is determined in a stable way without additional supplementary conditions by a recursive application of the EXAFS kernel.

RADIAL PAIR DISTRIBUTION FUNCTION. The PDF describes the density of interatomic distances in a material. The radial PDF, which is independent of orientation, is of special practical importance for the analysis of EXAFS spectra. It is a major descriptor for the atomic structure of amorphous materials and liquids.

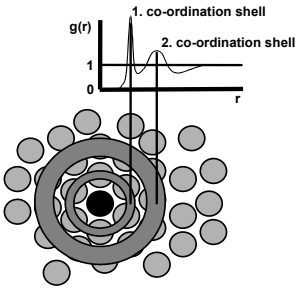

Fig. 1: Schematic illustration of a radial PDF.

A radial PDF has by definition the properties [1]:

(1) $g(r) \geq 0$ *for any* r,

(2) $g(r) \to 1$ *if* $r \to \infty$,

(3) $g(r) \to 0$ *if* $r \to r_{\min}$,

$g(r) = 0$ *if* $r < r_{\min}$

It means, that the PDF is a positive definite function. And for large distances, where the particles are uncorrelated, $g(r)$ goes to 1.

EXAFS EQUATION. The general EXAFS integral equation for a one-component system has the form:

$$\chi(k) = \int_0^\infty \frac{F(k,r)}{k} \exp\left(-\frac{2r}{\lambda(k)}\right) \sin\left[2kr + 2\delta(k) + \varphi(k,r)\right] g(r)\,\mathrm{d}r$$

where $\chi(k)$ is the normalized oscillating part of the measured x-ray absorption spectrum, k is the electron wave vector, and r is the distance from the central to the backscattering atoms. The functions backscattering amplitude $F(k,r)$, the phase shift of the central atom $\delta(k)$, the phase shift on the neighboring atoms $\varphi(k,r)$, and the mean free path of the photoelectron $\lambda(k)$ are obtained from the FEFF code.

The solution of the EXAFS equation is the PDF, i.e. $g(r)$.

If the density of interatomic distances is represented by separated Gaussian peaks

$$g(r) = \sum_{m=1}^{shells} \frac{N_m}{\sqrt{2\pi}\sigma_m r_m^2} exp\left(\frac{-(r-r_m)^2}{2\sigma_m^2}\right),$$

the above integral can be resolved and is reduced to the EXAFS equation for a number of coordination shells:

$$\chi(k) = \sum_{m=1}^{shells} \frac{N_m}{r_m^2} \frac{F_m(k,r_m)}{k} e^{-\frac{2r_m}{\lambda(k)}} e^{-2\sigma_m^2 k^2} \sin\left[2kr_m + 2\delta(k) + \varphi(k,r_m)\right].$$

N_m is the coordination number, r_m the distance and σ_m^2 the Debye-Waller factor of the back scattering atoms in the m^{th} shell.

Therefore, the knowledge of the complete PDF allows a much more general analysis of the EXAFS signal as the shell fit approach, see [2].

In the PDF approach the coordination number between two radii is defined as: $N = 4\pi \int_{r_1}^{r_2} r^2 g(r) dr$, the distances r_m are at the peaks of $g(r)$, and σ_m^2 are integral parts of $g(r)$.

ITERATION PROCEDURE. The EXAFS equation in operator form $Ag = \chi$, multiplied by αA^* (A^* is the conjugate transpose), is identically rewritten to: $g = (I - \alpha A^* A)g + \alpha A^* \chi$. Based on this equation with the initial condition $g_0 = 0$ and a parameter $\alpha > 0$, Landweber [3], suggested the iteration scheme:

$$g_{n+1} = g_n + \alpha A^* (\chi - A g_n).$$

Here n is the iteration number. This iteration procedure can be interpreted as the steepest descent algorithm to minimize the functional $\|Ag - \chi\|$ with α as convergence parameter. For our applications the optimal choice of α is:

$$\alpha^{EXAFS} = 1 / \left\| A^* A \right\|.$$

STOPPING PARAMETER. The mean problem in general iteration procedures is: when stops the iteration? If the iteration is too long, noise and errors dominate the iteration. If the iteration is too short, a loss of resolution will result.

If the total data error δ would be known, the stopping rule defining n_{opt}, is simply:

$$if \quad \left\| Ag_n - \chi \right\| \leq \delta : n = n_{opt}.$$

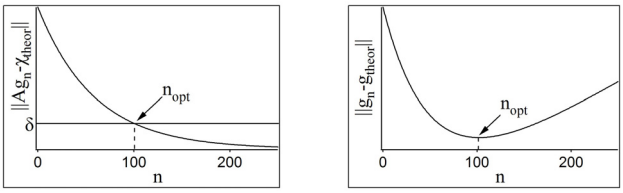

Fig. 2: Definition of n_{opt} for an idealized spectrum. Left: the difference of the iterated and the theoretical spectrum over n. Right: the difference of the iterated and the computed PDF over n.

L-CURVE CRITERION. For real EXAFS measurements the total error is not known. The concept of the L-curve criterion [4] is adapted for determining n_{opt}. In general, the L-curve is a log-log plot of the norm of an iterated solution versus the norm of the corresponding residual. Both norms depend parametrically on n_{opt}. The resulting curve shows a shape like the capital letter "L". n_{opt} is chosen as the maximum of the L curve curvature, corresponding to the corner of the “L”.

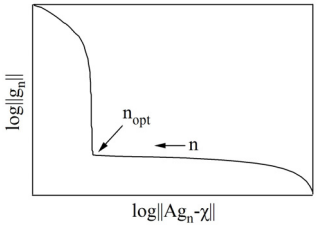

Fig. 3: A typical idealized L-curve. The function g_n is the PDF after the n^{th} iteration.

Some first applications of the presented iteration approach are presented in part II [2].

REFERENCES

[1] Babanov, Y. A. et al. (1981) *Phys. Stat. Sol.(B)* **105**, 747-757.
[2] Rossberg, A. et al. (2009) this report, p. 66.
[3] Landweber, L. (1951) *Am. J. Math. Manag. Technol.* **73**, 615-624.
[4] Kunicke, M. et al. (2005) *Physica Scripta* **T115**, 237-239.

Inversion of the EXAFS equation by a recursive iteration method. Part II - Application

A. Rossberg, H. Funke

For the first hydration sphere of the curium(III) aqua ion the Cm–O pair distribution function (PDF) is iteratively calculated from the L_{III} EXAFS spectrum. The asymmetric PDF is well described by two Gaussian distributions centered at 2.47 Å and 2.62 Å. The distribution of the Cm–O bond distances points out that the Cm(III) ion is coordinated by 9 water molecules in D_{3h} symmetry.

EXPERIMENTAL. The Cm L_{III} extended X-ray absorption fine structure (EXAFS) was measured at beamline 12-BM-B at the Advanced Photon Source (U.S.A.) [1]. The sample contains 0.523 M Cm(III) in 1 M perchloric acid [1].

RESULTS. In common shell fitting approaches the pair distribution function (PDF) is approximated by Gaussian peak shapes. If the PDF has a small asymmetric character then the cumulant expansion might be used for a better description of the PDF. In the most cases the shape of the PDF is not known *a priori*, hence the fitting model (symmetric, asymmetric or both) can not be clear defined. A fit with the wrong model for the PDF can lead to large errors in the EXAFS structural parameters. As discussed in Part I [2] the recursive iteration method is able to calculate the PDF directly from the EXAFS spectrum without *a priori* knowledge of its shape. In the following we test the performance of the iteration method on the basis of the well known structure of the Cm(III) aqua ion. The operator matrix A was calculated with FEFF8 in the R-range 1.3-4.0 Å with an increment of 0.02 Å. The amplitude reduction factor was set to $S_0^2 = 1$. The optimum number of iterations ($N_{opt} = 850$) were determined by using the L-curve criterion [2]. Figure 1 shows the experimental EXAFS spectrum and its reproduction by using the calculated PDF which is shown in Figure 2. Note that the small peaks at the right side in the PDF might arise from contributions of multiple scattering signals. In the range of 2.1-3.0 Å the integral of the PDF is equal to 9 O atoms.

A single Gaussian distribution cannot account for the observed large asymmetry of the calculated PDF. The asymmetric shape of the PDF is best reconstructed by using two Gaussians (Figure 2) which represents two O shells (shell A and shell B) at two different radial Cm–O distances. Each Gaussian is parameterized by a radial Cm–O distance (R), number of coordinated O atoms (CN), and the Debye-Waller factor (σ^2). The structural parameters calculated by the recursive iteration method are in favorable agreement with the literature data [1] (Table 1).

Note that in the shell fit approach the coordination numbers of the two shells must be fixed for stabilizing the fitting procedure [1]. The observed ratio between the areas of the two Gaussians is 2 : 1 and corresponds to the ratio between the number of O atoms in the short distance and the long distance. This ratio allows a 6-fold coordination (4 : 2), 9-fold coordination (6 : 3) and a 12-fold coordination (8 : 4). If one assumes a common error in determination of coordination numbers of 20% then both, the 6-fold and the 12-fold coordination can be ruled out because 9 ± 1.8 O atoms were observed by the integration of the PDF.

Tab. 1: Structural parameter for Cm(III) hydrate determined by the recursive iteration method and from literature [1].

Shell	CN	R[Å]	$\sigma^2 \cdot 10^3$ [Å^2]
A	6(2), 6*,f	2.47(1), 2.47*	6.1(2), 5.3*
B	3(2), 3*,f	2.62(6), 2.63*	10(6), 9*

() - 1σ error, * - [1], f – fixed during the shell fit.

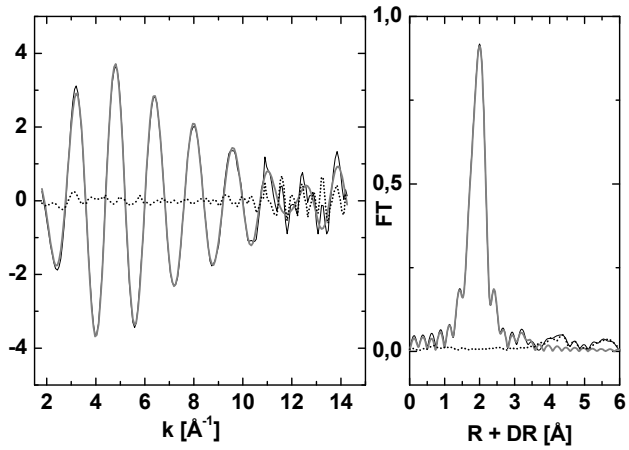

Fig. 1: Cm L_{III} EXAFS (left) with corresponding Fourier-transform (right). Experimental data (thin line), reproduction by using the PDF in Fig 2 (bold line), residual (dotted line).

Moreover the 9-fold coordination and the splitting in six short and three long Cm–O distances was also observed by DFT calculations which predicts a D_{3h} symmetry for the curium(III) aqua ion at room temperature [3].

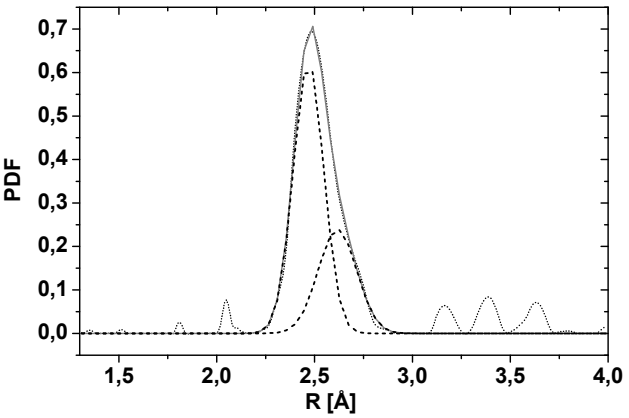

Fig. 2: Cm-O pair distribution function (dotted line), reproduction by using two Gaussians (dashed lines), sum of the Gaussians (solid line).

We showed that the iteration method is able to calculate the PDF without assumptions about the peak shape. This is a unique advantage in comparison with shell fitting procedures which use an underlying model function for the approximation of the true PDF.

ACKNOWLEDGEMENTS. We thank L. Soderholm for supplying the Cm EXAFS spectrum.

REFERENCES

[1] Skanthakumar, S. et al. (2007) *Inorg. Chem.* **46**, 3485-3491.
[2] Funke, H. et al. (2008) this report, p. 65.
[3] Hagberg, D. et al. (2007) *J. Am. Chem. Soc.* **129**, 14136-14137.

Biophysics

Introducing remarks to the new division of the IRC: Biophysics

K. Fahmy

In the statement of the Wissenschaftsrat (German Council of Science and Humanities) based on the evaluation of the Forschungszentrum Dresden-Rossendorf (FZD) in late 2007 a focusing of the scientific activities in the field of life sciences at the research center was appreciated. Accepting the recommendations of this statement, the biophysics division, formerly part of the program "Structural Dynamics of Biomolecules" (running from 2003 to 2009 at the FZD), has now become one of the pillars of the program "Actinides (metals) in biosystems". This realignment of the research topics is accompanied by a change of the institutional affiliation of the division within the FZD. Starting with 2008, our group constitutes now the fourth division of the Institute of Radiochemistry (IRC).

We provide reports of actual projects which reflect this period of transition and, therefore, are presented in an extra chapter of this Annual Report. The Biophysics Division is currently extending the protein-structural investigations to biomolecular metal coordination, including DNA as a prime target for intracellular coordination of multivalent cations. In this process, the application of complementary experimental approaches is of prime importance and has been successfully established in the preceding program. This is exemplified by the recently published investigation of the function of molecular motors, studied in collaboration with the Max Planck Institute of Molecular Cell Biology and Genetics, Dresden, Germany. The corresponding report shows how a combination of structure-sensitive spectroscopic methods, such as Circular Dichroism (CD), Fourier-transform infrared (FT-IR), and fluorescence spectroscopy allows determining protein structural changes and unfolding energies that are of direct importance to the biological function, here, the movement of cellular cargo (see pages 73, 74).

Regarding one of the scientific foci of the IRC, i.e. the interactions of actinides with biosystems, the investigation of metal binding using our previously established spectroscopic monitors of biomolecular structure, we expect synergies with ongoing radiochemical projects that will promote the understanding of fundamental, environmentally relevant molecular processes occurring in many organisms.

In the future, our contributions will be fully integrated into the two research programs of the IRC as they are presented in the preceding chapters.

Spectroscopic characterization of Au complexation and nanoclusters formation on *Bacillus sphaericus* JG-A12 S-layer

U. Jankowski, K. Fahmy, S. Selenska-Pobell, M. Merroun

Protein secondary structure and stability of S-layers from *B. sphaericus* JG-A12 in Au-complexes with Au(III) and in Au(0) nanoparticles, produced by reduction of Au(III), was studied by FTIR spectroscopy. The data show a different role of side chain carboxylates in complex formation as compared to an analogous study on complexation of Pd(II) or Pt(II).

EXPERIMENTAL. *B. sphaericus* JG-A12 was cultured in NB medium. The preparation of S-layer protein was performed as described in [1]. In the batch experiment 10 mg of protein were incubated in 100 ml 3 mM $HAuCl_4$ for 72 hours at room temperature in darkness. Afterwards, Au (III) was reduced by addition of a few drops of 100 mM DMAB to produce Au(0)-nanoparticles.
The suspension of the batch experiment was measured using Attenuated Total Reflection FT-IR on a Si-crystal (Bio-ATR-II).

RESULTS. The secondary structure of the S-layer of *B. sphaericus* JG-A12 is composed of mainly three components: turns, β-sheets, and random structures [2]. Spectral deconvolution in Fig. 1 shows a weakening of the peak at 1641 cm^{-1} and increased absorption at frequencies from 1660-1690 cm^{-1}, indicative of increased β-sheet structure from mainly unordered stretches upon Au(0)-nanoparticles formation.
Figure 2 shows the pH-dependent IR absorption of the Au treated samples. Weakening of asymmetric (1560 cm^{-1}) and symmetric (1400 cm^{-1}) stretching mode of carboxylates during acidification reveals the presence of ionized carboxylates. However, their contribution is distinctly lower, particularly in case of the S-layer loaded with Au(0)-nanoparticles, as compared to formerly studied Pd-bound S-layers [2,3]. This suggests that in Au(0)-nanoparticles-loaded S-layer, side chain carboxyls are mainly protonated which agrees with the shoulder at 1721 cm^{-1} (carboxyl C=O stretch) which persists even at alkaline pH. Thus, only a small fraction is available to become protonated by acidification which explains the reduced pH effect as compared to Pd-bound S-layers [2].
As is evident from the results presented in Fig. 3, where the asymmetric carboxylate stretch at ~1560 cm^{-1} is undisturbed by the amide-II absorption in D_2O, the ionized fraction appears to correspond to unusually acidic carboxyls as they cannot be fully neutralized even at pH 1.
In comparison to our previous studies [2,3], Au exhibits a complexation mechanism with S-layers that is different from that of Pt or Pd. Au appears to cause hydrophobic burial, and thus protonation of carboxyl side chains rather than engaging in ionic interactions as found with Pd. In both cases, however, protein secondary structure becomes highly stabilized against acidic denaturation. This property is of direct relevance to technical applications.

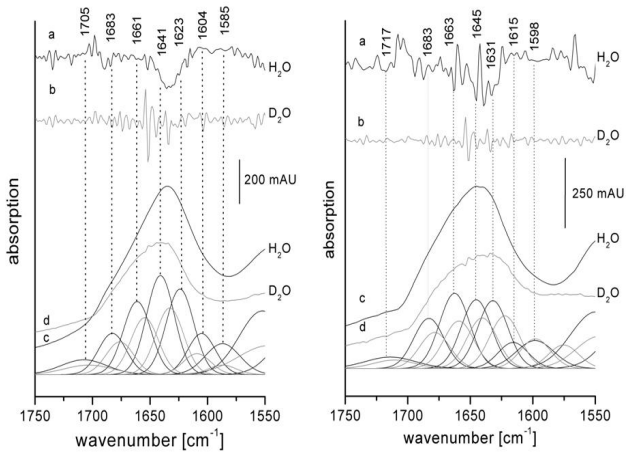

Fig. 1: IR spectra of Au(III)-bound S-layer (left) in H_2O (c) and in D_2O (d) and of Au(0)-nanoparticles-loaded S-layer (right). Simulated spectra are derived from the 2nd derivative (a ,b) of raw data.

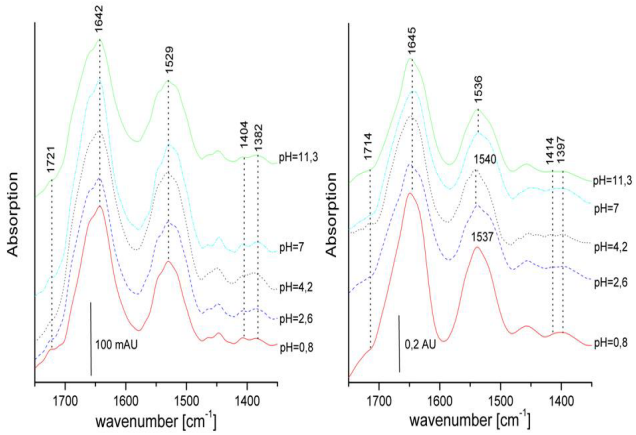

Fig. 2: pH dependence of the IR-absorption of Au(III)-bound S-layer (left) and of Au(0)-nanoparticles-loaded S-layer (right).

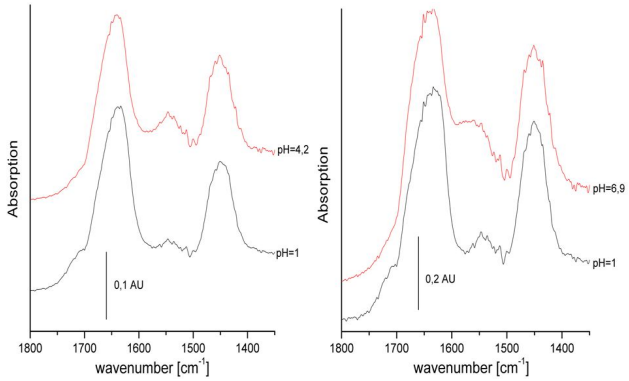

Fig. 3: pH dependence of the IR-absorption of Au(III)-bound S-layer (left) and of Au(0)-nanoparticles-loaded S-layer (right). Measurements after exchange of H_2O for D_2O, to resolve the asymmetric carboxylate stretch in the 1540-1560 cm^{-1} range.

REFERENCES

[1] Raff, J. (2002) Thesis, University of Leipzig, Leipzig.
[2] Fahmy, K. et al. (2006) *Biophys. J.* **91**, 996-1007.
[3] Jankowski, U. (2007) Diploma thesis, TU Bergakademie Freiberg, Freiberg.

Hydration-conformation coupling of biomolecules

H. Khesbak, O. Savchuk, K. Fahmy

In order to understand the mechanism of binding of biomolecules to each other or to inorganic ligands, it is important to explore the role of hydration water in the binding process. This is particularly important in binding to large ions such as actinides and heavy metals where hydration water gets replaced or restructured upon binding. We have established an experiment to reversibly induce fast transient hydration changes in biomolecular films while monitoring structural changes by time-resolved FT-IR spectroscopy. We have focused on DNA as a target that responds with structural changes to metal ions binding to its phosphate backbone. The method, however, is generally applicable, particular for complex systems at interfaces such as lipid membranes, peptidoglycans, and S-layers, where ions interact with biological diffusional barriers that govern entry into an organism in dependance of hydrated pathways through these barriers.

EXPERIMENTAL. The humidity of a DNA film is modulated by an electric current (0.3 mA, 1-4 s) sent through a heating wire in a saturated salt solution that is in equilibrium with the gas phase above the biofilm. Thereby, the humidity increases above the initial level determined by the salt solution. The ensuing water uptake and structural changes are monitored by FT-IR spectroscopy in time slices of 4 to 16 s for ~ 1 min. The reversibility and the fast response allows application of many current pulses such that time-resolved spectra can be co added from 10-20 independent automated experiments in about 1 h. This allows the recording of high S/N difference spectra at different defined hydration levels in successive experiments on an individual biomolecular film.

RESULTS. Preliminary hydration-modulated FT-IR difference spectra (Fig. 2) show different H-bonding patterns to the DNA-backbone (1260-1000 cm^{-1}) at different water potentials. Disruption of the water structure can thus be studied and experiments are underway determine formation of DNA-europium complexes. Isothermal titration calorimetry (ITC) has revealed the displacement of DNA-bound water by europium: the binding of Eu^{3+} to DNA as the reaction is entropically driven and enthalpically opposed (Fig. 3). By the combination of these approaches, structure and energetics of metal DNA interactions can be described.

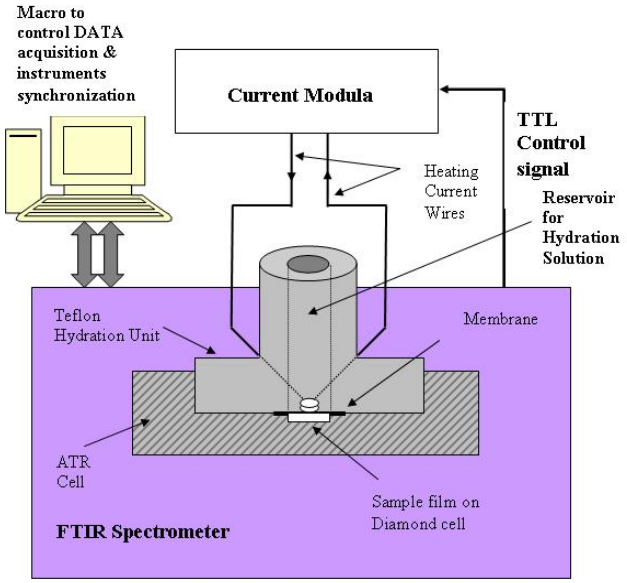

Fig. 1: Experimental setup.

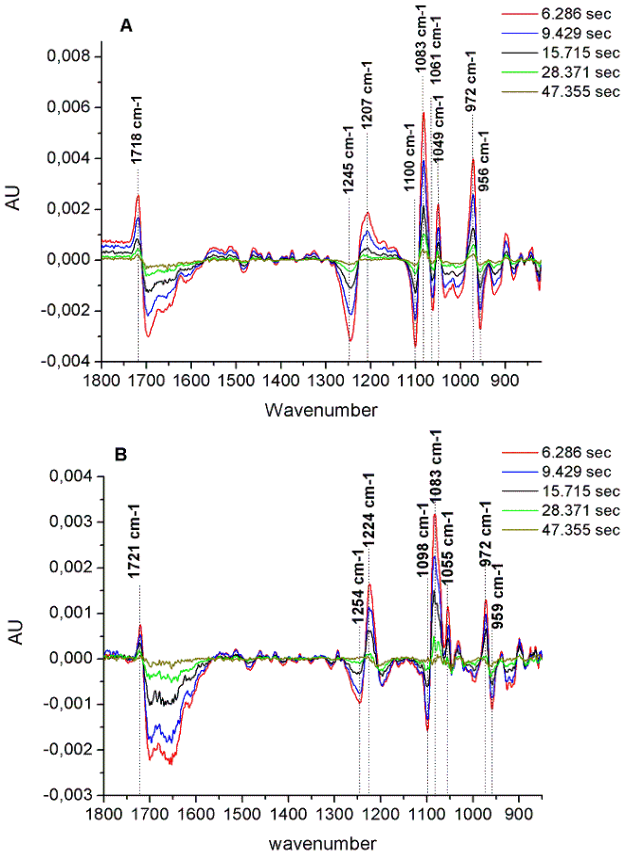

Fig. 2: Time-resolved FT-IR spectra: PO_2^- antisymmetric stretch (1222 cm^{-1}) witnesses larger frequency shift at RH = 65% (Fig. 2A) compared to RH = 75% (Fig. 2B). The same is also noticed for the CO stretch of the backbone sugar (1050 cm^{-1}).

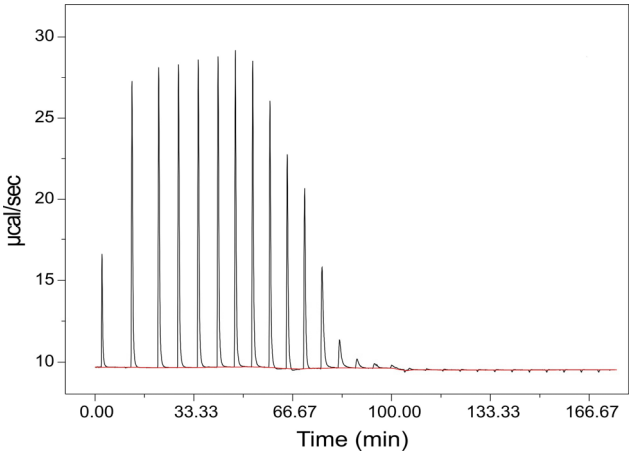

Fig. 3: ITC data of DNA (from Salmon Testes) titrated by Eu^{3+} (6 mM NaCl in the cell and syringe) at 50 °C. Each peak corresponds to the injection of 10 µL Eu^{3+}.

Eu^{3+}-DNA binding: Isothermal titration calorimetry and circular dichroism

O. Savchuk, K. Fahmy

Multivalent cations bind to extended DNA ultimately leading to condensation into compact particles. Our study focuses on structural and energetic description of the binding of large metal ions, here Eu^{3+}, to DNA whose negatively charged phosphate backbone represents the natural target for lanthanides, actinides, and many environmentally relevant metals. Beside clarifying health-related aspects, the understanding of metal DNA-interactions has implications for tailoring metal-specific complexes in biotechnology.

EXPERIMENTAL. Isothermal titration calorimetry (ITC) has been used to determine the thermodynamic parameters of metal-DNA binding interactions, whereas the accompanying structural changes were monitored by circular dichroism (CD).

RESULTS. Europium(III) binding to the short 144 bp plasmid DNA puc21 exhibits a two-stage behavior shown in Fig. 1 (red trace): up to a molar ratio $R = [Eu^{3+}]/[P]$ of 0.35 Eu^{3+} associates with the DNA phosphate backbone, whereas DNA condensation occurs in the range $0.35 < R < 0.8$, similar to binding of Co^{3+} [1]. In case of longer (on average 2000 bp) DNA there is no additional heat exchange attributable to condensation (Fig. 1, black trace). This difference is related to the capability of short DNA molecules to adjust more readily to become incorporated into a well ordered condensed structure, whereas the entropic cost is higher for the longer genomic DNA to adopt this state. The ITC data can be described by an electrostatic binding model that includes anticooperativity. This predicts that triply charged cations will bind to DNA with three times more negative free energy change than singly charged cations, and that binding constants of triply charged cations will equal the cube of the binding constant of singly charged cations. We are currently adopting this model to lanthanide binding.

The different phases of the calorimetric trace correlate well with structural transitions. CD spectroscopy shows that the short plasmid undergoes a negative B → Ψ transition after when $R > 0.35$ leading to condensation seen in Fig. 2, while the genomic DNA stays in a slightly altered B-form (Fig. 3). The spectral changes may reflect increasing dehydration of the phosphate backbone when water is replaced by Eu^{3+}, leading to conformational change not seen with Co^{3+} [2]. The coupling between secondary structure and metal binding may additionally depend on base sequence.

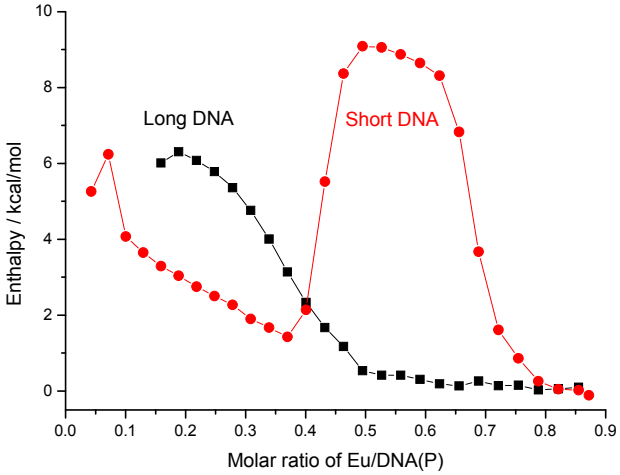

Fig. 1: ITC curves Eu^{3+} binding to short plasmid DNA and genomic (salmon testes) DNA at 50 mM NaCl, 30 °C.

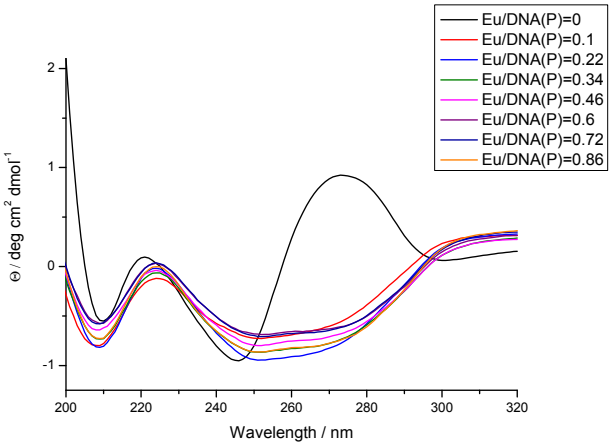

Fig. 2: CD spectra of short plasmid DNA at various concentration of Eu^{3+}, in 50 mM NaCl, 30 °C.

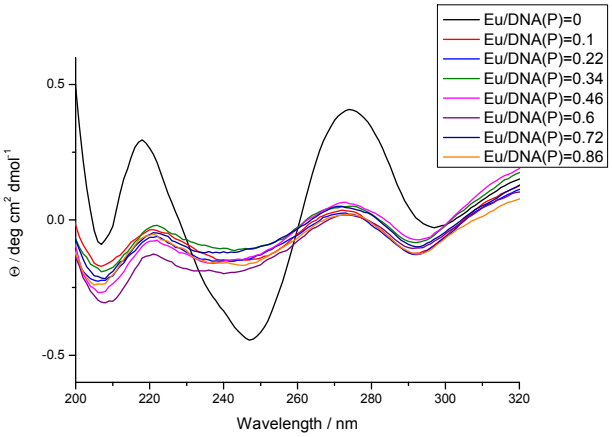

Fig. 3: CD spectra of genomic (salmon testes) DNA at various concentration of Eu^{3+}, in 50 mM NaCl, 30 °C.

REFERENCES

[1] Matulis, D. et al. (2000) *J. Mol. Biol.* **296**, 1053-1063.
[2] Kankia, B. I. et al. (2001) *Nucleic Acids Res.* **29**, 2795-2801.

Secondary structure and compliance of a predicted flexible domain in kinesin-1 necessary for cooperation of motors

A. H. Crevenna,[1] S. Madathil, D. N. Cohen,[1] M. Wagenbach,[2] K. Fahmy, J. Howard[1]

[1]Max Planck Institute of Molecular Cell Biology and Genetics, Dresden, Germany; [2]Physiology and Biophysics Department, University of Washington, Seattle, U.S.A.

We identified a 60-amino-acid-long domain, termed Hinge 1, in kinesin-1 from *Drosophila melanogaster*. Its deletion reduces microtubule gliding speed in multiple-motor assays but not in single-motor assays. Hinge 1 thus facilitates the cooperation of motors by preventing them from impeding each other.

Kinesin-1 is a molecular motor that moves cellular cargo along microtubules. Its functional mechanism is quite well-understood for individual motors. However, the way that many kinesin-1 motor proteins bound to the same cargo move together is not. We addressed the structural basis for this phenomenon using video-microscopy of single microtubule-bound full-length motors, Fourier-transform infrared (FT-IR), circular dichroism (CD), and fluorescence spectroscopy of Hinge 1 peptides.

EXPERIMENTAL. The preparation of model peptides and performance of FT-IR, CD, and fluorescence spectroscopy are described in detail in [1].

RESULTS. Peptides derived from the Hinge-1 region (Fig. 1A) show an unexpected profile of secondary structure-forming propensities.

Video-microscopy of single microtubule-bound full-length motors reveals the sporadic occurrence of high-compliance states alternating with longer-lived, low-compliance states (data not shown). The deletion of Hinge 1 abolishes transitions to the high-compliance state.

CD spectra of peptides 3 and 4 adjacent in the central Hinge-1 region evidence the partially helical structure which is absent in the N- and C-terminally flanking regions sampled by peptides 1, 2 and 5 which have a CD signature typical of unordered stretches (Fig. 1B). CD spectra are in general agreement with FT-IR spectra (Fig. 1C). Introduction of tryptophan as an intrinsic fluorophore does not alter helicity (Fig. 1D), allowing thermal unfolding to be monitored by fluorescence spectroscopy to determine unfolding enthalpy and entropy. [2]

From these results, we propose that low-compliance states correspond to an unexpected structured organization of the central Hinge 1 region, whereas high-compliance states correspond to the loss of that structure.

We hypothesize that strain accumulated during multiple-kinesin motility populates the high-compliance state by unfolding helical secondary structure in the central Hinge 1 domain flanked by unordered regions, thereby preventing the motors from interfering with each other in multiple motor situations.

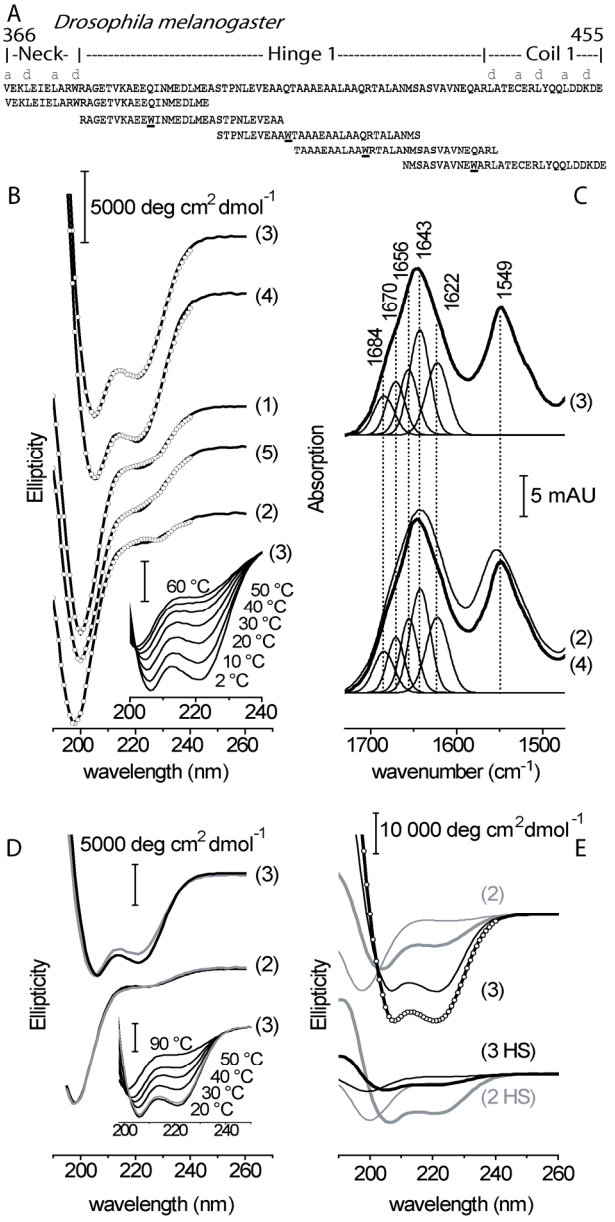

Fig. 1: (A) Sequence of the Hinge-1 of *Drosophila melanogaster* and of five peptides sampling different sections of the Hinge-1. (B) CD spectra of peptides 1-5. The insert shows reversible thermal unfolding.(C) IR spectra of peptide 3 (upper panel), and peptides 2 and 4 (lower panel). Major peaks in the spectra are indicated showing that peptides 3 and 4 can be fitted with identical spectral components. The higher absorption at 1643 cm^{-1} relative to 1656 cm^{-1} may indicate helix-helix interactions. For comparison, the broad amide absorptions of the unstructured peptide 2 are superimposed in the lower panel. (D) Overlaid CD spectra of peptide 2 (lower traces) and peptide 3 (upper traces) with either the native sequences (black) or with a tryptophan substitution at position 11 (gray, see also Fig. 1A). Insert: Thermal unfolding and refolding of peptide 3 carrying the native kinesin-1 sequence. After having been heated to 90 °C the CD spectrum at 20 °C (gray) reproduces the initial trace measured at 20 °C (black). (E) Comparison of the induction of secondary structure by TFE at 2 °C for peptides 2 and 3 derived from Hinge 1 of *Dm* (upper traces) and *Hs* (lower traces). Thin lines without TFE, thick lines with 32% TFE. Circles show the fit by CDSSTR resulting in 70% helicity for the *Dm* peptide 2.

REFERENCES

[1] Crevenna, A. H. et al. (2008) *Biophys. J.* **95**, 5216–5227.
[2] Crevenna, A. H. et al. (2009) this report, p. 74.

A novel fluorescence evaluation procedure for determination of enthalpy and entropy values of the unfolding of peptides

A. H. Crevenna,[1] S. Madathil, D. N. Cohen,[1] M. Wagenbach,[2] K. Fahmy, J. Howard[1]

[1]Max Planck Institute of Molecular Cell Biology and Genetics, Dresden, Germany; [2]Physiology and Biophysics Department, University of Washington, Seattle, U.S.A.

A novel fluorescence evaluation procedure was developed from which the enthalpy and entropy of unfolding of the central Hinge-1 region, a 60-amino-acid-long domain in kinesin-1 from *Drosophila melanogaster*, could be derived. The analysis is based on the altered temperature dependance of collisional quenching of tryptophan emission when exposed to a hydrophilic or hydrophobic environment.

EXPERIMENTAL. Model peptides were derived from the Hinge 1 sequence cut in to five 30-aa-long overlapping pieces. Each peptide was synthesized, high-performance-liquid-chromatography purified, and characterized by mass spectroscopy (ThermoElectron, Ulm, Germany). We used the intrinsic fluorescence of Trp to monitor temperature-induced structural transitions in the model peptides using a Perkin Elmer LS 55 instrument equipped with a temperature-controlled cuvette connected to a water-bath thermostat.

RESULTS. As shown in Fig. 1, the slope of a logarithmic plot of the normalized tryptophan emission versus temperature clearly increases with increasing solvent hydrophobicity. This has allowed evaluating the corresponding plots obtained with peptides 1-5 in a two state unfolding model where the final state exhibits a larger temperature sensitivity of the normalized emission due to the hydrophobic environment in the denatured/agregated state, whereas the initial state carries a water-exposed tryptophan, thereby resulting in a slope of the normalized log plot close to zero. Due to the intrinisic temperature dependance of tryptophane, its decrease with temperature is not per se an indication of unfolding. The normalization procedure introduced here resolves this problem and identifies the contribution that is directly related to structural transitions. The evaluation is generally applicable and provides a basis for the thermodynamic analysis of peptides and proteins containing native or engineered tryptophans. The curves in Fig. 1 are derived from the equation:

$$d\log\Phi_{pep}(T)/dT = p_U U_r(T) + p_N(1-U_R(T)) = \Delta p U_R(T) + p_N.$$

The relative concentration $U_r(T)$ of the unfolded state is given by $U_r(T) = 1/(1+K)$ with $K = U/N = e^{-\Delta G/RT}$ where N is the concentration of the native state. p_N and p_U are the slopes of the linear logarithmic relation between emission intensity and temperature in the native and unfolded state, respectively. Data are reproduced by substituting the appropriate values of ΔH and ΔS for ΔG. This results in values of 115 kJ and 367 JK^{-1}, respectively, for the most stable peptide 3. In agreement with the spectroscopic data, all of the less structured peptides show smaller unfolding entropies. Likewise, the unfolding enthalpy is close to the expected value for the unfolding of a 31-mer helical peptide [2]. Thus, the thermodynamic and spectroscopic data are in good agreement. The data suggest that the Hinge-1 is not required for single motor processivity. However, in an ensemble of many and potentially counteracting motors attached to the same cargo, motor interference is reduced by partial unfolding of the Hinge-1. The least structured flanking regions are supposedly the first to unfold, followed by breakage of the helical structure in the central part of the Hinge-1.

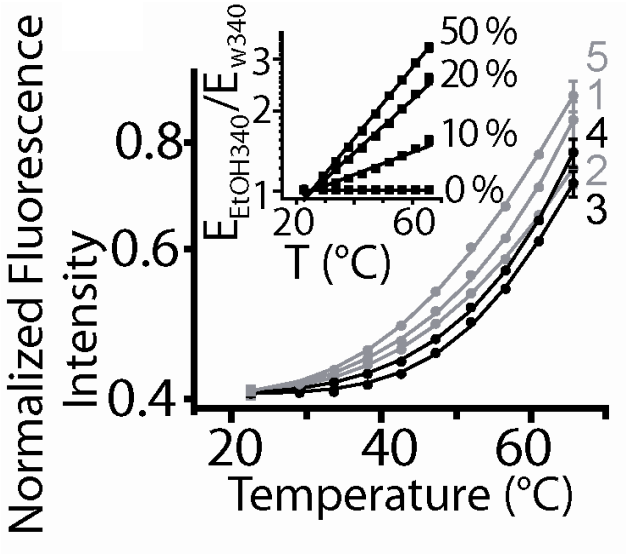

Fig. 1: Tryptophan fluorescence intensity plotted against temperature for the five *Dm* peptides. Solid lines are fits to a model in which equilibration occurs between a folded and an unfolded state. The plots obtained with the most stable peptides 3 and 4 (black lines) exhibit the strongest curvature (i.e. the largest change in $U_r = U/(N+U)$) at higher temperatures than the curves of less stable peptides (gray lines). Insert: Normalized fluorescence intensity of free Trp in 0, 10, 20, and 50% ethanol in water mixtures showing an increase of temperature sensitivity with increasing solvent hydrophobicity. T-dependence of Trp emission from the peptides corresponds to an increasingly hydrophobic environment as mimicked by high ethanol content.

We are currently adopting the combination of structure-sensitive spectroscopy with thermodynamic analyses to the study of structure and stability of metal-binding protein domains. The reliability of coordination models derived from spectroscopy can thus be verified by its consistency with energetic implications.

REFERENCES

[1] Crevenna, A. H. et al. (2008) *Biophys. J.* **95**, 5216–5227.
[2] Scholtz, J. M. et al. (1991) *Proc. Natl. Acad. Sci.U.S.A* **88**, 2854-2858.

Diffraction monitoring of IR-laser-induced solute transfer to a solid support by a thermal grating

G. Furlinski, H. Koezle, K. Fahmy

We describe a new method for material deposition on a solid support based on IR-laser evaporation in a transient holographic grating. Diffraction of a visible laser beam provides the monitor for the evaporation life time of the regularly deposited solute/solvent clusters. We show that the stereochemistry critically affects the life time of putative azeotropes deposited from solutions of butanediol isomers.

Figure 1 shows the interference of two coherent IR-CO_2-laser beams at the air, liquid, solid interface of an aqueous droplet on a glass substrate. Sample and substrate are strong IR absorbers. The interference field of the IR beam evaporates part of the solute, at the same time, it introduces a temperature grating on the glass surface. Thereby, the recondensing matter forms a relief-phase grating on the substrate. The lifetime of the grating depends on the composition and structure of the sample. The grating is read out by diffraction of a He-Ne laser. The life time of the grating is on the order of milliseconds and thus on the order of thermal effects in the glass, a prerequisite for these life time studies. The diffraction grating introduced in the liquid sample decays faster and reaches the millisecond regime only at high solvent viscosity. We have discovered the systematic dependencies of the transiently ordered solute deposition on physicochemical parameters:

– With increasing substrate thickness, and thus increasing heat flow perpendicular to the surface, the diffraction efficiency and lifetime of the induced gratings increase.
– The number of the diffraction orders, their efficiency and life time depend on the IR absorption properties of the sample, its mass, hydrophilic or hydrophobic nature, and isomeric state.
– IR-laser evaporation operates efficiently at very low solute concentrations. In glycerol solutions ranging from 10^{-9} to 1 M, a well defined concentration dependence of the diffraction efficiency has been observed.

EXPERIMENTAL. The potential sensitivity of the method to detect small differences in conformation and complex formation of solutes was investigated. Gratings of 1,2-butanediol and 1,4-butanediol were deposited from 45% and 30% aqueous solutions, respectively, on cover glasses coated with a layer of polyethylenimine and their lifetimes were measured. At these concentrations both compounds possess similar absorption at 9.6 µm laser wavelength resulting in equal energy input from a 240 mW IR beam in CW mode focused on the edge of a droplet and chopped into pulses of 40 µs duration at 1.75 Hz repetition rate. The He-Ne laser reading beam was chopped at 173 Hz.

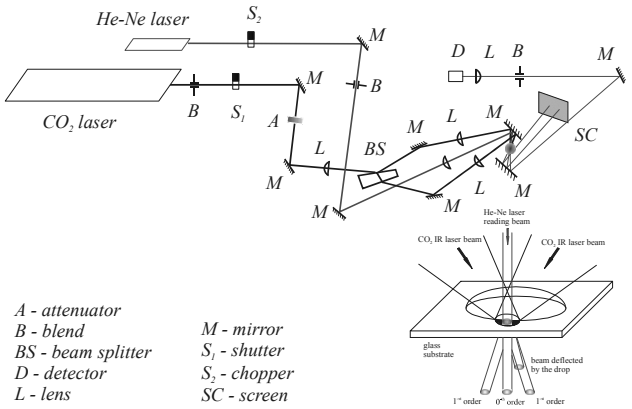

Fig. 1: Experimental setup.

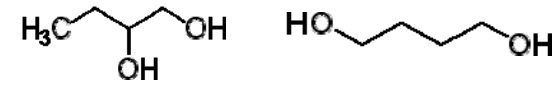

Fig. 2: Structural formulas of 1,2-butanediol and 1,4-butanediol.

RESULTS. The lifetime of the transiently deposited gratings was defined as the time during which the grating efficiency decreased from 90% to 10% of its maximum shown for the intensity of the first order diffraction from the ordered deposition of butanediols (Figs. 3,4). The lifetime range for both substances differs significantly. For 1,2-butanediol the maximal lifetime is limited to a few seconds to 2 min., and for 1,4-butanediol long-lived gratings exist for up to 2.5 hours. As boiling temperatures are 192 °C and 230 °C, respectively, and gratings were deposited in the same experimental conditions at 22 °C, we ascribe the significant difference to the formation of different water complexes that make up the evaporating unit. The technique has a potential for the stereoselective extraction of biomolecular water/metal complexes from dilute aqueous solutions.

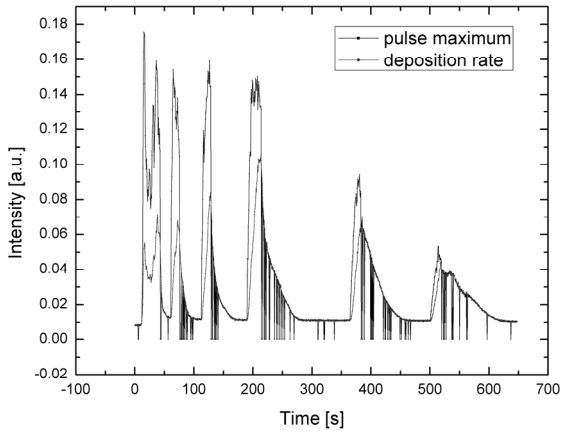

Fig. 3: First order of diffraction of 1,2-butanediol deposited grating.

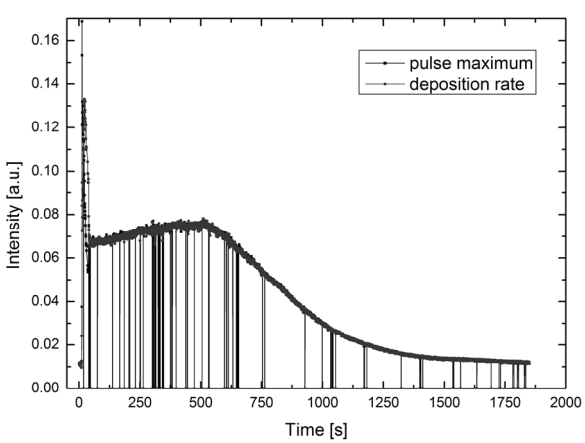

Fig. 4: First order of diffraction of 1,2-butanediol deposited grating.

- Articles (peer-reviewed)
- Proceedings, reports, contributions
- Lectures, oral presentations
- Posters
- Theses
- Diploma
- Bachelor
- Work placements

▶ Articles (peer-reviewed)

Abrasonis, G.; Scheinost, A. C.; Zhou, S.; Torres, R.; Gago, R.; Jimenez, I.; Kuepper, K.; Potzger, K.; Krause, M.; Kolitsch, A.; Möller, W.; Bartkowski, S.; Neumann, M.; Gareev, R. R.
X-ray spectroscopic and magnetic investigation of C : Ni nanocomposite films grown by ion beam cosputtering
Journal of Physical Chemistry C 112, 12628-12637 (2008).

Altmaier, M.; Brendler, V.; Hagemann, S.; Herbert, H. J.; Kienzler, B.; Marquardt, C. M.; Moog, H. C.; Neck, V.; Richter, A.; Voigt, W.; Wilhelm, S.
THEREDA – Ein Beitrag zur Langzeitsicherheit von Endlagern nuklearer und nichtnuklearer Abfälle
atw - International Journal for Nuclear Power 53, 249-253 (2008).

Barkleit, A.; Foerstendorf, H.; Heim, K.; Sachs, S.; Bernhard, G.
Complex formation of uranium(VI) with L-phenylalanine and 3-phenylpropionic acid studied by attenuated total reflection Fourier transform infrared spectroscopy
Applied Spectroscopy 62, 798-802 (2008).

Barkleit, A.; Moll, H.; Bernhard, G.
Interaction of uranium(VI) with lipopolysaccharide
Dalton Transactions, 2879-2886 (2008).

Baumann, N.; Arnold, T.; Foerstendorf, H.; Read, D.
Two spectroscopic verifications of a ultra thin mineral film on depleted uranium
Environmental Science & Technology 42, 8266-8269.

Creamer, N. J.; Deplanche, K.; Snape, T. J.; Mikheenko, I. P.; Yong, P.; Samyahumbi, D.; Wood, J.; Pollmann, K.; Selenska-Pobell, S.; Macaskie, L. E.
A biogenic catalyst for hydrogenation, reduction and selective dehalogenation in non-aqueous solvents
Hydrometallurgy 94, 138-143 (2008).

Crevenna, A. H.; Madathil, S.; Cohen, D. N.; Wagenbach, M.; Fahmy, K.; Howard, J.
Secondary structure and compliance of a predicted flexible domain in kinesin-1 necessary for co-operation of motors
Biophysical Journal 95, 5216-5227 (2008).

Geipel, G.; Amayri, S.; Bernhard, G.
Mixed complexes of alkaline earth uranyl cabonates: A laser-induced time-resolved fluorescence spectroscopic study
Spectrochimica Acta Part A 71, 53-58 (2008).

Glorius, M.; Moll, H.; Bernhard, G.
Complexation of curium(III) with hydroxamic acids investigated by time-resolved laser-induced fluorescence spectroscopy
Polyhedron 27, 2113-2118 (2008).

Glorius, M.; Moll, H.; Geipel, G.; Bernhard, G.
Complexation of uranium(VI) with aromatic acids such as hydroxamic and benzoic acid investigated by TRLFS
Journal of Radioanalytical and Nuclear Chemistry 277, 371-377 (2008).

Günther, A.; Raff, J.; Geipel, G.; Bernhard, G.
Spectroscopic identifications of U(VI) species sorbed by the green algae *Chlorella vulgaris*
BioMetals 21, 333-341 (2008).

Hennig, C.; Ikeda, A.; Schmeide, K.; Brendler, V.; Moll, H.; Tsushima, S.; Scheinost, A. C.; Skanthakumar, S.; Wilson, R.; Soderholm, L.; Servaes, K.; Görrler-Walrand, C.; van Deun, R.
The relationship of monodentate and bidentate coordinated uranium(VI) sulfate in aqueous solution
Radiochimica Acta 96, 607-611 (2008).

Hennig, C.; Kraus, W.; Emmerling, F.; Ikeda, A.; Scheinost, A. C.
Coordination of a uranium(IV) sulfate monomer in an aqueous solution and in the solid state
Inorganic Chemistry 47, 1634-1638 (2008).

Hennig, C.; Le Naour, C.; Den Auwer, C.
Double photoexcitation involving 2p and 4f electrons in L3-edge x-ray absorption spectra of protactinium
Physical Review B 77, 235102 (2008).

Hennig, C.; Servaes, K.; Nockemann, P.; van Hecke, K.; van Meervelt, L.; Wouters, J.; Görller-Walrand, C.; van Deun, R.
Species distribution and coordination of uranyl chloro complexes in acetonitrile
Inorganic Chemistry 47, 2987-2993 (2008).

Hübener, S; Taut, S; Vahle, A; Bernhard, G; Fanghänel, T.
Thermochromatographic studies of plutonium oxides
Radiochimica Acta 96, 781-785 (2008).

Ikeda, A.; Hennig, C.; Rossberg, A.; Tsushima, S.; Scheinost, A. C.; Bernhard, G.
Structural determination of individual chemical species in a mixed system by iterative transformation factor analysis (ITFA)-based X-ray absorption spectroscopy combined with UV-visible absorption and quantum chemical calculation
Analytical Chemistry 80, 1102-1110 (2008).

Ikeda-Ohno, A.; Hennig, C.; Rossberg, A.; Funke, H.; Scheinost, A. C.; Bernhard, G.; Yaita, T.
Electrochemical and complexation behavior of neptunium in aqueous perchlorate and nitrate solutions
Inorganic Chemistry 47, 8294-8305 (2008).

Kirsch R.; Scheinost A. C.; Rossberg A.; Banerjee D.; Charlet, L.
Reduction of antimony by nano-particulate magnetite and mackinawite
Mineralogical Magazine 72, 185-189 (2008).

Krawczyk-Bärsch, E.; Großmann, K.; Arnold, T.; Diessner, S.; Wobus, A.
Influence of uranium (VI) on the metabolic activity of stable multispecies biofilms studied by oxygen microsensors and fluorescence microscopy
Geochimica et Cosmochimica Acta 72, 5251-5265 (2008).

Křepelová, A.; Reich, T.; Sachs, S.; Drebert, J.; Bernhard, G.
Structural characterization of U(VI) surface complexes on kaolinite in the presence of humic acid using EXAFS spectroscopy
Journal of Colloid and Interface Science 319, 40-47 (2008).

Lehmann, S.; Geipel, G.; Foerstendorf, H.; Bernhard, G.
Syntheses and spectroscopic characterization of uranium(VI) silicate minerals
Journal of Radioanalytical and Nuclear Chemistry 275, 633-642 (2008).

López De Arroyabe Loyo, R.; Nikitenko, S.; Scheinost, A. C.; Simonoff, M.
Immobilization of selenium on Fe_3O_4 and Fe/FeC_3 ultrasmall particles
Environmental Science & Technology 42, 2451-2456 (2008).

Merroun, M.; Selenska-Pobell, S.
Bacterial interactions with uranium: An environmental perspective
Journal of Contaminant Hydrology 102, 285-295 (2008).

Moll, H.; Glorius, M.; Bernhard, G.
Curium(III) complexation with desferrioxamine B (DFO) investigated using fluorescence spectroscopy
Bulletin of the Chemical Society of Japan 81, 857-862 (2008).

Moll, H.; Glorius, M.; Bernhard, G.; Johnsson, A.; Pedersen, K.; Schäfer, M.; Budzikiewicz, H.
Characterization of pyoverdins secreted by a subsurface strain of *Pseudomonas fluorescens* and their interactions with uranium(VI)
Geomicrobiology Journal 25, 157-166 (2008).

Moll, H.; Johnsson, A.; Schäfer, M.; Pedersen, K.; Budzikiewicz, H.; Bernhard, G.
Curium(III) complexation with pyoverdins secreted by a groundwater strain of *Pseudomonas fluorescens*
BioMetals 21, 219-228 (2008).

Montes-Hernandez, G.; Charlet, L.; Renard, F.; Scheinost, A. C.; Bueno, M.; Fernández-Martínez, A.
Synthesis of a Se^0/calcite composite using hydrothermal carbonation of $Ca(OH)_2$ coupled with a complex selenocystine fragmentation
Crystal Growth & Design 8, 2497-2504 (2008).

Müller, K.; Brendler, V.; Foerstendorf, H.
Aqueous uranium(VI) hydrolysis species characterized by attenuated total reflection Fourier-transform infrared spectroscopy
Inorganic Chemistry 47, 10127-10134 (2008).

Richter, A.; Brendler, V.
Sparse and uncertain SCM parameter sets – What are the consequences?
Adsorption of Metals by Geomedia II: Variables, Mechanisms, and Model Applications (Series: Developments in Earth & Environmental Sciences, Vol. 7), (Barnett, M.O., Kent, D.B. eds.), Elsevier, Amsterdam, 267-291 (2008).

Sachs, S.; Bernhard, G.
Sorption of U(VI) onto an artificial humic substance-kaolinite-associate
Chemosphere 72, 1441-1447 (2008).

Scheinost, A. C.; Charlet, L.
Selenite reduction by mackinawite, magnetite and siderite: XAS characterization of redox products
Environmental Science & Technology 42, 1984-1989 (2008).

Scheinost, A. C.; Kirsch, R.; Banerjee, D.; Zaenker, H.; Funke, H.; Charlet, L.
X-ray absorption and photoelectron spectroscopy investigation of selenite reduction by FeII–bearing minerals
Journal of Contaminant Hydrology 102, 228-245 (2008).

Schwinté, P.; Foerstendorf, H.; Hussain, Z.; Gärtner, W.; Mroginski, M. A.; Hildebrandt, P.; Siebert, F.
FTIR study of the photoinduced processes of plant phytochrome *phyA* using isotope-labeled bilins and DFT calculations
Biophysical Journal 95, 1256-1267 (2008).

Steinborn, A.; Taut, S.; Brendler, V.; Geipel, G.; Flach, B.
TRLFS: Analysing spectra with an expectation-maximization (EM) algorithm
Spectrochimica Acta Part A: Molecular and Biomolecular Spectroscopy 71, 1425-1432 (2008).

Stephan, H.; Juran, S.; Born, K.; Comba, P.; Geipel, G.; Hahn, U.; Werner, N.; Vögtle, F.
Hydrophilic oxybathophenanthroline ligands: Synthesis and copper(II) complexation
New Journal of Chemistry 32, 2016-2022 (2008).

Tsushima, S.
Hydrolysis and dimerization of Th^{4+} ion
Journal of Physical Chemistry B 112, 7080-7085 (2008).

Tsushima, S.
Quantum chemical calculations of the redox potential of the Pu(VII)/Pu(VIII) couple
Journal of Physical Chemistry B 112, 13059-13063 (2008).

Wenzel, M.; Gloe, K.; Gloe, K.; Bernhard, G.; Clegg, J. K.; Ji, X. K.; Lindoy, L. F.
A new 34-membered N_6O_4-donor macrocycle: synthetic, X-ray and solvent extraction studies
New Journal of Chemistry 32, 132-137 (2008).

Wiebke, J.; Moritz, A.; Glorius, M.; Moll, H.; Bernhard, G.; Dolg, M.
Complexation of uranium(VI) with aromatic acids in aqueous solution – A combined computational and experimental study
Inorganic Chemistry 47, 3150-3157 (2008).

▶ Proceedings, reports, contributions

Banerjee, D.; Kirsch, R.; Scheinost, A. C.
X-ray photoelectron and absorption spectroscopy investigation of Se-IV and Sb-V reduction by mackinawite
Geochimica et Cosmochimica Acta 72, A51 (2008).

Barkleit, A.; Moll, H.; Bernhard, G.
Comparative investigation of the interaction of uranium with lipopolysaccharide and peptidoglycan
Uranium, Mining and Hydrogeology (Merkel, B.J.; Hasche-Berger, A. eds.), Springer Verlag, Berlin, 753-754 (2008).

Baumann, N.; Arnold, T.; Read, D.
Uranium ammunition in soil
Loads and fate of fertilizer-derived uranium (De Kok, L. J., Schnug, E., eds.), Backhuys Publishers, Leiden, 73-77 (2008).

Behrends, T.; Scheinost, A. C.; Shaw, S.; Benning, L.; van Cappellen, P.
Bacterial cell walls - Promoters and inhibitors of mineral nucleation
Geochimica et Cosmochimica Acta 72, A68 (2008).

Bernhard, G.; Geipel, G.; Steudtner, R.
Binding form of ingested uranium in human urine
2nd-INCC – 2nd International Nuclear Chemistry Congress, April 13-18, 2008, Cancun, Mexico, Abstract Book (Navarrete, M. ed.) Faculty of Chemistry, National Autonomous University of Mexico, Mexico City, Mexico (2008).

Foerstendorf, H.; Heim, K.
Sorption of uranium(VI) on ferrihydrite – Influence of atmospheric carbonate on surface complex formation investigated by ATR-FT-IR spectroscopy
NRC7 – 7th International Conference on Nuclear and Radiochemistry, August 24-29, 2008, Budapest, Hungary, Proceedings (Vértes, A.; Wojnárovits, L.; Vincze, Á. eds.), ISBN 978-963-9319-81-3 (2008).

Geipel, G.; Bernhard, G.
Uranium speciation - From mineral phases to mineral waters
2nd-INCC – 2nd International Nuclear Chemistry Congress, April 13-18, 2008, Cancun, Mexico, Abstract Book (Navarrete, M. ed.) Faculty of Chemistry, National Autonomous University of Mexico, Mexico City, Mexico (2008).

Geipel, G.; Bernhard, G.
Uranium speciation – From mineral phases to mineral waters
Uranium, Mining and Hydrogeology (Merkel, B.J.; Hasche-Berger, A. eds.), Springer Verlag, Berlin, 599-601 (2008).

Gester, S.; Altmaier, M.; Brendler, V.; Hagemann, S.; Herbert, H. J.; Marquardt, C.; Moog, H.; Neck, V.; Richter, A.; Voigt, W.; Wilhelm, S.
THEREDA – Thermodynamic reference database for nuclear waste disposal in Germany
Proceedings of the 12th International High-Level Radioactive Waste Management Conference, September 07-11, 2008, Las Vegas, U.S.A., American Nuclear Society, La Grange Park, U.S.A., 287-290 (2008).

Götz, C.; Geipel, G.; Bernhard, G.
Thermodynamical data of uranyl carbonate complexes from absorption spectroscopy
Uranium, Mining and Hydrogeology (Merkel, B.J.; Hasche-Berger, A. eds.), Springer Verlag, Berlin, 907-914 (2008).

Günther, A.; Rossberg, A.; Raff, J.; Geipel, G.; Bernhard, G.
U(VI) species sorbed on the green algae Chlorella vulgaris - A TRLFS and EXAFS study
NRC7 – 7th International Conference on Nuclear and Radiochemistry, August 24-29, 2008, Budapest, Hungary, Proceedings (Vértes, A.; Wojnárovits, L.; Vincze, Á. eds.), ISBN 978-963-9319-81-3 (2008).

Heller, A.; Barkleit, A.; Bernhard, G.
Complexation of Curium(III) and Europium(III) with Urea and in Human Urine
NRC7 – 7th International Conference on Nuclear and Radiochemistry, August 24-29, 2008, Budapest, Hungary, Proceedings (Vértes, A.; Wojnárovits, L.; Vincze, Á. eds.), ISBN 978-963-9319-81-3 (2008).

Hennig, C.; Tsushima, S.; Brendler, V.; Ikeda, A.; Scheinost, A. C.; Bernhard, G.
Coordination of U(IV) and U(VI) sulfate hydrate in aqueous solution
Uranium, Mining and Hydrogeology (Merkel, B.J.; Hasche-Berger, A. eds.), Springer Verlag, Berlin, 603-613 (2008).

Joseph, C.; Raditzky, B.; Schmeide, K.; Geipel, G.; Bernhard, G.
Complexation of uranium(VI) by sulfur and nitrogen containing model ligands in aqueous solution
Uranium, Mining and Hydrogeology (Merkel, B.J.; Hasche-Berger, A. eds.), Springer Verlag, Berlin, 539-548 (2008).

Kirsch, R.; Scheinost, A. C.; Rossberg, A.; Banerjee, D.; Charlet, L.
Reduction of antimony by nanoparticulate Fe_3O_4 and FeS
Geochimica et Cosmochimica Acta 72, A476 (2008).

Merroun, M.; Hennig, C.; Selenska-Pobell, S.
Uranium biomineralization by uranium mining waste isolates: a multidisciplinary approach study
Uranium, Mining and Hydrogeology (Merkel, B.J.; Hasche-Berger, A. eds.), Springer Verlag, Berlin, 723-723 (2008).

Moll, H.; Glorius, M.; Bernhard, G.
Curium(III) Speciation in Aqueous Solutions of Bacterial Siderophores
NRC7 – 7th International Conference on Nuclear and Radiochemistry, August 24-29, 2008, Budapest, Hungary, Proceedings (Vértes, A.; Wojnárovits, L.; Vincze, Á. eds.), ISBN 978-963-9319-81-3 (2008).

Müller, K.; Foerstendorf, H.; Brendler, V.
Infrared spectroscopic identification of aqueous neptunium species
Las Fronteras de la Física y Química Ambiental en Ibero América: Libro de actas del V congreso iberoamericano de física y química ambiental, Buenos Aires, Argentina, Universidad Nacional de San Martin, 39 (2008).

Müller, K.; Foerstendorf, H.; Brendler, V.; Bernhard, G.
Infrared spectroscopic comparison of the aqueous species of uranium(VI) and neptunium(VI)
NRC7 – 7th International Conference on Nuclear and Radiochemistry, August 24-29, 2008, Budapest, Hungary, Proceedings (Vértes, A.; Wojnárovits, L.; Vincze, Á. eds.), ISBN 978-963-9319-81-3 (2008).

Nebelung, C.; Brendler, V.
Uranium(VI) sorption on montmorillonite and bentonite: Prediction and experiments
Uranium, Mining and Hydrogeology (Merkel, B.J.; Hasche-Berger, A. eds.), Springer Verlag, Berlin, 525-526 (2008).

Pollmann, K.; Raff, J.; Fahmy, K.; von Borany J.; Grenzer, J.; Herrmannsdörfer, T.
Bacterial surface layers (S-layers) as building blocks for nanocomposites
Proceedings of Nanofair 2008, VDI Berichte 2027, VDI Verlag, Düsseldorf, 31-34 (2008).

Raditzky, B.; Schmeide, K.; Geipel, G.; Bernhard, G.
Complexation studies of uranium(VI) by sulfur and nitrogen containing model ligands in aqueous solution
NRC7 – 7th International Conference on Nuclear and Radiochemistry, August 24-29, 2008, Budapest, Hungary, Proceedings (Vértes, A.; Wojnárovits, L.; Vincze, Á. eds.), ISBN 978-963-9319-81-3 (2008).

Raff, J.; Marquard, A.; Günther, T.; Pollmann, K.
Multifunctional biocomposite layers for the elimination of pharmaceutical residues in water
Bremer Colloquium – Product integrated Water / Wastewater Technology 2008, Wastewater Technology of the future – Sustainable solutions, Proceedings (IUV, Institute of Environmental Process Engineering, University of Bremen and ProcessNet an initiative of DECHEMA and VDI-GVC eds.) (2008).

Read, D.; Black, S.; Beddow, H.; Trueman, E.; Arnold, T.; Baumann, N.
The fate of uranium in phosphate-rich soils
Loads and fate of fertilizer-derived uranium (De Kok, L. J., Schnug, E., eds.), Backhuys Publishers, Leiden, 65-71 (2008).

Reitz, T.; Merroun, M. L.; Selenska-Pobell, S.
Interactions *of Paenibacillus sp.* JG-TB8 and *Sulfolobus acidocaldarius* with U(VI): Spectroscopic and microscopic studies
Uranium, Mining and Hydrogeology (Merkel, B.J.; Hasche-Berger, A. eds.), Springer Verlag, Berlin, 703-710 (2008).

Richter, A.; Nebelung, C.; Brendler, V.
Component Additivity Approach for Uranium Retardation in Sandstone Host Rocks
XVII International Conference on Computational Methods in Water Resources (CMWR 2008), July 06-10, 2008, San Francisco, U.S.A. (2008). http://esd.lbl.gov/cmwr08/abstracts_all.html

Sachs, S.; Křepelová, A.; Schmeide, K.; Koban, A.; Günther, A.; Mibus, J.; Brendler, V.; Geipel, G.; Bernhard, G.
Migration behavior of actinides (uranium, neptunium) in clays: Characterization and quantification of the influence of humic substances.
Migration of Actinides in the System Clay, Humic Substances, Aquifer (Marquardt, C.M. ed.), Wissenschaftliche Berichte FZKA 7407, Forschungszentrum Karlsruhe, Karlsruhe, 23-140 (2008).

Satchanska, G.; Selenska-Pobell, S.; Groudeva, V.; Dimkov R.; Golovinski, E.
Heavy metal, uranium and phenol derivatives pollution in Bulgarian and German environments as a factor influencing bacterial diversity
Ecological Engineering and Environment Protection 7/2-3 (2008).

Schmeide, K.; Bernhard, G.
Spectroscopic study of the uranium(IV) complexation by organic model ligands in aqueous solution
Uranium, Mining and Hydrogeology (Merkel, B.J.; Hasche-Berger, A. eds.), Springer Verlag, Berlin, 591-598 (2008).

Schmeide, K.; Křepelová, A.; Sachs, S.; Bernhard, G.
Comparison of the americium(III), neptunium(V) and uranium(VI) sorption onto kaolinite in the absence and presence of humic acid
2nd-INCC – 2nd International Nuclear Chemistry Congress, April 13-18, 2008, Cancun, Mexico, Abstract Book (Navarrete, M. ed.) Faculty of Chemistry, National Autonomous University of Mexico, Mexico City, Mexico (2008).

Selenska-Pobell, S.; Geissler, A.; Flemming, K.; Merroun, M.; Geipel, G.; Reuther, H.
Biogeochemical changes induced by uranyl nitrate in a uranium waste pile
Uranium, Mining and Hydrogeology (Merkel, B.J.; Hasche-Berger, A. eds.), Springer Verlag, Berlin, 743-752 (2008).

Tits, J.; Macé, N.; Eilzer, M.; Geipel, G.; Wieland, E.
Uranium(VI) uptake by calcium silicate hydrates
Geochimica et Cosmochimica Acta 72(2008)12, A948 (2008).

Viehweger, K.; Geipel, G.
Extracellular defence reactions of rape cells caused by uranium exposure
Uranium, Mining and Hydrogeology (Merkel, B.J.; Hasche-Berger, A. eds.), Springer Verlag, Berlin, 691 (2008).

Vogel, M.; Günther, A.; Raff, J.; Bernhard, G.
Microscopic and spectroscopic investigation of the U(VI) interaction with monocellular green algae
Uranium, Mining and Hydrogeology (Merkel, B.J.; Hasche-Berger, A. eds.), Springer Verlag, Berlin, 693-702 (2008).

▶ Lectures, oral presentations

Arnold, T.
U(VI/IV) adsorption mechanism on biotite surfaces and clarification of the influence of redox reactions on the U(VI) adsorption
4th Semi-Annual RTDC-2 Meeting of FUNMIG, April 29-30, 2008, Larnaca, Cyprus.

Arnold, T.
Uranium in biofilms
7th Symposium on remediation in Jena – Metal stress: Biotic and abiotic factors, September 22-23, 2008, Jena, Germany.

Banerjee, D.; Kirsch, R.; Scheinost, A. C.
X-ray photoelectron and absorption spectroscopy investigation of Se-IV and Sb-V reduction by mackinawite
18th Annual V.M. Goldschmidt Conference 2008, July 13-18, 2008, Vancouver, Canada.

Barkleit, A.; Moll, H.; Bernhard, G.
Comparative investigation of the interaction of uranium with lipopolysaccharide and peptidoglycan
UMH V – 5th International Conference Uranium Mining and Hydrogeology, September 14-18, 2008, Freiberg, Germany.

Barkleit, A.; Moll, H.; Bernhard, G.
Interaction of uranium(VI) with peptidoglycan
NRC7 – 7th International Conference on Nuclear and Radiochemistry, August 24-29, 2008, Budapest, Hungary.

Baumann, N.; Arnold, T.
Analyzing of uranium species by fluorescence spectroscopy: A contribution for handling ecological problems caused by uranium mining activities in former Eastern Germany
Thailand Institute of Nuclear Technology (TINT), Radioactive Waste Management Center, November 03, 2008, Bangkok, Thailand.

Baumann, N.; Arnold, T.
Ecological problems in Saxony related to the former uranium mining activities – Fluorescence spectroscopy, a tool for analyzing the uranium binding form
Graduate School of Engineering, Faculty of Engineering, Hiroshima University, October 27, 2008, Hiroshima, Japan.

Behrends, T.; Scheinost, A. C.; Shaw, S.; Benning, L.; van Cappellen, P.
Bacterial cell walls - Promoters and inhibitors of mineral nucleation
18th Annual V.M. Goldschmidt Conference 2008, July 13-18, 2008, Vancouver, Canada.

Bernhard, G.
Wechselwirkung und Transport von Actiniden im natürlichen Tongestein unter Berücksichtigung von Huminstoffen und Tonorganika - Verbundprojekt "Actinidenmigration im natürlichen Tongestein"
Forschungsförderung zur Entsorgung gefährlicher Abfälle in tiefen geologischen Formationen – 8. Projektstatusgespräch, May 06-07, 2008, Karlsruhe, Germany.

Bernhard, G.; Geipel, G.
Binding form of uranium in environmental relevant compartments
SElS-08 – School cum Workshop on Trace Element Speciation, November 21-29, 2008, Kolkata, India.

Bernhard, G.; Geipel, G.
Chemistry of actinides
SElS-08 – School cum Workshop on Trace Element Speciation, November 21-29, 2008, Kolkata, India.

Bernhard, G.; Geipel, G.; Steudtner, R.
Binding form of ingested uranium in human urine
2nd-INCC – 2nd International Nuclear Chemistry Congress, April 13-18, 2008, Cancun, Mexico.

Funke, H.
Wavelet based XAFS data analysis
Workshop on X-ray absorption spectroscopy and advanced XAS techniques, October 6-10, 2008, Villigen, Switzerland.

Funke, H.; Scheinost, A. C.; Hennig, C.; Rossberg, A.; Banerjee, D.; Hesse, M.
The Rossendorf Beamline at ESRF: The next 10 years of actinide XAFS
Actinide XAS 2008, 5th Workshop on Speciation, Techniques, and Facilities for Radioactive Materials at Synchrotron Light Sources, July 15-17, 2008, Saint-Aubin, France.

Geipel, G.; Bernhard, G.
Complexation of actinides with organic and inorganic ligands
SElS-08 – School cum Workshop on Trace Element Speciation, November 21-29, 2008, Kolkata, India.

Geipel, G.; Bernhard, G.
Spectroscopic techniques in actinide speciation studies
SElS-08 – School cum Workshop on Trace Element Speciation, November 21-29, 2008, Kolkata, India.

Geipel, G.; Bernhard, G.
Uranium speciation - From mineral phases to mineral waters
2nd-INCC – 2nd International Nuclear Chemistry Congress, April 13-18, 2008, Cancun, Mexico.

Geipel, G.; Bernhard, G.
Uranium speciation - From mineral phases to mineral waters
UMH V – 5th International Conference Uranium Mining and Hydrogeology, September 14-18, 2008, Freiberg, Germany.

Geipel, G.; Bernhard, G.
Uranium speciation - From mineral to water
Faculty of Nuclear Sciences and Physical Engineering, Czech Technical University in Prague, May 28, 2008, Prague, Czech Republic.

Geipel, G.; Viehweger, K.; Bernhard, G.
Uranium speciation after contact with plant cells
BioMetals 2008, 6th International Biometals Symposium, July 14-18, 2008, Santiago de Compostela, Spain.

Geipel, G.; Viehweger, K.; Bernhard, G.
Uranium – Species trace analytics in the nanomolar concentration range
The Seminar Series of the Glenn T. Seaborg Center, December 10, 2008, Berkeley, U.S.A.

Gester, S.; Altmaier, M.; Brendler, V.; Hagemann, S.; Herbert, H. J.; Marquardt, C.; Moog, H.; Neck, V.; Richter, A.; Voigt, W.; Wilhelm, S.
THEREDA – Thermodynamic reference database for nuclear waste disposal in Germany
12th International High-Level Radioactive Waste Management Conference, September 07-11, 2008, Las Vegas, U.S.A.

Giachini, L.; Faure, S.; Meyer, M.; Nguyen, L. V.; Batifol, B.; Chollet, H.; Guilard, R.; Scheinost, A. C.; Hennig, C.
X-ray absorption studies of the interaction between uranium(VI) and silica-gel-bound tetraazamacrocycles
Actinide XAS 2008, 5th Workshop on Speciation, Techniques, and Facilities for Radioactive Materials at Synchrotron Light Sources, July 15-17, 2008, Saint-Aubin, France.

Günther, A.; Rossberg, A.; Raff, J.; Geipel, G.; Bernhard, G.
U(VI) species sorbed on the green algae Chlorella vulgaris - A TRLFS and EXAFS study
NRC7 – 7th International Conference on Nuclear and Radiochemistry, August 24-29, 2008, Budapest, Hungary.

Hennig, C.
Redox chemistry and coordination of uranium and neptunium sulfate in aqueous solution
Atelier PARIS "Redox et Actinides", Institute de Physique Nucleaire, January 21, 2008, Orsay, France.

Hennig, C.; Servaes, K.; Nockemann, P.; Van Deun, R.
Combining EXAFS, UV-vis and XRD to extract speciation and coordination in solution
Actinide XAS 2008, 5th Workshop on Speciation, Techniques, and Facilities for Radioactive Materials at Synchrotron Light Sources, July 15-17, 2008, Saint-Aubin, France.

Hennig, C.
Influence of ionic strength, pH and silicate on colloidal UO_2 formation
Ecole Polytechnique Federale Lausanne (EPFL), Environmental Microbiology Laboratory (EML), November 20, 2008, Lausanne, Switzerland.

Hennig, C.
Speciation and coordination of U(VI) and U(IV) sulfate in aqueous solution
UMH V – 5th International Conference Uranium Mining and Hydrogeology, September 14-18, 2008, Freiberg, Germany.

Hennig, C.
Uranium coordination in liquids and amorphous solids determined by EXAFS spectroscopy
Inorganic Chemistry, University of Siegen, November 24, 2008, Siegen, Germany.

Hennig, C.
X-ray absorption and X-ray scattering – Two complementary techniques to determine the coordination of solution species
Department of Chemistry, Katolieke Universiteit Leuven, August 05, 2008, Leuven, Belgium.

Hennig, C.; Ikeda-Ohno, A.; Tsushima, S.
EXAFS study of neptunium complex structures in aqueous solution
JAEA Actinide Network Workshop, October 29, 2008, Tokai, Japan.

Hennig, C.; Ikeda, A.; Tsushima, S.; Le Naour, C.; Den Auwer, C.; Wilson, R.
Coordinatiom of actinides in aqueous sulfate solution
Plutonium Futures "The Science" 2008, July 07-11, 2008, Dijon, France.

Joseph, C.
Sorption von U(VI) in Abwesenheit und Gegenwart von Huminsäure an Kaolinit und Opalinuston
Workshop zum Forschungsvorhaben "Wechselwirkung und Transport von Actiniden im natürlichen Tongestein unter Berücksichtigung von Huminstoffen und Tonorganika", April 01-02, 2008, Munich, Germany.

Joseph, C.; Schmeide, K.; Sachs, S.
Uranium sorption onto opalinus clay and uranium complexation with model ligands - New results
Workshop zum Forschungsvorhaben "Wechselwirkung und Transport von Actiniden im natürlichen Tongestein unter Berücksichtigung von Huminstoffen und Tonorganika", October 07-08, 2008, Speyer, Germany.

Kammer, F. von der; Baalousha, M.; Baun, A.; Hassellov, M.; Delay, M.; Thieme, J.; Zänker, H.; Neumann-Hensel, H.; Handy, R.; Hochella, M.
Natural and engineered nanoparticles in the environment: A presentation of current activities of the AK "Aquatic Nanoscience & Nanotechnology"
Wasser 2008. Jahrestagung der Wasserchemischen Gesellschaft, April 28-30, 2008, Trier, Germany.

Kirsch, R.; Scheinost, A. C.; Rossberg, A.; Banerjee, D.; Charlet, L.
Reduction of antimony by nanoparticulate Fe_3O_4 and FeS. X-ray photoelectron and absorption spectroscopy investigation of Se-IV and Sb-V reduction by mackinawite
18th Annual V.M. Goldschmidt Conference 2008, July 13-18, 2008, Vancouver, Canada.

Krawczyk-Bärsch, E.
The influence of microbes on the mobility and immobilization of radionuclides e.g. U(VI) in surface and subsurface environments: A microscopical and geochemical study
Institute of Chemistry, Cyprus University, May 02, 2008, Nicosia, Cyprus.

Krawczyk-Bärsch, E.; Arnold, T.
The immobilization of uranium in multispecies biofilms studied by microsensors and confocal microscopy
4th Semi-Annual RTDC-2 Meeting of FUNMIG, April 29-30, 2008, Larnaca, Cyprus.

Krawczyk-Bärsch, E.; Brockmann, S.; Arnold, T.; Hofmann, S.; Wobus, A.
The response of biofilms to uranium impacts
7th Symposium on remediation in Jena – Metal stress: Biotic and abiotic factors, September 22-23, 2008, Jena, Germany.

Krawczyk-Bärsch, E.; Brockmann, S.; Arnold, T.; Wobus, A.; Diessner, S.
The increase of metabolic activity in biofilms caused by uranium
Biofilms III, 3rd International Biofilm Conference, October 06-08, 2008, Munich, Germany.

Křepelová, A.; Sachs, S.; Geipel, G.; Bernhard, G.
Study of the influence of humic acid on the Am(III) sorption onto kaolinite
4th RTDC-1 Meeting of FUNMIG, May 20-21, 2008, Bürgenstock, Switzerland.

Marquard, A.
Photokatalytische Spaltung von Diclofenac mit an S-Layer gebundenen ZnO/TiO_2-Nanopartikeln
Meeting with Institute of Water Chemsistry, Dresden University of Technology, June 16, 2008, FZD,Dresden, Germany.

Martin, P.; Belin, R.; Valenza, P.; Pieragnoli, A.; Scheinost, A. C.
XAS study of $Am_2Zr_2O_7$ pyrochlore – Evolution under alpha self irradiation
Plutonium Futures "The Science" 2008, July 07-11, 2008, Dijon, France.

Martin, P.; Belin, R.; Valenza, P.; Scheinost, A. C.
XAS study of $Am_2Zr_2O_7$ pyrochlore – Evolution under alpha self-irradiation
Actinide XAS 2008, 5th Workshop on Speciation, Techniques, and Facilities for Radioactive Materials at Synchrotron Light Sources, July 15-17, 2008, Saint-Aubin, France.

Merroun, M.; Selenska-Pobell, S.
Bacteria –actinide interactions: An environmental perspective
38th Journées des Actinides 2008, April 12-15, 2008, Wroclaw, Poland.

Moll, H.; Bernhard, G.
Die Mobilisierung von Actiniden durch mikrobiell produzierte Liganden unter Berücksichtigung der Endlagerung von radioaktivem Abfall
8. Projektstatusgespräch zur Forschungsförderung zur Entsorgung gefährlicher Abfälle in tiefen geologischen Formationen, May 06-07, 2008, Karlsruhe, Germany.

Moll, H.; Glorius, M.; Rossberg, A.; Bernhard, G.
Uranium(VI) complexation with pyoverdins and related model compounds studied by EXAFS
Actinide XAS 2008, 5th Workshop on Speciation, Techniques, and Facilities for Radioactive Materials at Synchrotron Light Sources, July 15-17, 2008, Saint-Aubin, France.

Müller, K.; Foerstendorf, H.; Brendler, V.
Infrared spectroscopic identification of aqueous neptunium species
Vth Ibero-American Congress of Environmental Physics and Chemistry, April 14-18, 2008, Mar del Plata, Argentina.

Müller, K.; Foerstendorf, H.; Křepelová, A.; Baumann, N.; Brendler, V.
U(VI) sorption onto environmental relevant minerals: Vibrational spectroscopy and complementary tools
Seminar at National Commission of Atomic Energy (CNEA) of Argentina, April 21, 2008, San Martin, Argentina.

Nebelung, C.; Brendler, V.
Uranium(VI) sorption on montmorillonite and bentonite: Prediction and experiments
UMH V – 5th International Conference Uranium Mining and Hydrogeology, September 14-18, 2008, Freiberg, Germany.

Nebelung, C.; Jähnigen, P.; Bernhard, G.
Simultaneaous determination of beta nuclides by liquid scintillation spectrometry
LSC 2008, Advances in Liquid Scintillation Spectrometry, May 25-30, 2008, Davos, Switzerland.

Payne, T. E.; Brendler, V.; Comarmond, M. J.; Harrison, J. J.; Nebelung, C.
Applicability of surface area normalisation in interpreting distribution coefficients (K_d) for radionuclide sorption
SPERA'08 – 10th South Pacific Environmental Radioactivity Conference, November 24-27, 2008, Christchurch, New Zealand.

Pollmann, K.
Multifunctional multilayer-systems based on bacterial surface layers (S-layers)
Workshop zum DFG-Schwerpunktprogramm "Biomimetic Materials Research", July 07, 2008, Potsdam, Germany.

Pollmann, K.; Raff, J.
Nano-Biotechnologie für den Umweltschutz: Entwicklung neuer fotokatalytisch aktiver Verbundmaterialien
DECHEMA-Workshop zur Fördermaßnahme NanoNature des BMBF, August 26, 2008, Frankfurt, Germany.

Pollmann, K.; Raff, J.
NanoFoto - Neue Wege zur verwertungsorientierten Netzwerkbildung in der Nanobiotechnologie
Kick-Off Meeting, WGL-Workshop, March 11, 2008, Berlin, Germany.

Pollmann, K.; Raff, J.
S-Layer für neue Nanomaterialien
Leibniz Institute for Catalysis, April 17, 2008, Berlin, Germany.

Raditzky, B.
Komplexierung von U(VI) durch stickstoffhaltige Modellliganden
Workshop zum Forschungsvorhaben "Wechselwirkung und Transport von Actiniden im natürlichen Tongestein unter Berücksichtigung von Huminstoffen und Tonorganika", April 01-02, 2008, Munich, Germany.

Raditzky, B.
Non-covalent interactions between nucleosides and molecular clips – Comparison of phosphate, phosphonate and sulphate containing clips
5th SUPRAPHONE/4th WG Meeting COST D31, May 29-31, 2008, Prague, Czech Republic.

Raditzky, B.; Joseph, C.
Spectroscopic studies of the uranium(VI) interaction with nitrogen and sulfur containing model ligands
ACTINET 05-08 Project Meeting, October 27-31, 2008, Larnaca, Cyprus.

Raditzky, B.; Schmeide, K.; Geipel, G.; Bernhard, G.
Complexation studies of uranium(VI) by sulfur and nitrogen containing model ligands in aqueous solution
NRC7 – 7th International Conference on Nuclear and Radiochemistry, August 24-29, 2008, Budapest, Hungary.

Raff, J.
Bakterielle Hüllproteine (S-Layer) und ihre technische Anwendung
Sächsisches Textilforschungsinstitut e.V., November 18, 2008, Chemnitz, Germany.

Raff, J.
Metal removal and recovery by bacteria-based biocomposites
Max Bergmann Symposium 08 on Molecular Designed Biological Coatings, November 04-06, 2008, Dresden, Germany.

Raff, J.
Technologieplattform S-Layer
Meeting with Institute of Water Chemsistry, Dresden University of Technology, June 16, 2008, FZD,Dresden, Germany.

Raff, J.; Marquard, A.; Pollmann, K.
Multifunktionale Biokompositschichten zur Eliminierung von Arneimittelrückständen aus Wasser
Colloquium "Produktionsintegrierte Wasser-/ Abwassertechnik", September 22-23, 2008, Bremen, Germany.

Reitz, T.; Merroun, M. L.; Selenska-Pobell, S.
Interactions of *Paenibacillus sp.* JG-TB8 and *Sulfolobus acidocaldarius* with U(VI): Spectroscopic and microscopic studies
UMH V – 5th International Conference Uranium Mining and Hydrogeology, September 14-18, 2008, Freiberg, Germany.

Richter, A.; Brendler, V.
THEREDA - Online
Fachgespräch "Entwicklung einer thermodynamischen Referenzdatenbasis - THEREDA", November 12, 2008, Karlsruhe, Germany.

Rossberg, A.; Tsushima, S.; Scheinost, A. C.
The structure of polynuclear uranyl sorption complexes at the gibbsite/water interface
Actinide XAS 2008, 5th Workshop on Speciation, Techniques, and Facilities for Radioactive Materials at Synchrotron Light Sources, July 15-17, 2008, Saint-Aubin, France.

Rossberg, A.; Funke, H.; Scheinost, A. C
Pair distribution function, Monte Carlo modeling and Factor Analysis: New approaches to EXAFS analysis
2008 SSRL/LCLS Users' Meeting and Workshop, October 15-18, 2008, Stanford, U.S.A.

Sachs, S.
Formation of UO_2(OH)HA(I) studied by TRLFS
ACTINET 05-08 Project Meeting, October 27-31, 2008, Larnaca, Cyprus.

Sachs, S.
Synthetic humic acids for basic studies of humic acid complexation properties and migration processes
ACTINET 05-08 Project Meeting, October 27-31, 2008, Larnaca, Cyprus.

Scheinost, A. C.
Quantitative chemical speciation in environmental systems: statistical approaches to EXAFS
School on Synchrotron X-ray and IR Methods Focusing on Environmental Sciences, January 21-23, 2008, Karlsruhe, Germany.

Scheinost, A. C.
The Rossendorf Beamline: X-Ray Absorption Spectroscopy for Radiochemistry
Ecole Polytechnique Federale Lausanne (EPFL), Environmental Microbiology Laboratory (EML), November 20, 2008, Lausanne, Switzerland.

Schierz, A.; Zänker, H.
Colloidal carbon nanotubes and their influence on dissolved uranium
Environmental Effects of Nanoparticles and Nanomaterials, September 15-16, 2008, Birmingham, Great Britain.

Schierz, A.; Zänker, H.; Bernhard, G.
Einfluss der Oberflächeneigenschaften von Kohlenstoffnanotubes auf ihr Verhalten in der Umwelt
2. Symposium "Nanotechnology and Toxicology in Environment and Health", April 02-03, 2008, Leipzig, Germany.

Schmeide, K.
Redox properties of humic substances in the systems Np(V)/(IV) and U(VI)/(IV)
ACTINET 05-08 Project Meeting, October 27-31, 2008, Larnaca, Cyprus.

Schmeide, K.; Bernhard, G.
Spectroscopic study of the uranium(IV) complexation by organic model ligands in aqueous solution
UMH V – 5th International Conference Uranium Mining and Hydrogeology, September 14-18, 2008, Freiberg, Germany.

Schmeide, K.; Křepelová, A.; Sachs, S.; Bernhard, G.
Comparison of the americium(III), neptunium(V) and uranium(VI) sorption onto kaolinite in the absence and presence of humic acid
2nd-INCC – 2nd International Nuclear Chemistry Congress, April 13-18, 2008, Cancun, Mexico.

Satchanska, G.; Selenska-Pobell S.; Groudeva, V.; Dimkov, R.; Golovinski, E.
Heavy metal, uranium and phenol derivatives pollution in Bulgarian and German environments as a factor influencing bacterial diversity
Ecology Meeting, April 17-18, 2008, Sofia, Bulgaria.

Selenska-Pobell, S.
Bacteria heavy metal interactions: Biomineralization and nanoclusters formation
Ben Gurion University of the Negev, April 02, 2008, Negev, Israel.

Selenska-Pobell, S.
Biogeochemical changes induced in uranium mining wastes by increased uranium concentrations
Institute of Molecular Biology, Bulgarian Academy of Sciences, October 6, 2008, Sofia, Bulgaria.

Selenska-Pobell, S.
The impact of microorganisms on the behaviour of actinides in natural environments
Actinide XAS 2008, 5th Workshop on Speciation, Techniques, and Facilities for Radioactive Materials at Synchrotron Light Sources, July 15-17, 2008, Saint-Aubin, France.

Steudtner, R.
Synthesis and spectroscopic analysis of uranyl sugar complexes
5th SUPRAPHONE/4th WG Meeting COST D31, May 29-31, 2008, Prague, Czech Republic.

Tsushima, S.
Structures and stoichiometry of actinide complexes: Challenges of combining EXAFS and quantum chemistry
Actinide XAS 2008, 5th Workshop on Speciation, Techniques, and Facilities for Radioactive Materials at Synchrotron Light Sources, July 15-17, 2008, Saint-Aubin, France.

Tsushima, S.
Theoretical study on the highest oxidation states of Pu
Plutonium Futures "The Science" 2008, July 07-11, 2008, Dijon, France.

Viehweger, K.; Geipel, G.
Extracellular defence reactions of rape cells caused by uranium exposure
UMH V – 5th International Conference Uranium Mining and Hydrogeology, September 14-18, 2008, Freiberg, Germany.

Viehweger, K.; Geipel, G.
How can plants deal with the relatively high toxic uranium?
The Seminar Series of the Glenn T. Seaborg Center, December 10, 2008, Berkeley, U.S.A.

Vogel, M.; Günther, A.; Raff, J.; Bernhard, G.
Microscopic and spectroscopic investigation of the U(VI) interaction with monocellular green algae
UMH V – 5th International Conference Uranium Mining and Hydrogeology, September 14-18, 2008, Freiberg, Germany.

Zänker, H.
***In-situ* measurements on suspended nanoparticles with X-rays, visible laser light and infra-red light**
Ladenburger Diskurs der Gottlieb Daimler- und Karl Benz-Stiftung "Engineered Nanoparticles in the Aquatic Environment", June 30- July 01, 2008, Ladenburg, Germany.

▶ Posters

Brockmann, S.; Großmann, K.; Krawczyk-Bärsch, E.; Arnold, T.; Wobus, A.
Visualization of uranium in living biofilms in relation to biofilm structure and geochemical conditions
Biofilms III, 3rd International Biofilm Conference, October 06-08, 2008, Munich, Germany.

Crouzet, C.; Delorme, F.; Battaglia-Brunet, F.; Burnol, A.; Scheinost, A. C.; Morin, D.; Touzelet, S.
Characterisation of dissolved thioarsenite complexes and precipitated arsenic species in a low-pH sulphate-reducing bioreactor
2nd International Congress: As in the environment, May 21-23, 2008, Valencia, Spain.

Foerstendorf, H.; Heim, K.
Sorption of uranium(VI) on ferrihydrite – Influence of atmospheric carbonate on surface complex formation investigated by ATR-FT-IR spectroscopy
NRC7 – 7th International Conference on Nuclear and Radiochemistry, August 24-29, 2008, Budapest, Hungary.

Geipel, G.; Viehweger, K.; Bernhard, G.
Uranium speciation after contact with plant cells
The American Society for Cell Biology, 48th Annual Meeting, December 13-17, 2008, San Francisco, U.S.A.

Götz, C.; Geipel, G.; Bernhard, G.
Thermodynamical data of uranyl carbonate complexes from absorption spectroscopy
UMH V – 5th International Conference Uranium Mining and Hydrogeology, September 14-18, 2008, Freiberg, Germany.

Heller, A.; Barkleit, A.; Bernhard, G.
Complexation of curium(III) and europium(III) with urea
NRC7 – 7th International Conference on Nuclear and Radiochemistry, August 24-29, 2008, Budapest, Hungary.

Jankowski, U.; Fahmy, K.; Hennig, C.; Selenska-Pobell, S.; Merroun, M.
Spectroscopic characterization of Pt-complexation and nanoparticle formation on S-layer protein of *bacillus sphaericus* JG-A12
School on Synchrotron X-ray and IR Methods Focusing on Environmental Sciences, January 21-23, 2008, Karlsruhe, Germany.

Joseph, C.; Raditzky, B.; Schmeide, K.; Geipel, G.; Bernhard, G.
Complexation of uranium(VI) by sulfur and nitrogen containing model ligands in aqueous solution
UMH V – 5th International Conference Uranium Mining and Hydrogeology, September 14-18, 2008, Freiberg, Germany.

Kirsch, R.; Scheinost, A. C.; Rossberg, A.; Banerjee, D.; Charlet, L.
Reduction of antimony by nanoparticulate magnetite and mackinawite
GES 8 – Geochemistry of the Earth's Surface 8, August 18, 2008, London, Great Britain.

Knobel, M.; Wagner, M.
Rückgewinnung von Neptunium aus Probelösungen zur radioökologischen Forschung
10. Sächsischer Landeswettbewerb zur Umsetzung der Agenda 21 in der beruflichen Ausbildung 2007/2008, July 07, 2008, Dresden, Germany.

Krawczyk-Bärsch, E.; Arnold, T.; Großmann, K.
Influence of biofilms on the migration behavior of radionuclides
IP FUNMIG Final Workshop, November 24-27, 2008, Karlsruhe, Germany (2008).

Li, B.; Raff, J.; Rossberg, A.; Foerstendorf, H.
A study of uranium phosvitin complexation using ATR FT-IR and EXAFS spectroscopy
BioMetals 2008, 6th International Biometals Symposium, July 14-18, 2008, Santiago de Compostela, Spain.

Macé, N.; Harfouche, M.; Dähn, R.; Tits, J.; Scheinost, A. C.; Wieland, E.
EXAFS investigation of U(VI) speciation in cementitious materials
Actinide XAS 2008, 5th Workshop on Speciation, Techniques, and Facilities for Radioactive Materials at Synchrotron Light Sources, July 15-17, 2008, Saint-Aubin, France.

Macé, N.; Wieland, E.; Tits, J.; Dähn, R.; Kunz, D.; Geipel, G.; Scheinost, A. C.
Spectroscopic investigations of U(VI) speciation In cementitious materials
Cement 08 – 2nd International Workshop on Mechanism and Modelling of Waste/Cement Interaction, October 12-16, 2008, Le Croisic, France.

Marques Fernandes, M.; Dähn, R.; Baeyens, B.; Scheinost, A. C.; Bradbury, M. H.
Influence of carbonate complexation on the sorption of U(VI) on montmorillonite
Actinide XAS 2008, 5th Workshop on Speciation, Techniques, and Facilities for Radioactive Materials at Synchrotron Light Sources, July 15-17, 2008, Saint-Aubin, France.

Moll, H.; Glorius, M.; Bernhard, G.
Curium(III) Speciation in Aqueous Solutions of Bacterial Siderophores
NRC7 – 7th International Conference on Nuclear and Radiochemistry, August 24-29, 2008, Budapest, Hungary.

Müller, K.; Foerstendorf, H.; Brendler, V.; Bernhard, G.
Infrared spectroscopic comparison of the aqueous species of uranium(VI) and neptunium(VI)
NRC7 – 7th International Conference on Nuclear and Radiochemistry, August 24-29, 2008, Budapest, Hungary.

Müller, M.; Schott, J.; Acker, M.; Taut, S.; Barkleit, A.; Bernhard, G.
Absorption spectroscopy of Eu and Am with a liquid waveguide capillary cell
NRC7 – 7th International Conference on Nuclear and Radiochemistry, August 24-29, 2008, Budapest, Hungary.

Pollmann, K.; Raff, J.
Nano-Biotechnologie für den Umweltschutz: Entwicklung neuer fotokatalytisch aktiver Verbundmaterialien
DECHEMA-Workshop zur Fördermaßnahme NanoNature des BMBF, August 26, 2008, Frankfurt, Germany.

Pollmann, K.; Raff, J.; Fahmy, K.; von Borany, J.; Grenzer, J.; Herrmansdörfer, T.
Bacterial surface layers (S-layers) as building blocks for nanocomposites
Nanofair 2008, March 11-12, 2008, Dresden, Germany.

Pollmann, K.; Raff, J.; Marquard, A.; Scholz, A.
Bacterial surface layers (S-layers) as building blocks for photocatalytic nanocomposites
NanoBioEurope2008, June 09-13, 2008, Barcelona, Spain.

Radeva, G.; Kenarova, A.; Buchvarova, V.; Flemming, K.; Selenska-Pobell, S.
Bacterial and archaeal communities – Composition of uranium-contaminated soils in Bulgaria
XII. International Congress of Bacteriology and Applied Microbiology, August 05-09, 2008, Istanbul, Turkey.

Raff, J.; Pollmann, K.
Biodiversität im Filter: Wie Forscher helfen, Uran-Altlasten zu beseitigen
Parlamentarischer Abend der Leibniz-Gemeinschaft, May 06, 2008, Berlin, Germany.

Raff, J.; Pollmann, K.
Nanoskalige Biokompositmaterialien zur Eliminierung von Arzneimittelrückständen
Biotechnica 2008, October 07-09, 2008, Hannover, Germany.

Reitz, T.; Merroun, M. L.; Selenska-Pobell, S.
Interactions of *Paenibacillus sp.* JG-TB8 and *Sulfolobus acidocaldarius* with U(VI)
12th International Symposium on Microbial Ecology, August 17-22, 2008, Cairns, Australia.

Reitz, T.; Merroun, M. L.; Selenska-Pobell, S.
Interactions of U(VI) with members of a microbial consortium recovered from a uranium mining waste pile: Spectroscopic and microscopic studies
School on Synchrotron X-ray and IR Methods Focusing on Environmental Sciences, January 21-23, 2008, Karlsruhe, Germany.

Richter, A.; Nebelung, C.; Brendler, V.
Component additivity approach for uranium retardation in sandstone host rocks
CMWR 2008 – Computational Methods in Water Resources, July 06-10, 2008, San Francisco, U.S.A.

Schierz, A.; Zänker, H.; Bernhard, G.
Influence of acid treatment of multiwall carbon nanotubes on the sorption of U(VI) and on the stability of aqueous suspensions
NanoECO – Nanoparticles in the Environment – Implications and Applications, March 02-07, 2008, Monte Verità, Ascona, Switzerland.

Schmeide, K.; Bernhard, G.
Neptunium(V) reduction by humic substances of varying functionality
Plutonium Futures "The Science" 2008, July 07-11, 2008, Dijon, France.

Selenska-Pobell, S.; Geissler, A.; Flemming, K.; Merroun, M.; Geipel, G.; Reuther, H.
Biogeochemical changes induced by uranyl nitrate in a uranium waste pile
UMH V – 5th International Conference Uranium Mining and Hydrogeology, September 14-18, 2008, Freiberg, Germany.

Suess, E.; Scheinost, A. C.; Bostick, B. C.; Merkel, B. J.; Wallschlaeger, D.; Planer-Friedrich, B.
Structural identification of thioarsenates and their differentiation from thioarsenites by EXAFS
2008 AGU Fall Meeting, December 15-19, 2008, San Francisco, U.S.A.

Suess, E.; Scheinost, A. C.; Bostick, B. C.; Merkel, B. J.; Wallschlaeger, D.; Planer-Friedrich, B.
Structural identification of thioarsenates by EXAFS
Synchrotron Environmental Science IV, December 11-13, 2008, San Francisco, U.S.A.

Tits, J.; Macé, N.; Eilzer, M.; Geipel, G.; Wieland, E.
Uranium(VI) uptake by calcium silicate hydrates
18th Annual V.M. Goldschmidt Conference 2008, July 13-18, 2008, Vancouver, Canada.

Viehweger, K.; Geipel, G.
Extracellular defence reactions of rape cells caused by uranium exposure
BioMetals 2008, 6th International Biometals Symposium, July 14-18, 2008, Santiago de Compostela, Spain.

Viehweger, K.; Geipel, G.
The importance of the intracellular glutathione pool of rape cells exposed to heavy metal stress
The American Society for Cell Biology, 48th Annual Meeting, December 13-17, 2008, San Francisco, U.S.A.

▶ Theses

Großmann, K.
Zur Lokalisation und Bindungsform des Urans in Biofilmen
Dresden University of Technology, Dresden, Germany (2008).

Diploma

Behrendt, F.
Herstellung und Optimierung fotokatalytisch aktiver Schichten auf der Basis bakterieller Hüllproteine
University of Applied Sciences, Dresden, Germany (2008).

Hauptmann, T.
Die Planung und Durchführung von Marktanalysen zur Unterstützung der Verwertung technologischer Inventionen – Eine Fallstudie am Beispiel des Projektes Aquapures
Dresden University of Technology, Dresden, Germany (2008).

Lederer, F.
Heterologe Expression und Modifikation eines S-layer Proteins von einem uranbindenden Bacillus - Isolat
University of Rostock (2008)

Weinert, U.
Modifizierung bakterieller Hüllproteine zur Erzeugung funktioneller Schichten für die Bindung und Detektion von Uran
University of Applied Sciences, Dresden, Germany (2008).

Bachelor

Meusel, T.
Sorption von Uran(VI) an TiO_2-Phasen: Schwingungsspektroskopische Charakterisierung der molekularen Wechselwirkungen
Dresden University of Technology, Dresden, Germany (2008).

Schott, J.
Temperaturabhängige Untersuchungen zur Komplexbildung von Eu(III) mit dem Huminstoff-Modellliganden 2,5-dihydroxybenzoesäure
Dresden University of Technology, Dresden, Germany (2008).

Wimmer, C.
Vergleichende Untersuchungen zu den Fluoreszenzeigenschaften biologisch relevanter Verbindungen bei Raumtemperatur und tiefen Temperaturen
Dresden University of Technology, Dresden, Germany (2008).

Work placements

Krause, M.
Untersuchungen zur technischen Anwendbarkeit von selbstorganisierenden bakteriellen Hüllproteinen in der Nanotechnologie
University of Applied Sciences, Dresden, Germany (2008).

Rossmann, J
Medienoptimierung für verschiedene Haldenisoalte zur Steigerung der Biomasse- und Hüllproteinausbeute
University of Applied Sciences, Dresden, Germany (2008).

- Seminars (Talks of visitors)
- Workshops
- Teaching activities

Seminars

Dr. Tim Payne
Institute for Environmental Research, Australian Nuclear Science and Technology Organisation, Menai, Australia.
NEA sorption project – Overview at start phase III
January 24, 2008

Prof. Dr. Ingmar Grenthe
Department of Chemistry, Royal Institute of Technology, Stockholm, Sweden.
The coordination chemistry of lanthanide(III) and actinide(III) ions – Implications for the design of separation methods
February 08, 2008

Dr. Roland Hellmann
Environmental Geochemistry Group, Université J. Fourier, Grenoble, France.
The role of near-surface alteration at the fluid-mineral interface: Evolving views on the mechanisms of dissolution
March 03, 2008

Prof. Dr. Hendrik Küpper
Department of Biology, Universität Konstanz, Germany.
Heavy metal accumulation in hyperaccumulator plants – Analysis of a complex biological system with physiochemical and biophysical methods
April 09, 2008

Dr. Grégory Lefèvre
Ecole Nationale Supérieure de Chimie de Paris, Paris, France.
Reactivity of particles surface: sorption and adhesion processes
July 07, 2008

Dr. Arnd Junghans
FZD – Institute of Radiation Physics, Dresden, Germany.
Kernenergieforschung mit Neutronen
July 08, 2008

Prof. Dr. Winkelmann
Institute of Microbiolog, Department of Microbiology/Biotechnology, Eberhard-Karls-Universität, Tübingen, Germany
Sidophore – Stabilität und umweltrelevante Eigenschaften
September 29, 2008

Dipl.-Ing. Michael Sailer
Öko-Institut e.V., Darmstadt, Germany.
Zur aktuellen Situation in der Endlagerung
October 20, 2008

Prof. Dr. Hermann Heilmeier
Interdisciplinary Environmenal Research Centre (IÖZ), Technische Universität Bergakadmie Freiberg.
Stress responses in plants: Signalling from the cellular to the whole plant level
November 12, 2008

Prof. Dr. Thomas Schrader
Department of Chemistry, University Duisburg-Essen.
Fundamental biological processes and artificial receptors*
November 13, 2008

Dr. Tilmann Rothfuchs
Gesellschaft für Anlagen- und Reaktorsicherheit (GRS), Braunschweig
Sicherheitsforschung für die Endlagerung radioaktiver Abfälle in Deutschland
December 09, 2008

* Seminar in cooperation with the Institute of Radiopharmacy, FZD.

▶ Workshops (organized by the IRC)

Workshop of the Rossendorf-Beamline (ROBL) at the ESRF, Grenoble, France

FZD, Dresden, Germany, January 15, 2008.

van Deun, R. (KU Leuven)
Absorption spectroscopy of the uranyl ion: Using symmetry to predict spectra

Hennig, C.; van Deun, R.
Coordination and species distribution of uranium chlorides in aqueous and nonaqueous solution

Ikeda, A.
Electrochemical and complexation behavior of U and Np in aqueous solutions

Moll, H.; Glorius, M; Barkleit, A.; Rossberg, A.; Bernhard, G.
U(VI) coordination in biological systems. Part A: U(VI) complexation with pyoverdins and related model compounds. Part B: U(VI) interaction with lipopolysaccharide

Günther, A.; Rossberg, A.
EXAFS structure parameters of uranyl complexes in algae in dependance of the sample preparation

Banerjee, D.
Molecular spectroscopic techniques in environmental chemistry: Reactions at the solution-solid interface

Tsushima, S; Hennig, C.; Rossberg, A.; Ikeda, A.; Scheinost, A. C.
Structures and stoichiometry of actinide complexes: Challenges of combining EXAFS and quantum chemistry

Rossberg, A.; Funke, H.; Kunicke, M.
A recursive approach for determining the radial pair distribution function from EXAFS spectra

Funke, H.; Comin, N.; Chinchio, E.
HAMAGUI: a windows-oriented program for wavelet analysis of EXAFS spectra

Henning. C.
Status report 2007 and outlook

Workshop of the joint project "THEREDA – Thermodynamic Reference Database"

FZD, Dresden, Germany, February 6, 2008.

Hagemann, S. (Gesellschaft für Anlagen- und Reaktorsicherheit (GRS) mbH, Braunschweig)
THEREDA – Zwischenstand Frühjahr 2008

Neck, V. (Institute for Nuclear Waste Disposal, Forschungszentrum Karlsruhe)
Richtlinien zur Datenauswahl und Bewertung

Voigt, W. (TU Bergakademie Freiberg)
Ozeanisches System und Carbonate

Marquardt C. (Institute for Nuclear Waste Disposal, Forschungszentrum Karlsruhe)
Datenbasis Radionuklide

Brendler, V.
Datenbasis Radionuklide – Teil II: Uran

Hagemann, S. (Gesellschaft für Anlagen- und Reaktorsicherheit (GRS) mbH, Braunschweig)
Anorganische Schadstoffe und Matrixelemente in THEREDA

Wilhelm, S. (AF-Colenco Ltd., Baden)
Entwicklung einer thermodynamischen Referenzdatenbasis für Zement

Moog, H. (Gesellschaft für Anlagen- und Reaktorsicherheit (GRS) mbH, Braunschweig)
THEREDA – Struktur und Werkzeuge

Richter, A.
THEREDA im Internet / Intranet

NanoNature-Meeting

FZD, Dresden, Germany, September 26, 2008.

Participants:
Hartmann, J. (Hochschule Anhalt)
Jaehnisch, K. (Leibniz Institute for Catalysis, Berlin)
Längin, A. (Universitätsklinikum, Freiburg)
Lippok, D. (pro aqua, Mainz)
Meyer, A. (UMEX, Dresden)
Pollmann, K.
Raff, J.
Steinfeldt, N. (LIKAT, Berlin)
Strehlitz, B. (Centre for Environmental Research, UFZ, Leipzig)
Worch, E. (Dresden University of Technology)

Workshop of the Institute of Radiochemistry (IRC) and the Institute for Waste Disposal (INE), Karlsruhe, Germany

FZK, Karlsruhe, Germany, October 23-24, 2008.

Li, B.
Spectroscopic characterization of uranium(VI) protein interaction at a molecular level

Polly, R.
Theoretical investigation of sorption at the cprundum surface

Raff, J.
Microbial binding forms of uranium – Base of innovative material development

Scheinost, A. C.
X-ray absorption and photoelectron spectroscopy investigation of selenite reduction by Fe(II)-bearing minerals

Schmidt, M.
Site-selective TRLFS zum Einbau dreiwertiger Lanthaniden und Actiniden in Ca^{2+}-haltige Mineralphasen

Skerencak, A.
TRLFS studies of Cm(III) and Eu(III) with inorganic ligands at elevated temperatures

Tsushima, S.
Actinide speciation with quantum chemical calculations

Vogel, M.
Microscopic and spectroscopic investigation of U(VI) interaction with monocellular green algae

Walther, C.
Investigation of An(IV) polymerization by ESI-TOF, LIBD and XAFS

Workshop of the Institute of Radiochemistry (IRC) and the Paul Scherrer Institute (PSI), Villigen, Switzerland

FZD, Dresden, Germany, November 03-04, 2008.

Bradbury, M.
Überblick Entsorgung Schweiz / LES

Brendler, V.
THEREDA – A thermodynamic reference database for nuclear waste disposal sites in Germany

Curti, E.
Rück- und Ausblicke auf mehr als 15 Jahre Glas-Auflösung

Foerstendorf, H.
Sorption of U(VI) onto ferrihydrite and of Np(V) onto titaniumoxide investigated by *in situ* ATR FT-IR spectroscopy

Gimmi, T.
Solute diffusion and retention in opalinus clay at the field scale

Jordan, N.
Retention of selenium (IV) onto iron oxides. Influence of silicic acid

Joseph, C.
Sorption of uranium(VI) onto opalinus clay in absence and presence of humic acid

Lehmann, S.
Fluorescence spectroscopic studies on the complexation of uranium(IV) with fluoride and phosphate

Marques, M.
Influence of carbonate on the sorption of Eu and trivalent actinides on montmorillonite: A combined macroscopic and microscopic (TRLFS, EXAFS) approach

Moll, H.
Uranium(VI) complexation with pyoverdins and related model compounds studied by EXAFS

Nebelung, C.
Uranium(VI) sorption on montmorillonite and bentonite: Prediction and experiments

Workshop of the Rossendorf-Beamline (ROBL) at the ESRF, Grenoble

FZD, Dresden, Germany, December 18, 2008.

Banerjee, D.
X-ray photoelectron and absorption spectroscopy investigation of Se^{IV} and Sb^{V} reduction by mackinawite

Funke, H.
Inversion of the EXAFS equation by a recursive iteration method. Part I: Theory

Hennig, C.
Interaction of U(IV) with silicate in aqueous solution - An attempt to determine the resulting structures

Kirsch, R.
Sorption of Sb^{V} to and reaction with magnetite

Lucks, C.
Aqueous U^{VI} complexes with tartaric acid: A combined XAFS and UV-vis study

Rossberg, A.
Inversion of the EXAFS equation by a recursive iteration method. Part II: Application

Saito, T.
Structural characterization of uranyl surface complexes on gibbsite in the presence of silicic acid using EXAFS spectroscopy and DFT calculations

Scheinost, A. C.
Towards a micro-XAS beamline for actinide research: First results on uranium oxidation state mapping and micro-XAS from SSRL

The Rossendorf Beamline in 2008 and outlook into 2009 and beyond

Takao, K.
Stability and structures of Np^{VI} and Np^{V} acetate complexes from UV-vis and X-ray absorption spectroscopy

Tsushima, S.
Photochemical reduction of UO_2^{2+} studied by DFT calculations

Teaching activities

Lectures

Bernhard, G.
Radiochemistry – Radiochemical methods
Dresden University of Technology
Summer term 2006

Bernhard, G.
Environmental analysis (Trace analysis)
Dresden University of Technology
Summer term 2006

Bernhard, G.
Environmental chemistry (Environment – Substance – Energy)
Dresden University of Technology
Winter term 2006/2007

Merroun, M.
Lixiviación y Recuperación de Metales: Bioleaching and removal of metals
Centro de Ensenanzas Virtuales de la Universidad de Granada – Fundación Empresa Universidad de Granada & Escuela Superior de Ensenanza Abierta
Study course: Máster de Biotecnología – Master of Biotechnoogy

Courses

The IRC provided one experiment of the laboratory course "Instrumental Analysis" held by the Institute for Analytical Chemistry, Dresden University of Technology, during winter term:

- Alpha spectrometric isotope dilution analysis of uranium

Adviser:
Foerstendorf, H.

Teaching Assistants:
Brockmann, S. (WT 08/09)
Dreissig, I. (WT 07/08)
Götz, C. (WT 07/08)
Günther, T. (WT 08/09)
Joseph, C. (WT 07/08)
Lucks, C. (WT 08/09)
Reitz, T. (WT 07/08)
Vogel, M. (WT 08/09)
Weiß, S. (WT 07-09)

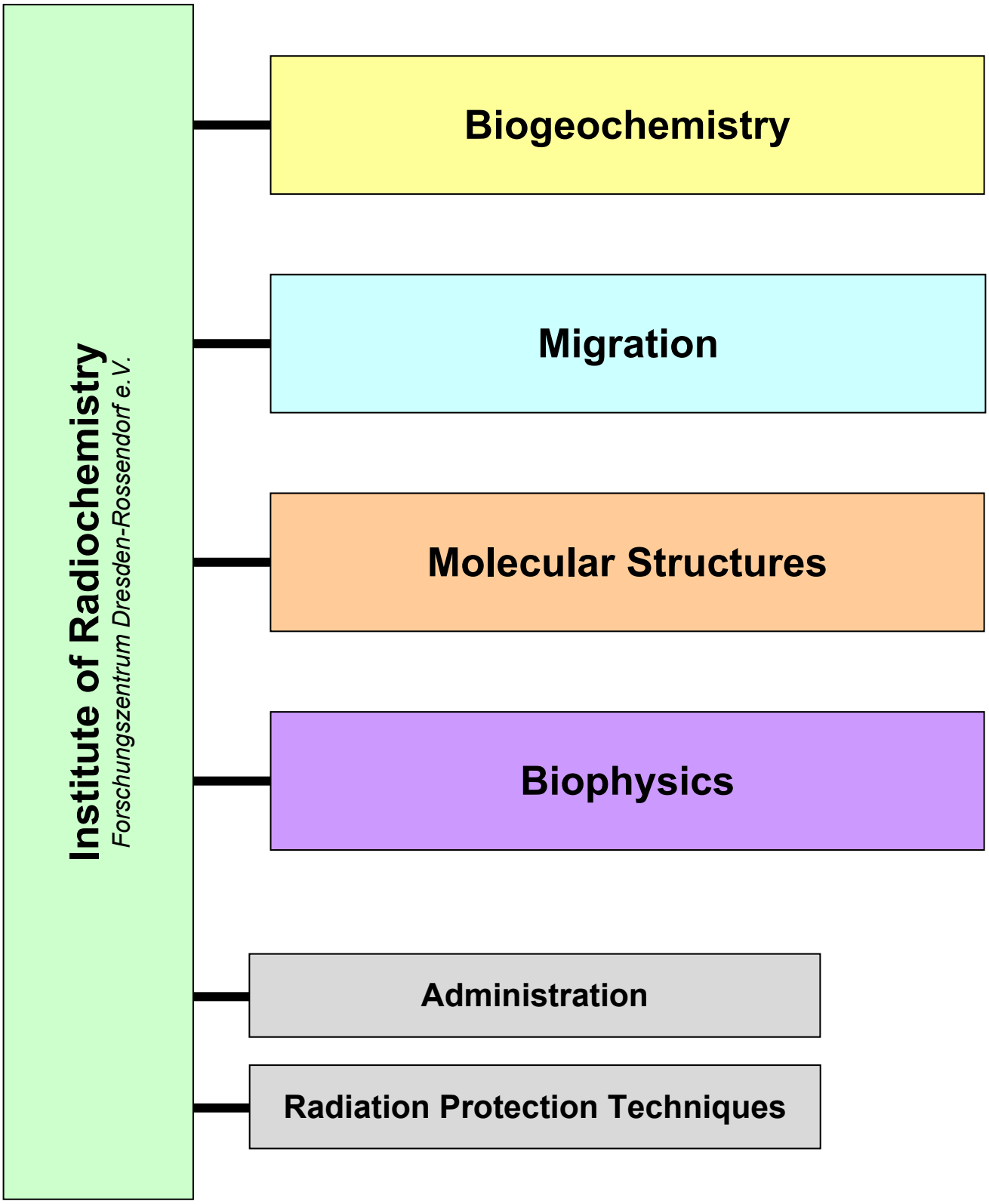
Institute of Radiochemistry
Forschungszentrum Dresden-Rossendorf e.V.
Biogeochemistry
Migration
Molecular Structures
Biophysics
Administration
Radiation Protection Techniques

Prof. Dr. habil. G. Bernhard (Director)

Administration
Kirmes, Claudia; Kovács, Jenny; Barthold, Sylvia;* Pietsch, Mareen* (*: temporary employee)

Radiation Protection Techniques
Heim, Heidemarie; Falkenberg, Dirk; Henke, Steffen; Hiller, Bernd; Rumpel, Annette

D I V I S I O N S

BIOGEO-CHEMISTRY

Dr. Geipel, Gerhard

Dr. Arnold, Thuro
Dr. Barkleit, Astrid
Dr. Günther, Alix
Dr. Ikeda-Ohno, Atsushi
Dr. Krawczyk-Bärsch, Evelyn
Dr. Kutschke, Sabine
Dr. Merroun, Mohamed L.
Dr. Moll, Henry
Dr. Pollmann, Katrin
Dr. Radeva, Galina
Dr. Raff, Johannes
Dr. Sachs, Susanne
Dr. Schmeide, Katja
Dr. Selenska-Pobell, Sonja
Dr. Viehweger, Katrin

Ph. D. students
Glorius, Maja
Götz, Christian
Günther, Tobias
Heller, Anne
Joseph, Claudia
Lederer, Franziska
Lehmann, Sandra
Raditzky, Bianca
Reitz, Thomas
Steudtner, Robin
Tanh Jeazet, Harold B.
Vogel, Manja

Diploma/Bachelor
Behrendt, Frank
Frost, Laura
Schott, Juliane
Wimmer, Christin

Technical Staff
Dudek, Monika
Eilzer, Manuela
Flemming, Katrin
Grambole, Genia
Gürtler, Sylvia
Heller, Sylvia
Marquard, André
Ritter, Aline

MIGRATION

Dr. Brendler, Vinzenz

Dr. Baumann, Nils
Dr. Foerstendorf, Harald
Gester, Sven
Dr. Jordan, Norbert
Nebelung, Cordula
Dr. Richter, Anke
Dr. Stockmann, Madlen
Dr. Schierz, Ariette
Dr. Zänker, Harald

Ph. D. students
Dreissig, Isabell
Li, Bo
Müller, Katharina
Schreppel, Katja

Bachelor
Meusel, Tilmann

Technical Staff
Bruder, Mandy
Eckardt, Carola
Eidner, Irmgard
Fröhlich, Christine
Heim, Karsten
Müller, Christa
Neubert, Heidrun
Schaefer, Ursula
Weiß, Stephan

MOLECULAR STRUCTURES

Dr. habil. Scheinost, Andreas C.

Dr. Banerjee, Dipanjan
Dr. Funke, Harald
Dr. Hennig, Christoph
Dr. Rossberg, André
Dr. Takao, Koichiro
Dr. Takao, Shinobu
Prof. Dr. Tsushima, Satoru

Ph. D. students
Kirsch, Regina
Lucks, Christian

Administration
Glückert, Marion

Technical Staff
Hesse, Marco

BIOPHYSICS

Dr. habil. Fahmy, Karim

Dr. Savchuk, Olesya
Dr. Sczepan, Martin

Ph. D. students
Eichler, Stefanie
Furlinski, Georgi I.
Khesbak, Hassan
Madathil, Sineej

Technical Staff
Philipp, Jenny

EXIST – Fellowship for business start up

BIOREM
Hauptmann, Tobias
Lehmann, Falk
Richter, Lars
Weinert, Ulrike

NANOLAB
Dr. Großmann, Kay
Sobirai, Dirk
Trepte, Paul

External Ph. D. students
Brockmann, Sina
Müller, Melanie
Pürschel, Madlen

GRADUATE ASSISTANTS, STUDENT ASSISTANTS, TRAINEES

Aleithe, Susanne	Harnisch, Kristin	Meierhöfer, Claudia	Seidel, Peggy
Bernhard, Jörg	Heller, Tina	Meurich, Maria	Stolze, Karoline
Fajardo Uribe, Carlos H.	Herrmann, Stefanie	Mizera, Jens	Ulrich, Alessandra
Falkenberg, Anne	Husar, Richard	Müller, Christian	Wenzel, Marco
Gensch, Tobias	Jankowski, Ulrike	Riemer, Michaela	Winkler, Marion
Goméz-Garcia, Liliana	Jähnigen, Peggy	Rossmann, Julia	Zirakadze, Lana
Gregus, Maria-Alexandra	Jentsch, Annegret	Schleith, Kathrin	Zirnstein, Isabel
Gründig, Ines	Krause, Martin	Schmidt, Kristin	
Hänsch, Samuel	Kuhnert, Elisabeth	Sebald, Peter	

GUEST SCIENTISTS

S. K. Andhirka	*Indian Institute of Technology Madras, Chennai, India*
V. Bucharova	*Institute of Molecular Biology, Bulgarian Academy of Sciences, Sofia, Bulgaria*
Dr. M. J. Comarmond	*Institute for Environmental Research, Australian Nuclear Science and Technology Organisation, Menai, Australia*
Prof. Dr. E. Golovinsky	*Institute of Molecular Biology, Bulgarian Academy of Sciences, Sofia, Bulgaria*
R. Illgen	*Faculty of Mathematics / Natural Sciences Hochschule Zittau/Görlitz (FH) – University of Applied Sciences*
Dr. O. Kataeva	*A. E. Arbuzov Institute of Organic and Physical Chemistry, Kazan Research Centre of the Russian Academy of Sciences, Kazan, Russia*
Dr. V. Kiselev	*Izhevsk State Technical University Izhevsk, Russia*
Dr. G. Lefèvre	*Laboratoire d'Electrochimie et de Chimie Analytique, École Nationale Supérieure de Chimie de Paris, Paris, France*
S. Meca Fàbrega	*CTM Centre Tecnològic, Environmetal Technology Area Manresa, Spain*
F. Morcillo de Amueda	*Depertamento de Microbiología, Facultad de Ciencias, University of Granada, Spain*
V. Pavlov	*Institute of Microelectronics Technology, Russian Academy of Sciences, Chernogolovka, Russia*
Dr. G. Radeva	*Institute of Molecular Biology, Bulgarian Academy of Sciences, Sofia, Bulgaria*

ACKNOWLEDGEMENTS

The Institute of Radiochemistry is part of the Forschungszentrum Dresden-Rossendorf e. V. (FZD) which is financed in equal parts by the ***Federal Republic of Germany*** and the ***Free State of Saxony***.

The Commission of the European Communities (EU) supported the following projects:

- ACTINET Network for Actinide Sciences:
  Contract No.: FIR1-CT-2002-20211
  Contract No.: FI6W-CT-2004-508836
- ACTINET-6 Pooled Facility:
  Actinides and lanthanides solution chemistry in water stable room temperature ionic liquids(RTILs) – Part II
  Contract No.: 05-26
  Actinide selective recognition by bio mimetic molecules
  Contract No.: 05-01
  Batch experiments and spectroscopic studies of Np(V) sorption on montmorillonite
  Contract No.: 05-22
  Combining XAS at variable energy and theoretical calculations to investigate bonding in actinide molecules
  Contract No.: 07-06
  Free and silica-gel-bound tetraazamacrocycles as complexing agents of actinide cations: investigation of the solid-state and solution coordination scheme
  Contract No.: 07-05
  Influence of carbonate on actinides sorption on clay minerals
  Contract No.: JRP 06-02
  Microscale investigations of the speciation and mobility of uranium in cementitious materials
  Contract No.: JRP 06-13
  Physico-chemical and redox properties of protactinium
  Contract No.: JRP 07-20
  Probing the interaction of actinides with the functional species of mineral/electrolyte interfaces by sum frequency vibrational spectroscopy
  Contract No.: 05-11
  Reduction of uranium(VI) by adsorbed Fe(II) on several clays and by structural Fe(II) in smectite in O_2,, CO_2 free atmosphere
  Contract No.: JRP 06-08
  Contract No.: JRP 07-21
  Speciation of actinides and fission products nanoparticles embedded into the mesoporous matrices
  Contract No.: JRP 07-16
- ACTINET Sorption Board:
  Knowledge infrastructure and education
  Contract No.: 02-23
  Managing experiments, models and data
  Contract No.: 02-24
- Integrated project FUNMIG:
  Fundamental processes of radionuclide migration
  Contract No.: 516514
  Redox phenomena controlling systems (RECOSY)
  Contract No.: 212287

Eight projects were supported by the ***Bundesministerium für Wirtschaft und Technologie (BMWi)*** and by the ***Bundesministerium für Bildung und Forschung (BMBF)***:

- Integriertes Sorptionsdatenbanksystem für Wechselwirkungen chemisch-toxischer und radioaktiver Kontaminanten mit mineralischen Systemen in geologischen Formationen (ISDA-FZR)
  Contract No.: BMBF 02C1144
- Mobilisierung von Actiniden durch mikrobiell produzierte Liganden unter Berücksichtigung der Endlagerung von radioaktivem Abfall
  Contract No.: BMWi 02E9985
- NanoFoto – Neue Wege zur verwertungsorientierten Netzwerkbildung in der Nanobiotechnologie
  Contract No.: BMBF 01SF0717
- Thermodynamische Referenzdatenbasis THEREDA, Teilvorhaben FZR, gefördert durch das BMBF
  Contract No.: 02C1436
- Thermodynamische Referenzdatenbasis THEREDA, Teilvorhaben FZR, gefördert durch das BMWi
  Contract No.: 02E10136
- Verbundprojekt: Actinidenmigration im natürlichen Tongestein: Charakterisierung und Quantifizierung des Einflusses von Tonorganika auf die Wechselwirkung von U und Am im Ton
  Contract No.: BMWi 02E10156
- Verbundprojekt: Realitätsnahe Einbindung von Sorptionsprozessen in Transportprogramme für die Langzeitsicherheitsanalyse (ESTRAL)-TV2
  Contract No.: 02E10528
- Wissenschaftlich-Technologische Zusammenarbeit (WTZ) Indien: Strukturbiophysik G-Protein gekoppelte Rezeptoren
  Contract-No.: IND 061030

Five projects were supported by the ***Deutsche Forschungsgemeinschaft (DFG)***:

- Bindungsform von Cm(III) und Eu(III) in menschlichen Biofluiden (Speichel, Urin)
  Contract No.:BE 2234/10-1
- In-situ Speziation von Uran in Biofilmen
  Contract No.: AR 584/1-1
- In situ-Strukturuntersuchungen von Neptunium-Spezies in wässriger Lösung unter reduzierenden Bedingungen
  Contract No.: HE 2297/2-1
- Sorptionsprozesse von Np(V) an Alumosilikaten. Schwingungsspektroskopische Untersuchungen
  Contract No.: FO 619/1-1
- Strukturbestimmung von ternären aquatischen U(VI)-Sorptionskomplexen mittels neuester entwickelter kombinierter EXAFS-Auswertemethoden (ITFA, MCTFA)
  Contract No.: RO 2254/3-1

The ***Project Management Jülich*** supported the EXIST grants for business start-up:

- BIOREM
  Contract-No.: 03EGSSN014
- Nanolab Microsystems, Gesellschaft für Technologie- und Umweltberatung
  Contract-No.: 03EGSSN019

The ***Bundesamt für Strahlenschutz (BfS)*** supported one project:

- Entwicklung einer thermodynamischen Referenzdatenbasis (Teilprojekt Spaltprodukte und Zement: THEREDA-SZ)
  Contract-No.: VA3252 - AN550550 - UA2671

One project was supported by ***Deutscher Akademischer Austauschdienst (DAAD)***:

- Nanoparticles for fuell cell technology, DAAD Großbritannien
  Contract No. D/08/08913

The ***University of Manchester, Department of Chemistry***, Great Britain supported one project:

- Access to beamtime at Rossendorf Beamline at ESRF in the frame of a scientific collaboration

The ***University of Jena*** supported one project:

- Uranaufnahme
  Contract-No.: 02S8517

Prof. Dr. S. Tsushima is a research fellow of the ***Alexander von Humboldt Foundation***.

V. Bucharova and Dr. G. Radeva were granted by the ***Sächsisches Staatsministerium für Wissenschaft und Kunst (SMWK)***.

INDEX OF AUTHORS